VOLUME 102 | SUPPLEMENT 1 | MARCH 2022

LI

LABORATORY INVESTIGATION

THE BASIC AND TRANSLATIONAL PATHOLOGY RESEARCH JOURNAL

ABSTRACTS (851–976)

HEMATOPATHOLOGY

2022

USCAP 111TH ANNUAL MEETING

REAL INTELLIGENCE

MARCH 19–24, 2022 LOS ANGELES, CALIFORNIA

Published by
SPRINGER NATURE
www.ModernPathology.org

USCAP
Creating a Better Pathologist
AN OFFICIAL JOURNAL OF THE UNITED STATES AND CANADIAN ACADEMY OF PATHOLOGY

EDUCATION COMMITTEE

Rhonda K. Yantiss
Chair

Kristin C. Jensen
Chair, CME Subcommittee

Laura C. Collins
Chair, Interactive Microscopy Subcommittee

Yuri Fedoriw
Short Course Coordinator

Ilan Weinreb
Chair, Subcommittee for Unique Live Course Offerings

Carla L. Ellis
Chair, DEI Subcommittee

Adebowale J. Adeniran
Kimberly H. Allison
Sarah M. Dry
William C. Faquin
Karen J. Fritchie
Jennifer B. Gordetsky
Levon Katsakhyan, Pathologist-in-Training
Melinda J. Lerwill
M. Beatriz S. Lopes
Julia R. Naso, Pathologist-in-Training
Liron Pantanowitz
Carlos Parra-Herran
Rajiv M. Patel
Charles "Matt" Quick
David F. Schaeffer
Lynette M. Sholl
Olga K. Weinberg
Maria Westerhoff

ABSTRACT REVIEW BOARD

Benjamin Adam
Oyedele Adeyi
Mariam Priya Alexander
Daniela Allende
Catalina Amador
Vijayalakshmi Ananthanarayanan
Tatjana Antic
Manju Aron
Roberto Barrios
Gregory R. Bean
Govind Bhagat
Luis Zabala Blanco
Michael Bonert
Alain C. Borczuk
Tamar C. Brandler
Eric Jason Burks
Kelly J. Butnor
Sarah M. Calkins
Weibiao Cao
Wenqing (Wendy) Cao
Barbara Ann Centeno
Joanna SY Chan
Kung-Chao Chang
Hao Chen
Wei Chen
Yunn-Yi Chen
Sarah Chiang
Soo-Jin Cho
Shefali Chopra
Nicole A. Cipriani
Cecilia Clement
Claudiu Cotta
Jennifer A. Cotter
Sonika M. Dahiya
Elizabeth G. Demicco
Katie Dennis
Jasreman Dhillon
Anand S. Dighe
Bojana Djordjevic
Michelle R. Downes
Charles G. Eberhart
Andrew G. Evans
Fang Fan
Julie C. Fanburg-Smith
Gelareh Farshid
Michael Feely
Susan A. Fineberg
Dennis J. Firchau
Gregory A. Fishbein
Agnes B. Fogo
Andrew L. Folpe
Danielle Fortuna
Billie Fyfe-Kirschner
Zeina Ghorab
Giovanna A. Giannico
Anthony J. Gill
Tamar A. Giorgadze
Alessio Giubellino
Carolyn Glass
Carmen R. Gomez-Fernandez
Shunyou Gong
Purva Gopal
Abha Goyal
Christopher C. Griffith
Ian S. Hagemann
Gillian Leigh Hale
Suntrea TG Hammer
Malini Harigopal
Kammi J. Henriksen
Jonas J. Heymann
Carlo Vincent Hojilla
Aaron R. Huber
Jabed Iqbal
Shilpa Jain
Vickie Y. Jo
Ivy John
Dan Jones
Ridas Juskevicius
Meghan E. Kapp
Nora Katabi
Francesca Khani
Joseph D. Khoury
Benjamin Kipp
Veronica E. Klepeis
Christian A. Kunder
Stefano La Rosa
Stephen M. Lagana
Keith K. Lai
Goo Lee
Michael Lee
Vasiliki Leventaki
Madelyn Lew
Faqian Li
Ying Li
Chieh-Yu Lin
Mikhail Lisovsky
Lesley C. Lomo
Fang-I Lu
aDeqin Ma
Varsha Manucha
Rachel Angelica Mariani
Brock Aaron Martin
David S. McClintock
Anne M. Mills
Richard N. Mitchell
Hiroshi Miyamoto
Kristen E. Muller
Priya Nagarajan
Navneet Narula
Michiya Nishino
Maura O'Neil
Scott Roland Owens
Burcin Pehlivanoglu
Deniz Peker Barclift
Avani Anil Pendse
Andre Pinto
Susan Prendeville
Carlos N. Prieto Granada
Peter Pytel
Stephen S. Raab
Emilian V. Racila
Stanley J. Radio
Santiago Ramon Y Cajal
Kaaren K Reichard
Jordan P. Reynolds
Lisa M. Rooper
Andrew Eric Rosenberg
Ozlen Saglam
Ankur R. Sangoi
Kurt B. Schaberg
Qiuying (Judy) Shi
Wonwoo Shon
Pratibha S. Shukla
Gabriel Sica
Alexa Siddon
Anthony Sisk
Kalliopi P. Siziopikou
Stephanie Lynn Skala
Maxwell L. Smith
Isaac H. Solomon
Wei Song
Simona Stolnicu
Adrian Suarez
Paul E. Swanson
Benjamin Jack Swanson
Sara Szabo
Gary H. Tozbikian
Gulisa Turashvili
Andrew T. Turk
Efsevia Vakiani
Paul VanderLaan
Hanlin L. Wang
Stephen C. Ward
Kevin M. Waters
Jaclyn C. Watkins
Shi Wei
Hannah Y. Wen
Kwun Wah Wen
Kristy Wolniak
Deyin Xing
Ya Xu
Shaofeng N. Yan
Zhaohai Yang
Yunshin Albert Yeh
Huina Zhang
Xuchen Zhang
Bihong Zhao
Lei Zhao

To cite abstracts in this publication, please use the following format: **Author A, Author B, Author C, et al. Abstract title (abs#). In "File Title."** ***Laboratory Investigation*** **2022; 102 (suppl 1): page#**

851 Immunophenotypic and Molecular Profiling of Chronic Myeloid Leukemia (CML) in T-cell lineage Blast Phase

Romany Abdelmalak[1], Qi Gao[1], Kseniya Petrova-Drus[1], Yanming Zhang[1], Wenbin Xiao[1], Mikhail Roshal[1], Pallavi Galera[1]
[1]*Memorial Sloan Kettering Cancer Center, New York, NY*

Disclosures: Romany Abdelmalak: None; Qi Gao: None; Kseniya Petrova-Drus: None; Yanming Zhang: None; Wenbin Xiao: None; Mikhail Roshal: None; Pallavi Galera: None

Background: Chronic Myeloid Leukemia (CML) arises from pluripotent hematopoietic stem cells that have the ability to differentiate various lineages including lymphoid. T-cell lineage blast phase in the context of CML is a rare phenomenon with less than 50 cases being described in the literature. The molecular landscape of these is currently unknown.

Design: 3 CML cases in blast phase (Table 1) with the blasts showing T cell differentiation were identified. Clinical, histologic, flow cytometric, cytogenetic, and molecular features were reviewed.

Results: All 3 patients were female, ages ranging from 43–76-year-old.

Patient1: started on imatinib for CML in chronic phase, she was non-compliant. She presented fever, neck swelling. The BM revealed a hypercellular marrow with 25% blasts. By flow cytometry (FC) the blast were cCD3+(bright), sCD3-, CD1a-, CD2+, CD5+(dim), CD7+, CD4-, CD8-, CD34+(partial), TDT-, CD117-, MPO-, CD14-, CD56-, CD10+(partial), CD19-, CD20-, CD22-, (s)light chain- and focally positive for TdT by IHC. Molecular studies showed MED12 mutation. Post induction chemotherapy (HyperCVAD) patient underwent HSCT and is now disease-free.

Patient 2 initially diagnosed as CML, subsequently presented in blast phase, 85% blasts. By FC blasts revealed cCD3+(bright), sCD3 -, CD11+(partial), CD19+(partial),CD2-,CD5-,CD7-,CD10-, cCD79a-,CD117+, CD34+, CD15+(partial), MPO+(partial) consistent with a T/Myeloid diff. Molecular studies revealed ABL1 mutation.

Patient3 presented with leukocytosis, basophilia, 21% PB blasts. The blasts by FC were cCD3+, sCD3+(partial), CD11b, CD19+ & cCD79a (subset), CD2+, CD5+(partial), CD7+(partial), CD10+ (partial), CD117+,CD34+, CD15-, MPO- consistent with T, B and myeloid diff. CG studies showed t(9;22)/complex karyotype (table) indicative of CML. Molecular studies revealed HIST1H1D mutation, treated with FLA-IDA & subsequent HSCT.

PATIENT	AGE	SEX	DIAGNOSIS	BLAST CRISIS	CBC AT BLAST CRISIS	BM AT BLAST CRISIS	FLOW FINDINGS	MUTATION PROFILE	Cytogenetic results
1	43	FEMALE	CML	T-cell Blasts	ANC:127, ALC:80, AMC:21, AEC:2, ABC:0 WBC: 236 RBC:2.99 HGB: 8.7 HCT: 26.6% PLT: 80 L:24.0% M: 9.0% N: 54.0% Meta:3.0% Myelo:3.0% Blasts: 4.0% B: 0% E:1.0% nRBC 1.0%	25% blasts Hypercellular marrow>95% Reticulin fibrosis 3/3	cCD3+ sCD3- CD1a- TdT- CD2+ CD5+ CD7+ CD38+ CD10+p CD34+p CD4- CD8- HLA-DR- CD117- MPO CD33- CD36- CD14- CD56- CD19- CD20- CD22- surface kappa and lambda(-).	MED12 (NM_005120) exon29 p.P1371Lfs*5 (c.4112delC)	FISH studies performed on flow cytometry (FC) sorted T-blasts revealed t(9;22) supporting the diagnosis.
2	76	FEMALE	CML	T/myeloid blasts	ANC:1.7, ALC:3.4, AMC:0.5,	85% blasts Hypercellular marrow>95%	cCD3+ bright sCD3-	ABL1 (NM_005157) exon6	trisomy 8 in addition to t(9;22)

					AEC:0.2, ABC:0 Blasts 18.5 WBC 24.4 RBC 3. HGB 10.9 HCT 33.8 PLT: 23 N:7.0% M: 2.0% E: 1.0% B: 0% Blast 76.0%	Reticulin fibrosis 0/3	CD11+P CD19+P CD2- CD5- CD7- CD38 +P CD10- cCD79a- CD117+ HLA-DR- CD34+ CD15+P	p.T315I (c.944C>T)	
3	74	FEMALE	CML	Myeloid, B, and T-cell differentiation blasts	ANC:3.2, ALC:3.7, AMC:2.2, AEC:0.4, ABC:1 Blasts 2.9 WBC 13.8 RBC 2.43 HGB 7.6 HCT 22.8 PLT: 235 N:23.0% M: 16.0% E: 7.0% B: 7% Blast 21.0%	48% blasts Hypercellular 70% Reticulin fibrosis 1/3	cCD3+ sCD3+p CD11b+ CD19+P CD2+ CD5+p CD7+p CD8- CD38 +P CD10+p cCD79a+p CD117+ HLA-DR+ CD34+ CD15- MPO-	HIST1H1D (NM_005320) exon1 p.S2P (c.4T>C)	revealed complex karyotype, including t(9;22), inv(3q), an unbalanced translocation between chromosomes 2 and 5 along a deletion of 5q, and a ring chromosome 7

Conclusions: Mutations in *CDKN2A/B* and *IKZF1* have been reported in CML in lymphoblastic transformation (predominantly B-lineage). However, specific genetic aberrations leading to T cell differentiation in CML are not well understood. MED12 somatic mutations (as identified in patient 1) are rare and have been reported in T- and NK-cell post-transplant lymphoproliferative disorders and pediatric T-cell acute lymphoblastic leukemia T-ALL). Hierarchical clustering has shown them to be early events in T-ALL. Evaluation of the molecular landscape of these rare cases can provide us an insight into drivers of T cell differentiation in CML.

852 Comparison of BRAF Testing Modalities in Histiocytic Neoplasms

Aldo Acosta-Medina[1], Jithma Abeykoon[1], Ronald Go[1], Gaurav Goyal[2], Susan Schram[1], Aishwarya Ravindran[1], Karen Rech[1]
[1]Mayo Clinic, Rochester, MN, [2]The University of Alabama at Birmingham, Birmingham, AL

Disclosures: Aldo Acosta-Medina: None; Jithma Abeykoon: None; Ronald Go: None; Gaurav Goyal: None; Susan Schram: None; Aishwarya Ravindran: None; Karen Rech: None

Background: The diagnostic and therapeutic approach to histiocytic neoplasms, such as Erdheim-Chester Disease (ECD) and Langerhans Cell Histiocytosis (LCH), has been revolutionized by the demonstration of mutations in the MAPK pathway, most commonly *BRAF*^{V600E}. We compared the performance of IHC and NGS in detection of *BRAF*^{V600E} in histiocytic disorders.

Design: Review of pathology records identified patients with a diagnosis of a histiocytic disorder and *BRAF* evaluation by BRAF^{V600E} IHC or targeted NGS on tissue biopsy. IHC was performed using the VE1clone (Abcam) on the Ventana Benchmark ULTRA with Optiview AMP detection.

Results: A total of 121 patients had 160 tissue samples. Diagnoses included ECD (*n*=60), LCH (*n*=56), histiocytic sarcoma (*n*=3), Rosai-Dorfman disease (*n*=2).

IHC was done in 110 biopsies, with failed staining in 2 (1.8%) and equivocal staining in 8 (7%). Among patients with IHC on multiple biopsies, all were concordant except 2 cases where equivocal staining on a decalcified sample was confirmed positive on a no.

In 45 patients, both NGS and IHC were successfully performed (Table 1). With NGS as gold standard, IHC showed high sensitivity (82.4%) and specificity (96.4%) for detection of *BRAF*^{V600E}. Three false-negative IHC results included 2 with a *BRAF*^{V600E} variant allele frequency (VAF) <6% by NGS. VAF in the 14 NGS positive samples ranged from 1.9%–20.6% and 50% were ≤5%. A false-positive IHC in a lung biopsy showed cytoplasmic staining in histiocytes although NGS was negative. As the VE1 antibody is known to cross-react with ciliary axonemal components, it is hypothesized that the histiocytes had engulfed cells sloughed from the respiratory epithelium.

Table 1. Comparison of immunohistochemistry (IHC) for detection of BRAF^{V600E} to next-generation sequencing (NGS).

		Next-generation sequencing		
		Positive	Negative	Total
Immunohistochemistry	Positive	14	1	15
	Negative	3	27	30
	Total	17	28	45

Conclusions: IHC is a useful method for detection of BRAF^{V600E} in histiocytic neoplasms with high sensitivity and specificity. In cases with negative or equivocal IHC results, confirmation by a sensitive molecular technique should be performed. A targeted NGS panel can detect *BRAF*^{V600E} at the low VAF frequently seen in histiocytic neoplasms and has the additional advantage of detecting other pathogenic mutations along the MAPK pathway. An important caveat is recognition of the cross-reactivity of the VE1 antibody clone against axonemal components in biopsies containing ciliated epithelium.

853 Cytopenic Patients with Negative Bone Marrow Next Generation Sequencing Studies Have Little to No Risk of Subsequent Progression to Myeloid Neoplasms

Raniah Alamri[1], Erika Moore[2], Bryan Rea[2]
[1]UPMC Presbyterian Hospital, Pittsburgh, PA, [2]University of Pittsburgh School of Medicine, Pittsburgh, PA

Disclosures: Raniah Alamri: None; Erika Moore: None; Bryan Rea: None

Background: Unexplained cytopenia(s) are a common indication for bone marrow (BM) biopsy but commonly lack sufficient morphologic abnormalities to explain such cytopenias. Such cases may receive a diagnosis of idiopathic cytopenia of undetermined significance (ICUS), or if a mutation is present by next generation sequencing (NGS), clonal cytopenia of undetermined significance (CCUS). While a few studies have shown CCUS cases can progress to myeloid neoplasms, the outcomes of patients with non-diagnostic BMs and negative NGS are less certain. Here, we investigate cytopenic patients with negative BM NGS to determine their subsequent risk of myeloid neoplasms, and, to our knowledge, this is the largest series of such cases.

Design: We collected 184 BMs with negative NGS for an indication of cytopenia from 2017-2021. The NGS panel included either 37 (2017-2019) or 54 genes (2019-2021) recurrently mutated in myeloid neoplasms. Cases with a previous or current diagnosis of a myeloid neoplasm were excluded. 150 total cases remained for detailed clinicopathologic evaluation and extended clinical follow-up.

Results: Of 150 cases, 13 (8%) had diagnostic evidence of a myeloid neoplasm based on cytogenetic findings. A total of 137 cases with unexplained cytopenia, non-diagnostic marrow morphology, and negative NGS/cytogenetics remained. The median age was 61 years (range, 8-98 years) with a male:female ratio of 0.6:1. 69 cases (50%) had single lineage cytopenia, 38 (28%) had bicytopenia, and 30 (22%) had pancytopenia. With a median follow-up time of 22 months (range 1-53 months), none of the 137 cases developed a myeloid neoplasm over the study period. 15 cases (11%) had repeat BM biopsies performed for unexplained cytopenia, none of which identified a myeloid neoplasm. The negative predictive value (NPV) for negative NGS in a non-diagnostic BM was 91% while negative cytogenetics and negative NGS had a NPV of 100%.

Conclusions: This data highlights the importance of negative NGS findings in the evaluation of cytopenia, and it also demonstrates the diagnostic role of cytogenetic testing in a subset of cases. The risk of subsequent diagnosis of a myeloid neoplasm was zero in cases with a non-diagnostic BM and negative NGS/cytogenetic studies. Although even longer term follow-up will be important, these findings may indicate that cytopenic patients with no morphologic evidence of a myeloid neoplasm and negative genetic studies do not need extensive clinical follow-up and may not benefit from subsequent BMs.

854 Flow Cytometric Evaluation of CD1c and CD180 in Low Grade B-cell Lymphomas

Khaled Alayed[1], Howard Meyerson[2]
[1]King Saud University, Case Western Reserve University, University Hospitals/Case Medical Center, Aurora, OH, [2]University Hospital Case Medical Center, Cleveland, OH

Disclosures: Khaled Alayed: None; Howard Meyerson: None

Background: CD1c (BDCA-1) is a membrane glycoprotein of the CD1 family. It is expressed on a major subpopulation of myeloid dendritic cells. In blood, CD1c is also expressed on subset of CD19+ small resting B lymphocytes. CD180 is a toll-like receptor (TLR) expressed by human B lymphocytes, monocytes, and some dendritic cells. It plays crucial roles in innate immune response by recognizing specific molecule on pathogens. The aims of this study are to evaluate flow cytometric (FCM) expression of CD1c and CD180 in B-cells of different subtypes of low grade B-cell lymphomas and determine their diagnostic relevance in routing clinical analysis.

Design: Low grade B-cell lymphoma cases with the desired FCM testing were collected. Cases were diagnosed according to the 2017 WHO classification. Six-color FCM assay were performed using these antibodies: CD1c, CD5, CD10, CD11c, CD19, CD20, CD23, CD25, CD38, CD43, CD45, CD56, CD79b, CD180, IgD, Kappa and Lambda. Mean Fluorescence Intensity (MFI) was used to evaluate CD1c and CD180 analysis.

Results: 54 cases were included with mean age of 70 years (range: 25-94). 18 (33%) cases were females and 36 (67%) were males. The site of involvement was bone marrow (BM) in 34 (63%) cases, peripheral blood (PB) in 11 (20.4%), lymph node (LN) in 8 (14.8%) and orbit in 1 (1.8%). CLL/SLL diagnosis was established in 12 (22%) cases, MCL in 6 (11%), FL in 2 (4%), LPL in 16 (30%), MZL in 7 (13%), SMZL in 7 (13%), HCL in 2 (4%), and HCLv in 2 (4%). Multiple comparisons testing showed significantly lower expression of CD1c in CLL/SLL cases compared to MCL, LPL, MZL and SMZL (adj. *P,* 0.001, 0.0006, 0.0004, 0.01, respectively). No association between CD1c and age, gender, disease site or any other diagnoses comparisons. CD180 showed significant higher expression in SMZL (adj. *P* 0.49) and nearly significant higher expression in MCL (adj. *P* 0.054) compared to CLL/SLL cases. No other CD180 associations were detected.

Conclusions: We observed that CD1c and CD180 showed significant under expression in CLL/SLL cases compared to other subtypes of low grade B-cell lymphomas. These findings might therefore necessitate the need of including them in FCM panels for diagnosis of low grade B-cell lymphomas. An evaluation of these markers in large cohorts with multivariate analysis might revealed more insights regard their pathogenesis and diagnostic relevance in low grade B-cell lymphomas.

855 PET Scan Assessment in Follicular Lymphoma (FL) with High Proliferation Index (HPI)

Mahmoud Aldyab[1], Ammoura Ibrahim[2], Tipu Nazeer[2]
[1]Albany Medical Center, Albany, NY, [2]Albany Medical College, Albany, NY

Disclosures: Mahmoud Aldyab: None; Ammoura Ibrahim: None; Tipu Nazeer: None

Background: Positron Emission Tomography (PET) is commonly utilized to evaluate for histologic progression of follicular lymphoma (FL) to diffuse large cell lymphoma (DLCL) and assist in targeted biopsy for confirmation. Low grade (LG) FL with high proliferation index (HPI) have been reported to behave like high grade (HG) FL and may require a different therapeutic approach. Currently, they are recognized only at the microscope.

This study was undertaken to evaluate the utility of PET scan in identifying sites that harbor LG FL with HPI for targeted biopsy

Design: One hundred and twenty-four FL cases at the pathology department at Albany Medical Center between years 2013-2019 were collected. Cases showing evolution to diffuse large cell lymphoma were excluded. FL grade, KI67 index and proliferation pattern (diffuse vs nodular) were recorded. PET scan reports were matched with the location and date of biopsy. Cases with no PET scans were excluded as well as cases where the PET scan was done >30 days before or after the biopsy.

Of the 63 cases that were included, 36 were grade1 including 12 cases with HPI, 10 cases grade2, 5 of which had a HPI, and 17 cases of high grade. A high proliferation index using two cut offs (KI67≥40% and KI67>20%) was utilized for analysis.

Results: 37 cases were excisional Bx and 26 Core Bx. The male to female ratio was: 1.1:1, and the age ranged from 35-92 with a mean of 65. The mean SUV for grade 1 FL was: 9.27, for grade 2 was: 11.59 and for grade 3: 13.05 The mean SUV for grade1 FL

with HPI was: 10.56, and for grade 2 FL with HPI was: 11.08 SUV means were compared using an independent sample t test and the results demonstrated in the table for KI67≥40% and >20%. No statistical significance was found for PET SUV in differentiating grade 1 or grade 2 FL with HPI from HGFL when using KI67≥40% (P= 0.231 for grade1 with HPI vs HG and P=0.472 for grade2 with HPI vs HG). No statistical significance was found for PET SUV in differentiating grade1 FL or grade2 FL with HPI (KI67≥40%) from grade1 FL or grade2 FL with low proliferation index (LPI). Similar results were obtained for KI67>20%.

Grade 1 FL with HPI (KI67≥40%) vs high grade FL				
	t	df	P	CI
PET-SUV	-1.224	27	0.231	-6.675 – 1.686
Grade 2 FL with HPI (KI67≥40%) vs high grade FL				
PET-SUV	-0.732	20	0.472	-7.592 – 3.646
Grade 1 FL with HPI (KI67≥40%) vs Grade 1 FL with Low proliferation index				
PET-SUV	-1.082	34	0.287	-5.553 – 1.695
Grade 2 FL with HPI (KI67≥40%) vs Grade 2 FL with Low proliferation index				
PET-SUV	-0.861	44	0.394	-4.957 - 1.989
Grade 1 FL with HPI (KI67>20%) vs high grade FL				
PET-SUV	-1.644	32	0.110	-6.586 – 0.704
Grade 2 FL with HPI (KI67>20%) vs high grade FL				
PET-SUV	-1.554	22	0.134	-8.594 – 1.231
Grade 1 FL with HPI (KI67>20%) vs Grade 1 FL with Low proliferation index				
PET-SUV	-0.941	34	0.353	-5.026 – 1.845
Grade 2 FL with HPI (KI67>20%) vs Grade 2 FL with Low proliferation index				
PET-SUV	-0.149	44	0.882	-3.634 – 3.133

Conclusions: Our findings indicate that the low grade FL with HPI, while clinically distinct from low grade FL with LPI and more similar to HG FL, seem to occupy a continuum between these two extremes and cannot be reliably identified for targeted biopsy by PET scan.

856 Clinicopathologic Features of Amyloidosis Harboring Gains/Amplification of Chromosome 1q

Mohamed Alshal[1], Caroline Astbury[1], Jack Khouri[1], Megan Nakashima[1]
[1]Cleveland Clinic, Cleveland, OH

Disclosures: Mohamed Alshal: None; Caroline Astbury: None; Jack Khouri: None; Megan Nakashima: *Consultant*, Blueprint Medicines

Background: AL amyloidosis (AL-amy) and multiple myeloma (MM) share similar chromosomal aberrations, but the prognostic impact of certain chromosomal aberrations in AL amyloidosis has not been widely studied. The presence of additional copies of chromosome 1q is a poor prognostic marker in MM, regarded as a secondary genetic event, often seen in association with other high risk genetic abnormalities. It has been subcategorized into gain of 1q (3 copies) and amplification (amp) of 1q (≥4 copies), the latter of which has a worse prognosis. Gain of 1q has also been associated with an adverse prognosis in AL amyloidosis; however, these cases have not been well-described.

Design: Cases were selected by cross-referencing FISH results from 4/2018 to 03/2021 against patients with a clinical encounter for AL-amy in the electronic medical record. FISH was performed on CD138-enriched plasma cells. The routine panel included probes for 1p (*CDKN2C*)/1q (*CKS1B*), 13q (*RB1*)/17p (*TP53*), CEP 9/CEP 15, *IGH (*BAP), and *IGH/CCND1*. *IGH/MMSET* and *IGH/MAF* were tested if *IGH* BAP was positive and *IGH/CCND1* negative. Cases were considered “amp 1q” if >20% of plasma cells had ≥4 copies of 1q. Correlation between variables was calculated using Fishers exact test.

Results: 146 patients with AL-amy and adequate FISH results were identified. Of these, 25 (17.1%) had reported gain of 1q, 15 with symptomatic MM and 10 with AL-amy only. There were 12 women and 13 men with average age 67.3 years (range 53-89). Sixteen cases were lambda, 8 kappa, and 1 biclonal. Seven cases had amp of 1q (1 AL-amy only, 6 MM). The majority of patients had cardiac involvement by amyloid (19). Eleven patients had expired, including all 7 amp 1q cases (p=0.02), but there was no significant correlation with presence of cardiac amyloidosis. Nineteen (76%) cases were positive for *IGH* rearrangement, 4 with *IGH/CCND1*, 4 with *IGH/MAF*, and 2 with *IGH/MMSET*. Loss of *RB1* was present in 13 (52%) cases and gain of both chromosomes 9&15 (suggestive of hyperdiploidy) was present in 8 (32%). FISH abnormalities associated with amp 1q were gain of both chromosomes 9&15 (5 with both, p= 0.02), and gain of *TP53* (4 with both, p=0.01).

		Amp 1q (n=7)	%	Gain 1q (n=18)	%
Age (yrs)	Median	71		66.5	
	Range	58-79		53-89	
PCs by CD138 IHC	Average	37.1		21.3	
	Range	10-75		3-75	
Diagnosis	AL amyloid only	1	14.3%	9	50.0%
	Symptomatic MM	6	85.7%	9	50.0%
Gender	Male	4	57.1%	9	50.0%
	Female	3	42.9%	9	50.0%
Light chain	Kappa	1	14.3%	7	38.9%
	Lambda	6	85.7%	10	55.6%
	Biclonal	0	0.0%	1	5.6%
Heavy chain	IgG	4	57.1%	7	38.9%
	IgA	1	14.3%	2	11.1%
	IgM	0	0.0%	1	5.6%
	IgA and IgG	0	0.0%	1	5.6%
	Light chain only	2	28.6%	7	38.9%
Other	Deceased	6	85.7%	5	27.8%
	Cardiac AL	6	85.7%	15	83.3%
	BMBx amyloid	4	57.1%	8	44.4%
	Abnl karyotype	3 (of 6)	50.0%	3 (of 16)	18.8%

Figure 1 - 856

Conclusions: Gain of 1q was seen in a smaller subset of AL amyloid patients than reported for MM (40%). Cases with amp of 1q showed worse overall survival than those with gain of 1q, and were associated with hyperdiploidy and gain of *TP53* in this small study.

857 Distinct Expression of MYC and Ki-67 in Molecular Subtypes of Peripheral T-Cell Lymphoma, Not Otherwise Specified (PTCL-NOS)

Ahmad Alshomrani[1], Sunandini Sharma[1], Alyssa Bouska[1], Timothy Greiner[1], German Ott[2], Andreas Rosenwald[3], Phil Raess[4], Sarah Ondrejka[5], James Cook[5], Lisa Rimsza[6], Dennis Weisenburger[7], Wing Chan[7], Javeed Iqbal[1], Catalina Amador[8]

[1]University of Nebraska Medical Center, Omaha, NE, [2]Robert-Bosch-Krankenhaus, Stuttgart, Germany, [3]Universität Würzburg, Wuerzberg, Germany, [4]Oregon Health & Science University, Portland, OR, [5]Cleveland Clinic, Cleveland, OH, [6]Mayo Clinic, Scottsdale, AZ, [7]City of Hope National Medical Center, Duarte, CA, [8]University of Miami, Miami, FL

Disclosures: Ahmad Alshomrani: None; Sunandini Sharma: None; Alyssa Bouska: None; Timothy Greiner: *Consultant*, Daiichi Sankyo, Inc., Daiichi Sankyo, Inc.; German Ott: None; Andreas Rosenwald: None; Phil Raess: *Primary Investigator*, Scopio Labs; Sarah Ondrejka: None; James Cook: None; Lisa Rimsza: None; Dennis Weisenburger: None; Wing Chan: None; Javeed Iqbal: None; Catalina Amador: None

Background: Peripheral T-cell lymphoma (PTCL) is a heterogeneous group of disorders of which ~40% of cases cannot be further classified into WHO-defined entities and are hence designated as PTCL-not otherwise specified (PTCL-NOS). We identified two major molecular subgroups using gene expression profiling (GEP), PTCL-TBX21 and PTCL-GATA3, showing distinct transcriptomic signatures and significant differences in overall survival (OS). Subsequently, we described a subset of cases within PTCL-TBX21 having a cytotoxic phenotype. This abstract evaluates differences in expression of MYC and Ki-67 in these subgroups of PTCL-NOS.

Design: Tissue microarrays (TMAs) were constructed from 50 PTCL-NOS cases subclassified by GEP (HG-U133 Plus2, Affymetrix Inc., n=22) or digital GEP (nCounter, NanoString Inc., n=28). The TMAs were stained for H&E and immunohistochemistry was done for CD3, MYC, Ki-67, and cytotoxic markers (TIA1, granzyme B, and perforin). H&E and CD3 were used to evaluate the percentage of tumor cell involvement. Blinded to the GEP classification, the percentage of tumor cells staining for KI67 and MYC was visually estimated for each case and recorded in 5% increments. Cytotoxic phenotype was defined by strong qualitatively expression of one or more of the cytotoxic markers.

Results: GEP subclassified PTCL-NOS into 22 (44%) PTCL-GATA3 and 28 (56%) PTCL-TBX21. PTCL-TBX21 was significantly associated with a cytotoxic phenotype (25% of cases vs. 5%, $p<0.05$). MYC expression was significantly higher in PTCL-GATA3 (average MYC= 20%) versus PTCL-TBX21 (average MYC= <5% in both cytotoxic and non-cytotoxic subgroups, $p< 0.05$). MYC positivity greater than 30% was only found in the PTCL-GATA3 subgroup (22% of cases vs. 0%, $p< 0.05$). When evaluating Ki-67 expression, we observed that both cytotoxic-PTCL-TBX21 (average KI67= 60%) and PTCL-GATA3 (average KI67= 60%) have significantly higher expression compared to non-cytotoxic PTCL-TBX21 (average KI67= 30%, $p<0.05$).

Conclusions: Our findings delineate immunophenotypic differences in molecular subtypes of PTCL-NOS and further differentiate between cytotoxic and non-cytotoxic cases of PTCL-TBX21.

858 An 18.5-year Retrospective Review of Diagnostic Acute Promyelocytic Leukemia Samples from a Large Cytogenomics Laboratory with Concurrent Conventional Chromosome and PML/RARA Dual-Color Dual-Fusion FISH Studies

Holly Berg[1], Jess Peterson[2], Reid Meyer[1]

[1]Mayo Clinic, Rochester, MN, [2]Medical College of Wisconsin, Milwaukee, WI

Disclosures: Holly Berg: None; Jess Peterson: None; Reid Meyer: None

Background: Acute promyelocytic leukemia (APL) is a distinct subtype of acute myeloid leukemia that is sensitive to all-trans retinoic acid therapy. Detection of *PML/RARA* (and other *RARA* gene fusion variants) is required for the diagnosis of APL and is considered highly time sensitive. The goal of this study is to report concurrent chromosome and *PML/RARA* dual-color dual-fusion fluorescence *in situ* hybridization (D-FISH) results over an 18.5-year period from a large cytogenomic laboratory.

Design: A retrospective review (01/2003-05/2021) of the Mayo Clinic cytogenomic database was performed to identify diagnostic APL samples (bone marrow and/or blood) with concurrent chromosome and *PML/RARA* D-FISH (Abbott Molecular, Abbott Park, IL) studies. Samples indicating prior diagnosis, treatment of APL, or cytogenetic variants of APL were excluded. When available, 20 metaphases and 500 interphase nuclei were analyzed.

Results: A total of 831 unique patients with chromosome and *PML/RARA* fusion detected by D-FISH were identified (Figure 1). Of these, 514 (62%) had a t(15;17)(q24;21) as the sole cytogenetic abnormality and a balanced *PML/RARA* rearrangement by D-FISH studies. Two-hundred and nine patients (25%) demonstrated a balanced t(15;17) with additional chromosomal abnormalities by chromosomes and a balanced *PML/RARA* rearrangement by D-FISH studies. The most common secondary abnormalities were trisomy/tetrasomy 8, del(7q), del(9q) and trisomy/tetrasomy 11. Fifty patients (6%) had atypical chromosome results [visible abnormalities involving chromosomes 15 and/or 17 in the absence of a classical t(15;17)] with *PML/RARA* fusion by D-FISH. Forty-eight patients (6%) had an apparently balanced t(15;17) by chromosomes but atypical *PML/RARA* rearrangements [any *PML/RARA*-positive signal pattern (indicated by at least one fusion signal) other than one green, one red and two fusions] by D-FISH. Six patients (0.5%) had a cytogenetically cryptic *PML/RARA* fusion (no visible abnormalities involving chromosomes 15 or 17). Lastly, four patients (0.5%) had a near-triploid/tetraploid clone with t(15;17) and *PML/RARA* fusion by D-FISH.

Figure 1 - 858

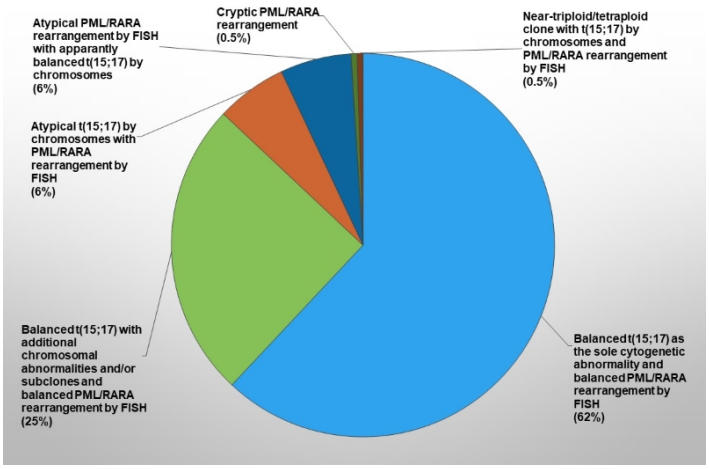

Conclusions: We describe the largest cohort to date of diagnostic APL cases with concurrent chromosome and *PML/RARA* D-FISH studies. While the majority of newly diagnosed APL cases harbor t(15;17) with balanced *PML/RARA* rearrangements by D-FISH, a significant number have atypical t(15;17) and/or *PML/RARA* D-FISH results.

859 Development of Interactive Hematology Atlas/Teaching Database for Resident Education and Resident Attitudes and Feedback Toward Full Field Microscopy

Swati Bhardwaj[1], Aiswarya Irri[1], Bella Liu[1], Nazire Albayrak[1], Francine Dembitzer[1], Christian Salib[1], Siraj El Jamal[1], Bruce Petersen[1], Shafinaz Hussein[2], Julie Teruya-Feldstein[3]
[1]Icahn School of Medicine at Mount Sinai, New York, NY, [2]Mount Sinai Hospital, New York, NY, [3]New York, NY

Disclosures: Swati Bhardwaj: None; Aiswarya Irri: None; Bella Liu: None; Nazire Albayrak: None; Francine Dembitzer: None; Christian Salib: None; Siraj El Jamal: None; Bruce Petersen: None; Shafinaz Hussein: None; Julie Teruya-Feldstein: *Advisory Board Member*, Astellas Pharma, Blueprint Medicines; *Consultant*, Histowiz, Curio Science, Scopio Anthem Edge

Background: With the temporary eclipse of standard in-person teaching by the pandemic, digital histopathology served as an important alternative. While this modality has been used in Anatomic Pathology, the field of hematology has not yet witnessed an equivalent explosion in digital pathology. We aimed to develop and utilize an online, cloud-based hematology educational database with some degree of user interactivity.

Design: We utilized a novel full-field digital technology platform to scan peripheral blood smears that simulates real-life evaluation (https://scopiolabs.com/). Using this platform, residents are able to develop both localization and identification skills. Educationally valuable smears were scanned over a period of 6 months to establish a digital teaching set of 369 cases. A web-linked datasheet was compiled as an index, with linked flow cytometry and molecular results. A survey was subsequently conducted, in order to obtain resident feedback.

Results: A total of 369 cases were scanned and uploaded to an online database. The average scan time was approximately 7 minutes per slide. Pancytopenic smears (defined as WBC $<3.5x10^3$/uL) required the use of a full field-cytopenia mode for scanning.

Residents were provided login credentials for accessing the database, the case index with the correct diagnoses, linked to flow cytometry results, and molecular results. Cases included benign entities, such as macrocytic anemia, neutrophilia, and eosinophilia, as well as examples of malignant entities, e.g., acute myeloid leukemia, with tagged features such as cup-shaped blasts, folded nuclei, etc. Residents were able to freely assess peripheral smears at low power in order to identify optimal fields, with the ability to then observe areas of interest at up to x1000 magnification, to arrive at a diagnosis. Out of a total of 23 resident respondents, 66.7% preferred this online teaching set over traditional hematology atlases, 28.6% considered textbook and hematology atlases to be of equivalent educational value, while 4.5% preferred a textbook atlas. All but one respondent (95.4%) preferred the use of full field scanned images for daily sign-outs as well.

Example: https://demo.scopiolabs.com/#/view_scan/82a49cd1-3f7d-4258-9ec6-b3c45ab32afc

Figure 1 - 859

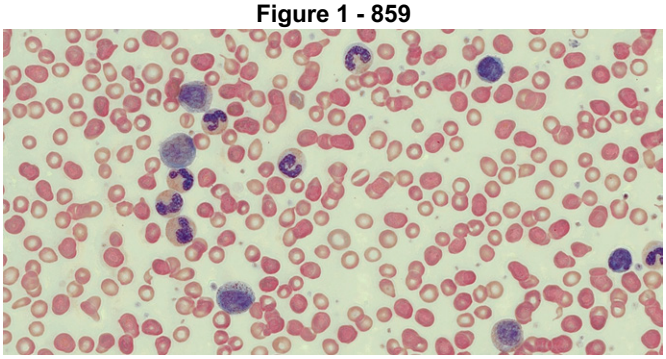

Figure 2 – 859

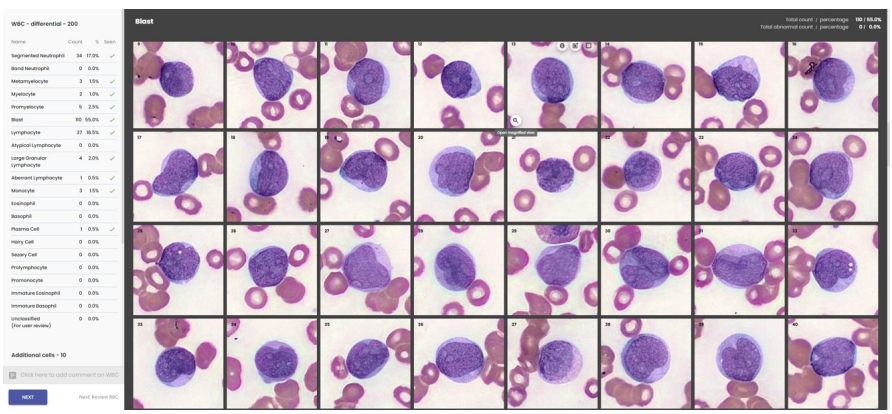

Conclusions: Full field digital morphology provides a more comprehensive educational alternative to textbook atlases. The ability to interact with scanned images provides a better learning experience than static images of cells alone, and can thus serve as an important educational tool for residents.

860 Clinicopathologic features of IgM MGUS with and without IgM-Related Disorders

Frido Bruehl[1], Megan Nakashima[2], Peter Mannion[1], Elisha Barbato[2], James Cook[2]
[1]Cleveland Clinic Foundation, Cleveland, OH, [2]Cleveland Clinic, Cleveland, OH

Disclosures: Frido Bruehl: None; Megan Nakashima: *Consultant*, Blueprint Medicines; Peter Mannion: None; Elisha Barbato: None; James Cook: None

Background: The 2017 WHO classification defines IgM monoclonal gammopathy of undetermined significance (MGUS) as a monoclonal serum IgM protein (<30g/L) with <10% bone marrow lymphoplasmacytic infiltration. The term “IgM-related disorder

(IgM-RD)" has been used to describe the subset of IgM MGUS patients with symptoms including neuropathy, cryoglobulinemia (CRYG), or cold agglutinin disease (CAD). We sought to define the clinicopathologic features of IgM MGUS with and without IgM-RD in a large cohort of patients.

Design: We identified 240 patients with IgM MGUS from departmental databases. Patients with coexisting myeloid neoplasms (12), primary amyloidosis (15), and previously diagnosed lymphoproliferative disorders (20) were excluded, for a final cohort of 193 patients. Neuropathy attributable to paraproteinemia, CRYG, and CAD were defined as IgM-RD.

Results: The clinicopathologic features of IgM cases with (87/193, 45%) or without IgM-RD (106/193, 55%) are shown in Table 1. Among IgM-RD, neuropathy was the most frequent symptom (73/193, 38%), followed by CRYG (21/193, 11%), and CAD (10/193, 5%). CRYG was seen concurrently with CAD or neuropathy, but overlap between neuropathy and CAD was not identified (Figure 1A). More males (67%) than females (33%) had IgM-RD (p=0.0916). Patients with IgM-RD had significantly higher hemoglobin (Hgb) than IgM MGUS without IgM-RD (12.2 vs. 13.0 g/dL; p=0.0146), but Hgb was lower in CAD patients than IgM MGUS without IgM-RD (10.3 g/dL). Morphologic evaluation demonstrated lymphoid aggregates in slightly more cases with IgM-RD (53% vs. 39%, p=0.156). Patients with and without IgM-RD showed a similar incidence of clonal plasma cells by IHC (22/74, 30% vs. 24/85, 28%, p=0.836), clonal B-cells by flow cytometry (24/72, 33% vs 20/87, 23%, p= 0.157), *MYD88* L265P mutation (21/29, 72% vs. 14/27, 52%, p=0.112), and abnormal karyotype (10/77, 13% vs. 12/97, 12.4%, p=0.903). No differences were observed in progression-free survival (PFS) during the available follow-up interval (median follow-up: 2.4 years; Figure 1B).

		All IgM MGUS		IgM MGUS without IgM-RD		IgM MGUS with IgM-RD		*P*
Total		193	100%	106	55%	87	45%	
Sex	Male	116	60%	58	55%	58	67%	0.092
	Female	77	40%	48	45%	29	33%	
Age [Years] at bone marrow biopsy		69.6	44-94	70.5	44-94	68.5	45-90	0.155
Age [Years] at first detection of M-Protein		68.9	44-94	70.1	44-94	67.6	44-90	0.080
IgM Serum [mg/dL]		677.1	720.6	708.6	679.5	639.7	768.8	0.546
Abnormal κ/λ FLC ratio		86	51%	48	52%	38	49%	0.715
Paraprotein type	Kappa	118	61%	65	61%	53	61%	*ns*
	Lambda	46	24%	23	22%	23	26%	*ns*
	Multiple bands	12	6%	6	6%	6	7%	*ns*
	Poorly defined bands	17	9%	12	11%	5	6%	*ns*
WBC [k/μL]		6.8	2.5	6.9	2.5	6.6	2.6	0.507
Hgb [g/dL]		12.6	2.2	12.2	2.1	13.0	2.1	**0.015**
PLT [k/μL]		233	83	225	84	242	81	0.135
PCs on biopsy [%]		4.4	1.7	4.2	1.7	4.6	1.6	0.149
Clonal PCs (by IHC)		46	29%	24	28%	22	30%	0.836
Clonal B-cells (by FC)		44	28%	20	23%	24	33%	0.147
Lymphoid aggregates		49	46%	22	39%	27	53%	0.157
Abnormal karyotype		22	13%	12	12.4%	10	13.0%	0.903
MYD88 L265P mutated		35	63%	14	52%	21	72%	0.112

Figure 1 - 860

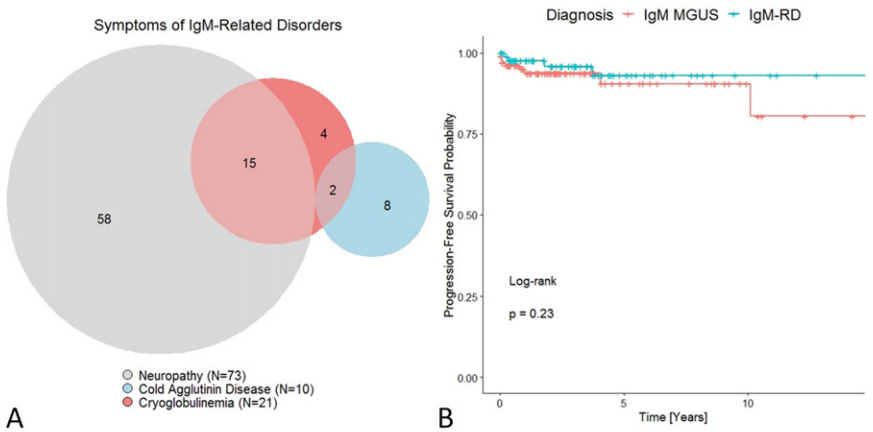

Conclusions: IgM-RD represents a significant proportion of patients with IgM MGUS as currently defined, with neuropathy being the most common symptom. IgM MGUS patients with and without IgM-RD show few pathologic differences and no difference in PFS. These results emphasize the importance of correlation with clinical features and laboratory testing for CRYG and CAD in the workup of patients with IgM MGUS for appropriate classification and management.

861 Clinicopathologic and Molecular Analysis of Normal Karyotype Therapy-related and De Novo Acute Myeloid Leukemia: A Multi-institutional Study by the Bone Marrow Pathology Group

Miguel Cantu[1], Rashmi Kanagal-Shamanna[2], Carlos Bueso-Ramos[2], Sanjay Patel[3], Julia Geyer[4], Wayne Tam[4], Peng Li[5], Tracy George[6], Meredith Nichols[7], Heesun Rogers[7], Yen-Chun Liu[8], Nidhi Aggarwal[9], Jason Kurzer[10], Danielle Maracaja[11], Eric Hsi[12], Feras Zaiem[13], Daniel Babu[14], Kathryn Foucar[14], Dorottya Laczko[15], Adam Bagg[16], Attilio Orazi[17], Daniel Arber[18], Robert Hasserjian[19], Olga Weinberg[1]

[1]UT Southwestern Medical Center, Dallas, TX, [2]The University of Texas MD Anderson Cancer Center, Houston, TX, [3]Weill Cornell Medical College, New York, NY, [4]Weill Cornell Medicine, New York, NY, [5]ARUP Laboratories, University of Utah, Salt Lake City, UT, [6]The University of Utah, Salt Lake City, UT, [7]Cleveland Clinic, Cleveland, OH, [8]St. Jude Children's Research Hospital, Memphis, TN, [9]University of Pittsburgh School of Medicine, Pittsburgh, PA, [10]Stanford Medicine/Stanford University, Stanford, CA, [11]Wake Forest School of Medicine, Winston-Salem, NC, [12]Wake Forest Baptist Health, Winston-Salem, NC, [13]University of New Mexico School of Medicine, Albuquerque, NM, [14]University of New Mexico, Albuquerque, NM, [15]Perelman School of Medicine, Hospital of the University of Pennsylvania, Philadelphia, PA, [16]University of Pennsylvania, Philadelphia, PA, [17]Texas Tech University Health Science Center, El Paso, TX, [18]University of Chicago, Chicago, IL, [19]Massachusetts General Hospital, Harvard Medical School, Boston, MA

Disclosures: Miguel Cantu: None; Rashmi Kanagal-Shamanna: None; Carlos Bueso-Ramos: None; Sanjay Patel: None; Julia Geyer: None; Wayne Tam: None; Peng Li: None; Tracy George: None; Meredith Nichols: None; Heesun Rogers: None; Yen-Chun Liu: None; Nidhi Aggarwal: None; Jason Kurzer: None; Danielle Maracaja: None; Eric Hsi: None; Feras Zaiem: None; Daniel Babu: None; Kathryn Foucar: None; Dorottya Laczko: None; Adam Bagg: None; Attilio Orazi: None; Daniel Arber: None; Robert Hasserjian: None; Olga Weinberg: None

Background: Therapy-related acute myeloid leukemias (t-AML) are aggressive neoplasms that arise following iatrogenic exposure to mutagenic agents, typically ionizing radiation and cytotoxic chemotherapy for malignancy. t-AMLs are often associated with chromosomal aberrations and the current diagnostic recommendation is to distinguish t-AML from other AMLs with similar cytogenetic findings. However, few studies have evaluated the clinicopathologic characteristics and mutational landscape of normal karyotype (NK) t-AML in comparison to NK de novo AML (dn-AML).

Design: We retrospectively reviewed 331 NK AMLs (74 t-AML, 257 dn-AML) from 11 academic institutions. Clinicopathologic features, next generation sequencing (NGS) and targeted sequencing data were analyzed. Fisher's exact and Mann-Whitney tests were performed on categorical and continuous variables, respectively. P-values were two-tailed and values <0.05 were considered significant. Overall survival (OS) and relapse free survival (RFS) were assessed by Kaplan-Meier method. Multivariate Cox proportional hazard analysis (MVA) was performed to determine the impact of variables on RFS for all t-AML patients and those treated with induction therapy.

Results: Patients with NK t-AML were significantly older (Table 1A) and had shorter median OS and RFS (Figure 1) compared to dn-AML. All t-AML patients received chemotherapy and/or radiation for prior malignancy (Table 1B). Breast and hematologic malignancies together accounted for >50% of the preceding malignancies. Leukocyte count, bone marrow (BM) blast percentage, and BM cellularity were significantly lower in t-AML compared to dn-AML. *NPM1*, *TET2*, *FLT3*, *DNMT3A*, and *RUNX1* were among the most frequently mutated genes in both groups (Figure 2). Significant differences in the frequency of *DMNT3A*, *KRAS*, *EZH2*, and *GATA2* variants and median total somatic mutations detected by NGS were observed between t-AML and dn-AML (Table 1A and Figure 2). MVA for factors influencing RFS of NK AML patients identified ELN score (intermediate/adverse) and higher BM cellularity as adverse predictors while treatment with stem-cell transplant and *NPM1* mutation predicted more favorable RFS in patients treated with induction (Table 1C & 1D).

Table 1A. Clinicopathologic characteristics	NK t-AML (N=74)	NK De novo AML (N=257)	P value	
Age (year, median)	70	63	<0.0001	
Sex, M/F ratio	0.6	1.1	0.0251	
Median Follow-up (month)	36.5	38.5		
Patients who expired (%)	71.6	45.5	0.0001	
Patients who relapsed (%)	24.3	45.5	0.0012	
Patients who achieved remission (%)	61.2	76.3	0.0205	
Therapy (%)				
Supportive care	5.4	2.7	0.2728	
Low-intensity chemotherapy	2.7	2.4	0.6554	
Hypomethylating agents	40.5	16.3	<0.0001	
Induction chemotherapy	51.3	79	<0.0001	
Bone marrow transplant	25.7	53.7	<0.0001	
Pathologic findings				
WBC (x10^9/L, median)	6.5	14	0.0389	
PB blast (%, median)	17	25	0.062	
BM blast (%, median)	42	69.5	0.0006	
BM Cellularity (%, median)	80	90	0.0011	
Molecular genetics				
Presence of somatic mutations (%)	92.9	95.3	0.5036	
Total somatic mutations per case, median (range)	3 (0-11)	4 (0-10)	0.0121	
DNMT3A (%)	22.6	39.3	0.0276	
KRAS (%)	15.1	4.3	0.0072	
EZH2(%)	9.4	2.7	0.037	
GATA2 (%)	11.3	1.56	0.0023	
FLT3 (%) (TKD/ITD %)	20 (5.5/16.4)	33.5 (14/23.7)	0.0549	
NPM1 (%)	32.1	47.8	0.1009	
1B. Prior malignancy characteristics in NK t-AML (N=74)				
Prior Malignancy				
Breast, # (%)	33 (44.6)			
Hematologic, # (%)	15 (20.3)			
Colorectal, # (%)	11 (14.8)			
Prostate, # (%)	5 (6.8)†			
Lung, # (%)	3 (4)			
Head & Neck, # (%)	3 (4)			
Gynecologic, # (%)	2 (2.7)††			
Renal, # (%)	1 (1.4)			
Bladder, # (%)	1 (1.4)			
Soft tissue, # (%)	1 (1.4)			
Pancreaticobiliary, # (%)	1 (1.4)			
Prior Therapy				
Chemotherapy-only (%)	50			
Radiation therapy-only (%)	18.6			
Chemotherapy and radiation (%)	31.4			
†One patient with history of hematologic and prostatic malignancies				
††One patient with history of hematologic and gynecologic malignancies				
1C. Multivariate analysis to predict variable impact on RFS, all t-AML patients				
Variable	Pr > Chi²	Hazard ratio	Hazard ratio Lower bound (95%)	Hazard ratio Upper bound (95%)
BM cellularity	0.019	1.017	1.003	1.031
HMA-based therapy	0.002	0.212	0.000	0.571
Induction therapy	0.001	0.200	0.000	0.533
BMT	0.000	0.216	0.000	0.476
ELN Intermediate/Adverse	0.014	3.292	1.269	8.540
1D. Multivariate analysis to predict variable impact on RFS, induction-only t-AML patients				
Variable	Pr > Chi²	Hazard ratio	Hazard ratio Lower bound (95%)	Hazard ratio Upper bound (95%)
BMT	0.000	0.130	0.000	0.408
NPM1 mutation	0.035	0.339	0.000	0.927

Figure 1 - 861

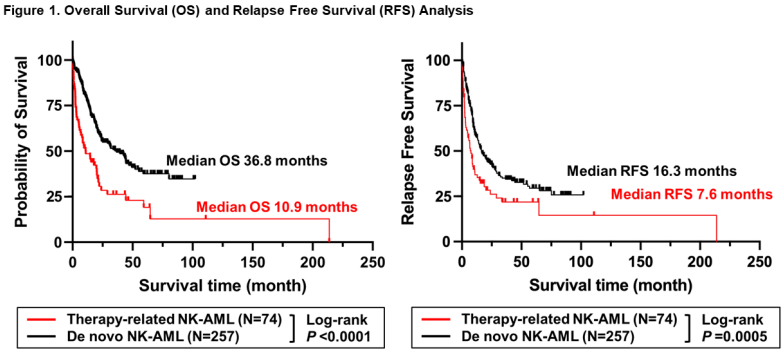

Figure 2 – 861

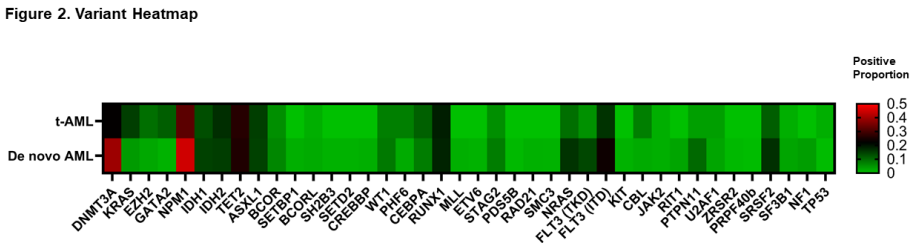

Conclusions: This is the largest study to date to comprehensively evaluate NK t-AML. NK t-AML exhibits significantly shorter OS and RFS compared to dn-AML. Though NGS findings showed some overlap, the frequency of *EZH2*, *GATA2*, and *KRAS* mutations were significantly higher in NK t-AML*, which may indicate underlying genetic ontogeny in NK t-AML compared to NK de novo AML. NPM1* mutation was seen in almost one third of NK t-AML patients and predicted favorable RFS in those treated with induction.

862 Benchmarking Cyclin D1 Immunohistochemistry in Multiple Myeloma Relative to CCND1 Gene Expression and Fluorescence In-Situ Hybridization for t(11;14)

Mario Capitano[1], Christina Turpin[2], Bob Argiropoulos[1], Etienne Mahe[3]
[1]Alberta Precision Laboratories, University of Calgary, Calgary, Canada, [2]Alberta Precision Laboratories, Calgary, Canada, [3]University of Calgary, Calgary, Canada

Disclosures: Mario Capitano: None; Christina Turpin: None; Bob Argiropoulos: None; Etienne Mahe: None

Background: Multiple myeloma (MM) is a molecularly complex entity, with a number of potential recurrent structural abnormalities, some known to be of prognostic value. MM with t(11;14) has been described as a relatively low risk entity, one that may be associated with upregulated cyclin D1 expression.

Design: We undertook a review of cyclin D1 and *CCND1* expression in MMs submitted for prognostic Fluorescence In-Situ Hybridization (FISH) analysis in our referral region over the course of a calendar year. To assist with this analysis, we devised an interactive immunohistochemistry (IHC) segmentation algorithm to quantify the percent of positive nuclei.

Results: Over the 2019 calendar year, 137 cases of MM were submitted for fluorescence in-situ hybridization (FISH) analysis, including FISH for t(11;14), t(4;14), t(14;16) & del(17p). Of these, 36 were excluded from further analysis owing to absent archival materials or to an absence of residual disease in available materials. Of the remaining 101 specimens, all were stained with cyclin D1 (Dako Clone EP12) & 54 were also assessed using the Illumina TruSight RNA Fusion Panel (NGS).

Seventeen percent of cases were abnormal by t(11;14) FISH, all of which also had elevated *CCND1*expression by NGS. An additional 26% of cases demonstrated abnormally elevated *CCND1* expression (based on established laboratory cut-offs) without associated t(11;14). By receiver-operator characteristic (ROC) analysis t(11;14) cases could be classified by cyclin D1 IHC percent nuclear positivity with an area-under the curve (AUC) of 0.91 (95%CI 0.85-0.97). A separate ROC analysis of cyclin D1 IHC relative to *CCND1* over-expression resulted in an AUC of 0.81 (95%CI 0.72-0.90).

In the 67% of new diagnoses there was a significantly lower level of cyclin D1 IHC in those cases with non-*CCND1* associated molecular abnormalities (t=3.7, p=0.001). When combined with high-level burden of disease (i.e. aspirate plasma cell count at least 60%), low cyclin D1 IHC (i.e. less than 15% nuclei positive) predicted a non-*CCND1* associated molecular abnormality with a PPV of 0.97 (95%CI 0.43-0.99).

Figure 1 - 862

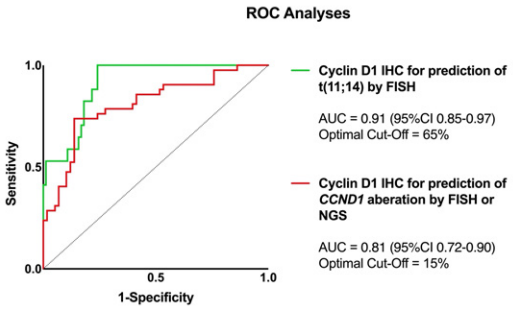

Conclusions: Our data support the use of cyclin D1 IHC as a predictive biomarker in the setting of myeloma. In addition, when combined with other laboratory parameters, cyclin D1 IHC might assist with triaging myeloma cases for follow-up molecular studies.

863 Distinctive Immunophenotypic Features of Thyroid MALT Lymphomas, Including Frequent IRTA1 Expression, Are Unlike Hashimoto Thyroiditis or Class-Switched Primary Cutaneous Marginal Zone Lymphomas (PCMZL)

Eric Carlsen[1], Adam Davis[2], James Cook[3], Steven Swerdlow[4]
[1]Duke University Medical Center, Durham, NC, [2]University of Pittsburgh Medical Center Presbyterian Shadyside, Pittsburgh, PA, [3]Cleveland Clinic, Cleveland, OH, [4]University of Pittsburgh School of Medicine, Pittsburgh, PA

Disclosures: Eric Carlsen: None; Adam Davis: None; James Cook: None; Steven Swerdlow: None

Background: Like PCMZL, thyroid MALT lymphomas often show plasmacytic differentiation with class-switched heavy chains. Whether they have other features of class-switched PCMZL, like frequent IgG4 positivity and limited expression of IRTA1, is uncertain. It is also unclear how IRTA1 staining might compare to that in Hashimoto thyroiditis, which often accompanies and can obscure focal MALT lymphomas.

Design: Clinicopathologic features of 18 thyroid MALT lymphomas were assessed, including their heavy and light chain, CD20, CD138, CD19 (17 cases), CD56 (12) and IRTA1 (16) expression by immunohistochemistry. IRTA1 expression was also assessed in 5 cases of florid Hashimoto thyroiditis. All lymphomas appeared to be primary to thyroid based on clinical examination and available imaging studies, although some cases had regional adenopathy and 1 case with coexistent diffuse large B-cell lymphoma had regionally advanced disease.

Results: Patients were all adults (median age 57.5 yrs, range 30-90 yrs, M:F 4:14) with median follow-up of 9.6 yrs (2 lost to follow-up). Only 1 patient with regionally advanced lymphoma died of disease. All cases had parenchymal destruction with variably sized B-cell rich areas. Plasmacytic differentiation was present in 15 cases and was extensive with sheet-like areas of plasmacytic cells in 12. 14/15 of these cases were IgG+ (2 were IgG4+) with 12 κ+ and 2 both κ- and λ- (Figure 1). 1/15 with plasmacytic differentiation was IgAλ+. Plasmacytic cells were CD138+ in only 8/15 cases but were uniformly CD19+ (14/14), CD20- (15/15) and CD56- (11/11). Some IRTA1 positivity was present in 16/16 cases, ranging from scattered or focally clustered cells to >50% of cells. IRTA1 positivity was often concentrated in “MALT-ball”-type lymphoepithelial lesions (LEL), perifollicular regions, and sometimes in follicles. IRTA1 positivity in Hashimoto thyroiditis was restricted to scattered cells that were sometimes concentrated in perifollicular regions and occasionally in other small clusters (Figure 2).

Figure 1 - 863

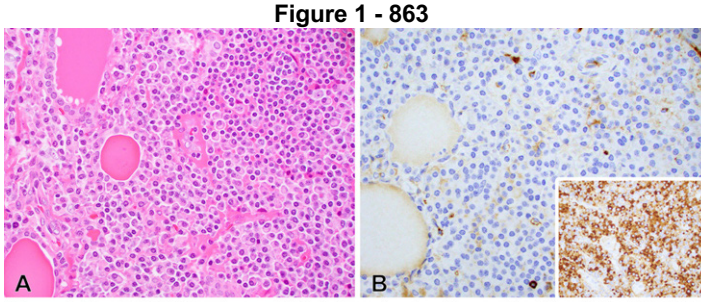

Figure 1. Thyroid MALT lymphoma. (A) Note the extensive plasmacytic differentiation (B) which was essentially negative for CD138 (inset: note the cytoplasmic IgG with punctate staining in many cells, a pattern of positivity seen in 3 additional cases). Original magnification 50x.

Figure 2 - 863

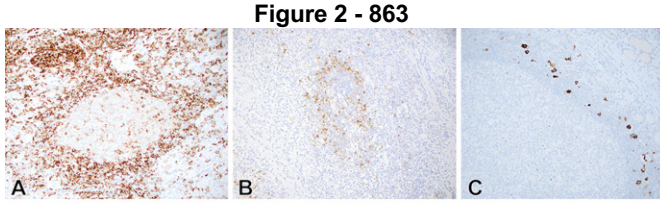

Figure 2: IRTA1 immunohistochemistry. (A) Note the strong positivity in perifollicular areas and in "MALT ball"-type lymphoepithelial lesions in this MALT lymphoma. (B) This lymphoma had only scattered IRTA1+ cells that were more numerous in the perifollicular regions. (C) This case of florid Hashimoto thyroiditis has scattered IRTA1+ cells in the perifollicular region around a very large, reactive germinal center. Original magnification 20x.

Conclusions: Although thyroid MALT lymphomas share some features with class-switched PCMZL, they are otherwise more like classic MALT lymphomas with IRTA1 positivity, prominent LEL, and infrequent IgG4 positivity. Plasmacytic differentiation is common and can be extensive, mimicking a plasmacytoma, but plasmacytic cells are CD19+ like those associated with B-cell neoplasms, and are sometimes CD138-. IRTA1 positivity may help distinguish MALT lymphomas from Hashimoto thyroiditis.

864 Clinical, Pathologic and Genomic Comparison of Myeloproliferative Neoplasm in Blast Phase (MPN-BP) with AML with Unfavorable Cytogenetics

Dong Chen[1], Julia Geyer[2], Adam Bagg[3], Robert Hasserjian[4], Olga Weinberg[5]
[1]Clin-Path Associates, PLC, Tempe, AZ, [2]Weill Cornell Medicine, New York, NY, [3]University of Pennsylvania, Philadelphia, PA, [4]Massachusetts General Hospital, Harvard Medical School, Boston, MA, [5]UT Southwestern Medical Center, Dallas, TX

Disclosures: Dong Chen: None; Julia Geyer: None; Adam Bagg: None; Robert Hasserjian: None; Olga Weinberg: None

Background: Essential thrombocythemia (ET), polycythemia vera (PV), and primary myelofibrosis (PMF), are the three major Philadelphia chromosome (BCR-ABL1) negative myeloproliferative neoplasms (MPNs), with variable tendency to progress to blast phase of disease (BP). Although MPN-BP often shows complex cytogenetic aberrations and has short survival, its relationship to de novo AML with complex karyotype is unclear.

Design: We identified 104 patients in MPN-BP and 145 patients AML with complex karyotype (AML-CK) with available pathologic, cytogenetic, and molecular data. CK was defined as having >3 or more unrelated abnormalities. Mann-Whitney tests were used to compare the data. 47 AML-CK patients were therapy-related. After diagnosis of AML, standard induction therapy, hypomethylating agents, or other low-intensity agents were administered in 55, 72 and 7 patients respectively. In the MPN-BP group, allogenic bone marrow transplant, hydroxyurea, Jakafi, and other chemotherapy were administered in 39, 28, 21 and 32 patients.

Results: AML-CK and MPN-BP patients show similar age distribution (64.7 vs 68.8, p=0.078) but with different bone marrow blast count (51% vs 28%, p<0.0001). WBC and platelet counts are higher in patients with AML-CK than MPN-BP (WBC: 8.6 vs 2.8, p<0.0001; PLT: 106 vs 57, p<0.0001) with similar hemoglobin levels (HGB: 8.3 vs 8.5, p=0.10). Patients with MPN-BP show different mutation profiles from AML-CK, with more frequent *JAK2* (56% vs 2%), *CALR* (11% vs 0%), *ASXL1* (22% vs 4%), *IDH2* (10% vs 3%), *SETBP1* (4% vs 1%) and *SRSF2* (9% vs 1%) and less frequent *TP53* (17% vs 75%) and *DNMT3A* (5% vs 12%). The AML-CK (108/145) and MPN-BP (15/104) patients carried *TP53* mutation and presented with similar platelet count (73 vs 51, p=0.3542), bone marrow cellularity (90% vs 75%, p=0.1093), and higher hemoglobin (9.3 vs 8.3, p=0.0339), bone marrow blasts (52% vs 25%, p=0.0147) and WBC (6.13 vs 3.09, p=0.0418) in AML-CK-TP53. In MPN-BP, *ASXL1* are mainly detected in ET and PMF, associated with poorer prognosis such as shorter progression time. Overall survival of AML-CK and MPN-BP patients was similar.

Conclusions: We find that, compared to AML-CK, patients with MPN-BP present show differences in blood counts and mutational profile. However, the outcomes of these two groups is similar, which suggests that MPN in blast phase may be equivalent to high-risk AML.

865 Clinicopathologic Features of Relapsed CD19(-) B-ALL in CD19-Targeted Immunotherapy: Insights Into Mechanism of Relapse and LILRB1 as a Novel B-cell Marker for CD19(-) B Lymphoblasts

Dong Chen[1], Franklin Fuda[2], Flavia Rosado[3], Silvia Saumell[4], Samuel John[2], Prasad Koduru[2], Weina Chen[2]
[1]Clin-Path Associates, PLC, Tempe, AZ, [2]UT Southwestern Medical Center, Dallas, TX, [3]University of Pittsburgh Medical Center, Pittsburgh, PA, [4]Hospital Universitari Vall d'Hebron, La Vall d'Hebron, Spain

Disclosures: Dong Chen: None; Franklin Fuda: None; Flavia Rosado: None; Silvia Saumell: None; Samuel John: None; Prasad Koduru: None; Weina Chen: None

Background: Recently developed CD19-targeting immunotherapy, Kymriah [CART-19, chimeric antigen receptor (CAR) T-cells targeting CD19] and blinatumomab (bispecific protein anti-CD19 and anti-CD3), has emerged as promising therapy in treating relapsed/refractory B-lymphoblastic leukemia (B-ALL). However, a subset of patients relapsed with either CD19(-) B-ALL or CD19(+) B-ALL. Our study aims to analyze clinicopathologic features of relapsed B-ALL after anti-CD19 immunotherapy and to assess the novel B-cell marker, LILRB1 (type I transmembrane inhibitory leukocyte immunoglobulin-like receptor subfamily B member), for detecting CD19(-) B lymphoblasts.

Design: Six patients (3 males and 3 females, median age of 15 years) with relapsed B-ALL were analyzed for clinicopathological features including cytogenetic profile and immunophenotype by flow cytometry (Table 1).

Results: Relapsed B-ALL in anti-CD19 therapy (with a median interval of 5.8 months) were all CD19(-) except one case with both CD19(+) and CD19(-) lymphoblasts. All cases had B-cell aplasia before the first relapse, indicative of persistent effect of CART or blinatumomab. Importantly, LILRB1 was variably expressed on all CD19(-) B lymphoblasts, strong on CD34(+) lymphoblasts and dim or partial on CD34(-) lymphoblasts; the pattern is comparable to strong and dim/partial LILRB1 expressions on CD34(+) and CD34(-) hematogones, respectively. In patients 2 and 5, converting from CD19(+) lymphoblasts to CD19(-) lymphoblasts was accompanied by different cytogenetic findings, indicative of clonal selection. In patient 4, relapsed B-ALL consisted of both CD19(+)/CD24(-) lymphoblasts and CD19(-)/CD24(+) lymphoblasts, indicative of clonal heterogeneity.

Figure 1 - 865

	Samples	Interval (month)	Blast %	B-cell Aplasia#	CD10	CD19	CD22	CD24	CD34	CD38	CD45	LILRB1	CG/FISH
Case 1 (20/M)					**Kymriah**								
Pre	PB		80		+	+	Var+	ND	Pt+	+	Pt+	ND	del(9)(p21p23);ishdel(9)(D9Z1+,p16-)/del(*16P*)
Post	PB/RL	2	29	yes	+	-	-	+	Pt+	Var+	Pt+	Dim+	ND
Case 2 (35/M)					**Blinatumomab**								
Pre	BM		77	N/A	+	+	Pt+	ND	+	Pt+	Var+	ND	ND
Post 1	BM	2.7	6	yes	+	+	Var+	ND	+	Var+	+	ND	t(1;12)(q42;q13),inv(5)(p13q33),del(6)(q13q23) *
Post 2	BM	4	5.8	yes	+	-	Var+	ND	+	+	+	+	t(3;4)(p25;q25),del(14)(q22q32)
Post 3	CSF	4.7	36	N/A	+	+	-	ND	+	Var+	Var+	ND	ND*
Case 3 (4/F)					**Kymriah**								
Pre	BM		12		+	+	+	+	Pt+	Var+	-		ND
Post	BM	6	34	yes	+	-	+	+	Pt+	Var+	-	Dim+	Complex abnormalities**
Case 4 (7/F)					**Kymriah**								
Pre	BM		80		+	+	+	+	-	+	-	ND	t(1;19)(q21;p13.3) (presumed *TCF3-PBX1*)
Post 1	BM	5.5	11	yes	+	+	+	-	-	+	+	Pt dim+	Normal***
			3.9		+	-	+	+	-	+	+	Pt+	Normal***
Case 5 (10/F)					**Kymriah**								
Pre	BM		58		+	+	+	ND	+	Pt+	+		47,XX,+21c
Post 1	BM	6.0	33	yes	+	-	+	+	Pt+	Pt+	+	ND	47,XX,t(X;14)(p22.3;q32),t(3;16)(p25;p11.2),+21c[13]/47,XX,+21c
Post 2	BM	24	4.9		+	-	+	ND	+	Pt+	Pt+	+	47XX,t(1;5)(p22;q13),t(2;9)(p13;q34),t(3;16)(p25;p11.2), inv(7)(p13q22),add(19)(q13.1),+21c
Case 6 (20/M)					**Kymriah**								
	PB		90		+	+	+	ND	+	Pt+	Dim+	ND	Normal karyotype
Pre	CSF (relapse)		1.3		+	+	+	ND	+	Pt+	Dim+	ND	ND
Post	PB	8.5	92	yes	+	-	+	ND	+	Pt+	Dim+	+	ND

Table 1. Clinicopathologic findings in B-ALL patients with anti-CD19 immunotherapy

Abbreviations: BM, bone marrow; CSF, cerebrospinal fluid; F, female; M, male; pt, partial; ND, not done; N/A, not available; age, years
#: lack of B cells (<0.2% of total cells) before the relapse
*case 2: given short interval and CD19(+) B-ALL, the cytogenetic abnormality likely arising in the *selected* original leukemia clone
**case 3: 42,X,X,der(1)add(1)(p36.1)add(1)(q44),add(2)(p11.2),del(3)(p21),-4,+add(6)(p23),-12,-15,add(16)(q24),-17
***: case 4: CD19(+)/(-) clones both detected post-therapy, indicative of heterogeneity of leukemia clones

Conclusions: Our study demonstrates that the emergence of CD19(-) relapsed B-ALL in post immunotherapy is likely associated with complex oncogenic pathways, which provides insights into the mechanisms of relapses, including clonal heterogeneity and clonal selection. Furthermore, LILRB1 may represent a promising novel B-cell marker to identify CD19(-) B lymphoblasts and to aid in monitoring treatment efficacy during immunotherapy.

866 Clinicopathologic Significance of Epstein-Barr Virus Infection in Nodular Sclerosis Classical Hodgkin Lymphoma: A Retrospective Study of 363 Cases

Jiang Chen[1], Jianchang Fu[1], Jihao Zhou[2], Yuhua Huang[3]
[1]Cancer Center of Sun Yat-sen University, Guangzhou, China, [2]Shenzhen, China, [3]Sun Yat-sen University Cancer Center, Guangzhou, China

Disclosures: Jiang Chen: None; Jianchang Fu: None; Jihao Zhou: None; Yuhua Huang: None

Background: Nodular Sclerosis Classical Hodgkin Lymphoma (NSCHL) is the most common subtype of Classical Hodgkin Lymphoma (CHL). Although it is well known that a portion of NSCHL is associated with Epstein-Barr Virus (EBV) infection, the clinicopathologic significance of EBV infection in NSCHL has not been well characterized. Thus, a systematic and deeper understanding is required.

Design: A total of 363 consecutive NSCHLs from Sun Yat-sen University Cancer Center were retrospectively evaluated using *in situ hybridization* for EBV-encoded RNA (EBER), the clinicopathological parameters, therapeutic response and patients' outcome between EBV-positive and EBV-negative NSCHLs were comprehensively compared. Other potential prognostic factors were also examined.

Results: The prevalence of EBV infection in NSCHL was 23.4% (85/363). EBV-positive NSCHL showed the highest incidence (80.0%, 12/15) in patients under 10 years. EBV infection was significantly related to male (*P*=0.001), elevated LDH level (*P*=0.005) and advanced clinical stages (*P*=0.018). Interestingly, EBV infection was associated with lower complete response (CR) rate (46.3% vs 61.6%, *P*=0.016) and higher relapse rate in CR patients (40.0 % vs 19.4%, *P*<0.001). Additionally, EBER-positive was associated with worse 5-year overall survival (OS) and progression-free survival (PFS) than EBER-negative patients (Both *P*<0.01). Notably, EBER presence was correlated with poorer OS in patients with advanced disease (*P*=0.004) and unfavorable PFS in early-stage patients (*P*=0.001). Finally, Cox regression model suggested EBER as an independent prognostic factor.

Figure 1 - 866

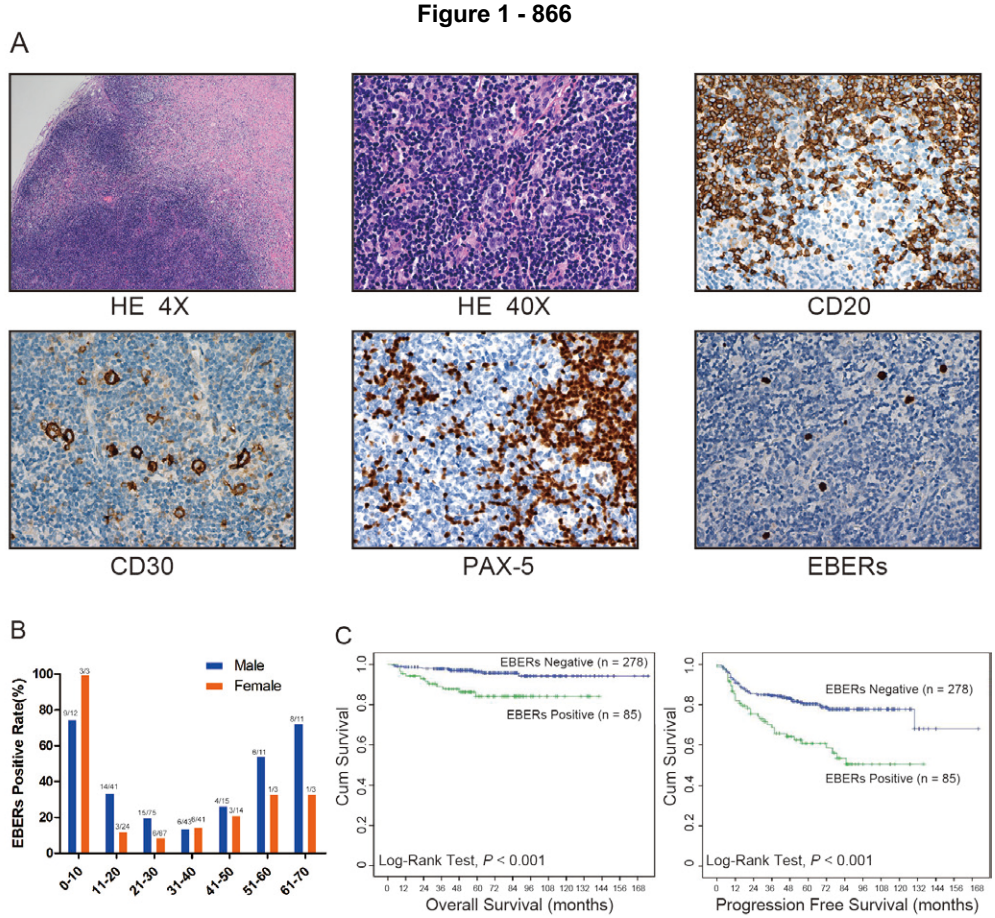

Conclusions: EBV-positive NSCHL has unique clinicopathological characteristics. EBV infection was related to adverse NSCHL profile and correlated with poor treatment response, higher relapse rate and may represent a poor prognostic factor in NSCHL. Examination of EBER-ISH in NSCHL patients is recommended as a routine pathological practice.

867 IRTA1 and MNDA Are Useful Markers in The Differential Diagnosis Of Marginal Zone Lymphoma

Yanping Chen[1], Wenwen Zhang[1], Longfeng Ke[1], Jianping Lu[1], Gang Chen[1]
[1]Fujian Cancer Hospital, Fuzhou, China

Disclosures: Yanping Chen: None; Wenwen Zhang: None; Longfeng Ke: None; Jianping Lu: None; Gang Chen: None

Background: The diagnosis of marginal zone lymphoma (MZL) is frequently challenging and, in some cases, remains one of exclusion. This study aimed to assess the potential diagnostic utility of immune receptor translocation-associated protein 1 (IRTA1)and myeloid nuclear differentiation antigen (MNDA) in MZLs.

Design: We evaluated whole-tissue sections from 361 cases including 43 lymphoid reactive follicular hyperplasias, 135 MZLs, 78 follicular lymphomas (FLs), 41 mantle cell lymphomas (MCLs), 36chronic lymphocytic leukaemia/small lymphocytic lymphomas (CLL/SLLs), 8 lymphoplasmacytic lymphomas (LPLs) and 20 diffuse large B-cell lymphomas (DLBCLs), NOS. Immunohistochemistry for IRTA1, MNDA and other markers (CD10, BCL-6, CD5, CD23, CyclinD1,SOX-11 and LEF-1) were performed on Ventana-Benchmark XT automated instruments at the Department of Pathology.

Results: IRTA1 expression was detected in 93 (68.89%)of 135 MZLs vs22 (9.73%) of 226 other small B-cell neoplasms (P <0.005). MNDA staining was positive in 88 (65.19%) of 135 MZLs vs 60 (26.55%) of 226 non-MZLs(P <0.005). Notably, the specificity of IRTA1 (90.27%) in MZLs was higher than that of MNDA(73.45%).Expression of either IRTA1 or MNDA was found in 109(80.74%) of 135MZLs, while coexpression of both markers were less frequently seen (72/135, 53.33%).Within MZLs, IRTA1 and MNDA expressions in NMZLs (63.64% and 54.55%, respectively) were lower than in MALT (71.00% and 68.00%, respectively). IRTA1 expression was not seen in LPLs and CLL/SLLs(0%and 0%, respectively).IRTA1 and MNDA expression were less frequent in MZLs with plasma cell differentiation.

Table 1: The diagnostic value of MNDA and IRTA-1

Maker	Sensibility (%)	Specificity (%)	Accuracy (%)	Positive predictive value	Negative predictive value
MNDA	65.18	73.45	70.36	59.46	77.93
IRTA-1	68.89	90.27	82.27	80.87	82.93
Either	80.74	67.70	72.58	59.89	85.47
Both	53.33	96.02	80.06	88.89	77.50

Figure 1 - 867

Fig 1: Representative hematoxylin and eosin staining of a case of nodal MZL (NMZL).

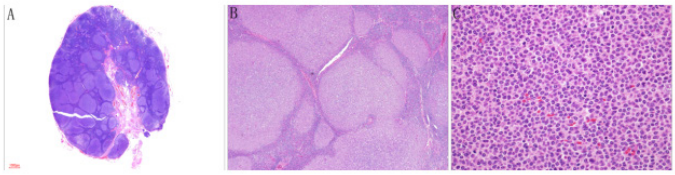

Figure 2 - 867

Fig 2: Representative immunostaining of CD21(A), CD20(B), CD10(C), Bcl-6(D), Bcl-2（E）, Ki-67(F), IRTA1(G，H) and NMDA(I) in a case of NMZL (Fig 1).

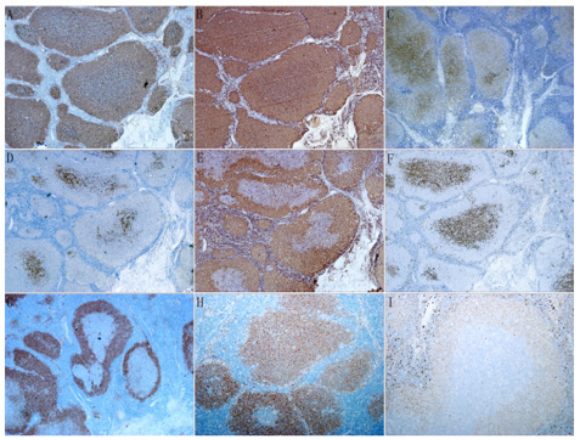

Conclusions: Overall, our findings indicate thatIRTA1 and MNDA are highly sensitive and useful markers in the differential diagnosis of MZLs.IRTA1 offers particular advantages in differential diagnosis as it appears to be highly specific for MZLs, being rarely expressed in other lymphomas examined. Therefore, combined use of IRTA1 and MNDA are more helpful to distinguish MZLs from other histologic mimics.

868 Frequent Detection of CBFA2T3/GLIS2 Fusion and RAM Phenotype with Possible Novel Relationship between RAM Phenotype and Aberrant Cytoplasmic CD3 Expression in Pediatric Non-Down Syndrome Acute Megakaryoblastic Leukemia

Yan Chen Wongworawat[1], Ghazaleh Eskandari[2], Amos Gaikwad[1], Andrea Marcogliese[3], Lizmery Ferguson Schires[1], Julienne Brackett[1], Jyotinder Punia[1], M. Tarek Elghetany[4], Reshma Kulkarni[4], Pulivarthi Rao[1], Jo Ringrose[1], Dolores Lopez-Terrada[3], Angshumoy Roy[2], Choladda Curry[1], Kevin Fisher[1]

[1]Baylor College of Medicine/Texas Children's Hospital, Houston, TX, [2]Baylor College of Medicine, Houston, TX, [3]Texas Children's Hospital, Baylor College of Medicine, Houston, TX, [4]Texas Children's Hospital, Houston, TX

Disclosures: Yan Chen Wongworawat: None; Ghazaleh Eskandari: None; Amos Gaikwad: None; Andrea Marcogliese: None; Lizmery Ferguson Schires: None; Julienne Brackett: None; Jyotinder Punia: None; M. Tarek Elghetany: None; Reshma Kulkarni: None; Pulivarthi Rao: None; Jo Ringrose: None; Dolores Lopez-Terrada: None; Angshumoy Roy: None; Choladda Curry: None; Kevin Fisher: None

Background: *CBFA2T3/GLIS2* fusions, identified in pediatric non-Down syndrome acute megakaryoblastic leukemia (non-DS-AMKL), are associated with the prognostically unfavorable RAM immunophenotype (RAM: bright CD56, dim-to-negative CD45 and CD38, and absent HLA-DR). Rarely, cytoplasmic CD3 (cCD3) is observed in non-DS-AMKL in infants, making mixed phenotype acute leukemia (MPAL) a controversial diagnostic consideration. We investigated cCD3, RAM immunophenotype, and *CBFA2T3/GLIS2* fusions in pediatric non-DS-AMKL.

Design: Non-DS-AMKLs from 2014-2021 were identified. cCD3 expression and RAM immunophenotype were confirmed by CD3 immunohistochemical staining (IHC) and flow cytometric data. *CBFA2T3/GLIS2* fusions were tested using targeted next-generation-sequencing (RNA-NGS) or reverse-transcriptase PCR (RT-PCR) of leukemic RNA. Cases with RAM phenotype status and RNA testing were included in the study. Statistical analysis was performed using Fisher's exact test for correlation analysis.

Results: Nineteen non-DS-AMKL patients (age 0.9 month-18 years, median 24.1 months; M:F ratio 1.4) were studied. Molecular profiling of 17 cases revealed six *CBFA2T3/GLIS2* fusions (35.3%), four *KMT2A* rearrangements, one *RBM15/MLK1*, one *PICALM/MLLT10* and one *NUP98/KDM5A* fusion. Four cases had no fusions and two failed RNA testing. Nine patients (47.4%, age 0.9-41.3 months, median 19.1 months; M:F ratio 2:1) demonstrated RAM immunophenotype. Aberrant cCD3 expression was identified in 6 (31.6%); 4 by flow cytometry (31-49% of blasts expressing cCD3) and 2 by IHC. RAM immunophenotype significantly correlated with *CBFA2T3/GLIS2* fusion (p=0.001). A trend to correlation between cCD3 and RAM immunophenotype (p=0.057) was observed. Our pediatric non-DS-AMKL cohort had poor outcomes; patients were treated with

variable chemotherapy regimens including 14 (73.7%) with bone marrow transplant. Fourteen (73.7%) had relapsed/refractory diseases, and only 7 patients (36.8%) were alive at follow-up including 3 (15.8%) without evidence of disease.

Conclusions: The dismal outcomes in pediatric non-DS-AMKL require more effective therapeutic interventions. The identification of *CBFA2T3/GLIS2* fusions and/or RAM-immunophenotype is highly desirable as anti-CD56 may serve as a potential therapeutic intervention. The possible relationship between aberrant cCD3 and RAM immunophenotype in non-DS-AMKL is a novel finding. Despite aberrant cCD3 expression in this setting, non-DS-AMKL should be considered as AML and not MPAL.

869 Genomic and Clinical Heterogeneity in TP53 Mutant Myelodysplastic Syndromes

Zachary Coty-Fattal[1], Madina Sukhanova[2], Xinyan Lu[2], Kristy Wolniak[3], Juehua Gao[4], Amir Behdad[2]
[1]McGaw Medical Center of Northwestern University, Chicago, IL, [2]Northwestern University Feinberg School of Medicine, Chicago, IL, [3]Northwestern University, Chicago, IL, [4]Northwestern Memorial Hospital, Chicago, IL

Disclosures: Zachary Coty-Fattal: None; Madina Sukhanova: None; Xinyan Lu: None; Kristy Wolniak: None; Juehua Gao: None; Amir Behdad: *Speaker*, Lilly, Roche/Foundation Medicine China, Thermo Fisher Scientific, Bayer

Background: Myelodysplastic syndromes (MDS) are a heterogenous group of neoplasms characterized by one or more cytopenias and dysplasia in hematopoetic precursors. MDS with *TP53* mutations have been associated with poor clinical outcomes and increased risk of transformation to acute myeloid leukemia (AML). However, recent literature has demonstrated that there is heterogeneity amongst *TP53*-mutant MDS. The goal of this study is to further stratify MDS with *TP53* mutations.

Design: We retrospectively studied clinicopathologic and genetic characteristics of 23 patients diagnosed with MDS and with confirmed *TP53* mutations between 2017 and 2020. Patients with *TP53* mutations were divided into two subgroups based on *TP53* variant allele frequency (VAF): High VAF (≥25%, or with isolated *TP53* mutation; HVAF) and low VAF (VAF<25%; LVAF). Comparative analysis of clinicopathologic data, cytogenetic findings and co-occurring mutations detected by NGS was performed between the two groups.

Results: Age, gender distribution, WHO sub-classification at diagnosis, and blast count at diagnosis were not significantly different between the HVAF and LVAF groups (Table 1). The HVAF group did not have a significantly different time of progression to AML (p=0.28), but had poorer overall survival (p=0.036; Figure 2) compared to the LAVF group. The most common cytogenetic abnormalities in the HVAF group included complex karyotypes (92.9%), deletions of 5q (71.4%) and deletions of 7q (42.9%), while in the LVAF group the cytogenetic abnormalities included complex karyotypes (33.3%), deletions of 5q (44.4%), gain of chromosome 8 (22.2%) and deletions of 13q (44.4%). VAFs of *TP53* variants in the LVAF group was 8.5±6%, compared to 56.9±22.7% observed in the HVAF group (p<0.01). NGS analysis revealed a higher number of co-occurring mutations per case (1.9±0.8) in the LVAF group compared to the HVAF group (1.1±1.3; p=0.07). The vast majority of the HVAF cases (85.7%) had ≤1 additional mutations. LVAF cases commonly harbored co-mutations in spliceosome genes (*U2AF1*, 33.3%; *SRSF2*, 33.3%), *ASXL1* (33.3%), *TET2* (33.3%), *BCOR* (22.2%), and *RUNX1* (11.1%). The HVAF group had mutations most commonly in *RUNX1* (21.4%), *IKZF1* (14.3%), and *ASXL1* (14.3%).

Figure 1 - 869

	HVAF (>25%) or Isolated TP53 Mutation (N=14)	LVAF (<25%) (N=9)	P-value
Age at Diagnosis			
Mean (SD)	63.6 (13.9)	65.3 (12.4)	0.754
Median [Min, Max]	69.0 [32.0, 80.0]	66.0 [42.0, 88.0]	
Gender			
F	8 (57.1%)	4 (44.4%)	0.68
M	6 (42.9%)	5 (55.6%)	
WHO Subclassification			
MDS-EB-1	4 (28.6%)	3 (33.3%)	0.482
MDS-EB-2	4 (28.6%)	2 (22.2%)	
MDS-MLD	2 (14.3%)	3 (33.3%)	
MDS/MPN	3 (21.4%)	0 (0%)	
t-MDS	1 (7.1%)	0 (0%)	
MDS del(5q)	0 (0%)	1 (11.1%)	
Blast Count at Diagnosis			
Mean (SD)	6.23 (4.96)	6.73 (6.50)	0.845
Median [Min, Max]	3.90 [0.500, 15.0]	4.50 [0, 18.5]	

Figure 2 - 869

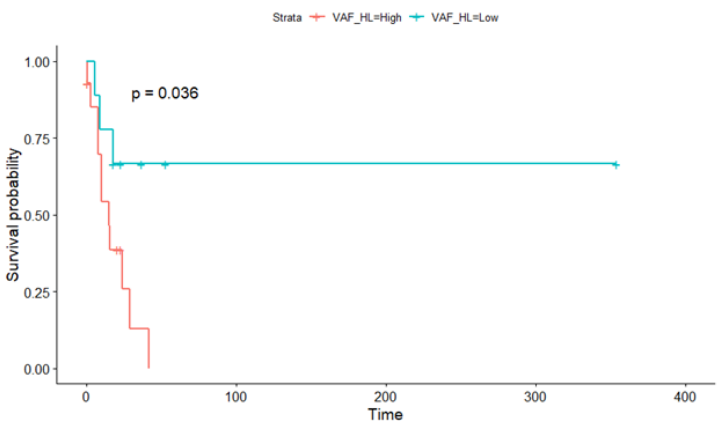

Conclusions: In our study, MDS cases with LVAF *TP53* mutations have a distinct genomic landscape compared to those with HVAF *TP53* mutations, demonstrating frequent driver mutations in spliceosome genes. Our data also revealed that MDS cases with LVAF *TP53* mutations are associated with lower rate of progression to AML and better overall survival.

870 Higher Infiltration of FOXP3+ Lymphocytes and CD8+ T Lymphocytes Associated with Nodal Location of Diffuse Large B-cell Lymphoma

Elizabeth Courville[1], Mark Girton[2], Lisa Friedman[2]
[1]*University of Virginia Health System, Charlottesville, VA,* [2]*University of Virginia, Charlottesville, VA*

Disclosures: Elizabeth Courville: None; Mark Girton: None; Lisa Friedman: None

Background: Diffuse large B-cell lymphoma is a common type of lymphoma in the adult population, and may present with nodal or extranodal disease. Up to 40% of cases are confined to extranodal sites at least initially. Prior studies have evaluated the density of intratumoral FOXP3+ regulatory T cells in diffuse large B-cell lymphoma (DLBCL), with higher infiltration found to correlate with nodal disease location in one study (references PMID 18223287 and 32962457).

Design: In this study, we evaluated CD3, CD4, CD8, LAG3, and FOXP3 expression in tumor infiltrating lymphocytes (TLI) using a tumor microarray (TMA) and immunohistochemical stains. The tumor microarray was constructed using 0.6 mm punches, in triplicate, taken from tumor-rich areas, and included cases of diffuse large B-cell lymphoma from our institutional files over years 2000 - 2019. Cases with EBV positivity or unknown status by in-situ hybridization were excluded from this study. CD3, CD4, CD8, LAG3, and FOXP3 immunohistochemical stains were performed on separate TMA slides using standard techniques, and evaluated by two pathologists (EC and LF) at a multiheaded microscope. For each immunohistochemical stain, positivity was graded as 0-3+ on a relative scale in the background lymphocytes as identified using cytomorphology/counterstain.

Results: Our cohort of DLBCL cases included 35 cases in an extranodal location and 19 cases in lymph node. Extranodal locations included spleen (n=3), small intestine (5), thyroid (2), ovary (1), testicle (1), pancreas (1), parotid (1), breast (1), tonsil/base of tongue (2), lung (2), stomach (1), pericardial mass (1), colon (3), bone/surrounding soft tissue (2), soft tissue (8), and scalp (1) . The median age at biopsy was 60 years old (range 22-86), with a male to female ratio of 1:1. There was a statistically significant difference in the distribution of CD3, CD8, and FOXP3 expression in the TIL between the nodal and extranodal groups (p=0.006, 0.009, and 0.028, respectively, by independent samples Mann-Whitney U test). No statistically significant difference was identified in CD4 or LAG3 expression (p=0.057 and 0.415, respectively).

Figure 1 - 870

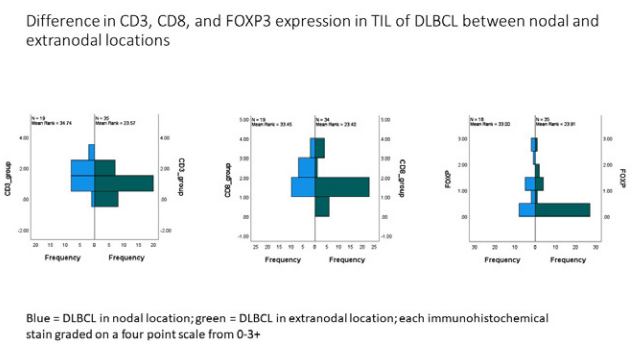

Figure 2 - 870

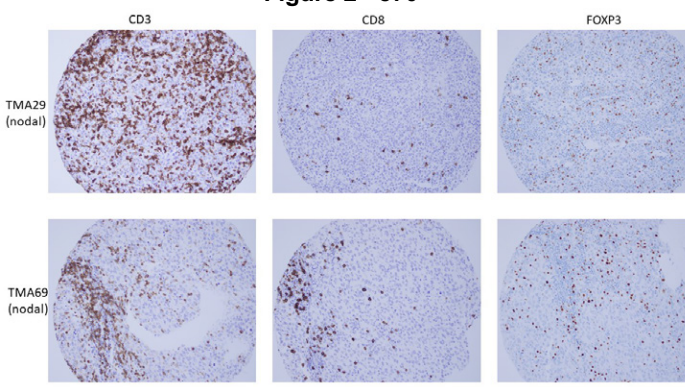

Conclusions: Our findings support the previously identified association between higher FOXP3+ lymphocyte infiltration and a nodal location. Differences in the TIL between nodal and extranodal locations emphasizes the importance of biopsy location when studying the tumor microenvironment, particularly in neoplasms of the lymphoid system such as DLBCL.

871 Clinicopathologic Features of IDH2 R172 Mutated Myeloid Neoplasms

Adam Davis[1], Briana Canady[2], Nidhi Aggarwal[3], Nathanael Bailey[4]
[1]University of Pittsburgh Medical Center Presbyterian Shadyside, Pittsburgh, PA, [2]University of Pittsburgh, Pittsburgh, PA, [3]University of Pittsburgh School of Medicine, Pittsburgh, PA, [4]University of Pittsburgh, UPMC, Pittsburgh, PA

Disclosures: Adam Davis: None; Briana Canady: None; Nidhi Aggarwal: None; Nathanael Bailey: None

Background: *IDH1* and *IDH2* are among the most commonly mutated genes in myeloid neoplasms (MNs). In contrast to other *IDH2*-mutated tumors, most *IDH2* mutations occur at codon R140 in MN rather than at R172. It has been proposed that *IDH2* R172 mutations (mR172) define a molecular subtype of acute myeloid leukemia (AML), but the clinicopathologic features of AML with mR172 have not been fully described.

Design: We retrospectively identified all specimens in our archive with an mR172 MN for comparison to a similar number of randomly selected and temporally matched cases with other *IDH* mutations, including *IDH2* R140 (mR140) and *IDH1* R132 (mR132) mutated cases. We collected demographic information and evaluated hematologic parameters, bone marrow morphology, immunophenotypic and genetic characteristics at diagnosis, treatment, and survival.

Results: Our cohort consists of 39 patients with *IDH*-mutated MNs with increased blasts, including 14 with mR172, 12 with mR140, and 13 with mR132. The clinical and pathologic features are presented in the Table. The diagnostic categories included AML (n=35) and other MNs with excess blasts (n=4, minimum 17% blasts). Non-mR172 cases presented with significantly higher leukocyte counts and peripheral blood blast percentages than mR172 cases (p=0.002 & p=0.03, respectively) and had higher bone marrow cellularity (p=0.02) (Figure 1A). mR172 AML cases had only FAB M0-M2 morphology, while the non-mR172 cases sometimes showed monocytic differentiation (Figure 1B). 11 of 14 mR172 cases had a significant proportion of blasts (>10%) with unusual, highly invaginated nuclei that sometimes led to a binucleated appearance that could cause consideration of microgranular acute promyelocytic leukemia on morphologic grounds (Figure 2). mR172 cases consistently expressed CD34, HLA-DR, CD117, and CD13 by flow cytometry (Figure 1B). However, mR172 cases frequently were negative or had very dim expression of CD33 in a minor subset of blasts (odds ratio vs non-mR172 = –2.8, p=0.01). mR172 never occurred with *NPM1* or favorable-risk translocations; however, two cases had mutated *RUNX1,* one case had a *TP53* mutation and a total of 3 cases (including one *RUNX1*- and one *TP53*-mutated case) had an adverse karyotype. There was a trend toward better survival in mR172 cases vs non-mR172 cases (p=0.06, Figure 1C).

	***IDH2* R172**	***IDH2* R140**	***IDH1* R132**
Demographic			
Number of Patients	14	12	13
Age (years, median)	73.5	73	68
Sex, M/F ratio	1.3	0.3	0.6
Diagnostic Category			
Acute Myeloid Leukemia	11	12	12
AML with minimal differentiation (M0)	2	0	0
AML without maturation (M1)	2	6	4
AML with maturation (M2)	7	3	5
Acute myelomonocytic leukemia (M4)	0	2	2
Acute monoblastic and monocytic leukemia (M5)	0	1	1
Myelodysplastic syndrome with excess blasts-2	3	0	0
Blast phase myeloproliferative neoplasm	0	0	1
Hematologic parameters			
WBC ($x10^9$/L, mean)	1.9	33.7	31.1
Hgb (g/dL, mean)	8.9	8.6	9.1
Platelet ($x10^9$/L, mean)	94.3	96.8	99.2
PB Blast (%, mean)	12.4	47.2	34.5
ANC ($x10^9$/L, mean)	0.42	3.06	1.71
ALC ($x10^9$/L, mean)	1.01	2.76	3.41
AMC ($x10^9$/L, mean)	0.08	1.33	3.19
Morphologic Features			
BM Cellularity (%, mean)	56.5	78.6	70.0
BM Blasts (%, mean)	44.7	66.1	54.77

Figure 1 - 871

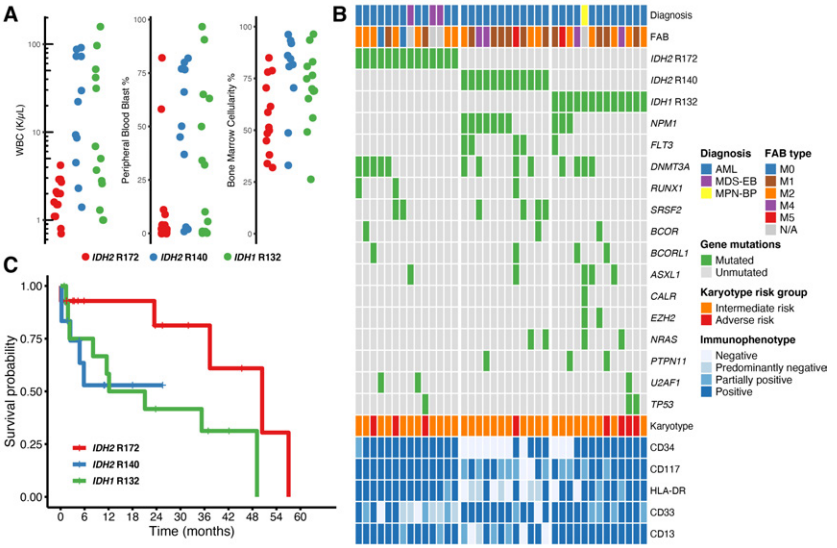

Figure 2 - 871

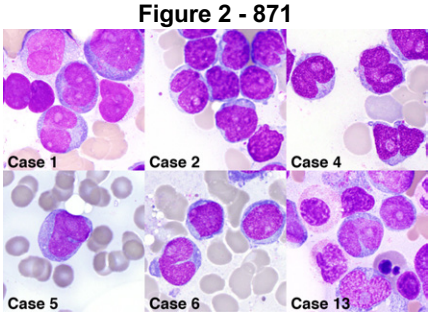

Conclusions: Our findings support that MNs with mR172 represent a morphologically and phenotypically distinct subtype. Our small retrospective cohort exhibited favorable short-term survival.

872 Comparison Between Integrated Genomic DNA/RNA Profiling and Fluorescence In Situ Hybridization in the Detection of MYC, BCL-2, and BCL-6 Gene Rearrangements in Large B-Cell Lymphomas: An Update

Luiz Paulo De Lima Guido[1], Jennifer Chapman[2], Daniel Cassidy[3]
[1]University of Miami Miller School of Medicine/Jackson Memorial Hospital, Miami, FL, [2]University of Miami, Miller School of Medicine, Miami, FL, [3]Jackson Memorial Hospital/ University of Miami Hospital, Miami, FL

Disclosures: Luiz Paulo De Lima Guido: None; Jennifer Chapman: None; Daniel Cassidy: None

Background: Large B-cell lymphomas (LBCLs) are a heterogeneous group of lymphoid neoplasms whose molecular and cytogenetic profile has predictive and prognostic implications. Fluorescence in-situ hybridization (FISH) is the current gold standard for detecting rearrangements in LBCLs, but various FISH probe options have varying sensitivities depending upon the specific breakpoint present. In theory, this limitation should be abrogated by the technology used in comprehensive genomic profiling (CGP) studies. Data comparing the sensitivity of CGP and FISH for detection of these rearrangements is lacking. This study intends to produce data to guide testing algorithms for detection of *MYC*, *BCL-2* and *BCL-6* rearrangements in LBCLs.

Design: FISH and CGP were performed in 131 unselected LBCLs. FISH studies included probes for *IGH-BCL2* dual fusion, *BCL-6* break apart, *MYC* break apart, and *IGH-MYC* dual fusion. Commercially performed CGP results were analyzed. Discrepancies between FISH and CGP results were analyzed.

Results: 98 rearrangements were identified including 43 *BCL6*, 36 *IGH-BCL2*, 10 *IGH-MYC* and 9 non-*IGH-MYC*. 23 (17.5%) cases had discordant results between FISH and CGP. CGP was more sensitive than FISH in detecting *IGH-BCL2* and *IGH-MYC*, while FISH was more sensitive for detection of *BCL6* and non-*IGH-MYC* (Tables 1, 2). 13 HGBCL with *MYC* and *BCL-2* and/or *BCL-6* rearrangement (DHL) were detected using combined FISH/CGP approach. FISH testing did not identify 23% of DHLs (Table 3). CGP testing did not identify 31% of DHLs (Table 3). Every DHL missed by CGP was the result of lack of CGP sensitivity in detecting non-*IGH-MYC* rearrangements.

Rearrangements detected by FISH and CGP in cases with discordant results. Missed HGBCLs in red		
Case No.	**Rearrangement Detected by FISH**	**Rearrangement Detected by CGP**
1	None	*IGH-BCL-2*
2	*IGH-MYC*	*IGH-BCL-2 and IGH-MYC*
3	*BCL-6*	*IGH-BCL-2 and BCL-6*
4	*IGH-MYC and BCL-6*	*IGH-BCL-2, IGH-MYC and BCL-6*
5	None	*IGH-MYC*
6	Non-*IGH-MYC and IGH-BCL-2*	*IGH-BCL-2*
7	Non-*IGH-MYC and BCL-6*	*BCL-6*
8	Non-*IGH-MYC*	None
9	Non-*IGH-MYC*	None
10	Non-*IGH-MYC*	None
11	Non-*IGH-MYC* and *BCL-6*	None
12	Non-*IGH-MYC* and *IGH-BCL-2*	*IGH-BCL-2*
13	Non-*IGH-MYC*	None
14	*IGH-MYC*	*IGH-MYC* and *BCL-6*
15	*IGH-BCL-2* and *BCL-6*	*IGH-BCL-2*
16	*IGH-BCL-2* and *BCL-6*	*IGH-BCL-2*
17	*IGH-BCL-2*	*IGH-BCL-2* and *IGH-MYC*
18	*BCL-6*	None
19	*BCL-6*	None
20	None	*BCL-6*
21	None	*BCL-6*
22	None	*BCL-6*
23	*BCL-6*	None

Figure 1 - 872

Figure 1: Overall sensitivities of FISH and CGP in the detection of *MYC, BCL2* and *BCL6* gene rearrangements

Rearrangement	FISH positives	CBP positives
IGH-MYC	9/10 (90%)	10/10 (100%)
Non-*IGH-MYC*	9/9 (100%)	1/9 (11%)
IGH-BCL2	32/36 (89%)	36/36 (100%)
BCL6	39/43 (91%)	37/43 (86%)

Figure 2 - 872

Figure 2: Sensitivities of FISH and CGP in the detection of HGBCL.

FISH positives	CGP positives	CGP + FISH using *MYC* breakapart probe only
10/13 (77%)	9/13 (69%)	13/13 (100%)

Conclusions: CGP appears more sensitive than FISH in detection of *IGH-BCL2* and *IGH-MYC* rearrangements. FISH testing is superior for detection of non-*IGH-MYC*. Neither FISH nor CGP detect all DHLs. CGP appears at least as sensitive as FISH in detection of most rearrangements in DHLs with the notable exception of non-*IGH-MYC*. These findings are largely in agreement with what we have previously reported and provide further support that the best approach to maximize detection of DHLs while limiting waste seems to be a combination of CGP and *MYC* break apart FISH, the latter to capture non-*IGH-MYC* events. Some studies have suggested that non-*IGH-MYC* and *BCL-6* rearrangements may not confer the same poor prognosis as *IGH-MYC* and *IGH-BCL-2* rearrangements in the context of DHLs, which may further support that CGP data may be more useful than FISH data in these lesions.

873 Axillary Lymph Node Core Biopsy Following SARS-CoV-2 Vaccination

Carl Dernell[1], Julie Jorns[1], Abraham Bogachkov[1], Shelly Reimer[1], Anubha Wadhwa[1], Shadie Majidi[1], John Astle[1]
[1]Medical College of Wisconsin, Milwaukee, WI

Disclosures: Carl Dernell: None; Julie Jorns: None; Abraham Bogachkov: None; Shelly Reimer: None; Anubha Wadhwa: None; Shadie Majidi: None; John Astle: None

Background: Atypical axillary lymph nodes identified on breast cancer screening often result in axillary lymph node core biopsy (ALNB). However, similar changes may occur after vaccination. Recent trends of mass vaccination for SARS-CoV-2 have resulted in new guidelines, specifically delay to biopsy following vaccination to avoid false positives and unnecessary biopsy, with notable exceptions in the context of breast cancer. We aimed to evaluate ALNB pathology, clinical and imaging features in patients who had received SARS-CoV-2 vaccination.

Design: We evaluated ALNB specimens from patients who received SARS-CoV-2 vaccine before biopsy (1/2021 - 6/2021) at our enterprise (1 academic and 2 community hospital sites). Clinicopathologic features were assessed by chart and slide review, with pathology review by a dedicated hematopathologist and imaging review by dedicated breast radiologists.

Results: Of 135 patients with ALNB, 48 (35.6%) had vaccination prior to biopsy. Patients were predominantly female (47/48; 97.9%), with a mean age of 55.1 years (range 19.9-91.3). 34 of 48 (70.8%) were benign, 12 (25%) had metastatic carcinoma, 1 (2.1%) hematologic malignancy (CLL/SLL), and 1 (2.1%) metastatic melanoma. In non-vaccinated patients, the rate of malignancy was similar (24/87; 27.6%) (p=0.73).

All ALNB with metastatic carcinoma were from patients with concurrent breast carcinoma and the patient with metastatic melanoma had a history of melanoma. Of patients with benign ALNB, 10 (29.4%) had concurrent, 1 (2.9%) recent (within 2 years) and 3 (8.8%) remote (>2 years) history of breast cancer. Most (37/48; 77.1%) ALNB specimens could be traced to abnormal breast imaging (Table 1).

SARS-CoV-2 vaccine was ipsilateral in 18 (37.5%), contralateral in 14 (29.2%) and side was not documented in 16 (33.3%). Median time from 1st dose to ALNB was 10.6 weeks (range 1.9-23.9) and from 2nd dose to ALNB was 7.7 weeks (range 0-20.9). 16 (33.3%) had a dose within the prior 6 weeks.

Benign ALNB in patients who underwent vaccination prior to biopsy comprised: 21 (61.8%) without specific features, 10 (29.4%) reactive follicular hyperplasia, 2 (5.9%) dermatopathic change and 1 (2.9%) tattoo pigment. Reactive follicular hyperplasia was significantly less frequent (4/63; 6.3%) in patients who did not undergo vaccination prior to biopsy (p<.01).

Table 1. Imaging features of all cases (N=48) and subset with benign pathology (N=34) in patients who underwent vaccination prior to biopsy

		Total N(%)	Benign N(%)
Method of Lymph Node Detection	Screening mammogram	14 (29.2)	13 (38.2)
	Diagnostic mammogram	15 (31.3)	8 (23.5)
	MRI	8 (16.7)	7 (20.6)
	Palpable	6 (12.5)	3 (8.8)
	Other	5 (10.4)	3 (8.8)
Axillary Lymphadenopathy Distribution	Unilateral	38 (79.2)	27 (79.4)
	Bilateral	10 (20.8)	7 (20.6)
Lymph Node Cortical Thickening Pattern	Focal	17 (35.4)	11 (32.4)
	Diffuse	31 (64.6)	23 (67.6)
Cortical Thickness	3-4 mm	9 (18.8)	7 (20.6)
	4-5 mm	12 (25)	10 (29.4)
	5+ mm	27 (56.3)	17 (50)
Lymph Node Fatty Hilum Presence	No	14 (29.2)	6 (17.6)
	Yes	34 (70.8)	28 (82.4)

Conclusions: Some patients who underwent SARS-CoV-2 vaccination with reactive changes may have avoided ALNB if there were more time between imaging, vaccination and breast cancer diagnosis.

874 Proliferation Center-Focused Artificial Intelligence Algorithm Enhances Detection of Accelerated Phase Chronic Lymphocytic Leukemia

Siba El Hussein[1], Pingjun Chen[2], John Boom[3], Ignacio Wistuba[2], L. Jeffrey Medeiros[2], Jia Wu[2], Joseph Khoury[2]
[1]University of Rochester Medical Center, Rochester, NY, [2]The University of Texas MD Anderson Cancer Center, Houston, TX, [3]Duke University, Durham, TX

Disclosures: Siba El Hussein: None; Pingjun Chen: None; John Boom: None; Ignacio Wistuba: None; L. Jeffrey Medeiros: None; Jia Wu: None; Joseph Khoury: None

Background: Discrimination between CLL and aCLL can be challenging. Current criteria for aCLL are limited to identifying confluent PCs exceeding a 20x field and increased Ki67 proliferation index >40%/ PC, and/or mitotic figures >2.4/ PC. Based on a combination of additional morphologic and architectural features of PCs, we developed an artificial intelligence tool to distinguish CLL from aCLL in excisional biopsy (EB) and CNB specimens.

Design: The study included 13 CLL (6 CNB; 7 EB) and 19 aCLL (9 CNB; 10 EB) cases. We extracted a total of 112 PCs (52 CLL; 60 aCLL) (***Figures A1-2 & B1-2)***. Annotation was based on morphologic identification of PCs. We then analyzed morphologic (*area*, *circularity, solidity* & *shape similarity*) and architectural features (*neighboring PC distance, distance to tissue border* & *PC/ biopsy length ratio)* within EB of CLL and aCLL groups within CNB of CLL and aCLL cases ***(Figures A3-7 & Figure B3-6).*** We defined *area* as the surface occupied by each PC; *circularity* as the degree of resemblance of PCs to circles; *solidity* as the ratio of PC area to the area of its convex hull; *shape similarity as the morphologic proximity* to other PCs within the same sample; *neighboring PC distance* as the distance of a designated PC centroid to its nearest PC centroid; *distance to tissue border* as the nearest distance to CNB edge; and, *PC/biopsy length ratio* as the ratio of the PC segment bordering the CNB edge and the PC total length. We then overlaid our results on Ki67 values.

Results: PCs in aCLL were more likely to occupy a larger surface area, have a non-circular shape characterized by convexities and concavities, exhibit dissimilarities to PCs within the same EB specimen and longer neighboring PC *distance* ***(Figure A3-7)***. These features correlated with areas of increased Ki-67 proliferation in aCLL relative to CLL ***(Figure A8-12).*** In CNB, PCs in aCLL were more likely to occupy a larger surface area , demonstrate a non-circular shape, exhibit shorter distance *to tissue border*, and larger PC/biopsy length ratio in comparison to PCs in CLL ***(Figure B3-6).*** These features correlated with areas of increased Ki-67 proliferation in aCLL relative to CLL ***(Figure B7-9)***. Using the Leave One Out Cross Validation Technique (LOOCV), we obtained robust diagnostic accuracy and precision values of 0.934 & 0.974 in EB, and 0.838 & 0.810 in CNB specimens, respectively.

Figure 1 – 874

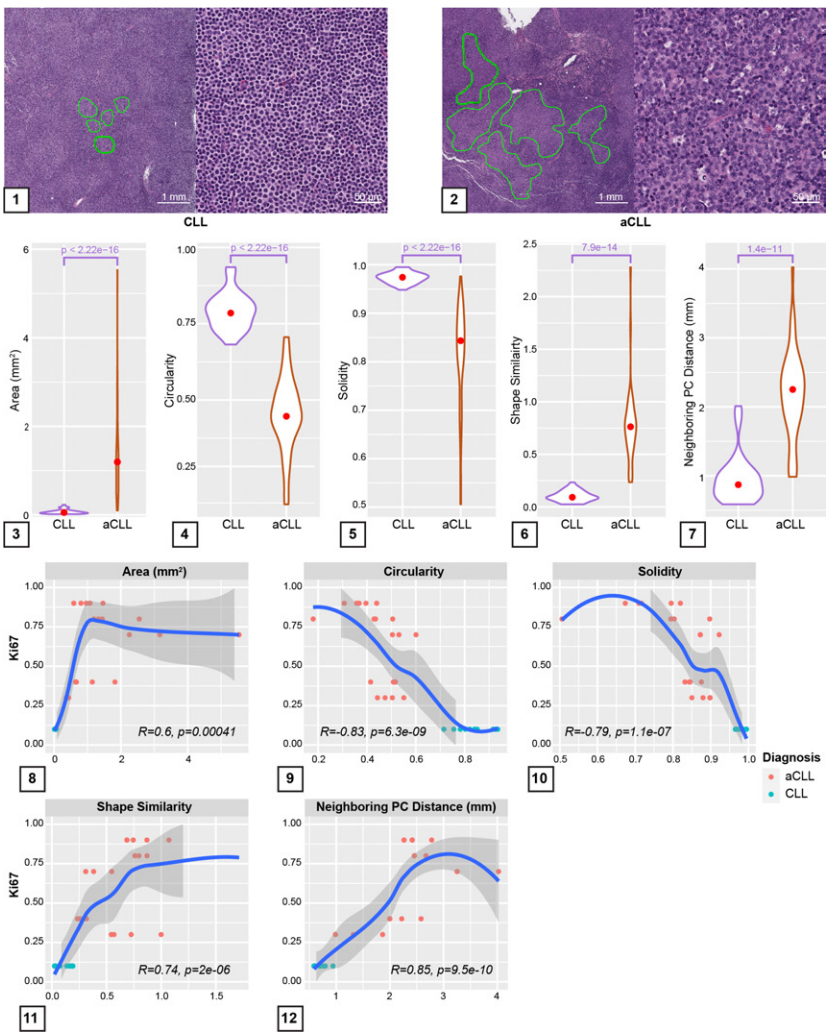

Figure 2 – 874

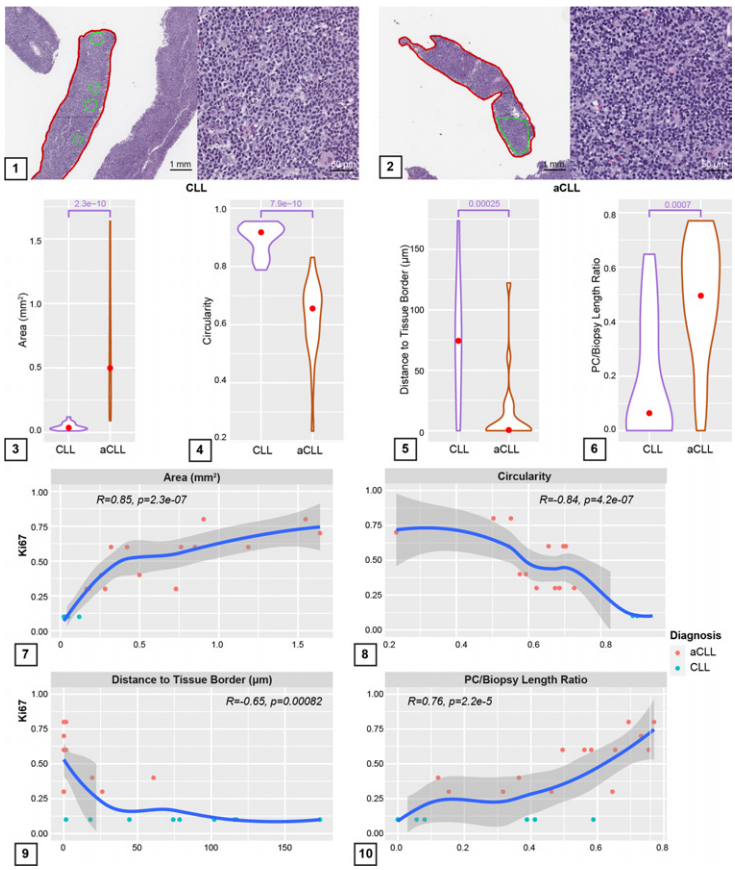

Conclusions: Our approach has the potential of providing diagnostic assistance in evaluating patients with suspicion of progressive CLL.

875 Mutation Burden Comparison Between Chronic Myelomonocytic Leukemia with Progression to Acute Myeloid Leukemia and De Novo Acute Myeloid Leukemia M4/M5

Ismail Elbaz Younes[1], Austin Ellis[1], Xiaohui Zhang[2], Lee Syler, Jinming Song[2], Yun Seongseok[2], Mohammad Hussaini[2], Ling Zhang[2]

[1]H. Lee Moffitt Cancer Center & Research Institute, University of South Florida, Tampa, FL, [2]H. Lee Moffitt Cancer Center & Research Institute, Tampa, FL, [3]University of South Florida, Tampa

Disclosures: Ismail Elbaz Younes: None; Austin Ellis: None; Xiaohui Zhang: None; Lee Syler: None; Jinming Song: None; Yun Seongseok: None; Mohammad Hussaini: None; Ling Zhang: None

Background: Chronic myelomonocytic leukemia (CMML) is frequently associated with *TET2, SRSF2*, *SETBP1* and *ASXL1* mutations. Approximately 15% of CMML cases are at risk to transform to acute myeloid leukemia (AML ex CMML). Driver mutations leading to the transformation are not well studied. Mutations involved in leukemogenesis of AML with myelomonocytic differentiation (AML M4/M5) are unclear. Our study aims to illustrate the differences of mutation profiles between groups of AML ex CMML and AML M4/M5and correlate them with prognosis and overall survival (OS).

Design: We retrospectively identified 70 *de novo* AML M4/M5 and 52 cases of AML ex CMML from our next-generation sequencing (NGS) data pool. The patients who had a history of *de novo* AML with recurrent cytogenetic changes, AML arising from myelodysplastic syndromes or with biallelic mutation of *CEBPA,* therapy-related AML were excluded. *NPM1* and *RUNX1* mutations

are kept in both groups for analysis. Categorical data were analyzed with Chi-square test. The Kaplan-Meier test was used to compare the OS.

Results: AML ex CMML showed more frequent mutations (>=3) when compared with AML M4/M5 (84% vs 54%, $p<0.001$). *ASXL1, SRSF2, TET2*, and *RUNX1* mutations were more commonly identified in AML ex CMML (all $p<0.01$, Table 1), while *NPM1*, *U2AF1* and *TP53* mutations were more frequently found in AML M4/M5 ($p<0.001$, $p=0.055$, and $p=0.07$, respectively). When compared the OS of the two groups, AML M4/M5 had better OS than AML ex CMML (7.6 vs. 6 months (mos), p=0.101). *TET2* mutation was associated with worse OS in both groups (6.4 vs. 11.6 mos, and 5.7 vs. 10.6 mos, respectively; overall $p=0.003$. Figure 1-2). Interestingly, when stratified with *ASXL1*, only *ASXL1*^{wildtype}/*TET2*^{mutated} group had worse OS than *ASXL1*^{wildtype}/*TET*^{wildtype} group in AML M4/M5 (5.5 vs 11.6 mos, $p=0.015$) but not in AML ex CMML. Complex karyotypes were associated with worse OS in AML ex CMML (1.7 vs 8.5 mos, $p=0.021$). Del(7q)/monosomy 7(-7) was associated with worse OS in AML M4/M5 (5.5 vs 9.9 mos, $p=0.049$) but not in our AML ex CMML cohort

Table 1. Clinical and molecular findings between patients diagnosed with *de novo* AML M4/5 and AML ex CMML

Variables	De novo AML M4/M5 (n=70)	CMML with progression to AML (n=52)	*p*-value (Chi-square test)
Gender			0.082
Male	39 (55.7%)	37 (71.1%)	
Female	31(44.3%)	15 (28.9%)	
Age			0.002
Median age (years)	73	65	
Range (years)	42-94	25-89	
Mutation results per NGS study (n, %)			
DNMT3A	22(31.4%)	11 (21.1%)	0.206
NPM1	19 (27.1%)	2 (3.8%)	**<0.001***
TET2	19 (27.1%)	27 (51.9%)	**0.005***
ASXL1	15 (21.4%)	30 (57.6%)	**<0.001***
RUNX1	12 (17.1%)	22 (42.3%)	**0.002***
U2AF1	10 (14.2%)	2 (3.8%)	0.056
IDH2	10 (14.2%)	3 (5.7%)	0.132
FLT3	8 (11.4%)	5 (9.6%)	0.748
TP53	7 (10%)	1 (1.9%)	0.075
SRSF2	7 (10%)	19 (36.5%)	**<0.001***
NRAS	7(10%)	9 (17.3%)	0.399
KRAS	7(10%)	3 (5.7%)	0.400
IDH1	7 (10%)	2 (3.8%)	0.198
SETBP	4 (5.7%)	5 (9.6%)	0.415
EZH2	4 (5.7%)	7 (13.4%)	0.140
>= 3 mutations	40 (57.1%)	44 (84.6%)	**0.001***
Karyotyping			0.168
>=3 cytogenetic abnormalities	13 (18.5%)	5 (9.6%)	
< 3 cytogenetic abnormalities	57 (81.5%)	47 (90.4%)	
17p abnormalities	5 (7.1%)	1 (1.9%)	0.187
Del(7q)/-7	5 (7.1%)	8 (15.3%)	0.145

*Statistically significant ($p<0.05$).

Figure 1 - 875

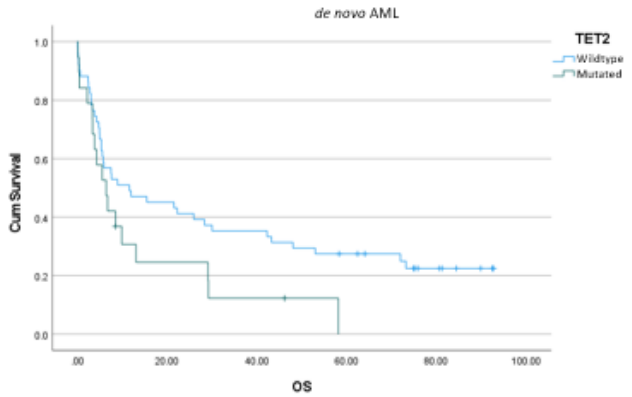

Figure 2 - 875

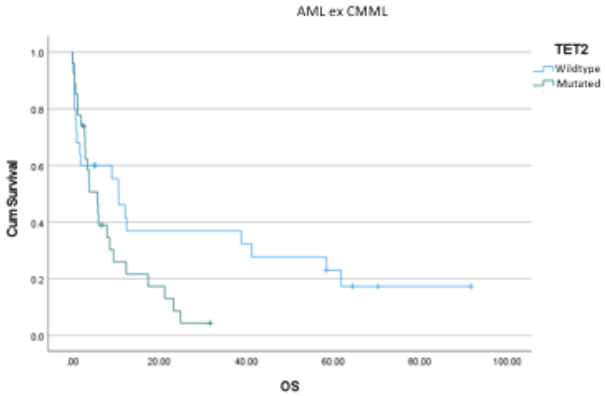

Conclusions: AML ex CMML and *de novo* AML M4/M5 have different mutation profiles. Acquisition of *RUNX1* mutation in CMML might be critical for leukemic transformation. The presence of *TET2* mutations predicts a worse outcome in both groups. Complex karyotypes are associated with worse OS in AML ex CMML and del(7q)/-7 is associated with worse OS in AML M4/M5. Multi-center cohorts including CMML without transformation to AML are to be performed for validation.

876 A Pathologic Study of Acute Myeloid Leukemia with Mutations in Clonal Hematopoiesis Related Genes: A Single Institution Experience

Mostafa Elhodaky[1], Madina Sukhanova[1], Lawrence Jennings[2], Xinyan Lu[1], Amir Behdad[1], Barina Aqil[1], Qing Chen[1], Yi-Hua Chen[3], Juehua Gao[3]

[1]Northwestern University Feinberg School of Medicine, Chicago, IL, [2]Northwestern University, Feinberg School of Medicine, Chicago, IL, [3]Northwestern Memorial Hospital, Chicago, IL

Disclosures: Mostafa Elhodaky: None; Madina Sukhanova: None; Lawrence Jennings: None; Xinyan Lu: None; Amir Behdad: *Speaker*, Lilly, Roche/Foundation Medicine China, Thermo Fisher Scientific, Bayer; Barina Aqil: None; Qing Chen: None; Yi-Hua Chen: None; Juehua Gao: None

Background: Genes commonly mutated in clonal hematopoiesis (CH) are found in a subset of patients with acute myeloid leukemia (AML). Although these mutations can occur early in AML evolution, they are not alone sufficient to cause AML, and their role in disease development and evolvement is still poorly understood.

Design: We searched all AML cases with mutations in three major CH genes: *DNMT3A, TET2, and ASXL1.* Only mutations of known or possible clinical significance were included. Mutations of unknown clinical significance were excluded from this study. We evaluated the pathologic diagnosis, cytogenetics, complete molecular profiling, and follow up information.

Results: Fifty-nine cases were identified from 44 males and 15 females (age 33~88, median 68). These cases included 15 AML with mutated NPM1 (25%), 13 AML-MRC (22%), 17 AML NOS (29%), 5 t-AML, 2 AML with t (8;21), 1 APL, 1 mixed lineage acute leukemia, 1 AML with biallelic CEBPA mutations, 2 AML transformed from PMF or PV, 1 myeloid sarcoma, and 1 blastic plasmacytoid dendritic cell neoplasm. Blasts often show monocytic differentiation, seen in most of the AML with mutated *NPM1*, and in 5/17 of AML, NOS. Among 55 patients with available cytogenetic data, 27 (49%) had normal karyotype. MDS related cytogenetic abnormalities were common and included complex karyotype, del(5q), del(7q), +8, and +20. Other copy number changes and balanced translocations were also present. Mutations in CH genes, if present at the time of AML diagnosis or persistent disease, were almost always accompanied by other driver mutations (39/41, 95%), most frequently *NPM1*, followed by cell signaling (*FLT3, RUNX1, KRAS, CBL*), splicesome *(SRSF2, U2AF1, ZRZF2*), *IDH1/2* and rarely *TP53*. Mutations in CH genes can persist after the patients achieved morphologic remission, and were often associated with disappearance of the accompanying mutations (11/13, 85%) except in two cases with persistent *U2AF1*. The VAF of the mutated CH related genes, during remission, remained similar, indicating relatively stable clone size over time. In 3 of the 4 cases with relapsed disease, additional mutations in *CEBPA*, *IDH2*, *FLT3* ITD and *PHF6* were acquired.

Conclusions: Mutations in CH related genes are present in different types of AML, but most frequently in AML with mutated NPM1, AML-MRC and AML with monocytic differentiation. They alone are not sufficient to cause AML, and can stably persist during remission. Relapse is often accompanied by acquisition of additional mutations.

877 Clinicopathologic Distinction Between Acute Myeloid Leukemia with Mutated NPM1 and Acute Myeloid Leukemia with Myelodysplasia-Related Changes in Cases with Multilineage Dysplasia

Austin Ellis[1], Ismail Elbaz Younes[1], Mohammad Hussaini[2], Jinming Song[2], Lynn Moscinski[2], Onyee Chan[2], Ling Zhang[2], Hammad Tashkandi[3]

[1]H. Lee Moffitt Cancer Center & Research Institute, University of South Florida, Tampa, FL, [2]H. Lee Moffitt Cancer Center & Research Institute, Tampa, FL, [3]University of Pittsburgh Medical Center, Pittsburgh, PA

Disclosures: Austin Ellis: None; Ismail Elbaz Younes: None; Mohammad Hussaini: None; Jinming Song: None; Lynn Moscinski: None; Onyee Chan: None; Ling Zhang: None; Hammad Tashkandi: None

Background: Misclassification of acute myeloid leukemia with mutated NPM1 (AML-*NPM1*^{mut}) as AML with myelodysplasia-related changes (AML-MRC) may occur in patients without a prior history of malignancy when the bone marrow harbors multilineage dysplasia since mutational status results lag morphologic assessment. The WHO classifies AML-*NPM1*^{mut} as a distinct entity with a favorable prognosis, while AML-MRC confers a poor prognosis, highlighting the need for proper classification.

Design: We retrospectively identified 51 cases of *de novo* AML with multilineage dysplasia by morphology in patients with no history of cytotoxic or radiotherapy for an unrelated disease and without biallelic mutation of *CEBPA* from 6500 patients in a next-generation sequencing (NGS) data pool. We divided the patients into two groups, AML-*NPM1*^{mut} (n=21) and AML-MRC (n=30) and assessed the clinical, laboratory, flow cytometric, and molecular findings at diagnosis. We analyzed continuous data and categorical data with Student's t-test and Fisher exact test, respectively.

Results: Due to the presence of multilineage dysplasia and pending NGS data which resulted between one and two weeks later, initial misclassification of AML-*NPM1*^{mut} as AML-MRC occurred in 43% (9/21) of cases. Except for higher platelet count in AML-*NPM1*^{mut} (88 vs 44 x109/L) (*P*=.026), we found no significant difference in age (*P*=.081), sex (*P*=.394), white blood cell count (*P*=.272), or hemoglobin level (*P*=.917). AML-*NPM1*^{mut} blasts more often expressed CD33 (20/21 vs 21/30) and had negative CD34 expression (14/21 vs 2/30) compared to AML-MRC blasts (*P*=.034 and *P*=<.001, respectively). A myelodysplastic syndrome (MDS) fluorescence in-situ hybridization (FISH) panel with probes for 5q, 7q, 17p, 20q, and trisomy 8 identified cytogenetic abnormalities sufficient for the diagnosis of AML-MRC in 0/12 AML-*NPM1*^{mut} cases and 21/27 AML-MRC cases (*P*=<.001). AML-MRC cases more commonly had TP53 mutations (14/28 vs 0/21) (*P*=<.001). Patients in the AML-MRC group had shorter survival than the AML-*NPM1*^{mut} group (median survival 10 months vs not reached) (*P*=.001).

Variables	**AML-*NPM1*^{mut}** (n=21)	**AML-MRC** (n=30)	***P* value**
Age, median (range), years	57 (27-83)	68 (32-83)	.081
Sex			.394
Male	8 (38%)	16 (53%)	
Female	13 (62%)	14 (47%)	
CBC at diagnosis	median (range)	median (range)	
WBC (k/μL)	9.09 (0.92-92.72)	3.84 (1.11-71.53)	.272
Hgb (g/dL)	8.1 (7.1-11.0)	8.1 (6.8-10)	.917
Platelets (k/μL)	88 (8-238)	41 (9-314)	.026
Blasts, median (range)			
Peripheral blood	20% (0-50%) n=19	11% (0-82%) n=27	.876
Bone marrow	45% (6.5-89%)	51% (20-75%)	.847
AML			
De novo	21 (100%)	30 (100%)	
Preceding MDS or MDS/MPN	0	0	
Therapy related	0	0	
FISH	n=12	n=27	<.001
-5/-5q	0	15 (56%)	
-7/7q	0	13 (48%)	
-20/20q	0	4 (15%)	
-17/17p	0	10 (37%)	
+8	0	6 (22%)	
Karyotype			<.001
≥3 cytogenetic abnormalities	0	18 (60%)	
<3 cytogenetic abnormalities	21 (100%)	12 (40%)	

Immunophenotype			
CD33 positive	20 (95%)	21 (70%)	.034
CD34 negative	14 (66%)	2 (7%)	<.001
CD117 positive	19 (90%)	29 (97%)	.561
Mutation			
NPM1	21 (100%)	0	
TP53	0	14 (50%) n=28	<.001
biallelic *CEBPA*	0	0	
Median survival	Not reached	10 months	.001

Figure 1 - 877

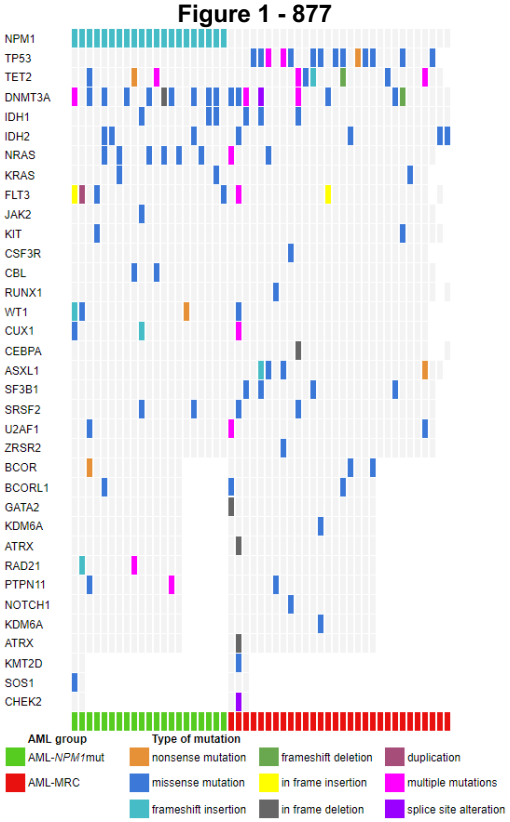

Figure 2 - 877

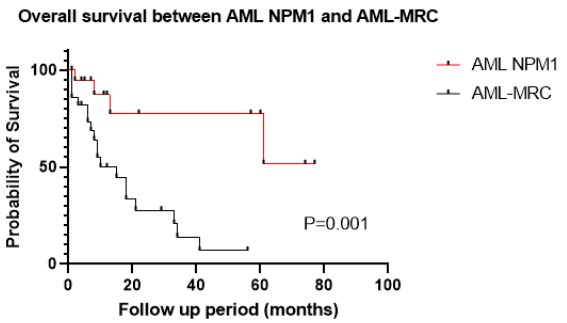

Conclusions: Distinguishing between AML-*NPM1*^{mut} with multilineage dysplasia and AML-MRC leads to critical differences in therapy and clinical outcome. AML-*NPM1*^{mut} more frequently expresses CD33 and lacks CD34. AML-MRC more frequently has MDS FISH abnormalities and lower platelet counts. Correlating these variables might help avoid misclassification before knowing whether *NPM1* has a mutation or not.

878 Bone Marrow Pathologic Abnormalities in Myelodysplastic Syndrome (MDS) Patients with Underlying TERT/TERC Germline Alterations

Mark Evans[1], Joseph Khoury[1], Courtney DiNardo[1], Guillermo Garcia-Manero[1], Hui Yang[1], Sanam Loghavi[1], Guillermo Montalban-Bravo[1], Keyur Patel[1], Andres Quesada[1], Sergej Konoplev[1], Sofia Garces[2], Gokce Toruner[1], Carlos Bueso-Ramos[1], L. Jeffrey Medeiros[1], Rashmi Kanagal-Shamanna[1]

[1]The University of Texas MD Anderson Cancer Center, Houston, TX, [2]The Hospital of the University of Pennsylvania, Philadelphia, PA

Disclosures: Mark Evans: None; Joseph Khoury: None; Courtney DiNardo: None; Guillermo Garcia-Manero: None; Hui Yang: None; Sanam Loghavi: None; Guillermo Montalban-Bravo: None; Keyur Patel: None; Andres Quesada: None; Sergej Konoplev: None; Sofia Garces: None; Gokce Toruner: None; Carlos Bueso-Ramos: None; L. Jeffrey Medeiros: None; Rashmi Kanagal-Shamanna: None

Background: The World Health Organization category of myeloid neoplasms arising in the setting of telomere biology disorders are characterized by *TERT* and *TERC* mutations. Unlike sporadic myeloid neoplasms (MNs), interpretation of bone marrow (BM)

morphologic findings in MNs with germline alterations is challenging. Understanding the significance of these findings in the context of other cytogenetic/mutational studies is warranted. The goal of this study is to characterize MNs in patients (pts) with germline *TERT/TERC* alterations.

Design: Baseline BM morphologic features were reviewed from 10 unrelated pts with a myelodysplastic syndrome (MDS), acute myeloid leukemia (AML), or clonal cytopenia of undetermined significance (CCUS) and with germline *TERT/TERC* mutations. Somatic alterations were evaluated using karyotyping and an 81-gene next-generation sequencing (NGS) panel [*TERT*: exons 1-16; *TERC*: RNA transcript sequence].

Results: There were 7 men and 3 women (median age, 62 years) with germline *TERT* (n=7) or *TERC* (n=3) mutations. All pts had peripheral blood cytopenias of variable duration (median, 18 months, range, 1-60+); 8 had lung/liver fibrosis or skin/hair abnormalities. All pts had a family history of cancer and/or short telomere-associated organ damage.

BM examination showed 7 (70%) cases of MDS, 1 (10%) case of AML with myelodysplasia-related changes (AML-MRC), and 2 (20%) cases of CCUS. All 7 cases of MDS were characterized by a low blast count [median 2%, (0-2)]. In 4 cases, ring sideroblasts were >15% (MDS-RS-MLD), and 3 cases had multilineage dysplasia (MDS-MLD). The median cellularity was 35% (5-75); 4 (58%) pts had hypocellular-for-age BM. Five pts showed trilineage and 2 pts showed either uni- or bilineage dysplasia. Except in 1 pt, megakaryocytes were either decreased or adequate in number. In 1 case the BM showed mild reticulin fibrosis.

All pts had at least 1 somatic (cytogenetic/molecular) abnormality (Figure 1). Four pts showed alterations involving chr(7). Recurrent somatic mutations involved spliceosome genes (n=5; 63%; *U2AF1*, *SF3B1*, *SRSF2*, *PRPF40B*) and *TP53* (n=3; 38%). CCUS pts showed low-level *TP53* and *TET2* mutations, with no changes in serial biopsies. Over a median follow-up of 27 months, 2 of 9 evaluable patients died.

Figure 1 - 878

		Patients									
	BM Diagnosis	MDS-MLD	MDS-MLD	MDS-MLD	MDS-RS-MLD	MDS-RS-MLD	MDS-RS-MLD	MDS-RS-MLD	CCUS	CCUS	AML-MRC
Karyotype Findings:	Diploid Karyotype										
	Alterations of Chromosome 7										
	Alterations of 1 or 2 Other Chromosome(s)										
	Complex Karyotype (3 or More Alterations)										
Molecular Findings:											
Genes with Somatic Mutations	*ASXL1*	p.L775*									
	U2AF1	p.S34F									p.Q157R
	SRSF2				p.R57Y						
	SF3B1				p.K700E		p.K700E				
	TP53					p.G262del		p.R337C c.782+1G>A	p.R249W		
	STAT5							p.T92M			
	PRPF-40B							p.S166L			
	TET2									p.Q599*	
	IDH1										p.R132C
	CUX1										p.A10G
	RUNX1										p.R320*
Germline Mutations of *TERT* or *TERC*	*TERT*	p.V664L		p.R865H		p.L864P	p.R972G	p.R979Q	p.P65A		p.V170M
	TERC		n.66C>T		n.381G>A					n.35C>T	

Conclusions: This is the first study to describe the unique BM and genetic features of MNs with germline *TERT/TERC* mutations that include presentations mimicking low-grade hypocellular MDS and frequent association with RS and spliceosome gene mutations.

879 Acute Promyelocytic Leukemia: Immunophenotype and Differential Diagnosis

Hong Fang[1], Sa Wang[1], Siba El Hussein[2], Sergej Konoplev[1], Huan Mo[1], Wei Liu[1], Zhuang Zuo[1], Shimin Hu[1], Fatima Zahra Jelloul[1], Zhenya Tang[1], L. Jeffrey Medeiros[1], Wei Wang[1]
[1]The University of Texas MD Anderson Cancer Center, Houston, TX, [2]University of Rochester Medical Center, Rochester, NY

Disclosures: Hong Fang: None; Sa Wang: None; Siba El Hussein: None; Sergej Konoplev: None; Huan Mo: None; Wei Liu: None; Zhuang Zuo: None; Shimin Hu: None; Fatima Zahra Jelloul: None; Zhenya Tang: None; L. Jeffrey Medeiros: None; Wei Wang: None

Background: Acute promyelocytic leukemia (APL) is a medical emergency and immediate recognition of this neoplasm is critical. In this study, we aimed to characterize the immunophenotype of APL by flow cytometric analysis and explore the differences between APL and other cases of acute myeloid leukemia (AML) with APL-like immunophenotype.

Design: Eighty-five cases were collected, including 47 APL, 26 *NPM1*-mutated AML with APL-like immunophenotype, and 12 *KMT2A*-rearranged AML with APL-like immunophenotype. All cases were analyzed using comprehensive panels of antibodies.

Results: APL cases showed four distinct patterns (patterns A-D) based on CD45/SSC plots. In patterns A-C, leukemic cells showed a continuous smear pattern on side scatter with cells ranging from low side scatter to cells with a very high side scatter. In contrast, leukemic cells in pattern D were located in the traditional blast gate with a low side scatter. APL cases with pattern D showed more frequent CD2 (p=0.0005) and CD34 (p=0.0002) expression when compared to APL cases with patterns A-C. No significant differences in other markers were found among these four patterns.

In pattern D of APL, cases were frequently positive for CD2 (8/13, 62%), CD13 (13/13, 100%), CD34 (7/13, 54%), CD64 (13/13, 100%), and MPO (13/13, 100%). All *NPM1*-mutated AML and all (but except one) *KMT2A*-rearranged AML cases with APL-like immunophenotype had low side scatter and dim CD45, similar to the pattern D in APL. Compared with APL, cases of *NPM1*-mutated AML were positive for CD13 (15/26, 58%; p=0.007) and CD64 (10/26, 38%; p=0.0003). In addition, only 4% of these cases were positive for CD34 and none were positive for CD2. Using the combination of uniform CD13 and positive CD64, the sensitivity and specificity to distinguish *NPM1*-mutated AML from APL-pattern D were 100% and 96%, respectively. In comparison with APL, *KMT2A*-rearranged AML cases were less often positive for MPO (4/11, 36%; p=0.001), with none being strongly positive. Similar to *NPM1*-mutated AML cases, *KMT2A*-rearranged AML cases were rarely positive for CD34 (1/11, 9%) and all were negative for CD2.

Conclusions: APL and its immunophenotypic mimics can be distinguished by markers including CD2, CD13, CD64, and MPO. CD2 expression is frequently seen in APL but not in its mimics. MPO is valuable to distinguish *KMT2A* rearranged cases from APL and *NPM1*-mutated cases. For the differential diagnosis between APL and *NPM1*-mutated AML, the combination of CD13 and CD64 has a high diagnostic value.

880 Molecular and Immunophenotypic Features of Pure Erythroid Leukemia

Hong Fang[1], Sa Wang[1], Joseph Khoury[1], Do Hwan Kim[1], Mehrnoosh Tashakori[2], Zhenya Tang[1], Shaoying Li[1], Zhihong Hu[3], Fatima Zahra Jelloul[1], Keyur Patel[1], Timothy McDonnell[1], L. Jeffrey Medeiros[1], Wei Wang[1]
[1]The University of Texas MD Anderson Cancer Center, Houston, TX, [2]University of Minnesota, Minneapolis, MN, [3]The University of Texas Health Science Center at Houston, Houston, TX

Disclosures: Hong Fang: None; Sa Wang: None; Joseph Khoury: None; Do Hwan Kim: None; Mehrnoosh Tashakori: None; Zhenya Tang: None; Shaoying Li: None; Zhihong Hu: None; Fatima Zahra Jelloul: None; Keyur Patel: *Consultant*, Astellas Pharma, Novartis Pharmaceutical Corporation; Timothy McDonnell: None; L. Jeffrey Medeiros: None; Wei Wang: None

Background: Pure erythroid leukemia (PEL) is a rare subtype of acute myeloid leukemia. Its mutation profiles and immunophenotypic features are not well characterized.

Design: Twenty-two PEL cases with comprehensive flow cytometric analysis were collected. For comparisons, 26 cases with reactive early erythroid precursors were included.

Results: There were 14 men and 8 women with a median age of 69 years (range, 37-81 years) and a median survival of 2.7 months. All (21) cases of PEL that underwent mutation analysis showed *TP53* mutations: 18 (85%) had one *TP53* mutation, 2

(10%) had two mutations, and 1 (5%) had three mutations. In total, 25 *TP53* mutations were detected and 19 (76%) were missense mutations. All patients had a complex karyotype with frequent -5/5q-, -7/7q-, and -17/17p-. Biallelic *TP53* loss-of-function manifested as *TP53* mutation in one allele and 17p/*TP53* region deletion in the other allele was seen in 76% of cases. The remaining (24%) cases showed no *TP53* region deletion, but most (75%) showed more than one *TP53* mutations. Using an NGS-based myeloid panel composed of 81 genes, 11 (55%) of 20 cases showed *TP53* as a sole mutation.

All cases exhibited mutant p53 expression patterns by immunohistochemistry; 16/21 (76%) had strong and uniform p53 expression (overexpression pattern); 5/21 (24%) had complete loss of p53 staining (truncated pattern). Among 5 cases with complete negative p53 protein, 3 had frameshift mutations, 1 had a nonsense mutation, and 1 had a splice-site mutation. For erythroid markers, CD71 was strongly positive in all cases. E-cadherin and CD117 were also positive, but often in a subset of cells consistent with early erythroid precursors. By flow cytometric analysis, the neoplastic cells were positive for CD36, CD71, CD117 and CD235. Compared to reactive erythroid precursors with uniform CD38 expression, 76% of PEL cases showed decreased or negative CD38. CD13, CD33, and uniform CD4 expression was more frequently seen in PEL cases than in reactive erythroid precursors. Although not increased in number, CD34-positive blasts in PEL showed an aberrant immunophenotype in 18 of 20 (90%) cases.

Conclusions: PEL is characterized by biallelic *TP53* gene alterations and aberrant p53 expression. Compared with reactive erythroid precursors, the neoplastic cells of PEL more frequently express CD13, CD33 and CD4 (uniform) and they often show decreased CD38. Aberrant CD34-positive blasts were frequently present in PEL cases but not in reactive erythroid hyperplasia.

881 Diagnostic Impact of Next Generation Sequencing Panels for Lymphoproliferative Neoplasms on Small Volume Biopsies

Fei Fei[1], Yasodha Natkunam[1], James Zehnder[1], Dita Gratzinger[2]
[1]Stanford Medicine/Stanford University, Stanford, CA, [2]Stanford University Medical Center, Stanford, CA

Disclosures: Fei Fei: None; Yasodha Natkunam: None; James Zehnder: None; Dita Gratzinger: None

Background: Despite the increasing application of next generation sequencing (NGS) panels in the clinical workup for lymphoproliferative disorders (LPDs), the diagnostic impact of NGS panels on small volume biopsies are largely unknown. The purpose of this study is to investigate the feasibility and utility of *IGH* and *TCR* rearrangements and targeted mutations by NGS panels for lymphoproliferative neoplasm in small volume biopsies.

Design: A retrospective review of NGS assays requested on small volume biopsies of LPDs from 2018 – 2021 identified 110 cases, consisting of 72 (65.5%) core needle biopsies and 38 (34.5%) fine needle aspirations (FNA). Stanford Actionable Mutation Panel for Hematologic neoplasms (Heme-STAMP), which detects single nucleotide variants (SNVs), short insertions and deletions, and selected gene fusions in over 160 genes recurrently altered in myeloid and lymphoid neoplasms was performed in 97 cases, *IGH*/*TCR* rearrangements were performed in 38 cases, and both assays in 24 cases. NGS-based *IGH* /*TCR* rearrangements detect clonal rearrangements in B- and T-cells to aid in the diagnosis of LPDs. Heme-STAMP and IGH/TCR assays were simultaneous performed on 60 cases. The findings were correlated with patient demographics and type of biopsy.

Results: The mean age was 60 years (range, 7 to 94), with a male to female ratio of 60 (54.5%) and 50 (45.5%) as summarized in Table 1. The mean tumor cell content was 55.4% (range, 1 – 99%). We found that Heme-STAMP, IGH/TCR assays or both confirmed/supported the final pathology diagnosis in 44 cases (40%), and led to the refinement of the diagnosis in a further 23 cases (21%). Among the latter 23 cases, 11 cases (48%) were mature T cell neoplasms and 6 cases (26%) were mature B cell neoplasms (Figure 2). A non-neoplastic diagnosis was confirmed in 3 cases (13%).

Table 1. Demographic and clinical characteristics.

Total sample	n = 110		
Age (Mean, Range)	60 (7 - 94)		
Gender, n (%)			
Male	60 (54.5%)		
Female	50 (45.5%)		
Sample type, n (%)			
Biopsy	72 (65.5%)		
FNA	38 (34.5%)		
Sample location, n (%)			
Lymph node	52 (47.3%)		
Soft tissue	16 (14.5%)		

GI	11 (10.0%)		
Lung	6 (5.5%)		
GU	5 (4.6%)		
ENT	4 (3.6%)		
Bone	4 (3.6%)		
Other	12 (10.9%)		
NGS panels			
Heme-STAMP, n (%)	97 (88.2%)		
IGH/TCR assay, n (%)	38 (34.5%)		
Heme-STAMP and IGH/TCR assay, n (%)	24 (21.8%)		
Tumor cell content, % (Mean, Range)	55.4% (1 - 95%)		

Abbreviations: FNA, fine needle aspiration; GI, gastrointestinal; GU, Genitourinary; ENT, ears, nose and throat; IGH, immunoglobulin heavy chain; TCR, T cell receptor.

Figure 1 - 881

Figure 1. Diagnostic impacts resulting from NGS.

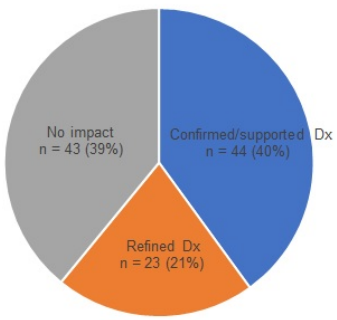

Figure 2 - 881

Figure 2. WHO classification categories for refined diagnosis according to results obtained by the NGS panel.

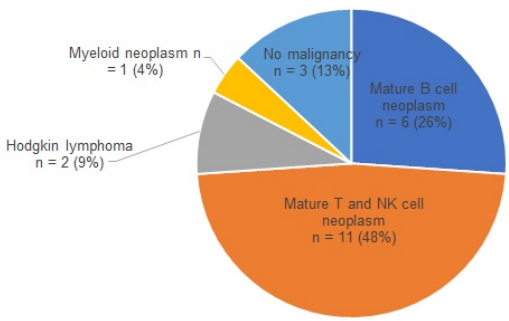

Conclusions: Overall, our study indicates that the implementation of the Heme-STAMP and/or *IGH/TCR* NGS assays on small volume biopsies benefits the diagnosis of lymphoproliferative neoplasms in most analyzed cases in the appropriate clinicopathologic context.

882 Small Volume Biopsy Diagnostic Yield at Initial versus Recurrence/Transformation of Follicular Lymphoma: A Retrospective Cyto-Heme Inter-Institutional Collaborative (CHIC) Study

Megan Fitzpatrick[1], Vandana Sundaram[2], Amy Ly[1], Ronald Balassanian[3], Srishti Gupta[4], Robert Hasserjian[5], Oscar Lin[6], Steven Long[3], Joshua Menke[7], Yasodha Natkunam[2], Roberto Ruiz-Cordero[3], Ashley Volaric[2], Linlin Wang[3], Kwun Wah Wen[3], Yi Xie[3], Sara Zadeh[2], Dita Gratzinger[8]

[1]Massachusetts General Hospital, Boston, MA, [2]Stanford Medicine/Stanford University, Stanford, CA, [3]University of California, San Francisco, San Francisco, CA, [4]University of Virginia, Charlottesville, VA, [5]Massachusetts General Hospital, Harvard Medical School, Boston, MA, [6]Memorial Sloan Kettering Cancer Center, New York, NY, [7]Stanford Health Care, Stanford, CA, [8]Stanford University Medical Center, Stanford, CA

Disclosures: Megan Fitzpatrick: None; Vandana Sundaram: None; Amy Ly: None; Ronald Balassanian: None; Srishti Gupta: None; Robert Hasserjian: None; Oscar Lin: *Consultant*, Hologic, Jansen; Steven Long: None; Joshua Menke: None; Yasodha Natkunam: None; Roberto Ruiz-Cordero: None; Ashley Volaric: None; Linlin Wang: None; Kwun Wah Wen: None; Yi Xie: None; Sara Zadeh: None; Dita Gratzinger: None

Background: Although surgical biopsy remains the gold standard for follicular lymphoma (FL) diagnosis, the use of small volume biopsies including fine needle aspiration (FNA) and needle core biopsy (NCB) has increased; yet no studies have compared diagnostic yield of these biopsies when performed for different clinical indications throughout the natural history of FL.

Design: We retrospectively identified FL workups from six institutions performed between 2012 and 2016. We included all workups that began with FNA+/- cellblock (CB) or NCB+/- FNA, performed for initial diagnosis or question transformation/recurrence. The primary intent of the study was to describe diagnostic yield of small volume biopsies for hypothesis generation. Diagnostic yield

was assessed by evaluating the mean number of biopsies per workup, the proportion of workups requiring >1 biopsy and the proportion with a specific diagnosis on initial biopsy, defined as a complete WHO diagnosis including histologic grade.

Results: We identified 676 clinical workups from 563 patients. 44% of the cohort was female with a mean age of 64 years. Compared to workups done for question FL transformation/recurrence, those done for initial FL diagnosis were significantly more likely to require >1 biopsy (p<0.01), had a higher mean number of biopsies per workup (1.7 vs 1.1, ASD=1.12) and a lower specific diagnosis rate (97/234, 41% vs 321/442, 73%) (Table 1, Figures 1-2).

At the time of initial FL diagnosis, beginning with NCB+/-FNA was associated with fewer biopsies per workup compared to FNA+/-CB (1.2 vs 1.9), fewer workups requiring >1 biopsy (22/94, 23% vs 116/140, 83%) and a higher specific diagnosis rate on initial biopsy (73/94, 78% vs 24/140, 17%). In contrast, at the time of question transformation/recurrence, beginning with NCB+/-FNA showed a similar mean number of biopsies per workup compared to FNA+/-CB (1.1 vs 1.2) and smaller differences in workups with >1 biopsy (17/279, 6% vs 31/163, 19%) and in specific diagnosis rate (222/279, 80% vs 99/163, 61%).

Table 1. Diagnostic Yield of Small Volume Biopsies by Clinical Indication

	Initial Diagnosis	Question transformation	Question recurrence	Statistical Comparison
Overall Number of biopsies per workup n Mean (SD) Median (IQR)	234 1.7 (0.62) 2.0 (1-2)	278 1.1 (0.33) 1.0 (1-1)	164 1.2 (0.38) 1.0 (1-1)	ASD=1.12[1]
Workups with >1 biopsy, n (%)	138 (59.0)	24 (9.0)	24 (15.0)	p=<0.01
Mean Biopsies per Workup by Initial Biopsy Type				
FNA (n=135) n Mean (SD) Median (IQR	66 2.0 (0.53) 2.0 (2-2)	29 1.1 (0.26) 1.0 (1-1)	40 1.2 (0.42) 1.0 (1-1)	NA
FNA+CB (n=169) n Mean (SD) Median (IQR)	74 1.8 (0.55) 2.0 (2-2)	59 1.2 (0.50) 1.0 (1-1)	35 1.2 (0.43) 1.0 (1-1)	NA
NCB+FNA (n=301) n Mean (SD) Median (IQR	80 1.2 (0.46) 1.0 (1-1)	151 1.1 (0.25) 1.0 (1-1)	69 1.1 (0.33) 1.0 (1-1)	NA
NCB (n=73) n Mean (SD) Median (IQR)	14 1.4 (0.63) 1.0 (1-2)	39 1.1 (0.27) 1.0 (1-1)	20 1.1 (0.31) 1.0 (1-1)	NA

Abbreviations: SD: standard deviation, IQR: interquartile range, FNA: fine needle aspiration, CB: cell block, NCB: needle core biopsy, ASD: absolute standardized deviation, NA: not assessed. [1]ASD values of 0.2, 0.5, and 0.8 correspond to small, moderate, and large differences, respectively.

Figure 1 - 882

Figure 1. Clinical Workups with 1 Biopsy or >1 Biopsy by Clinical Indication

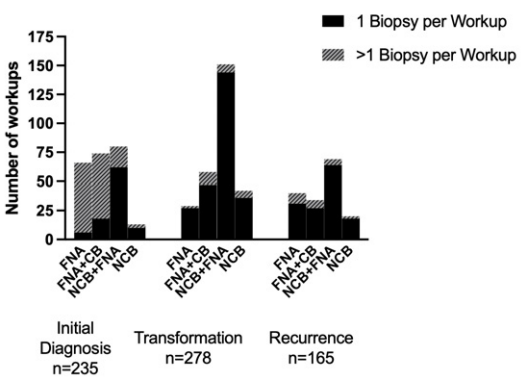

Abbreviations: FNA: fine needle aspiration, CB: cell block, NCB: needle core biopsy

Figure 2 - 882

Figure 2. Initial biopsy diagnostic categories by clinical indication

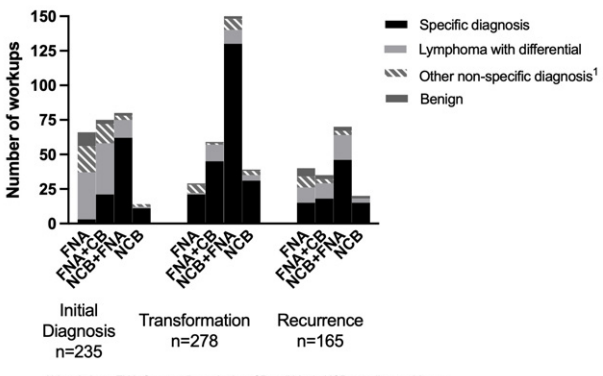

Abbreviations: FNA: fine needle aspiration, CB: cell block, NCB: needle core biopsy
[1]Includes suspicious for lymphoma, atypical, limited specimen and non-diagnostic

Conclusions: FNA provides a rapid and minimally invasive screening tool in distinguishing lymphoma from reactive and non-hematopoietic disease. Although in the initial diagnosis of FL, beginning with FNA was associated with more biopsies per workup relative to NCB, this suggests that FNA is effective at identifying patients in need of more extensive workup. In the setting of question transformation/recurrence, NCB and FNA showed similar diagnostic yield, suggesting that either biopsy alone may be sufficient.

883 Evaluating Novel Antigens for the Differentiation of Marginal Zone Lymphoma from Follicular Lymphoma by Flow Cytometry

Jonathan Fromm[1], Nathan Maris[1], Lorinda Soma[2], Sindhu Cherian[1], David Ng[3]
[1]University of Washington, Seattle, WA, [2]University of Washington Medical Center, Seattle, WA, [3]ARUP Laboratories, University of Utah, Salt Lake City, UT

Disclosures: Jonathan Fromm: *Grant or Research Support*, Merck; Nathan Maris: None; Lorinda Soma: None; Sindhu Cherian: None; David Ng: None

Background: Follicular lymphoma (FL) and marginal zone lymphoma (MZL) may resemble each other by morphology and can have immunophenotypic overlap. Consequently, novel antigens are required to help clarify the diagnosis. CD44, CD32, CD82, JAM-C, IRTA1, and TACI have displayed differential expression between the two lymphomas in prior immunohistochemical and genetic studies, and may represent potential targets for analysis by flow cytometry to help differentiate these two lymphomas.

Design: An initial screening cohort of FL, MZL and follicular hyperplasia (FH) cases (controls) were used to evaluate the novel antigens for differential expression. Based on these initial experiments and prior work in our laboratory, a 10-color combination was devised (CD40/kappa/CD75/CD19/lambda/CD44/ CD38/CD32/CD71/CD5) to comprehensively evaluate novel antigen expression levels and light scattering properties in larger test cohort of cases (33 FL, 27 MZL, and 20 FH). All experiments were performed on a modified 11-color LSR flow cytometer.

Results: In the initial screening cohort, JAM-C, IRTA1, and TACI had low fluorescence intensity and could not distinguish FL from MZL. CD82 was somewhat up-regulated in MZL cases, but it did not provide adequate separation from FL cases to be diagnostically useful. CD44, down-regulated in FL, showed the greatest separation between the two neoplasms; CD32, also down-regulated in FL, also could distinguish these lymphomas. The utility of CD44 (Figure 1) paired with CD32 (Figure 2) and forward scatter area (nominally increased in FL) were confirmed in the test cohort and a simple scoring algorithm was devised to predict the diagnosis. SSC-H was not helpful for separating the two lymphomas.

Figure 1 - 883

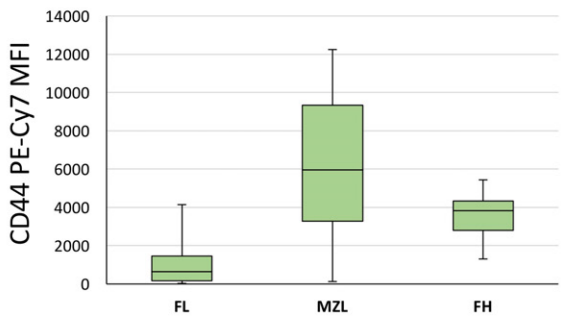

MFI boxplots of confirmation (test) cases for CD44. "Boxes" span from the first to the third quartile with the intermediate line representing the median, while "whiskers" span to the minimum and maximum values. Boxplots confirmed initial screening observations that FL generally downregulates and MZL generally upregulates CD44 expression relative to FH controls.

Figure 2 - 883

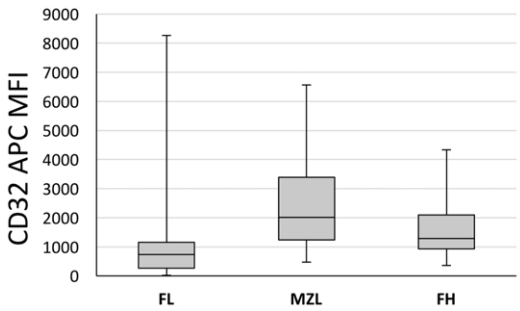

MFI boxplots of confirmation cases for CD32. By our qualifying criterion, CD32 is regarded as "significant" in distinguishing FL from MZL, as the FL third quartile and the MZL first quartile do not overlap. Note that the separation is not as great as with CD44 and CD32 is considered a complement to CD44 for the separation of FL from MZL.

Conclusions: CD44 expression, especially when evaluated alongside CD32, is a useful adjunct for distinguishing FL from MZL by flow cytometry.

884 Utility of T-Cell Receptor (TRBC1) Antibody JOVI-1 in Flow Cytometry Diagnosis of T-Cell Malignancies and Correlation with PCR Based T-Cell Receptor Gene Rearrangement: A Single Institution Experience

Mariam Ghafoor[1], Liam Nisenfeld[1], Ziver Sahin[1], Jerald Gong[2], Guldeep Uppal[3]
[1]Thomas Jefferson University Hospital, Philadelphia, PA, [2]Thomas Jefferson University, Philadelphia, PA, [3]Sidney Kimmel Medical College, Thomas Jefferson University, Philadelphia, PA

Disclosures: Mariam Ghafoor: None; Liam Nisenfeld: None; Ziver Sahin: None; Jerald Gong: None; Guldeep Uppal: None

Background: Recently discovered monoclonal IgG2a antibody (commonly available clone JOVI-1), targets T-cell receptor (TCR) β chain constant region 1 (TRBC1). It accurately determines the clonality of abnormal T-cells, aiding in the diagnosis of T-cell malignancies. Currently, molecular analysis, whether PCR or next generation sequencing (NGS), is considered to play an important role in the diagnosis of T-cell malignancies. These techniques, despite being accurate, are time consuming and require expertise. We analyzed utility of TRBC1 antibody flow cytometry in the diagnosis of T-cell malignancies.

Design: A retrospective evaluation of TRBC1 antibody analysis was performed on 25 cases of T-cell neoplasms and 25 control specimens from patients with no evidence of T-cell lymphoma/leukemia. Varieties of the specimens included were blood, bone marrow, lymph nodes, tissues, and body fluids. The following parameters were evaluated: age, gender, source of specimen, clinical history, phenotype, biopsy findings, and molecular results. The clone used was JOVI-1 from LifeSpan BioSciences Inc. (LSBio). Flow cytometry results were correlated with PCR-based clonality results. 24 of 25 positive cases were confirmed by either molecular analysis (21) or morphological interpretation (3). In the control group, we analyzed the expression of JOVI-1 in relation to CD3, CD4 and CD8 expression.

Results: In 24 out of 25 (96%) of the cases, the abnormal T-cells showed clonality by either completely negative or positive TRBC1 expression (95.9% average with a cut-off of >80%; Table 1, Image 1A). All the controls showed admixture of TRBC1 positive and negative cells consistent with the polyclonal expression (CD3: 60.2±6.8%, CD4: 57.1±4.5%; CD8: 67.5±9.8%), (Figure 1B). There was 100% correlation with molecular evidence of clonality and morphologic evidence of T-cell malignancies in 3 cases.

No.	Age	Gender	Source	JOVI +ve %	JOVI -ve %	Molecular Results (TCRG and/or TCRB)	Diagnosis
1	78	F	PB	7	93	positive	Cutaneous T-cell lymphoma (peripheral involvement)
2	80	F	PB	2	98	No follow-up	T-cell lymphoproliferative disorder, not further specified
3	81	M	PB	99	1	positive	LGL leukemia
4	56	F	PB	0	100	positive	LGL leukemia
5	73	F	PB	100	0	positive	T-CUS in AA
6	44	F	PB	48	52	positive	ATLL
7	90	M	PB	99	1	positive	LGL leukemia
8	10	M	orbital mass	4	96	positive	ALCL
9	52	M	pericardial fluid	0	100	Not done	T- LBL
10	70	M	PB	100	0	positive	AITL
11	86	F	PB	100	0	positive	PTCL
12	87	M	Pleural fluid	80	20	positive	AITL involving BM
13	44	M	PB	0	100	positive	LGL leukemia
14	67	F	PB	100	0	positive	AITL
15	69	F	BM	2	98	positive	LGL leukemia
16	39	F	BM	0	100	positive	LGL leukemia
17	33	F	PB	2	98	positive	LGL leukemia
18	86	F	LN	0	100	positive	AITL
19	22	F	Pleural fluid	0	100	positive	T-LBL
20	41	M	Pericardial fluid	83	17	positive	ATLL
21	38	F	LN	96	4	positive	PTCL NOS
22	81	M	BM	100	0	positive	LGL
23	89	F	BM	0	100	Not done	T-CUS in MDS/MPN
24	59	M	LN	89.2	10.8	Not done	PTCL, NOS
25	71	F	BM	0	100	positive	LGL Leukemia

Table1. Correlation of TRBC1 expression with molecular and clinical findings. (ALCL: Anaplastic large cell lymphoma; ATLL: Adult T-cell leukemia/lymphoma; AITL: Angioimmunoblastic T-cell lymphoma; AA: aplastic anemia; BM: Bone marrow; LGL: Large granular lymphocytes; LBL: Lymphoblastic lymphoma; LN: Lymph node; MDS/MPN: Myelodysplastic/myeloproliferative neoplasms; PB: Peripheral blood; T-CUS: T-cell clones of uncertain significance; TCRG: T-cell receptor gamma; TCRB: T-cell receptor beta; PTCL: Peripheral T-cell lymphoma)

Figure 1 - 884

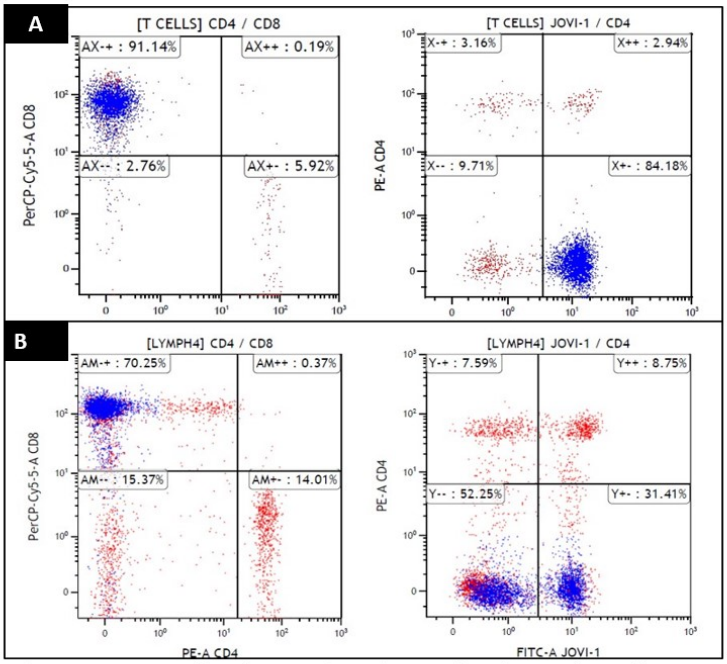

Figure 1, A. Monoclonal expression of JOVI-1 by abnormal T-cells;
B. Polyclonal expression of JOVI-1 by normal CD8 T-cells

Conclusions: The current pilot study included a variety of specimens including PB, BM, tissues, and body fluids. Most of the cases had TCR rearrangement results available and showed 100% concordance with flow cytometry results. Our results are concordant with studies by Horna et al. who also reported that the positive cases showed either complete positive or negative expression of TRBC1. TRBC1 flow cytometry analysis to determine T-cell clonality is 100% sensitive, effective, and a low-cost method of determining clonality. TRBC1 analysis has high potential of replacing laborious molecular testing in T-cell neoplasms expressing αβ receptor.

885 Effusion-Based Plasmablastic Lymphoma: A Clinicopathologic Review and Comparison to Solid Plasmablastic Lymphoma

Savanah Gisriel[1], Xiaojun Wu[2], Xueyan Chen[3], Mingyi Chen[4], Jenna McCracken[5], Endi Wang[6], Zenggang Pan[7]
[1]Yale School of Medicine, Yale New Haven Hospital, New Haven, CT, [2]Johns Hopkins School of Medicine, Baltimore, MD, [3]University of Washington, Seattle, WA, [4]UT Southwestern Medical Center, Dallas, TX, [5]Duke Health, Durham, NC, [6]Duke University Medical Center, Durham, NC, [7]Yale School of Medicine, New Haven, CT

Disclosures: Savanah Gisriel: None; Xiaojun Wu: None; Xueyan Chen: None; Mingyi Chen: None; Jenna McCracken: None; Endi Wang: None; Zenggang Pan: None

Background: Plasmablastic lymphoma (PBL) is a rare, highly aggressive B-cell lymphoma comprised of large neoplastic cells with a CD20-negative immunophenotype that occurs predominantly in immunocompromised patients. Effusion-based lymphomas with plasmablastic morphology and immunophenotype (EB-PBL) are extremely rare and it is unknown whether or not this lymphoma should be regarded as an entity distinct from conventional PBL that necessitates unique management.

Design: Ten cases of EB-PBL were collected from 2000-2020 across five different institutions and 20 cases of EB-PBL were identified in the literature; the clinicopathologic characteristics of the 30 total cases were summarized. Cases were considered EB-PBL if a human herpesvirus-8 (HHV-8)-negative lymphoma with plasmablastic morphology and immunophenotype presented solely as a body cavity effusion. Thirteen cases of conventional solid plasmablastic lymphoma (PBL) were included as a control cohort. The clinicopathologic characteristics of both cohorts are summarized in Table 1.

Results: The 30 cases of EB-PBL primarily affected males (M:F ratio of 2:1), with a median age of 71 years. Two of 19 (11%) and 2 of 9 (22%) of patients were positive for human immunodeficiency virus (HIV) and hepatitis C virus (HCV), respectively. The malignant effusions mostly involved the pleural and peritoneal cavities.

In this study, EB-PBL revealed similar clinicopathologic characteristics to solid PBL, apart from a statistically significant difference in EBER-ISH positivity (26% among EB-PBL and 69% among PBL, $p = 0.02$) (Table 1). Compared with solid PBL patients, EB-PBL patients had a statistically significant shorter median survival (2.5 months vs. 11 months, $p = 0.01$) (Figure 1).

	EB-PBL			**Solid PBL** (n=13)	***P*-value** (Total vs. solid)
	Our Study (n=10)	Literature (n=20)	Total Cases (n=30)		
Median age (years)	76.5 (60-94)	65 (29-91)	71 (29-94)	58 (32-82)	
Male/female (% male)	8/2 (80%)	12/8 (60%)	20/10 (67%)	12/1 (92%)	0.13
HIV+ (%)	1/6 (17%)	1/13 (8%)	2/19 (11%)	2/9 (22%)	0.57
HCV+ (%)	1/5 (20%)	1/12 (8%)	2/17 (12%)	0/7 (0%)	1.00
HHV-8+ (%)	0/10 (0%)	0/20 (0%)	0/30 (0%)	0/4 (0%)	1.00
EBER-ISH+ (%)	1/9 (11%)	6/18 (33%)	7/27 (26%)	9/13 (69%)	**0.02**
Follow-up (median, months)	3.5 (1-12)	1.5 (0.2-25.5)	2 (0.2-25.5)	8 (1-117.5)	
Overall survival (median, months)	4.5	1.9	2.5	11	**0.01**

Figure 1 - 885

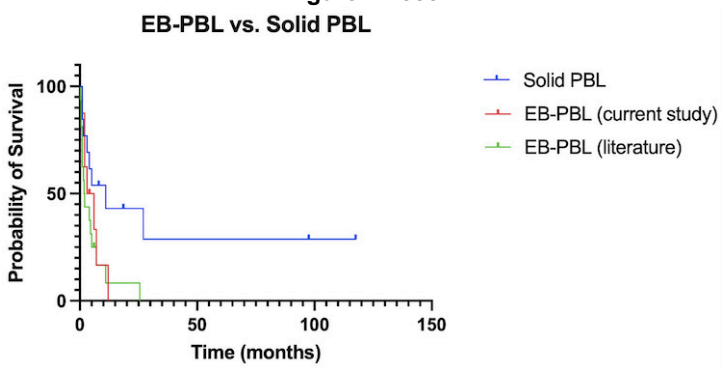

Conclusions: These findings suggest that EB-PBL may represent an entity distinct from solid PBL. Our results are limited by the rarity of both EB-PBL and PBL and the resultant small sample size. Further investigation with a larger sample size is warranted.

886 Burkitt-Like Lymphoma with 11q Aberration in Children Is Cytogenetically and Molecularly Heterogeneous

Shunyou Gong[1], Aida Richardson[1], Kai Lee Yap[1]
[1]*Ann & Robert H. Lurie Children's Hospital of Chicago, Chicago, IL*

Disclosures: Shunyou Gong: None; Aida Richardson: None; Kai Lee Yap: None

Background: Burkitt-like lymphoma with 11q aberration (BLL11q) is a recently recognized provisional entity with pathologic features closely resembling Burkitt lymphoma (BL) but lack *MYC* rearrangements. As its name implies, BLL11q is defined by recurrent chromosome (Chr) 11q alterations, requiring both proximal gains and telomeric losses per the updated WHO Classification. With a clinical course reportedly similar to BL, BLL11q has only a small number of cases published so far. Furthermore, it is also being debated whether BLL11q should be a separate entity, and whether proximal gain and distal loss are both needed for diagnosis. Lastly, the mutational profiles of BLL11q have not been well defined. Here we contribute to further characterize this entity clinically and pathologically and report the detailed cytogentic and molecular findings of 9 pediatric cases.

Design: 9 cases of *MYC*-negative Burkitt-like lymphoma cases with characteristic proximal gains and/or telomeric losses of Chr 11q were identified from our archive. Clinical, morphologic, and immunophenotypic data was collected. *MYC*, *BCL-2*, and *BCL-6* FISH, array comparative genomic hybridization (CGH), and pediatric oncomine next-generation sequencing panel were performed.

Results: 6 of 9 cases showed both proximal gains including at least 11q13-q23 and telomeric losses with minimally 11q24-qter. 2 cases had only proximal gains and 1 case revealed just telomeric loss. The cases included 8 males and 1 female, and age at initial diagnosis ranged from 6-22 years old. 8 of 9 cases occurred in head and neck areas (4 cervical lymph nodes, 2 tonsils and 2 nasopharyngeal masses). One case arose from the gastrointestinal tract (small bowel). All cases showed morphologic and immunophenotypic features resembling BL but lacked *MYC*, *BCL-2*, and *BCL-6* translocations. 8 cases had successful sequencing. None of them demonstrated mutational profiles of BL, specifically lacking alterations in *ID3*, *TCF3*, and *CCND3* genes, which altogether identify vast majority of BL cases. Instead, they showed recurrent mutations of *GNA13* (2/8), *TP53* (2/8), *PTEN* (2/8), *KRAS* (2/8), and non-recurrent mutations of *SMARCA4* and *KMT2D*.

Conclusions: BLL11q is more common in males, with remarkable predilection for head and neck areas. Although most cases harbor both proximal gain and distal loss of Chr 11q, fewer cases may have just one abnormality. The mutational profiles of BLL11q are largely different from those of BL, suggesting that it should be separately classified.

887 Age-Related Genomic Landscape of T-Lymphoblastic Leukemia/Lymphoma

Rohit Gulati[1], Rachel Kositsky[2], Lin Wang[1], Mary Ann Arildsen[3], Emily Mason[3], Ridas Juskevicius[3], Jonathan Galeotti[4], Yuri Fedoriw[4], Catalina Amador[5], Kacie Flaherty[6], Haley Martin[7], Sarah Ondrejka[8], Eric Hsi[9], Jean Koff[10], Colin O'Leary[10], Jennifer Chapman[11], Chad McCall[12], Amy Chadburn[13], Eric Tse[14], Dina Soliman[15], Jiong Yan[16], Andrew Evans[17], Chee Leong Cheng[18], Ilja Kalashnikov[19], Alexandra Kovach[20], C. Cameron Yin[21], Payal Sojitra[22], Neeraja Yerrapotu[23], Amber Landis[1], Cassandra Love[2], Utpal Dave[1], Kikkeri Naresh[24], Sandeep Dave, Magdalena Czader[25]

[1]Indiana University School of Medicine, Indianapolis, IN, [2]Duke University, Durham, NC, [3]Vanderbilt University Medical Center, Nashville, TN, [4]University of North Carolina, Chapel Hill, NC, [5]University of Miami, Miami, FL, [6]University of Nebraska Medical Center, Omaha, NE, [7]Massachusetts General Hospital, Boston, MA, [8]Cleveland Clinic, Cleveland, OH, [9]Wake Forest Baptist Health, Winston-Salem, NC, [10]Emory University, Atlanta, GA, [11]University of Miami, Miller School of Medicine, Miami, FL, [12]Carolinas Pathology Group/Atrium Healthcare, Charlotte, NC, [13]Weill Cornell Medical College, New York, NY, [14]The University of Hong Kong, Pokfulam, Hong Kong, [15]Hamad Medical Corporation, Doha, Qatar, [16]Laboratory Medicine Program, Departments of Anatomical Pathology, University Health Network and University of Toronto, Toronto, Canada, [17]University of Rochester Medical Center, Rochester, NY, [18]Singapore General Hospital, Singapore, Singapore, [19]University of Helsinki, Helsinki, Finland, [20]Keck School of Medicine of USC, Los Angeles, CA, [21]The University of Texas MD Anderson Cancer Center, Houston, TX, [22]Rutgers Robert Wood Johnson Medical School, New Brunswick, NJ, [23]Indiana University Health, Indianapolis, IN, [24]Fred Hutchinson Cancer Research Center, University of Washington, Seattle, WA, [25]Indiana University, Indianapolis, IN

Disclosures: Rohit Gulati: None; Rachel Kositsky: None; Lin Wang: None; Mary Ann Arildsen: None; Emily Mason: *Speaker*, Sysmex; Ridas Juskevicius: None; Jonathan Galeotti: None; Yuri Fedoriw: None; Catalina Amador: None; Kacie Flaherty: None; Haley Martin: None; Sarah Ondrejka: None; Eric Hsi: *Consultant*, Loxo, Seattle Genetics, Cytomx; *Grant or Research Support*, Abbvie, Eli Lilly; Jean Koff: *Grant or Research Support*, Oncternal Therapeutics, Viracta Therapeutics, Atara Biotherapeutics; *Advisory Board Member*, Janssen, MorphoSys, TG Therapeutics, Gamida Cell; Colin O'Leary: None; Jennifer Chapman: None; Chad McCall: None; Amy Chadburn: None; Eric Tse: None; Dina Soliman: None; Jiong Yan: None; Andrew Evans: None; Chee Leong Cheng: None; Ilja Kalashnikov: None; Alexandra Kovach: None; C. Cameron Yin: None; Payal Sojitra: None; Neeraja Yerrapotu: None; Amber Landis: None; Cassandra Love: None; Utpal Dave: None; Kikkeri Naresh: None; Sandeep Dave: *Stock Ownership*, Data Driven Bioscience; Magdalena Czader: *Speaker*, Beckman Coulter; *Grant or Research Support*, Beckman Coulter

Background: T-lymphoblastic leukemia/lymphoma (T-ALL/LBL) comprises 15% of pediatric and 25% of adult lymphoblastic leukemia/lymphoma cases. A number of driver genes such as *NOTCH1*, *CDKN2A* and *HOXA*, and aberrant activation of T-ALL/LBL-associated transcription factors have been previously identified in both pediatric and adult patients. Age is known to be a major determinant of survival following diagnosis; however, the biology underlying this association is not fully understood. To gain further insights into disease biology, we recruited 145 cases of T-ALL/LBL as part of the Atlas of Blood Cancer Genomes (ABC-G) initiative, a consortium consisting of 25 institutions.

Design: The study consists of 145 T-ALL/LBL cases with 64 matched normal controls. Formalin-fixed paraffin-embedded (FFPE) bone marrows and lymph nodes were included. All cases were reviewed centrally by an experienced panel of hematopathologists to ensure accurate diagnosis. Laboratory and clinical data including progression free survival, overall survival and treatment regimens were collected. Whole-exome DNA and RNA sequencing was performed using the Illumina platform, with mapping and alignment to GRCh38 assembly. Exonic variants were filtered using a set of paired normal samples and population-based databases to identify putative driver mutations, which were then aggregated at the gene level.

Results: Our cohort included children (age <15 years, 38%), adolescents/young adults (age 15-39, 48%) and older adults (age >40, 14%). We found a strong association between older age and prognosis (Fig. 1, P=0.0005, log-rank test). Nonsynonymous mutations and copy number changes were identified in 96% patients (Fig. 2). Previously reported genetic drivers including *NOTCH1*, *FBXW7*, *PFH6*, *PTEN*, *USP7*, *BCL11B*, *WT1* and *JAK3* occurred with similar frequency in our cohort. We found a number of additional potential drivers including *SPEN*, *ARID1B* and *DICER1*. The *FAT1*, *ARID1B* and *CXCR4* alterations correlated with a shorter survival (p<0.05). Gene expression analysis indicated a strong association of highly proliferative disease characterized by higher expression of genes related to cell cycle progression in pediatric population, whereas inflammatory response pathways were selectively upregulated in older patients.

Figure 1 - 887

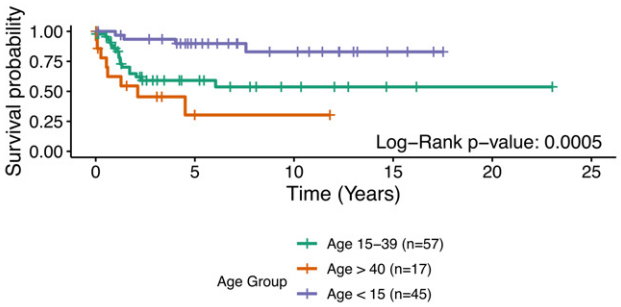

Figure 2 – 887

Conclusions: Our study, representing one of the largest comprehensive genomic and transcriptomic analyses of T-ALL/LBL, expands our understanding of its genomic landscape across age groups. It provides new evidence for biologically distinct disease subsets that are associated with age and prognosis in these patients.

888 Immunohistochemistry for CD123 is Specific for Littoral Cell Angiomas of the Spleen

Misty Hall[1], Pallavi Khattar[2], Rajeswari Jayakumar[3]
[1]Virginia Commonwealth University, Richmond, VA, [2]Icahn School of Medicine at Mount Sinai, New York, NY, [3]Virginia Commonwealth University Health System, Richmond, VA

Disclosures: Misty Hall: None; Pallavi Khattar: None; Rajeswari Jayakumar: None

Background: Vascular tumors are the most common primary neoplasms of the spleen and include hemangioma, splenic hamartoma, littoral cell angioma (LCA), sclerosing angiomatoid nodular transformation (SANT) and lymphangiomas to mention a few. LCAs are benign vascular tumors with malignant potential. LCAs have a distinct immunophenotypic pattern with endothelial and histiocytic markers and are positive for CD31, ERG, CD68, CD163 and CD21 and negative for CD8 and WT-1. Often a full panel of above mentioned stains are performed to distinguish LCA from other vascular tumors. CD123, also known as the alpha subunit of human interleukin-3 receptor is expressed on a variety of cells of the hematopoietic system and the dendritic cells of the spleen. We propose that CD123 is sufficient to distinguish LCA from other vascular tumors.

Design: 29 cases of splenic vascular lesions were identified from our archives (LCA=11, hemangioma=3, hamartoma =7, lymphangioma=2, SANT=7). One case had concurrent LCA and hemangioma. Immunohistochemistry for CD123 was performed on representative sections using a mouse monoclonal antibody at a dilution of 1:300.

Results: Review of the CD123 stained slides along with the hematoxylin and eosin slides for each case showed a strong and diffuse staining of the littoral cell angioma and negative staining in all other vascular lesions. CD123 also specifically stains only the LCA and normal littoral cells of splenic sinuses are negative. CD123 in normal spleen shows faint meshwork staining on the white pulp. CD123 also highlighted that LCAs arise in the periphery of the white pulp and identified early lesions (Figure 1). This also suggests the relationship between the pathogenesis of LCA and the dendritic cells of the spleen.

Figure 1 - 888

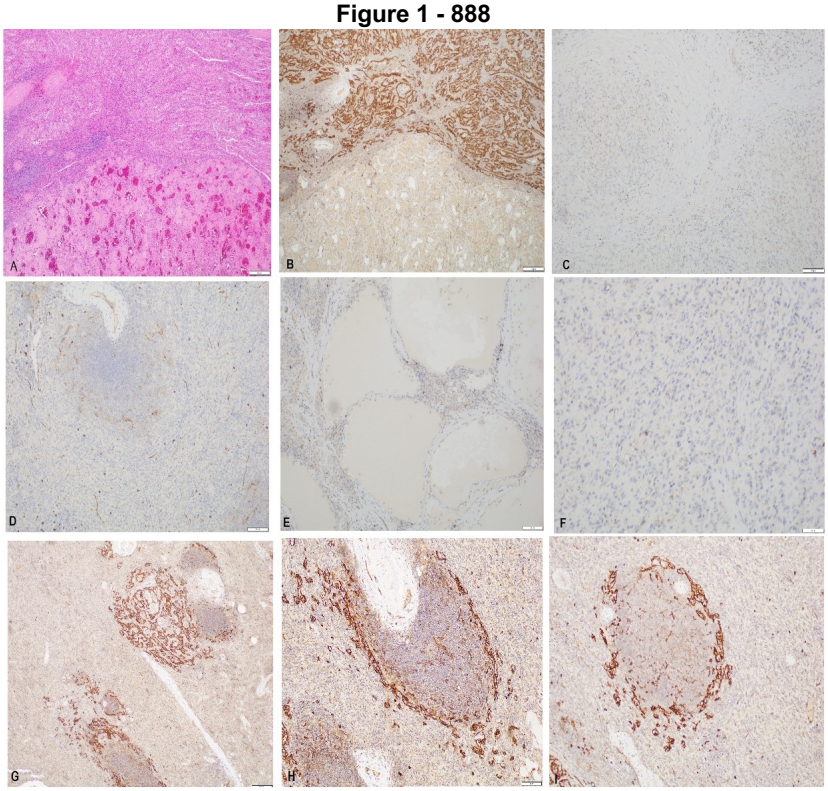

A. H&E image of concurrent Littoral cell angioma(lesion at the top) and hemagioma(lesion at the bottom); B. CD123 positive in LCA(lesion at the top) and negative in hemangioma; C. CD123 negative in SANT; D. CD123 showing faint meshwork staining in normal spleenic white pulp; E. CD123 negative in lymphangioma; F. CD123 negative in hamartoma; G,H and I. CD123 showing origin of LCA in the periphery of white pulp

Conclusions: CD123 specifically stains littoral cell angioma and enables distinction from other splenic vascular tumors and can replace the currently employed panel. It is negative on normal splenic sinusoidal littoral cells. This pattern of CD123 stain also favors an immunologic etiology for LCA.

889 Amyloidosis Associated with Low Grade B-Cell Lymphoma: A Report of 18 Cases

Zhihong Hu[1], C. Cameron Yin[2], Wei Wang[3], Pei Lin[2], William Glass[4], L. Jeffrey Medeiros[2], M. James You[2]
[1]The University of Texas Health Science Center at Houston, Houston, TX, [2]The University of Texas MD Anderson Cancer Center, Houston, TX, [3]McGovern Medical School at UTHealth, The University of Texas Health Science Center at Houston, Houston, TX, [4]The University of Texas Health Science Center at Houston/McGovern Medical School UTHealth, Houston, TX

Disclosures: Zhihong Hu: None; C. Cameron Yin: None; Wei Wang: None; Pei Lin: None; William Glass: None; L. Jeffrey Medeiros: None; M. James You: None

Background: Amyloidosis is rarely associated with low grade B-cell lymphomas. Thus far, the clinicopathologic features amyloidosis associated with low grade B-cell lymphomas are not well defined.

Design: We retrospectively reviewed cases of amyloidosis with associated low grade B-cell lymphoma during the interval of 1/1/2011- 8/1/2021. Clinicopathological findings, treatment regimens and patient outcomes were collected and analyzed. Liquid chromatography tandem mass spectrometry was used to type the amyloid.

Results: The study group is composed of 18 patients with amyloidosis with associated low grade B cell lymphomas. There were 13 F and 5 M; median age: 63.8 years (range, 46.4 – 83.0). Eight patients had history of malignancies, including breast carcinoma (n=2), squamous cell carcinoma (n=1), colonic adenocarcinoma (n=1), prostate carcinoma (n=1), hepatocellular carcinoma (n=1), DLBCL (n=1), and CLL/SLL (n=1). Seven patients had autoimmune diseases, including Sjogren syndrome (n=5), systemic lupus erythematosus (n=1), Hashimoto thyroiditis (n=1), and rheumatoid arthritis (n=1). The patients presented with a mass involving the lungs (n=8), skin (n=5), orbit (n=3), breast (n=1), submandibular gland (n=1), right knee (n=1), perinephric region (n=1), and bone marrow involvement (n=1). Four patients presented with lymphadenopathy. All 18 patients had resections of a mass containing amorphous material positive for Congo red stain with characteristic apple-green birefringence. Seventeen of 18 patients had extranodal MZL and the remaining patient had lymphoplasmacytic lymphoma. Amyloid typing was performed in six patients and in all a peptide profile consistent with immunoglobulin-derived light chain amyloidosis was identified (AL amyloid). No AA amyloid was detected. After mass resection, patients with localized masses were treated by observation (n=4), rituximab (n=3), radiation (n=2), autologous stem cell transplant (n=2), and RCHOP immunochemotherapy (n=1). With a median follow-up of 3.6 years (range, 0.2-14.2), two patients died of extensive disease, including one patient with lymphadenopathy and bone marrow involvement.

Conclusions: Amyloidosis associated with low grade B-cell lymphoma often occurs in patients who have other solid tumors and/or autoimmune diseases. Mass spectroscopy shows that the amyloid is of AL type. These patients who present with a localized mass have an indolent clinical course. A small subset of patients has extensive disease which portends a more aggressive clinical course.

890 PIM1 and CD79b Mutation Status Impacts the Outcome of Primary Diffuse Large B-cell Lymphoma of the CNS

Yuhua Huang, Jihao Zhou
[1]Sun Yat-sen University Cancer Center, Guangzhou, China, [2]Shenzhen People's Hospital, Shenzhen, China

Disclosures: Yuhua Huang: None; Jihao Zhou: None

Background: Primary diffuse large B cell lymphoma of the central nervous system (CNS DLBCL) is a rare malignancy with a distinct genetic profile. The molecular classification of systemic DLBCL does not seems to be applicable to predict patient outcomes in CNS DLBCL. Thus, a new molecular methodology is required for risk stratification and prognostic prediction.

Design: Forty cases of primary CNS DLBCL treated with high-dose methotrexate-based (HD-MTX) polychemotherapy were subjected to targeted exome sequencing covering 413 genes, including *MYD88*, *CD79b* and *PIM1*. In addition, transcriptional

sequencing was successfully performed in 6 cases. The relationship between the mutation patterns and clinicopathological features was further analyzed.

Results: Mutational analysis recognized two groups. The CDP (including *MYD88* and/or *CD79b* mutations) group was identified in 28 cases (70%), and the non-CDP (without *CD79b* and PIM1 mutations) group was identified in 12 cases (30%). The CDP group tended to occur in older patients (median age 57.0 vs. 48.4 y, p=0.015). Patients in the CDP group had a significantly longer 2-year overall survival (OS) (76% and 40%, p=0.0372) than those in the non-CDP group but not a significantly longer 2-year progression-free survival (PFS) (50.0% and 29%, p=0.078). Age less than 60 y, no c-Myc and Bcl2 double expression, and CDP subgroup were three independent risk factors indicating favorable OS. PyClone analysis revealed that tumor cells of the non-CDP group were genetically more heterogeneous than those of the CDP group. A total of 131 genes were significantly differentially expressed between these two groups. Gene Ontology (GO) enrichment analysis of these genes suggested that the major categories of biological processes that were significantly altered between these two groups were mainly related to intracellular metabolism mechanisms.

Variations	PFS				OS		
	No of Cases	Univariate	Multivariate		Univariate	Multivariate	
		P value	P value	Exp(95% CI)	P value	P value	Exp (95% CI)
Double expression by IHC: Yes vs No	15 vs 15	0.631	0.491	0.632	**0.036**	**0.044**	6.111
CDP vs nonCDP	27 vs 12	0.078	0.145	3.460	**0.037**	**0.025**	16.746
Age: <60 vs ≥60	25 vs 15	0.822	0.917	1.099	0.157	**0.036**	12.937
GCB vs nonGCB	11 vs 28	0.227	0.764	0.809	0.736	0.234	0.374
MCD vs nonMCD	12 vs 27	0.812	0.572	0.620	0.465	0.784	0.732

Figure 1 - 890

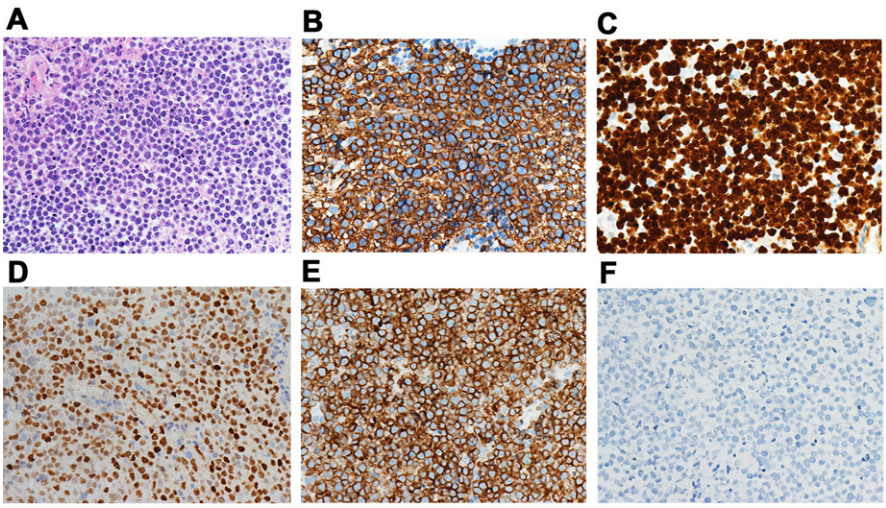

Figure 2 – 890

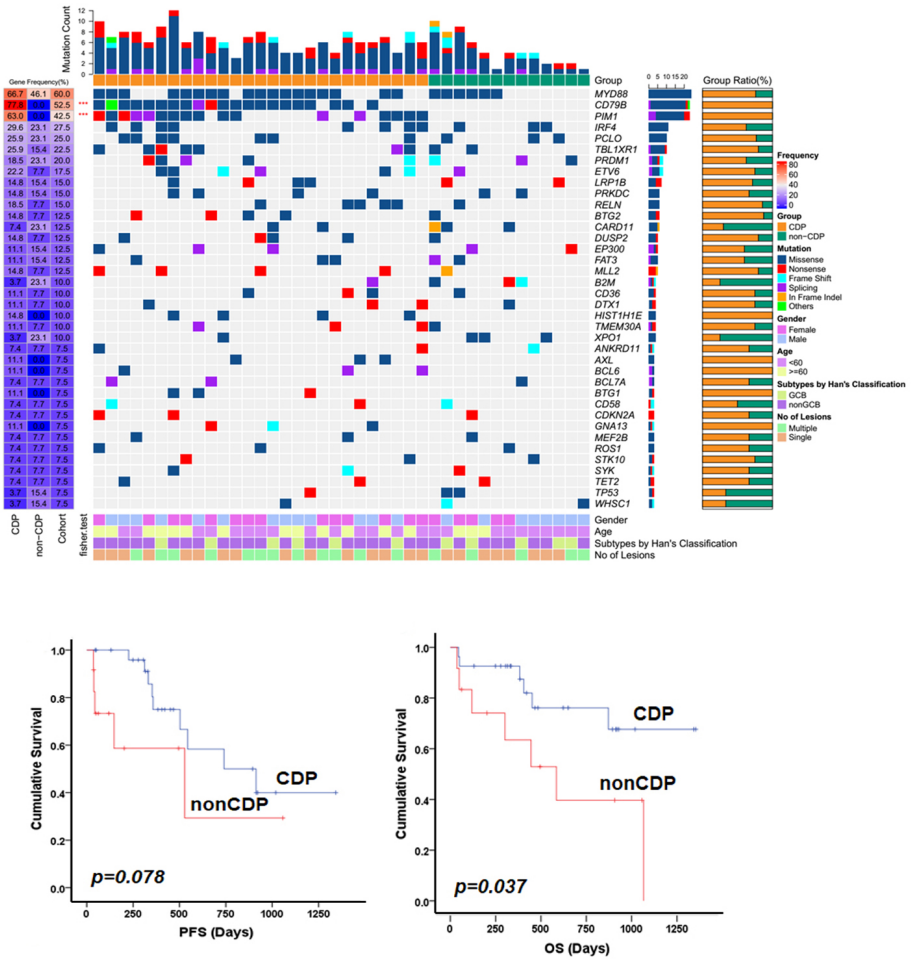

Conclusions: We developed a new molecular methodology to divide CNS DLBCL into CDP and non-CDP groups based on *CD79b* and *PIM1* mutational status. Patients without *PIM1* and *CD79b* mutations had unfavorable long-term survival after HD-MTX-based polychemotherapy, and the potential molecular mechanism awaits further investigation.

891 Clinicopathologic Features of Primary Central Nervous System (PCNS) Anaplastic Large Cell Lymphoma (ALCL): A Multicenter Study

Christopher Humphries[1], Robert Ohgami[2], Ken Young[3], Bangchen Wang[4], Francisco Vega-Vazquez[5], Mario Marques-Piubelli[5], Xiaoxian Zhao[6], James Rubenstein[2], Eric Hsi[1]

[1]Wake Forest Baptist Health, Winston-Salem, NC, [2]University of California, San Francisco, San Francisco, CA, [3]Duke University Medical Center, Chapel Hill, NC, [4]Duke University Medical Center, Durham, NC, [5]The University of Texas MD Anderson Cancer Center, Houston, TX, [6]Wake Forest Baptist Medical Center, Winston-Salem, NC

Disclosures: Christopher Humphries: None; Robert Ohgami: *Grant or Research Support*, Stemline Therapeutics; Ken Young: None; Bangchen Wang: None; Francisco Vega-Vazquez: None; Mario Marques-Piubelli: None; Xiaoxian Zhao: None; James Rubenstein: None; Eric Hsi: *Consultant*, Loxo, Seattle Genetics, Cytomx; *Grant or Research Support*, Abbvie, Eli Lilly

Background: Primary CNS ALCL is extremely uncommon with most cases reported as case reports. Thus, the clinical and pathologic characteristics are not well-characterized, including whether ALK-positivity of these primary lymphomas confers a favorable prognosis in the anatomically sensitive CNS.

Design: 12 primary CNS ALCL cases from four academic medical centers were retrospectively identified from 1998 to 2021. Demographic, pathologic, and outcome data and were extracted by medical record review. Progression free survival (PFS) and overall survival (OS) were evaluated (MedCalc, Ostend Belgium).

Results: The male to female ratio was 5.89 and the median age was 36 years (range, 4-73). Nine were ALK+ (75%) and three were ALK- (25%). ALK+ patients were younger than ALK- patients (median age of 27 vs. 67 years). CNS sites of disease included frontal lobe (5), parietal lobe (1), multifocal (4), pineal (1), and T12 spinal cord (1). In patients where CSF was sampled, 50% (5/10) had involvement by lymphoma. Pathologically, these had cytologic features compatible with the common pattern of ALCL. Six of nine ALK+ cases showed nuclear and cytoplasmic ALK staining compatible with an *NPM1-ALK* rearrangement; however, two cases showed a variant cytoplasmic pattern. One case had no staining pattern information. CD2,CD3, CD4, CD5, CD7, and CD8 were expressed in 66%, 40%, 100%, 0%, 50%, and 0% of cases tested. All seven cases in which more than one pan-T-cell marker was tested showed loss of at least one marker. The median follow-up time from initial diagnosis was 25 months. The 5-year OS rate was 77% and the 5-year PFS rate was 51%. Two patients succumbed to their disease (of ten known outcomes), while eight remained alive.

Table 1. Clinicopathologic Features of Primary Central Nervous System Anaplastic Large Cell Lymphoma

Case	Institution	Year of Diagnosis	Age	Gender	ALK Status	ALK Pattern	CNS Location	Leptomeninges	CSF	MTX with Therapy	Status from last F/U	Overall Survival (Months)
1	Site 1	2021	49	M	Positive	Nuclear and Cytoplasmic	Bilateral Hemisphere and Cerebellum	Y	Y	Y	Alive	5
2	Site 1	2003	27	M	Positive	Not Described	Occipital and Temporal	Unknown	Unknown	Unknown	Alive	2
3	Site 2	2004	4	M	Positive	Nuclear and Cytoplasmic	Pineal	Y	Y	N	Alive	200
4	Site 2	2006	28	M	Positive	Nuclear and Cytoplasmic	Cerebellum, Tentorium, Occipital, Midbrain	Y	N	N	Alive	98
5	Site 2	2018	13	F	Positive	Nuclear and Cytoplasmic	Frontal	Y	N	Y	Alive	31
6	Site 3	2010	6	M	Positive	Nuclear and Cytoplasmic	Frontal, Corpus Callosum	N	N	Y	Alive	18
7	Site 3	2005	19	M	Positive	Cytoplasmic	Spinal Cord	NA	Y	Y	Alive	68
8	Site 4	2013	61	M	Positive	Cytoplasmic	Frontal	Unknown	Y	Y	Dead	6
9	Site 4	2017	34	M	Positive	Nuclear and Cytoplasmic	Frontal	Unknown	N	Y	Alive	46
10	Site 4	2005	55	M	Negative	NA	Temporal, Cerebellum, Basal Ganglia, Brain Stem	N	Y	N	Dead	<1
11	Site 4	2021	73	M	Negative	NA	Parietal	Unknown	Unknown	Unknown	Unknown (No F/U)	NA
12	Site 4	2015	73	F	Negative	NA	Frontal	Unknown	N	Unknown	Unknown (No F/U)	NA

Note: ALK, anaplastic lymphoma kinase; CNS, central nervous system; CSF, cerebrospinal fluid; MTX, methotrexate; F/U, follow-up; Y, yes and/or involved; N, no and/or uninvolved

Figure 1 - 891

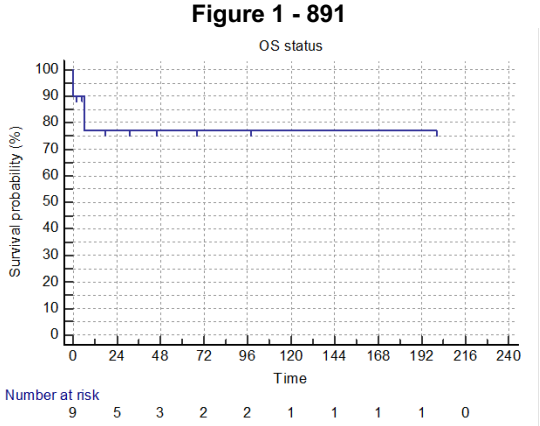

Figure 2 - 891

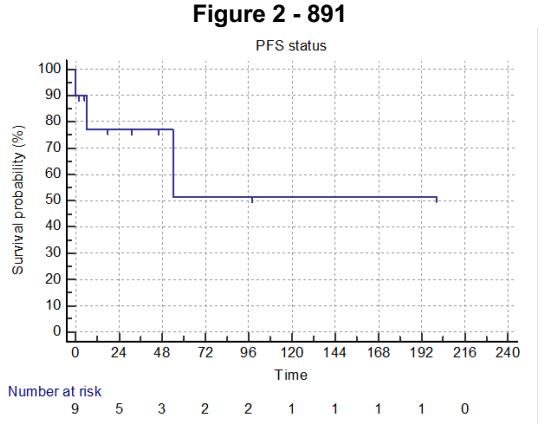

Conclusions: Primary CNS ALCL is rare and this is the largest reported series reported to date. Clinically, there is a marked male predominance and patients may present with localized or multifocal CNS disease. CSF involvement can be seen in 50% of cases. Pathologically, the common histologic pattern prevails. There appears to be a higher proportion of ALK+ primary CNS ALCLs (75%) compared to systemic ALCL (54%), which is also supported by a recent meta-analysis. Despite involving a sensitive anatomic site, our data indicate a relatively good 5-year OS. These data suggest that primary CNS ALCL may loosely parallel nodal disease with regard to ALK status and the associated clinicopathologic and prognostic features.

892 DNMT3A R882 Mutations Confer Unique Clinicopathologic Features in MDS Including a High Risk of AML Transformation

Majd Jawad[1], Michelle Afkhami[2], Yi Ding[3], Xiaohui Zhang[4], Peng Li[5], Mina Xu[6], Wei Cui[7], Young Kim[2], Stephanie Halene[8], David Viswanatha[1], Rong He[1], Dong Chen[1], Gang Zheng[1]

[1]Mayo Clinic, Rochester, MN, [2]City of Hope National Medical Center, Duarte, CA, [3]Geisinger Medical Center, Danville, PA, [4]H. Lee Moffitt Cancer Center & Research Institute, Tampa, FL, [5]ARUP Laboratories, University of Utah, Salt Lake City, UT, [6]Yale University, New Haven, CT, [7]University of Kansas Medical Center, Kansas city, KS, [8]Yale School of Medicine, New Haven, CT

Disclosures: Majd Jawad: None; Michelle Afkhami: None; Yi Ding: None; Xiaohui Zhang: None; Peng Li: None; Mina Xu: *Consultant*, Seattle Genetics, Pure Marrow, Blueprint Medicines; Wei Cui: None; Young Kim: None; Stephanie Halene: *Consultant*, FORMA Therapeutics; David Viswanatha: None; Rong He: None; Dong Chen: None; Gang Zheng: None

Background: DNMT3A mutations play a prominent role in clonal hematopoiesis with arginine (R)882 as a hotspot, and biochemical and in vitro studies suggest DNMT3A R882 mutations may have unique biological features when compared to non-R882 mutations. With the largest cohort of patients with DNMT3A R882 mutant MDS known to date, our multi-institution study set out to address whether DNMT3A R882 mutations confer unique clinicopathologic features in MDS.

Design: Targeted next generation sequencing data GENIE database (v.8.0, access date: April 10, 2020), and myeloid studies available in cBioPortal (access date: April 10, 2020) were retrieved. 124 patients with *DNMT3A* mutant MDS were identified by querying the clinical genomics database from seven institutions. Clinical information and follow-up data were obtained from the electronic medical records. This study was approved by the Institutional Review Boards (IRB) of all participating institutions.

Results: Shown with publicly accessible cancer genomics databases, the fraction of R882 mutations among all *DNMT3A* mutations is significantly higher in acute myeloid leukemia (AML) (53%) than myelodysplastic syndrome (MDS) (27%) or clonal hematopoiesis of indeterminate potential (CHIP) (10.6%) ($p < .001$), suggesting that as precursors of AML, MDS and CHIP harboring *DNMT3A* R882 mutations may have a higher risk of developing AML than those with non-R882 mutations. With clinical data collected from multiple institutions, *DNMT3A* R882 mutant MDS cases demonstrate more severe leukopenia (Table 1), enriched *SRSF2* and *IDH2* mutations (Figure 1), more cases with excess blasts (47% vs 22.5%, p=.004) (Table 1), markedly increased risk of AML transformation (25.8%, vs. 1.7%, p=.0001) (Figure 2a) and a worse progression-free survival (PFS) (Median 422 days vs.>1500, p=.009) (Figure 2b) than non-R882 mutant MDS group. *DNMT3A* R882 mutation is an independent risk factor for worse PFS by multivariate Cox proportional hazards model analysis (Figure 2c). The higher risk of AML transformation in *DNMT3A* R882 mutant MDS and the worse PFS are mitigated by coexisting *SF3B1* or *SRSF2* mutations (Table 1 and Figure 2d).

Table 1. Summary of the clinicopathologic features of *DNMT3A* (R882 vs. Non-R882) mutations in myelodysplastic syndromes.

	***DNMT3A* R882 (62)**	***DNMT3A* Non-R882 (62)**	**P Value**
Average age (range)	67 (29-91)	69 (23-86)	NS
Gender	39 M/23 F	32 M/30 F	NS
CBC*	41/54 (76%)	25/37 (67.5%)	NS
Anemia (Hg <10 g/dL)	17/54 (31%)	9/37 (24%)	NS***
Leukopenia (WBC<2 x 10^9/L)	32/54 (59%)	19/37 (51%)	NS
Thrombocytopenia (Plt <100 x 10^9/L)			
MDS-EB	29 (47%)	14 (22.5%)	0.004
Average bone marrow blast % (range)	8 (0-20)	1 (0-20)	
Cytogenetic Risk Group**	30/54 (55.5%)	39/58 (67%)	NS
Very good- good	11/54 (20%)	6/58 (10%)	NS
Intermediate	13/54 (24%)	13/58 (22%)	NS
Poor-very poor			
Average VAF%[#]	27 (2-49)	28 (5-66)	NS
Ring Sideroblasts	9/62 (35%)	15/62 (24%)	NS
Progressed to AML	15/58 (25.8%)	1/60 (1.7%)	0.0001
Survival[$]	29/58 (50%)	18/60 (30%)	0.02
Dead	29/58 (50%)	42/60 (70%)	
Alive			

M: male, F: Female, CBC: Complete blood counts, Hg: hemoglobin, WBC: white blood count, Plt: platelets, MDS-EB: Myelodysplastic syndrome with excess blasts, VAF: Variant allele frequency, AML: Acute myeloid leukemia, NS: not significant.

*CBC not available for 33 patients (8 R882, 25 non-R882), **Cytogenetic data not available for 12 patients. [#]VAF not available for 14 patients. [$]Survival data not available for 6 patients. ****p*=.02 by t-test comparing average white blood cell counts.

Figure 1 - 892

Figure 1

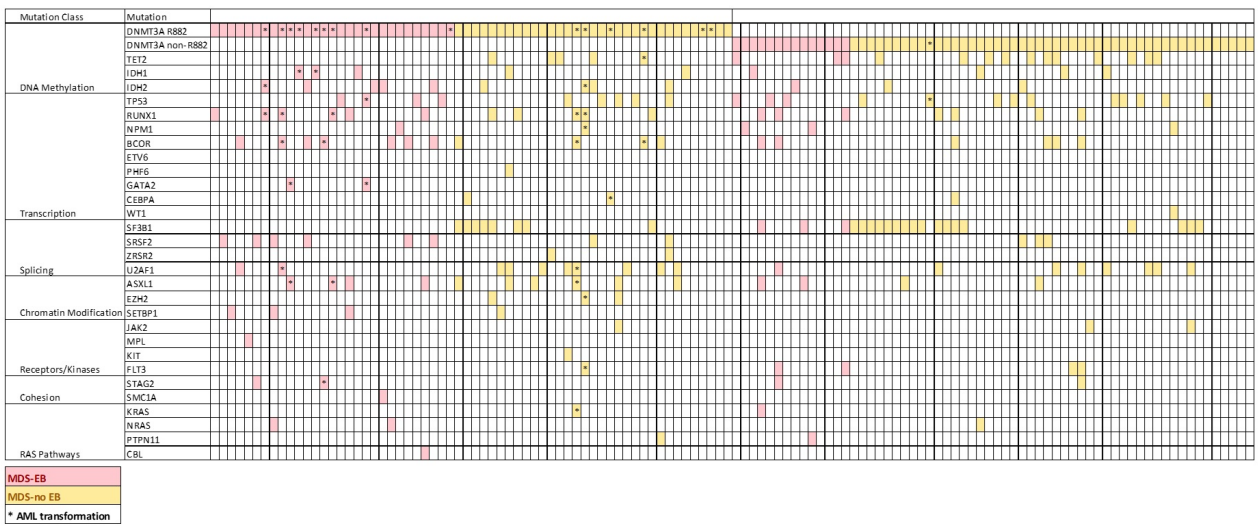

Figure 2 – 892

Figure 2

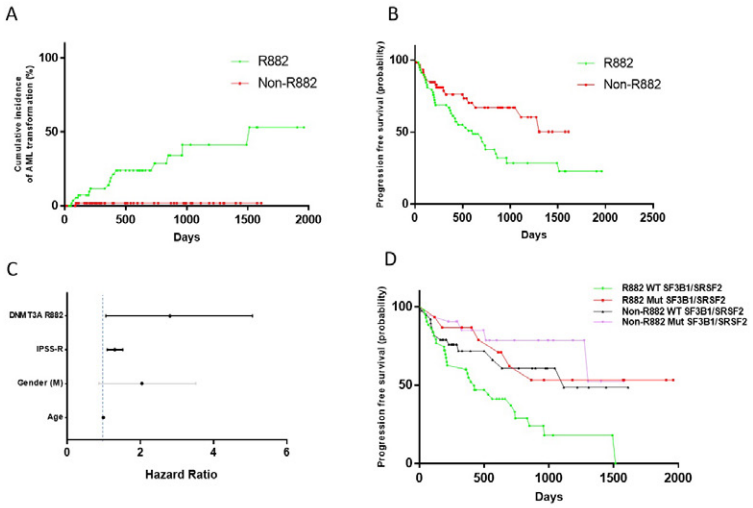

Conclusions: The unique clinicopathologic features of *DNMT3A* R882 mutant MDS shed light on the specific prognostic and therapeutic implications of *DNMT3A* R882 mutations.

893 No Bones About It: Disease Monitoring Using Next Generation Sequencing in Peripheral Blood for Patients with Myeloid Neoplasms

Nicole Joseph[1], Andrew Campbell[1], Yi Ding[1]
[1]Geisinger Medical Center, Danville, PA

Disclosures: Nicole Joseph: None; Andrew Campbell: None; Yi Ding: None

Background: Next Generation Sequencing (NGS) based mutation profiling on bone marrow aspirate plays a central role in aiding diagnosis, prognosis, and management of myeloid neoplasms, but has risks of procedure-related side effects. The aim of this project is to compare NGS results to determine if testing peripheral blood provides mutation information with comparable value as that of bone marrow biopsy.

Design: The results of NGS testing performed for patients with diagnosis or suspicion of myeloid disorders at our laboratory between December 2019 and June 2021 were reviewed. Patients with myeloid neoplasms and NGS of both blood and bone marrow specimens were selected. The NGS results included the variants, sequence depth, and their variant allele frequencies (VAF) from both sample types. Variants with a sequence depth < 500x or VAF < 5 % were excluded from the study.

Results: A total of 1793 consecutive hematologic NGS tests were reviewed and 52 paired of blood and bone marrow data is analyzed, including 27 cases with pathological diagnosis of myeloid neoplasms and 23 cases with cytosis or cytopenia without definitive diagnosis. 2 out of 52 patients with lymphoid neoplasms were excluded from this study. 85.2% (23/27) of blood NGS tests detected the same variants as the corresponding bone marrow NGS tests. 18.5% (5/27) had a subset of one or two variants detected only in the bone marrow (Figure 1). Impressively, there were 29.6% (8/27) cases where blood samples had more findings than bone marrow (Figure 2). Of the 10 cases of Acute Myeloid Leukemia (AML), blood testing identified all the variants detected in the 6 corresponding bone marrows. Five of these cases had variants detected in the blood that were not detected in the bone marrow, including two with *FLT3* mutations (Table 1). 4 cases of AML had a subset of one or two variants present only in bone marrow, including 2 cases with *FLT3* mutations. The VAF of these variants were ≤ 10.1%. Low VAF in initial bone marrow and

treatment between sample collection and testing may correlate with the absence of variants in blood, as in the 2 cases which had *FLT3* mutations in the bone marrow that were absent in the subsequent blood specimen.

Table 1: A Comparison of Gene Variants in Blood and Bone Marrow Across 10 Cases of AML

Case Number	1	2	3	4	5	6	7	8	9	10
Time Between Blood and Bone Marrow Testing (Days)	0	2	11	17	27	36	45	51	85	90
Number of Matching Variants	0/1	3/4	10/10	3/3	3/3	5/5	5/7	9/9	6/6	5/6
Non-Matching Variants Detected in Bone Marrow Only	*DDX41*	*MYC*					*FLT3* *NRAS*			*FLT3*
Variant Allele Frequency of Non-Matching Variant in Bone Marrow (%)	8.5	5.4					8.7 10			10.1
Number of Variants Detected in Blood Only			1		7	1		1		3
Variants Detected in Blood Only			*LUC7L2*		*FLT3* (2) *RUNX1* *KDM6A* *CEBPA* (3)	*FLT3*		*PTPN11*		*NRAS* *PTPN11* *WT1*

Figure 1 - 893

Figure 1: Number of matching gene variants from blood and bone marrow specimens in 27 patients with myeloid neoplasms who had NGS testing of both specimen types

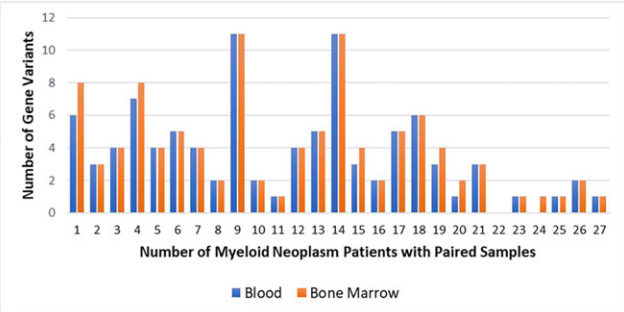

Figure 2 - 893

Figure 2: Number of gene variants found in blood specimens and not found in bone marrow specimens in 27 patients with myeloid neoplasm who had NGS testing of both specimen types

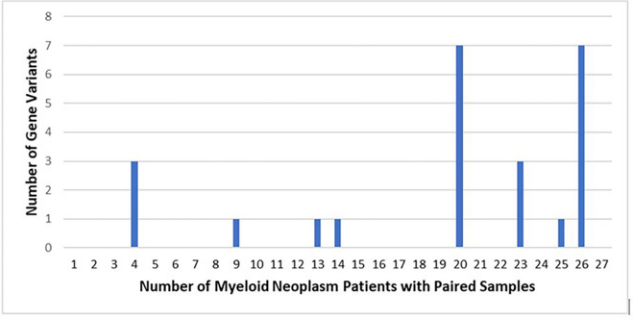

Conclusions: For patients with myeloid neoplasms, particularly AML, NGS of peripheral whole blood, as an alternative sample type, provides a less invasive and cheaper solution to reliably monitor disease status.

894 Heterogeneous Genomic Alterations of the IGH Locus and Their Clinical Implications in Multiple Myeloma

Amandeep Kaur[1], Barina Aqil[1], Juehua Gao[2], Madina Sukhanova[1], Yi-Hua Chen[2], Xinyan Lu[1]
[1]Northwestern University Feinberg School of Medicine, Chicago, IL, [2]Northwestern Memorial Hospital, Chicago, IL

Disclosures: Amandeep Kaur: None; Barina Aqil: None; Juehua Gao: None; Madina Sukhanova: None; Yi-Hua Chen: None; Xinyan Lu: None

Background: Multiple myeloma (MM) is cytogenetically heterogeneous. *IGH* translocations driving the abnormal expression of the partner fusion oncogenes is considered as a primary genomic alteration in the pathogenesis of MM. FISH based analysis to assess the *IGH* rearrangements on CD138+enriched plasma cells is a standard care. The *FGFR3-IGH, MAF-IGH* and *MAFB-IGH* fusions are high risk factors whereas the *CCND1-IGH* and *CCND3-IGH* fusions are standard risk factors. Most *IGH* fusions in MM are balanced however, unbalanced *IGH* fusions are frequent. The unbalanced fusions resulted from the 3'*IGH* deletion is of clinical importance, and the 5'*IGH* deletion is not well studied and often could be interpreted as physiological events due to the somatic V-D-J recombination of the *IGH* locus.

Design: To investigate the heterogeneous genomic alterations of the *IGH* locus and reevaluate the clinical significance of the 5'*IGH* deletions, we retrospectively analyzed the FISH results from a cohort of 1043 clinical MM cases that were tested using the *IGH* break apart and/or the *CCND1/MYEOV-IGH, FGFR3-IGH, MAF-IGH, MAFB-IGH, CCND3-IGH, MYC-IGH* duel color duel fusion probes at our institution.

Results: We identified 357 cases (34.2%) with *IGH* rearrangements including 225 balanced and 132 unbalanced which have been further described in Table 1. In addition, 43 cases showed a deletion of the entire IGH locus (or loss of chromosome 14) and 19 cases showed a gain of the *IGH* locus (or gain of chromosome 14). In the 5'*IGH* deleted group, most cases showed standard risk *IGH* fusions including CCND1-IGH (n=61) and CCND3-IGH (n=5); the high risk *IGH* fusions detected in 10 cases whereas, 19 remained to be unknown fusion partners. In addition, a partial deletion if the 5'IGH was observed in 6 cases, likely represents the physiological events with no known clinical significance.

Total IGH rearranged (n=357)	**Balanced group n=225 (63%)**	**Unbalanced group n=132 (37%)**	
		3'*IGH* deletion n=36 (27.3%)	**5'*IGH* deletion n=96 (72.7%)**
CCND1-IGH	n=129 (12.3%)	n=0	n=61 (62.5%)
FGFR3-IGH	n=22 (2.1%)	n=12 (33.3%)	n=2 (2.1%)
MAF-IGH	n=13 (1.2%)	n=0	n=4 (4.2%)
MAFB-IGH	n=13 (1.2%)	n=1 (2.7%)	n=4 (4.2%)
MYC-IGH	n=10 (0.9%)	n=0	n=1 (1%)
CCND3-IGH	n=6 (0.5%)	n=0	n=5 (5.2%)
Unknown fusion partner	n=32 (3%)	n=23 (63.8%)	n=19 (19.8%)

Conclusions: Our data demonstrated the cytogenetically heterogeneity of the *IGH* locus in MM, one third of the *IGH* translocations are unbalanced. The 3'*IGH* deletions are highly associated with high risk *IGH* fusions in MM, and the 5'*IGH* deletions are highly associated with the *CCND1-IGH* fusion. The 5'*IGH* deletions should not be interpreted as physiological events and all should be further assessed for fusion partners. The identification of the high frequency of the *CCND1-IGH* in 5'*IGH* deleted MM, could be clinically relevant for such patients to be eligible for clinically trials to receive targeted therapy.

895 Next-generation Sequencing Revealed Frequent TP53 mutation in Mantle Cell Lymphoma with Enhancer of Zeste Homolog 2 (EZH2) Expression

Do Hwan Kim[1], Shaoying Li[1], Rashmi Kanagal-Shamanna[1], Roberto Miranda[1], Francisco Vega-Vazquez[1], L. Jeffrey Medeiros[1], Chi Young Ok[1]
[1]*The University of Texas MD Anderson Cancer Center, Houston, TX*

Disclosures: Do Hwan Kim: None; Shaoying Li: None; Rashmi Kanagal-Shamanna: None; Roberto Miranda: None; Francisco Vega-Vazquez: None; L. Jeffrey Medeiros: None; Chi Young Ok: None

Background: Our group recently reported that expression of the enhancer of zeste homolog 2 (EZH2) is present in 38% of mantle cell lymphoma (MCL) patients and is associated with an inferior overall survival. To further elucidate genetic landscape of MCL with EZH2 expression (EZH2+ MCL), we conducted 11-gene panel next-generation sequencing (NGS).

Design: From our previously published dataset of MCL, DNA was extracted from formalin-fixed, paraffin-embedded tissue (n=80). Library preparation was performed using customized 11-gene (*ATM, BIRC3, CCND1, KMT2C, KMT2D, NOTCH1, NOTCH2, RB1, TP53, TRAF2* and *UBR5*) NGS panel and then subjected to the NovaSeq6000. Data analysis and annotation of mutation was conducted using vendor-provided tool. Clinicopathologic information was used from the published data.

Results: Total 76 cases passed quality check. In all cases, the most common mutation detected was *ATM* (56.4%), followed by *TP53* (32.1%) and *CCND1* (21.8%). There were 32 and 44 patients in EZH2+ and MCL without EZH2 expression (EZH2– MCL), respectively. At least one mutation was detected in 93.8% and 86.3% of EZH2+ and EZH2– MCL, respectively. The median number of mutations per case was similar (2 and 1.5). EZH2+ MCL cases demonstrated significantly higher frequency of *TP53* mutation compared with EZH2– MCL (43.8% vs. 20.5%, respectively, p=0.03). The median *TP53* mutant allelic frequency (MAF) was similar between the two groups (median MAF: 44% and 33%, respectively, p=0.56). Mutation frequency in the remaining genes was not significantly different between the two groups.

In all cases, *TP53*-mutated MCL patients demonstrated inferior overall survival (OS) compared with patients with wild-type *TP53* (p<0.01). In EZH2+ and EZH2– MCL subgroup analysis, *TP53*-mutated MCL patients showed a trend of worse outcome but it was not statistically significant (p=0.2 and p=0.1, respectively). However, in 4 group analysis based on EZH2 expression and *TP53* mutation status, EZH2+ MCL with wild-type *TP53* and EZH2– MCL with *TP53* mutation showed similar OS (median OS: 6.3 and 6.8 years, respectively) and cases with both EZH2 expression and *TP53* mutation showed the worst outcome (median OS: 2.6 years). In contrast, EZH2– MCL with wild-type *TP53* showed the best outcome (median OS: 11.7 years) (p<0.01).

Figure 1 - 895

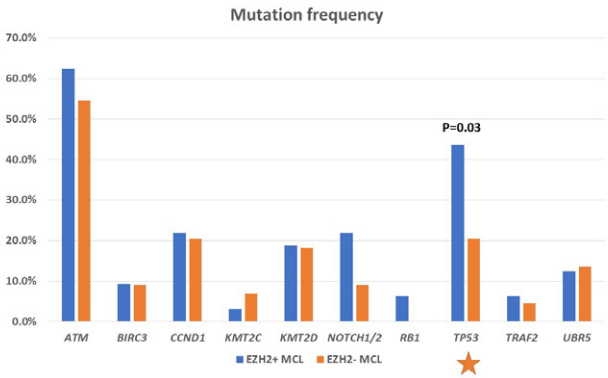

Figure 2 - 895

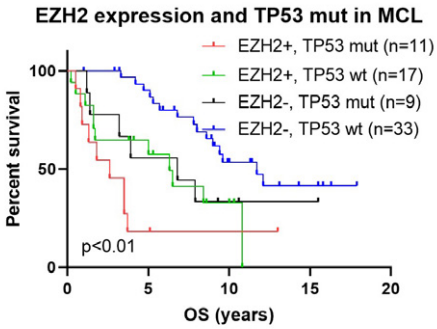

Conclusions: Among the assessed 11 genes, *TP53* mutation was significantly more frequent in EZH2+ MCL. Furthermore, we identified that EZH2 expression and *TP53* mutation may have a synergistic negative effect on the OS of MCL patients.

896 Acute Leukemias with Complex Karyotype Show a Similarly Poor Outcome Irrespective of Mixed, Myeloid and Lymphoblastic Immunophenotype: A Study from the Bone Marrow Pathology Group

Timothy Kirtek[1], Weina Chen[1], Dorottya Laczko[2], Adam Bagg[3], Prasad Koduru[1], Kathryn Foucar[4], Meredith Nichols[5], Heesun Rogers[5], Wayne Tam[6], Attilio Orazi[7], Eric Hsi[8], Robert Hasserjian[9], Daniel Arber[10], Olga Weinberg[1]
[1]UT Southwestern Medical Center, Dallas, TX, [2]Perelman School of Medicine, Hospital of the University of Pennsylvania, Philadelphia, PA, [3]University of Pennsylvania, Philadelphia, PA, [4]University of New Mexico, Albuquerque, NM, [5]Cleveland Clinic, Cleveland, OH, [6]Weill Cornell Medicine, New York, NY, [7]Texas Tech University Health Science Center, El Paso, TX, [8]Wake Forest Baptist Health, Winston-Salem, NC, [9]Massachusetts General Hospital, Harvard Medical School, Boston, MA, [10]University of Chicago, Chicago, IL

Disclosures: Timothy Kirtek: None; Weina Chen: None; Dorottya Laczko: None; Adam Bagg: None; Prasad Koduru: None; Kathryn Foucar: None; Meredith Nichols: None; Heesun Rogers: None; Wayne Tam: None; Attilio Orazi: None; Eric Hsi: None; Robert Hasserjian: None; Daniel Arber: None; Olga Weinberg: None

Background: Mixed phenotype acute leukemia (MPAL) is a heterogeneous group of acute leukemias characterized by leukemic blasts that express markers of multiple lineages. The WHO classification of MPAL excludes AML with myelodysplasia related changes (AML-MRC), including those with complex karyotype (CK), from a diagnosis of MPAL. Abnormal karyotype is frequent in MPAL and rate of CK in acute leukemias with mixed phenotypes is reported as 19-32%. The clinical and genetic features of MPAL with CK remain poorly characterized. This study aims to further characterize the genetic features of MPAL with CK in comparison to cases of AML and ALL with CK.

Design: Cases of newly diagnosed MPAL, AML, and B and T-ALL were collected from 8 institutions. The clinical, hematologic, pathologic, cytogenetic, and molecular data were reviewed where available. Variables including age, blood counts, bone marrow findings, genetic features, treatment with stem cell transplant, and overall survival (OS) were used to compare outcomes among the 3 groups. Complex karyotype was defined as having ≥3 unrelated abnormalities. OS was defined as time from diagnosis to death or last known follow up. Statistical analyses were performed using GraphPad Prism v9.2.0. Log-rank test was used to compare overall survival (OS) between groups.

Results: 23 cases of MPAL, 10 cases of ALL and 145 AML with CK were included. Among MPAL, 16 cases were B/myeloid, 5 T/myeloid, and 2 without lineages specified. Patients with ALL were younger on average than MPAL or AML (p=0.0003) and had higher bone marrow cellularity (p=0.0019) and blast percentage (p=0.0045) than AML. Cases of AML showed higher *TP53* mutation rates than that of ALL (p=0.012), but no significant difference when compared to MPAL (p=0.241). The most frequently mutated gene in MPAL was *FLT3* and was *TP53* in AML and ALL. Survival analysis did not show a statistically significant difference in OS between any group (Figure 1, p=0.372). Similarly, no significant difference in OS was identified among the subset of AML, ALL and MPAL patients lacking *TP53* mutation (p=0.275).

Table 1	MPAL	AML	ALL	P-value
Age (years)	60.49	66.65	46.78	0.0003
WBC (x10^9/L)	23.50	12.49	9.875	0.3045
Hgb (g/dL)	8.4	8.49	9.6	0.1205
Platelet (x10^9/L)	69.24	72.0	40.29	0.5691
PB Blast %	30.85	19.49	34.14	0.0764
BM Cellularity %	81.11	70.97	95.0	0.0019
BM Blast %	58.19	53.00	79.22	0.0045
General mutation rate (average # per case)	2.4	2.1	2.1	0.498
Cases with *TP53* mutation (%)	50	40	76	0.012

Figure 1 - 896

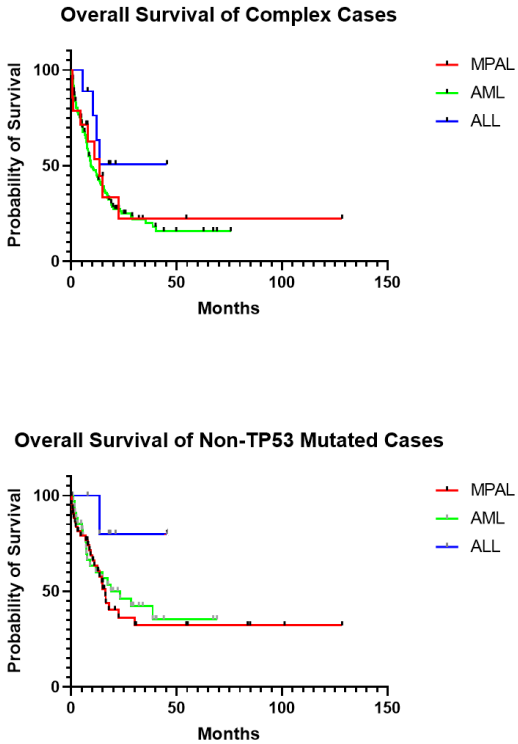

Conclusions: Our results suggested that acute leukemias with complex karyotype show a similarly poor outcome irrespective of lineage differentiation (mixed lineage, myeloid, or lymphoblastic) and mutations in *TP53*. Our results support the exclusion of immunophenotypic MPAL with CK from the MPAL category and their inclusion within AML-MRC.

897 The Genomic Landscape of Intravascular Large B Cell Lymphoma

Rohan Kodgule[1], Jie Chen[2], Pooja Khonde[3], Patrick Cimino[4], Eric Duncavage[5]
[1]Washington University School of Medicine, St. Louis, MO, [2]University of Nebraska Medical Center, Omaha, NE, [3]Barnes-Jewish Hospital/Washington University, St. Louis, MO, [4]University of Washington - Harborview, Seattle, WA, [5]Washington University in St. Louis, St. Louis, MO

Disclosures: Rohan Kodgule: None; Jie Chen: None; Pooja Khonde: None; Patrick Cimino: None; Eric Duncavage: None

Background: Intravascular large B cell lymphoma (IVLBCL) is a rare and aggressive type of extranodal diffuse large B-cell lymphoma (DLBCL) characterized by the presence of large B cells inside the lumen of blood vessels without substantial nodal or tissue involvement. The diagnosis of IVBCL is challenging as patients with IVLBCL usually present with non-specific clinical symptoms and obtaining a biopsy of involved vessels is difficult and many cases of IVLBCL are diagnosed at autopsy. The genomic landscape of IVBCL is poorly understood due to its rarity and difficulty in obtaining tissue specimens. In this study, we performed exome sequencing on six cases of IVLBCL patients.

Design: Formalin-fixed paraffin-embedded (FFPE) tumor and normal tissue were obtained from six patients who were diagnosed with IVLBCL either pre or postmortem. Slides were reviewed by a hematopathologist (ED) and neuropathologist (JC and PC) to confirm the diagnosis. Areas involved by IVLBCL were microdissected using 1mm core punches. Extracted DNA from each case was made into 4 independent exome libraries which were pooled and sequenced on an Illumina NovaSeq 6000. Sequence data were analyzed using the Illumina Dragen workflow and annotated using Annovar. Copy number alterations were called using CNVkit.

Results: Mean exome coverage per patient was 144.9x. Five cases from our cohort of IVLBCL had genetic aberrations that are part of the 'MCD type' of DLBCL which is characterized by *MYD88*L265P and *CD79B* mutations and the activated B-cell type. Across cases, the most common recurrent mutations were in *CD79B*, *SETD1B* (5 out of 6 cases), *MYD88* (p.L265P), *ETV6*, *OSBPL10*, *RAC2* (4 out of 6 cases), and *TBL1XR1*, *KLHL14*, and *BTG2* (3 out of 6 cases). Activation-induced cytidine deaminase (AID) is implicated in B cell lymphomagenesis. Mutations in PIM1 and *IGLL5* were detected in our data which are known targets of AID-related Somatic hypermutations. Copy number analysis showed no recurrent copy number gains or losses across cases.

Conclusions: Here we present data on the genomic landscape of IVLBCL using exome sequencing from FFPE tissue. To our knowledge, this is the first study using exome sequencing to characterize IVLBCL in FFPE tumor samples. Our data demonstrate that the mutation spectrum of IVLBCL is most like the MCD type of DLBCL which has been shown to have a higher incidence of extranodal involvement compared to other DLBCL subtypes.

898 Morphology and Immunophenotype Correlation Study of Peripheral Blood from COVID19 Patients

Kevin Kuan[1], John Liu[2], Mohammad Barouqa[3], Yang Shi[1], Xuejun Tian[1], Yanan Fang[1], Xiaoling Guo[1], Yanhua Wang[4]
[1]Albert Einstein College of Medicine, Montefiore Medical Center, Bronx, NY, [2]Rensselaer Polytechnic Institute, Bronx, NY, [3]Mayo Clinic, Rochester, MN, [4]Albert Einstein College of Medicine, Bronx, NY

Disclosures: Kevin Kuan: None; John Liu: None; Mohammad Barouqa: None; Yang Shi: None; Xuejun Tian: None; Yanan Fang: None; Xiaoling Guo: None; Yanhua Wang: None

Background: Since the first case of COVID19 infection in 2019, this RNA virus has led an unprecedented pandemic that infected more than 232 million people. Although the disease is studied extensively, much remains poorly understood. Here, we performed the first correlation study on the peripheral blood morphology and immunophenotype of the white blood cells (WBCs) from COVID19 patients.

Design: A total of 52 samples from COVID19 patients and 15 blood samples as control group were analyzed. COVID19 patients were divided into two groups based on clinical severity, severe (respiratory failure) or non-severe (hospitalized but stable). The controls were the patients with negative COVID19 results by PCR and antibody tests. The WBC morphology was examined either by blood smear review or via CellaVision DM analyzer captured images. Navios flow cytometer and Beckman Kaluza C software were used for immunophenotype analysis. Two-tailed T-test was performed on the COVID19 groups and the control group

Results: Almost all COVID19 patients showed marked neutrophilia and lymphopenia on the CBC tests. Morphologically, the neutrophils showed irregularities like hypogranulation, toxic granules and pseudo Pelger-Huet anomaly (Fig 1A). In severe COIVD19 group, there was an increase in neutrophils with immatures phenotypes, showing CD33 positivity while CD10, CD13 and CD16 negative (Fig 1B). Conversely, the CD10(+) mature neutrophils aberrantly expressed CD56 (Fig 1B). The percentage of CD56(+) neutrophils was significantly higher in both COVID19 groups, suggesting a stronger cellular adhesion and interaction.

The monocytes from the COVID19 patients had increased cytoplasm with cytoplasmic protrusion and vacuolization (Fig 2A). Phenotypically they were positive for CD13, CD33, CD38 and HLA-DR. The lymphocytes were also atypical, including increased cytoplasm with large granules and vacuoles. Phenotypically, they are activated, expressing CD38, HLA-DR, and mainly α/β subtype. Giant platelets with cytoplasmic vacuoles and projections were easily seen.

Platelet aggregations were observed (Fig 2B). These platelets were CD45(-) and expressed CD61 at lower-than-normal intensity, while expressing increased CD42b intensity when compared to the control group on a log scale.

Figure 1 - 898

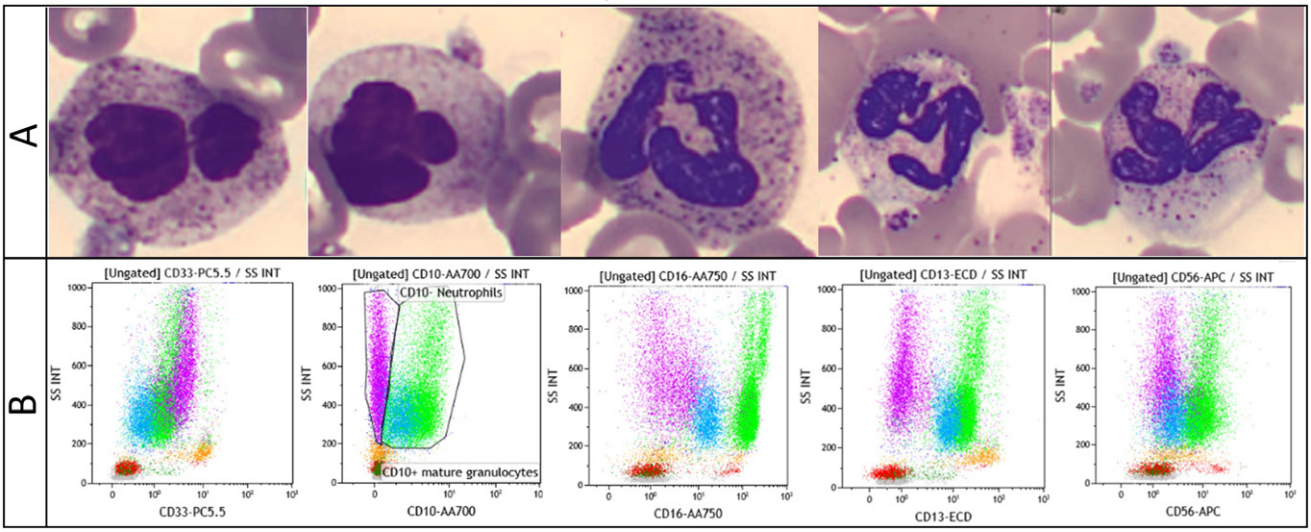

Figure 2 – 898

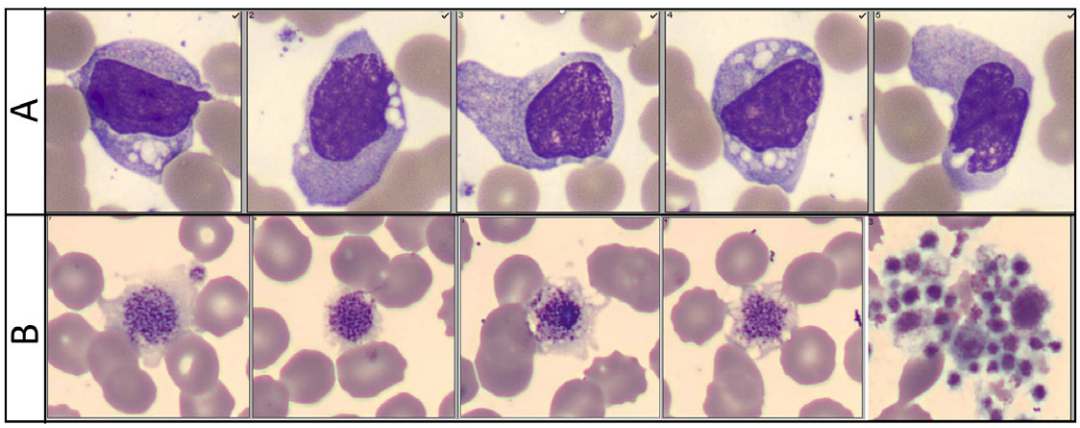

Conclusions: Despite being a small study, we were able to correlate the morphologic and phenotypic alterations of the WBCs in COVID19 patients. As such, this helped to explain some of the clinical hematologic manifestation of the disease.

899 Smoking Status in Acute Myeloid Leukemia is Associated with Worse Overall Survival, Prior Non-Hematopoietic Malignancies, Cytogenetic Abnormalities, and WHO Category

Jyoti Kumar[1], Samit Patel[2], Abraham Chang[2], Soham Mukherjee[3], Corinn Small[4], Sumanth Gollapudi[4], Olga Weinberg[5], Tracy George[6], James Zehnder[2], Robert Ohgami[4]

[1]Stanford University, Stanford, CA, [2]Stanford Medicine/Stanford University, Stanford, CA, [3]University of California, Berkeley, Berkeley, CA, [4]University of California, San Francisco, San Francisco, CA, [5]UT Southwestern Medical Center, Dallas, TX, [6]The University of Utah, Salt Lake City, UT

Disclosures: Jyoti Kumar: None; Samit Patel: None; Abraham Chang: None; Soham Mukherjee: None; Corinn Small: None; Sumanth Gollapudi: None; Olga Weinberg: None; Tracy George: *Consultant*, Celgene; James Zehnder: None; Robert Ohgami: *Grant or Research Support*, Stemline Therapeutics

Background: Acute myeloid leukemia (AML) is an aggressive disease of malignant myeloid cells. It has been shown that tobacco smoking is associated with worse outcomes in both hematopoietic and non-hematopoietic malignancies; however, no studies have

investigated the influence of smoking status on other clinical and diagnostic parameters in AML. The aim of our study was to evaluate the significance of smoking status relative to survival as well as other clinical and genetic parameters. We also sought to detect a genomic smoking signature using next-generation sequencing (NGS) data from an independent dataset.

Design: AML cases from 2005-2017 with ancillary data were identified. Clinical features (demographics, laboratory data, environmental exposures, treatment response and outcome) were collected. NGS data from 12 smoker patients (> 20 packs/year) and 12 never smoker patients from an independent dataset were bioinformatically analyzed to identify a genomic smoking signature based on the COSMIC database of mutational signatures (https://cancer.sanger.ac.uk/signatures/signatures_v2).

Results: Of 98 patients, 48 were smokers and 50 were non-smokers. There was decreased survival probability in the smoker population as compared to non-smokers ($p < 0.05$, Figure 1A). When stratifying by smoker status, male smokers had statistically significant decreased survival compared to female smokers ($p < 0.05$, Figure 2B), as well as compared to the population of smokers without a prior non-hematopoietic malignancy ($p < 0.05$, Figure 2C). A statistically significant decrease in survival was present within the WHO categories: AML, not otherwise specified (AML NOS) and AML with recurrent genetic abnormalities (AML RGA) ($p < 0.05$. Figure 2D-E). Smokers that demonstrated no cytogenetic abnormalities showed a statistically significant decrease in survival ($p < 0.05$) (Figure 2F).

Patients who were smokers, male, and older in age were associated with an increase in hazard ratio (HR) ($p < 0.05$, Table 1). There was a non-significant increase in the HR based on the number of cytogenetic abnormalities and presence of a prior non-hematopoietic malignancy.

Finally, molecular signature analysis identified a prominent smoking signature (Signature 4) in a subset of smokers (Figure 2). As defined by the COSMIC database, Signature 4 shows C>A mutations and is associated with smoking.

Characteristics	n	HR	95% CI	p value
Smoking Status				
Non-smoker	50	1.00	(reference)	
Smoker	48	2.0174	1.127-3.61	0.0181 *
Gender				
Female	47	1.00	(reference)	
Male	51	1.8469	0.5414-1.048	0.034 *
Age		1.03747	1.017-1.058	0.000247 ***
Cytogenetic Abnormalities				
None	43	1.00	(reference)	
1-2 abnormalities	35	1.5657	0.8449-2.901	0.154
3 or more	17	1.7162	0.7768-3.791	0.182
Prior Cancer				
No	85	1.00	(reference)	
Yes	13	2.25	0.9962-5.082	0.0511
AML Category				
AML NOS	17	1.00	(reference)	
AML RGA	31	1.157	0.4788-2.797	0.746
AML MRC	39	2.241	1.0000-5.022	0.05
AML-T	9	2.182	0.6474-7.358	0.208
AML-germline	1	0.000001274	NA	0.998

*p < 0.05; *** p < 0.001. AML, acute myeloid leukemia; NOS, not otherwise specified; RGA, recurrent genetic abnormalities; MRC, myelodysplasia-related changes; AML-T, therapy-related AML.

Figure 1 - 899

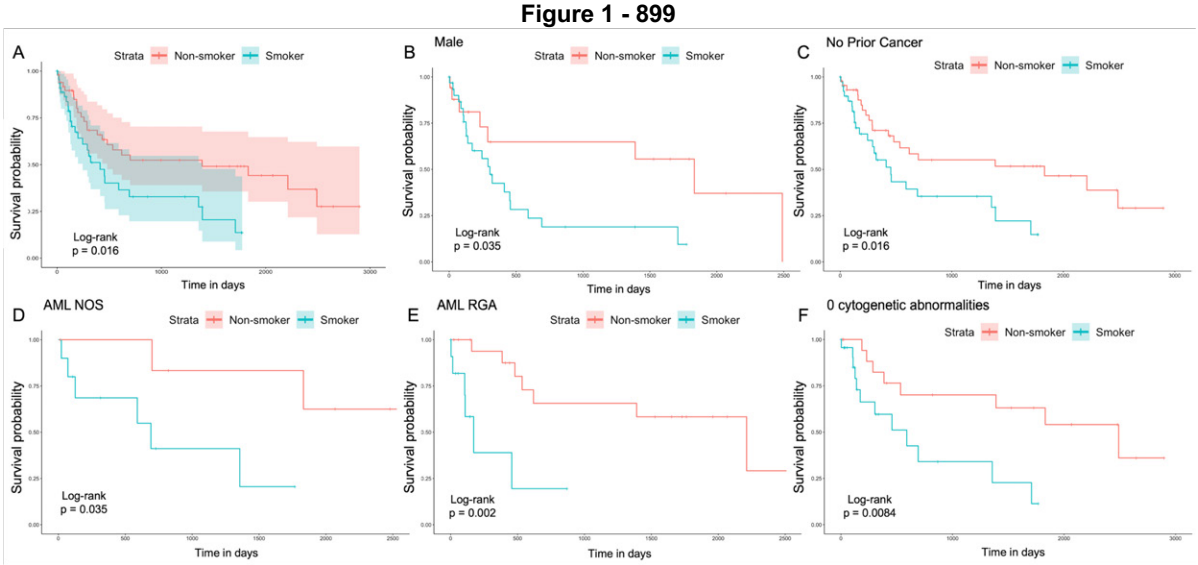

Figure 2 – 899

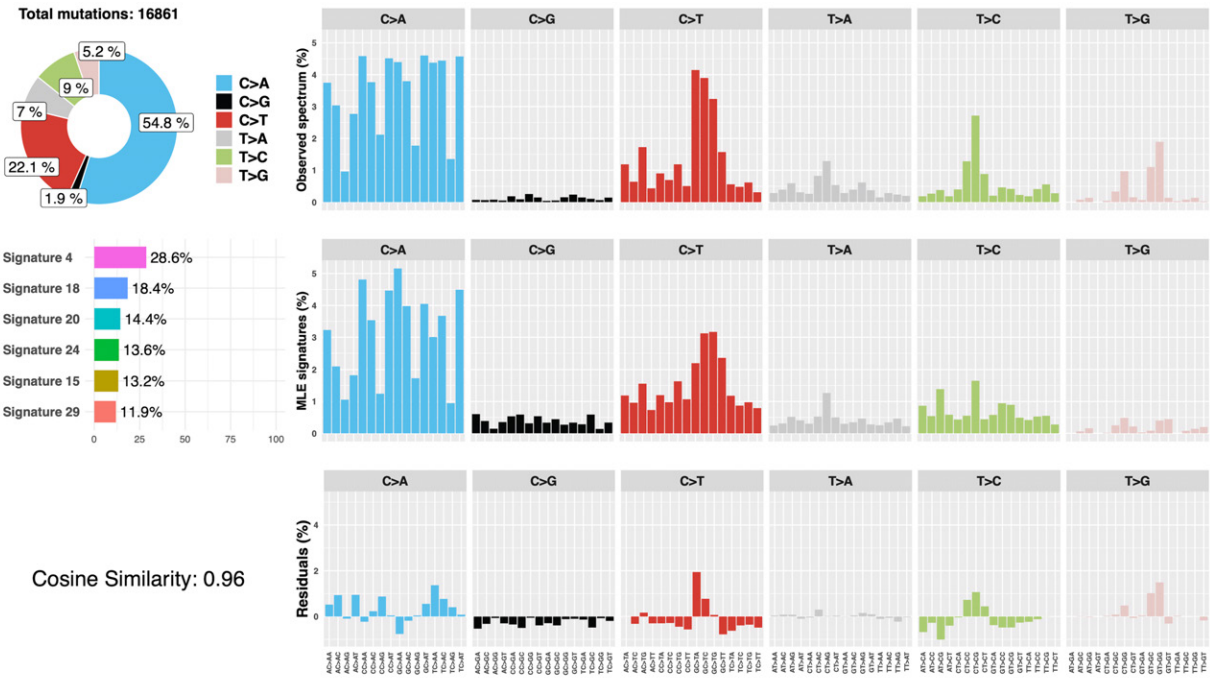

Conclusions: Smoking status significantly decreases overall survival in patients with AML. The impact of smoking status on overall survival is significantly modulated by other factors, including a prior malignancy, cytogenetic abnormalities, and WHO AML classification category. We also identified a genetic smoking signature; future studies are needed to further evaluate its prognostic significance.

900 Nonlinear Microscopy Enables Histological Evaluation of Hematopoietic and Lymphoid Tissue Within Minutes After Biopsy

Simon Lamothe[1], Tadayuki Yoshitake[2], Seymour Rosen[1], James Fujimoto[2], German Pihan[1]
[1]Beth Israel Deaconess Medical Center, Boston, MA, [2]Massachusetts Institute of Technology, Cambridge, MA

Disclosures: Simon Lamothe: None; Tadayuki Yoshitake: None; Seymour Rosen: None; James Fujimoto: None; German Pihan: None

Background: Histopathology of H&E-stained biopsy sections remains the gold standard in diagnosing hematopoietic and lymphoid (H&L) neoplasms. Histopathology diagnosis, however, is a lengthy multi-step process. Standard histology protocols take 16-24 hrs. to complete, and rapid protocols a minimum of 7 hrs. Frozen sections are unsuitable for diagnosis because of poor rendition of chromatin detail and consumption of precious tissue needed for subsequent phenotypic, and molecular studies. Nonlinear microscopy (NLM) enables rapid, non-destructive evaluation of fresh tissue without freezing or microtome sectioning.

Design: Shortly after collection, H&L biopsies were stained for one min with acridine orange and sulforhodamine solution and rinsed for 30 sec in saline. Biopsies were imaged with NLM in real-time (Fig.1). After imaging, tissue was processed for routine histopathology. Image fidelity was assessed by repeating comparisons of histological and cytological features between NLM and corresponding H&E images.

Results: NLM produced histological images within minutes after biopsy procurement. Moreover, image quality was comparable to standard H&E-stained sections. Indeed, chromatin detail and nucleocytoplasmic contrast was better enhanced with NLM than H&E, while RBC were not visualized with NLM. Specific cytoplasmic granules in neutrophil and eosinophils were more distinct with NLM. Illustrative representations (Fig. 2) show NLM and corresponding H&E images of bone marrow (a, b), germinal center (c, d), and splenic red pulp (e, f). NLM imaged virtually all marrow cell types (a) identified in the H&E section (b). Cytological detail in NLM images of a germinal center (c) rivaled those on H&E sections (d), and the splenic red pulp was imaged with good resolution (e), visualizing in littoral cells features not easily seen on H&E sections (f).

Figure 1 - 900

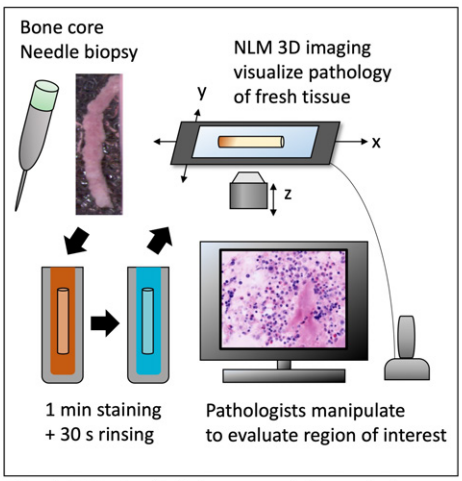

Figure 1: NLM protocol for fresh, unprocessed, biopsy evaluation. Fresh tissue biopsies stained with acridine orange and sulforhodamine were placed on the stage of the NLM microscope and a pathologist examined NLM image histologically in real time.

Figure 2 - 900

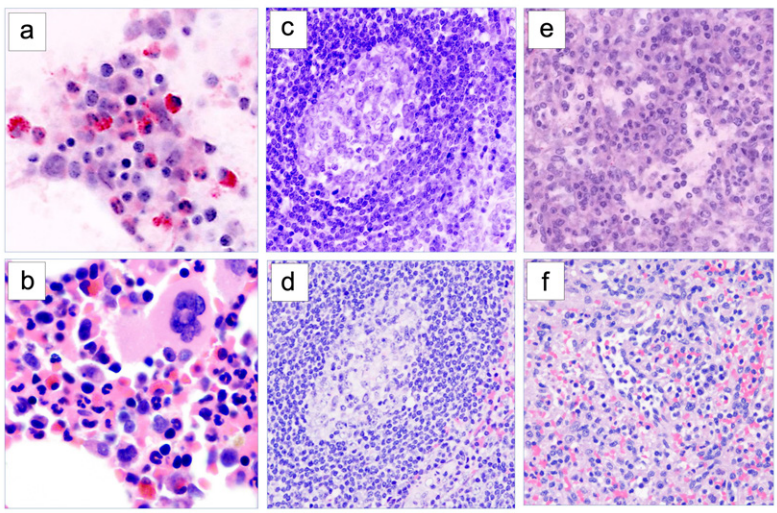

Fig 2. NLM (a,c,e) and H&E (b,d,f) images of bone marrow (a, b), a germinal center (c,d) and splenic red pulp (e,f). Original magnification H&E 200x, NLM 20x objective.

Conclusions: NLM imaged H&L nondestructively and within minutes after biopsy at a resolution comparable to standard H&E sections. Our observations suggest that NLM could be used to assess biopsy adequacy and to provide generic diagnoses, such as myelofibrosis, marrow aplasia, myeloma, and myeloproliferative disorders. With further technical refinements and larger blinded reading studies, it may be possible to use NLM for rapid primary diagnosis in patients with clinically aggressive leukemia and lymphoma, who would greatly benefit from expeditious diagnoses.

901 CD4-Positive Gamma-Delta T-cell Lymphomas Involving the Lymph Node

Daniel Larson[1], Andrew Feldman[1], Paul Kurtin[2], William Macon[1]
[1]Mayo Clinic, Rochester, MN, [2]None/retired, Rochester, MN

Disclosures: Daniel Larson: None; Andrew Feldman: *Grant or Research Support*, Zeno Pharmaceuticals; *Grant or Research Support*, Seattle Genetics; Paul Kurtin: None; William Macon: None

Background: Gamma-delta T-cell lymphomas are uncommon and usually negative for CD4 and CD8. CD4-positive gamma-delta T-cell lymphomas (CD4+ GDTCL) involving the lymph node are extremely rare with only four prior cases reported (Table 1). While most gamma-delta T-cells do not express CD4, approximately 1-4% of normal peripheral blood gamma-delta T-cells are CD4+/CD8-, have less cytotoxic activity than their CD8+ counterparts, and may function as bystander help to immunoglobulin-producing B-cells.

Design: We present the clinicopathologic features of three CD4+ GDTCLs involving the lymph node seen at a single institution over a period of eight years. Additionally, we incorporate data from the four other reported nodal CD4+ GDTCL.

Results: Clinicopathologic features of all seven cases are summarized in Table 1. All patients were male, aged 66-82. Lymphadenopathy was present in all cases, with the most common sites of involvement in cervical and inguinal nodes. One patient had B symptoms; two presented with normal CBC values, and case 2 presented with pancytopenia. Two cases (2 and 7) also had cutaneous involvement by CD4+ GDTCL. Case 3 had biopsy-proven involvement of the stomach on presentation and (along with case 7) showed low level bone marrow involvement. Morphologically, there was subtotal to total nodal effacement by a diffuse infiltrate of atypical lymphocytes. Cytologically, most cases showed small to intermediate-sized cells with round to oval nuclei, coarse chromatin, and abundant pale cytoplasm. Case 3 demonstrated more pleomorphism and higher N:C ratio (Figure 1). Immunophenotypically, neoplastic T-cells expressed CD2, CD3, CD4, CD5, and TCR delta with variable expression of CD7 and no expression of CD8 or TCR βF1 (Figure 2). Most cases lacked expression of TIA-1 (except case 6). Case 4 is unique in that it was composed of large cells that additionally coexpressed CD30. Therapy regimens varied and prognosis was poor: progression or relapse occurred in all, and overall survival was 2 months to 2 years after diagnosis (Table 1).

Clinicopathologic Characteristics of 7 Cases of CD4-Positive Gamma-Delta T-cell Lymphomas Involving Lymph Nodes

		Our Cohort			Cases Reported from the Literature			
		Case 1	Case 2	Case 3	Case 4 Ichinohasama *et al.* Hum Pathol. 1996;27(12):1370-1377	Case 5 Saito *et al.* Ann Oncol. 2002;13(11):1792-1798	Case 6 Saito *et al.* Ann Oncol. 2002;13(11):1792-1798	Case 7 Karner *et al.* J Hematopathology 2018;11(4):107-113
Clinical Presentation	Age (years)	66	72	82	72	66	79	66
	Sex	Male	Male	Male	Male	Male	.Male	Male
	Tissue Sites Involved	Cervical LN*	Skin* Inguinal LN* Supraclavicular LN*	Massive inguinal LAD* Extensive LAD Stomach* Spleen, Soft tissue	Cervical LN*, bilateral Thoracic LN	Cervical LN* Submandibular LN Inguinal LN Liver	Cervical LN* Inguinal LN	Skin* Axillary LN* Liver, Spleen
	Bone Marrow	unknown	Not involved	Involved, 10%	Not involved	NR	NR	Involved, low level
	Symptoms		No B symptoms	No B symptoms	No B symptoms			Rash, B symptoms
	CBC	unknown	Pancytopenia	Normal	Normal	NR	NR	NR
	LDH (IU/L)		400	718	304			NR
	Presentation	unknown	Skin patches Progressive LAD	DVT from inguinal LAD	Neck mass	LAD	LAD	Skin rash, nodules 1 year post renal XP
Morphology	Specimen	Cervical LN	Supraclavicular LN	Inguinal LN	Cervical LN			Axillary LN
	Type	Excision	Excision	Biopsy	Biopsy			Biopsy
	Architecture	Subtotal effacement	Effaced	Effaced	Subtotal Effacement			Effaced
	Growth	Diffuse/interfollicular	Diffuse	Diffuse with necrosis	Diffuse/interfollicular	NR	NR	Diffuse
	Cell Size	Small to medium	Small to medium	Small to medium	Large			Medium
	Nuclei	Round to oval	Round to oval	Irregular	Round to oval			Round to oval
	Chromatin	Coarse	Coarse	Coarse	Prominent nucleoli			Coarse
	Cytoplasm	Abundant, pale	Abundant, pale	Scant	Abundant, pale			Abundant, clear
Phenotype	CD2	+	+	+	+	NR	NR	+
	CD3	+	+	+	+	+	+	+
	CD4	+	+	+	+	+	+	+
	CD5	+	+	+	+	NR	+	+
	CD7	-	±	±	-	NR	NR	±
	CD8	-	-	-	-	-	-	-
	CD30	-	-	-	+	NR	NR	-
	TCRαβ	-	-	-	-	-	-	-
	TCRγδ	+	+	+	+	+	+	+
	TIA-1	NP	-	-	NR	-	+	NR
Treatment and Outcome	Therapy	unknown	Bexarotene (skin dz) Romidepsin (LN dz) CHOP Bendamustine	CHOP	VEPA MACOP-B with radiation	CHOP ESHAP Radiation	CHOP EPOCH	EPOCH with reduction of immunosuppression
	Response	unknown	Early cutaneous CR Progression of LAD	No response	Initial CR Relapse after 1 year	No response	No response	Initial PR Progression after 9 months
	Survival		2 years	2 months	2 years	5 months	3 months	NR

Legend: CBC complete blood count; CHOP cyclophosphamide, doxorubicin, vincristine, prednisone; CR complete response; DVT deep vein thrombosis; dz disease; EPOCH prednisone, etoposide, vincristine, cyclophosphamide, doxorubicin; ESHAP etoposide, methylprednisolone, cytosine arabinoside, cisplatin; LAD lymphadenopathy; LDH serum lactate dehydrogenase; LN lymph node; MACOP-B methotrexate, leucovorin, bleomycin, doxorubicin, cyclophosphamide, vincristine, dexamethasone; NP not performed; NR not reported; PR partial response; VEPA vincristine, cyclophosphamide, prednisone, adriamycin; XP transplant

*indicates biopsy-proven site of tissue involvement by lymphoma; other sites listed had presumed involvement by imaging studies

Figure 1 - 901

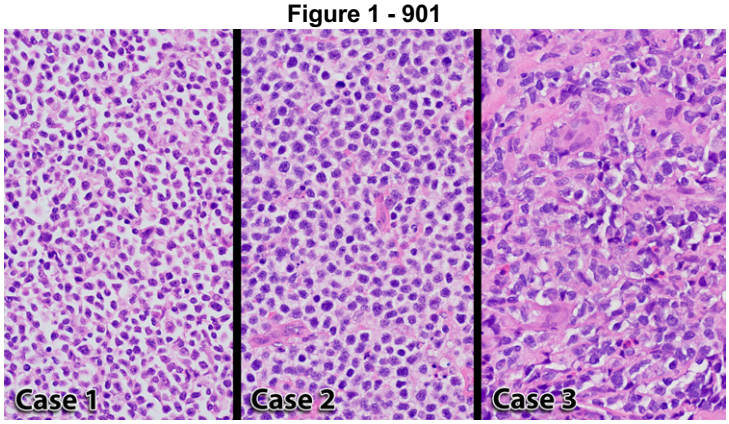

Figure 2 - 901

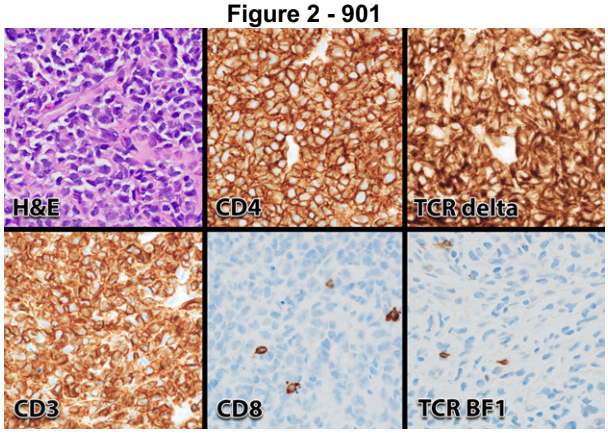

Conclusions: CD4+ GDTCL in lymph nodes is rare and appears to have an aggressive clinical course and poor outcomes. It is unknown whether CD4+ GDTCL arises from normal CD4+ G/D T-cells or represents aberrant expression of CD4 in a rare subset of GDTCL. Since these lymphomas express both CD4 and CD5, their gamma/delta phenotype type may be missed unless specific testing is performed.

902 LMO2 Expression is Frequent in T-lymphoblastic Leukemia and Correlates with Survival, Regardless of T-cell Stage

Kerri-Ann Latchmansingh[1], Xiaoqiong Wang[2], Ramiro Verdun[3], Francisco Vega-Vazquez[2], M. James You[2], Izidore Lossos[4], Jennifer Chapman[5]

[1]Jackson Memorial Hospital/ University of Miami Hospital, Miami, FL, [2]The University of Texas MD Anderson Cancer Center, Houston, TX, [3]University of Miami Health System, Miami, FL, [4]University of Miami/Sylvester Cancer Center, FL, [5]University of Miami, Miller School of Medicine, Miami, FL

Disclosures: Kerri-Ann Latchmansingh: None; Xiaoqiong Wang: None; Ramiro Verdun: None; Francisco Vega-Vazquez: None; M. James You: None; Izidore Lossos: None; Jennifer Chapman: None

Background: T- lymphoblastic leukemia / lymphoma (T-LL) is an aggressive malignancy of immature T-cells with poor overall survival (OS) and in need of new therapies. LIM-domain only 2 (LMO2) is a critical regulator of hematopoietic cell development that can be overexpressed in T-LL due to chromosomal abnormalities. Deregulated LMO2 expression contributes to T-LL development by inducing block of T-cell differentiation and continuous thymocyte self-renewal. However, LMO2 expression and its biologic significance in T-LL remain largely unknown.

Design: LMO2 expression was determined by immunohistochemistry in biopsies of T-LL and considered positive if nuclear signal was present in ≥ 30% of tumor cells (arbitrary but frequently used cut-off; LMO2 clone from Ventana, Tucson, Arizona, USA). LMO2 intensity was scored as 0 (negative), 1+ (dim compared to endothelial cells) or 2+ (equal or stronger than endothelial cells, Figure 1). Overall-survival (OS) was estimated using Gehan-Breslow-Wilcoxon test.

Results: 102 biopsies of T-LL were identified in 68 patients including 32 (47%) ETP -ALL, 26 (38%) cortical and 10 (15%) medullary type. 25 biopsies of post treatment relapse / persistence were also identified. Sites of biopsy included bone marrow (60), mediastinal mass (4), lymph node (3) and nasopharyngeal mass (1). Cytogenetic or molecular data was available in 47 (69%) cases. Mean patient age was 35 years (range 8 to 77 years), male:female ratio 2. LMO2 expression was positive in 50 (73.5%) initial biopsies of T-LL, showed an average of 87% positive tumor cells and average intensity of 1.9+ / 2+ (range 1-2). Eighteen (26.5%) cases were LMO2 negative. LMO2 was expressed in 84% of ETP, 70% of medullary and 62% of cortical T-LLs with no statistically significant difference (p=0.14). In all patients with follow up biopsies after therapy, LMO2 expression was stable. LMO2 expression was associated with longer OS (p=0.028) regardless of T-lymphoblast stage (Figure 2).

Figure 1 - 902

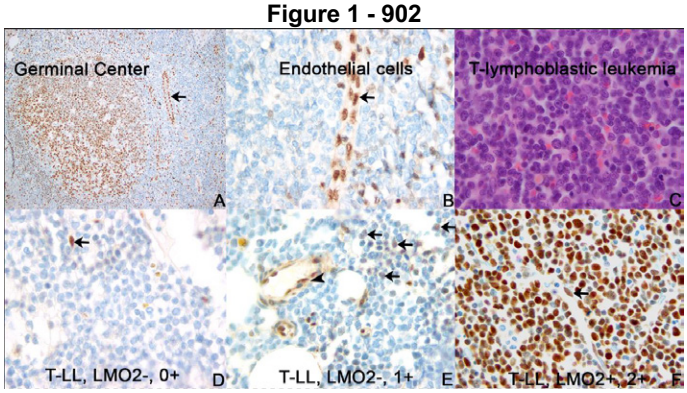

Figure 2 - 902

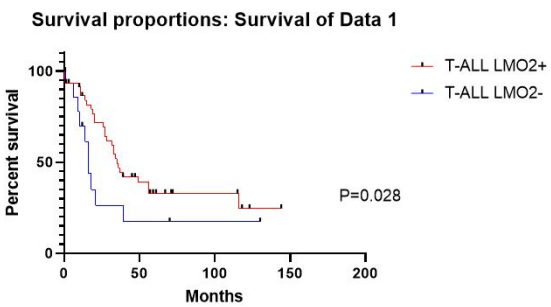

Conclusions: LMO2 protein is expressed in most (73.5%) of T-LL regardless of T-lymphoblast stage and correlates with OS, suggesting that LMO2 expression decreases DNA repair efficiency and thereby promotes response to chemotherapy, as has been previously observed in diffuse large B cell lymphoma (DLBCL). These findings provide support for further investigation of novel chemotherapy approaches in T-LL (i.e. PARP1/2 inhibitors), with selection of patients stratified by LMO2 expression.

903 Assessment of Minimal Residual Disease in AL-Amyloidosis by Multiplex Immunohistochemistry: A Comparative Analysis with Multiparametric Flow Cytometry

Julie Li[1], Sanket Choksi[1], Lawreen Connors[2], Andrew Staron[2], Vaishali Sanchorawala[2], Eric Burks[3]
[1]Boston Medical Center, Boston, MA, [2]Boston University, Boston Medical Center, Boston, MA, [3]Boston University Mallory Pathology Associates, Boston, MA

Disclosures: Julie Li: None; Sanket Choksi: None; Lawreen Connors: None; Andrew Staron: None; Vaishali Sanchorawala: None; Eric Burks: None

Background: Systemic light chain (AL) amyloidosis results from the organ deposition of misfolded light chain fibrils produced by clonal plasma cells in the marrow. Minimal residual disease (MRD) detection at a sensitivity level of 1 x 10^{-5} using multiparametric flow cytometry (MFC) predicts outcomes after treatment amongst patients with plasma cell neoplasms. In this study, we investigate whether dual immunohistochemical staining (dIHC) provides a sensitive alternative for identifying MRD in patients with AL amyloidosis.

Design: Bone marrow biopsy and aspirate samples (n=114) from 102 patients who completed treatment for AL amyloidosis were evaluated for the presence of MRD using both dIHC and MFC between January 2020 and August 2021. We applied dIHC for CD138/cyclinD1, CD56/Mum-1 and kappa/lambda on decalcified core biopsies. MFC using a 2-tube, 10-color antibody panel validated for MRD detection at 1 x 10^{-5} was performed on marrow aspirates. Statistical comparison was computed by Mann-Whitney U test.

Results: Among 114 paired samples, 100 (88%) were concordant for MRD status, including MFC+/dIHC+ (n=59) and MFC-/dIHC- (n=41) (Table). The majority of discordant MRD cases were MFC+/dIHC- (n=12), with only 2 being MFC-/dIHC+. Overt monotypic light chain expression was seen by dIHC kappa/lambda staining in 44 of 73 cases (60%) with MRD, whereas mild skewing of the light chain ratio or a normal light chain ratio was seen in 13 (18%) and 16 (22%) of cases, respectively. Mild light chain skewing (i.e., equivocal pattern) by dIHC was nonspecific for MRD as it was also observed in 2 of 41 (5%) cases with concordant MRD negativity (Table). Cyclin D1/CD138 and CD56/Mum-1 dIHC showed aberrant co-expression in 33 (45%) and 29 (40%) of MRD+ cases, respectively. Aberrant co-expression of cyclin D1/CD138 was detected in 6 of the 15 (40%) cases with mild light chain skewing (Table and Figure 1) and 5 cases with a normal dIHC light chain ratio. Conversely, CD56/Mum-1 co-expression was observed at low levels (i.e., 5-15% of plasma cells) in 7 of the 41 (17%) cases with concordant MRD negativity (Figure 1). The MRD disease burden as assessed by MFC was significantly higher among those with dIHC+ (median 1.0 x 10^{-3}; IQR 3.8 x 10^{-4} to 2.2 x 10^{-3}) compared to dIHC- (median 8.7 x 10^{-5}; IQR 5.4 x 10^{-5} to 1.9 x 10^{-4}), p<0.001 (Figure 2).

Table: Comparison of dIHC Expression Stratified by MRD Detection and MFC Concordance

	N	dIHC Kappa/Lambda Normal			dIHC Kappa/Lambda Equivocal			dIHC Kappa/Lambda Monotypic	
MRD+		16			13			44	
		CCND1+	CD56+		CCND1+	CD56+		CCND1+	CD56+
MFC+/dIHC+	59	3/3	0/3		6/12	4/12		22/44	23/44
MFC+/dIHC-	12	0/11	1/11		0/1	0/1		0/0	0/0
MFC-/dIHC+	2	2/2	1/2		0/0	0/0		0/0	0/0
		dIHC Kappa/Lambda Normal			dIHC Kappa/Lambda Equivocal			dIHC Kappa/Lambda Monotypic	
MRD-		39			2			0	
		CCND1+	CD56+		CCND1+	CD56+		CCND1+	CD56+
MFC-/dIHC-	41	0/39	6/39		0/2	1/2		0/0	0/0

Figure 1 - 903

Figure 1: Representative dIHC Patterns with Corresponding MFC

Top Panel: Aberrant Cyclin D1 expression in a subset of plasma cells showing mild kappa skewing with dIHC corresponding to 40% kappa-restricted plasma cells by MFC.

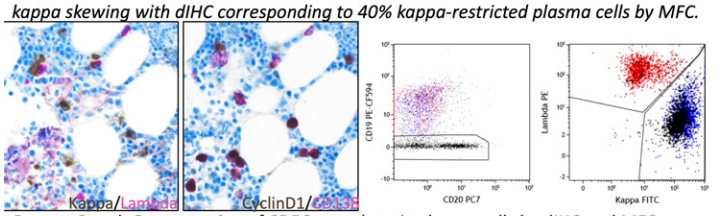

Bottom Panel: Co-expression of CD56 on polytypic plasma cells by dIHC and MFC.

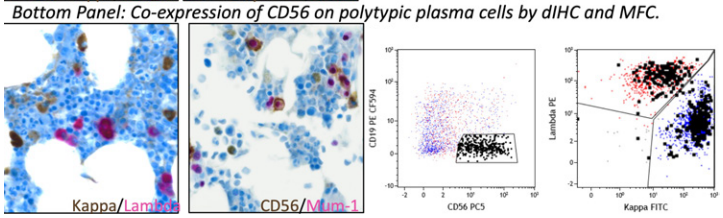

Figure 2 - 903

Figure 2: dIHC vs. MFC MRD Detection Level

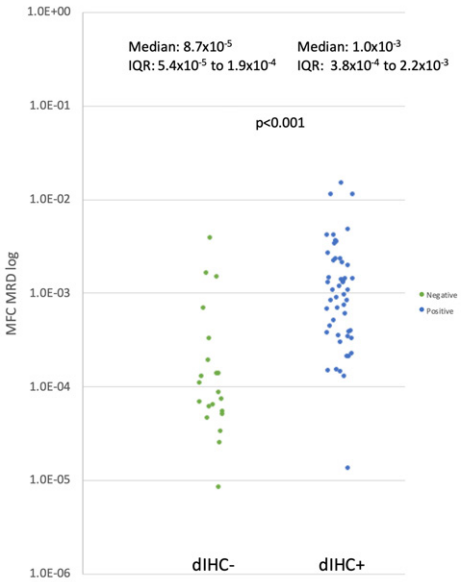

Conclusions: Conclusion: dIHC detects the majority (88%) of MRD positive cases following treatment for AL-amyloidosis but is inadequate for assessment of MRD at the level of 10^{-5}.

904 Post-induction Minimal Residual Disease Defined by Next-Generation Sequencing Predicts Poorer Clinical Outcomes in Patients with Acute Myeloid Leukemia

Yonghong Li[1], Jose Solis-Ruiz[2], Carmen Tong[1], Maedeh Mohebnasab[3], Frederick Racke[1], Felicitas Lacbawan[1], Richard Press[2]

[1]Quest Diagnostics, San Juan Capistrano, CA, [2]Oregon Health & Science University, Portland, OR, [3]Oregon Health & Science University, OR

Disclosures: Yonghong Li: None; Jose Solis-Ruiz: None; Carmen Tong: None; Maedeh Mohebnasab: None; Frederick Racke: None; Felicitas Lacbawan: None; Richard Press: None

Background: Patients who have been treated for acute myeloid leukemia (AML) may have minimal residual disease (MRD) owing to residual somatic mutations. This study assessed whether residual somatic mutations defined by next-generation sequencing (NGS) can serve as prognostic biomarkers for post-treatment AML patients.

Design: This is a retrospective study of AML patients (n=93) who underwent both pre-and post-treatment testing with a 42-gene NGS assay. Post-induction MRD status was assessed in each non-DAT (*i.e.,* excluding 3 preleukemic genes *DNMT3A*, *ASXL1* and *TET2*) gene that had a somatic mutation detected before treatment. Kaplan-Meier analysis was used

to compare survival (progression-free and overall) between MRD positive and negative patients. Cumulative incidence of relapse was estimated with non-disease death as a competing risk.

Results: The 93 patients evaluated were diagnosed with *de novo* AML (n=81) or secondary AML (n=12). The median (interquartile range [IQR]) age at diagnosis was 58 (43-65) years; 47 (51%) were women; the median (IQR) post-treatment NGS testing was 33 (28-41) days after therapy initiation; and the median (IQR) follow-up was 829 (252-1395) days. The most common mutations at diagnosis were in *FLT3* (34 [37%] patients), *NRAS* (29 [31%] patients), *NPM1* (27 [29%] patients) and *DNMT3A* (26 [27%] patients). Mutation clearance (to levels below the 0.5% assay detection limit) was achieved to various degrees after induction chemotherapy: for example, the *FLT3* mutations were undetectable in 26 (76%) of the 34 patients but the *DNMT3A* mutations were undetectable only in 4 (15%) of the 26 patients. Excluding patients with DAT mutations, there were 89 patients with at least one somatic mutation at diagnosis; the median was 2 mutations per patient. After treatment, 41 patients were MRD-negative and 48 were MRD-positive. Compared with the MRD-negative patients, the MRD-positive patients had shorter progression-free survival (median 742 days vs. 349.5 days; P=0.02), shorter overall survival (median 1078 days vs. 507.5 days; P=0.019), and a higher cumulative incidence of relapse (hazard ratio =2.13 [95%CI: 1.16-3.91]; P=0.016).

Conclusions: Post-induction MRD status, defined by the NGS results, is associated with poorer long-term clinical outcomes in AML patients. Additional therapies to achieve molecular MRD-negativity may be warranted in the higher-risk AML patients.

905 T-Cell Immunoreceptor with Ig and ITIM domains (TIGIT) Shows Distinct Expression Patterns Among Lymphoma Subtypes: Implications for Therapeutic Efficacy

Diane Libert[1], Shuchun Zhao[2], Sheren Younes[1], Yasodha Natkunam[2]
[1]Stanford Pathology, Stanford, CA, [2]Stanford Medicine/Stanford University, Stanford, CA

Disclosures: Diane Libert: None; Shuchun Zhao: None; Sheren Younes: None; Yasodha Natkunam: None

Background: Immune checkpoint inhibitors against PD-1/PD-L1 and CTLA-4/B7 axes have had limited success, requiring the need to explore alternative targets such as TIGIT/CD155 to improve durable clinical responses. TIGIT is a co-inhibitory receptor expressed in T- and NK-cells, which also binds to dendritic cells inducing IL-10 secretion, and leads to a tolerogenic microenvironment. We undertook this study to investigate the expression profile of TIGIT such that the potential efficacy of TIGIT/CD155 blockade could be mapped among lymphoma subtypes.

Design: Tissue microarrays (TMAs) of 638 lymphoma samples were used with Institutional Review Board approval. Immunohistochemistry was performed using an anti-TIGIT rabbit monoclonal (BLR047F at 1:300 dilution; Abcam, Cambridge, UK). Moderate to strong membrane staining in 10% of lymphoma cells was scored positive. For classic Hodgkin lymphoma (CHL), diffuse large B-cell lymphoma (DLBCL), and anaplastic large cell lymphoma (ALCL), TIGIT expression was also assessed in the tumor microenvironment (TME).

Results: Among B-cell lymphomas, TIGIT was highly expressed in follicular, marginal zone, and mantle cell lymphomas, whereas DLBCL, primary mediastinal large B, lymphoplasmacytic, and plasmablastic lymphomas were mostly negative. TIGIT was positive in 85% of the DLBCL TMEs evaluated. Although Hodgkin cells lacked TIGIT, TME cells were positive in over 70% of the CHL cases. Among T-cell lymphomas, angioimmunoblastic T-cell lymphoma (AITL) retained TIGIT expression in a high proportion of cases (90.9%) whereas the majority of other T and NK lymphomas showed decreased expression. TIGIT was expressed in 68% of the ALCL TMEs evaluated (Table 1, Figure 1).

Diagnosis	No. of cases	Expression in lymphoma cells	
		Positive (%)	Negative (%)
B-cell lymphomas			
Follicular lymphoma	87	75 (86.2)	12 (13.8)
Marginal zone lymphoma (all types)	68	52 (76.5)	16 (23.5)
Mantle cell lymphoma	28	16 (57.1)	12 (42.9)
Burkitt lymphoma	4	2 (50)	2 (50)
Small lymphocytic lymphoma	49	24 (49.0)	25 (51.0)
Post-transplant lymphoproliferative disorder (DLBCL)	35	16 (45.7)	19 (54.3)
B lymphoblastic lymphoma/leukemia	7	3 (42.9)	4 (57.1)
Lymphoplasmacytic lymphoma	3	1 (33.3)	2 (66.6)
Diffuse large B-cell lymphoma	100	25 (25)	75 (75)
Primary mediastinal large B cell lymphoma	3	0 (0)	3 (100)
Plasmablastic lymphoma	2	0 (0)	2 (100)

Classic Hodgkin Lymphoma	95	0 (0)	95 (100)
T and NK cell lymphomas			
Angioimmunoblastic T cell lymphoma	11	10 (90.9)	1 (9.1)
Peripheral T cell lymphoma, NOS	12	5 (41.7)	7 (58.3)
NK/T cell lymphoma	6	2 (33.3)	4 (66.7)
Gamma/delta T-cell lymphoma	5	1 (20)	4 (80)
Anaplastic large cell lymphoma (all types)	115	10 (8.7)	105 (91.3)
T lymphoblastic lymphoma/leukemia	8	0 (0)	8 (100)
Total	**638**	**242 (37.9)**	**396 (62.1)**
Expression in Tumor Microenvironment			
Selected Diagnosis (Evaluable Cases)	**No. of cases**	**Positive (%)**	**Negative (%)**
Classic Hodgkin Lymphoma	95	67 (70.5)	28 (29.5)
Diffuse large B-cell lymphoma	53	45 (85)	8 (15)
Anaplastic large cell lymphoma	98	31 (31.6)	67 (68.4)

Figure 1 - 905

Figure 1: TIGIT expression in lymphoma subtypes

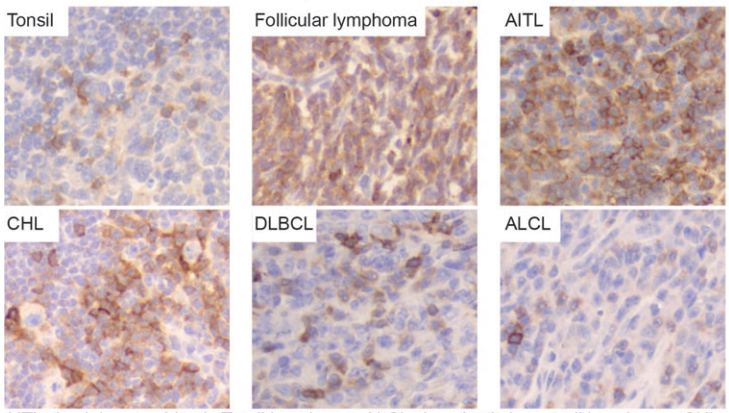

AITL: Angioimmunoblastic T-cell lymphoma, ALCL: Anaplastic large cell lymphoma, CHL: Classic Hodgkin lymphoma, DLBCL: Diffuse large B-cell lymphoma. All images taken at 20X magnification.

Conclusions: TIGIT expression in both the lymphoma cells and the TME show distinctive profiles among lymphoma subtypes. Small B cell and select T-cell lymphomas demonstrated high TIGIT expression in lymphoma cells whereas DLBCL, CHL, and ALCL showed high expression in TME cells. Given different modes of immunosuppression promoted by TIGIT/CD155 signaling, susceptibility to TIGIT blockade is likely to differ depending on TIGIT expression patterns. TIGIT positivity in lymphoma cells may explain why some lymphomas may be more refractory to checkpoint blockade and require co-blockade or alternative strategies to restore immune surveillance. Our data is likely to facilitate correlation of lymphoma biology with therapeutic response in clinical trials targeting TIGIT.

906 Genetic Characteristics of CD5+ Diffuse Large B-cell Lymphoma

Hui Liu[1], Dongshen Ma, Yuanyuan Ma, Chenxi Xiang
[1]Xuzhou Medical University, Xuzhou, China, [2]The Affiliated Hospital of Xuzhou Medical University, Xuzhou, China

Disclosures: Hui Liu: None; Dongshen Ma: None; Yuanyuan Ma: None; Chenxi Xiang: None

Background: CD5+ diffuse large B-cell lymphoma (CD5+ DLBCL) accounts for about 5%-10% of DLBCL cases, which has invasive biological behavior and poor prognosis. Morphologically, CD5+ DLBCL shows no significant differences from CD5- DLBCL. From the perspective of cell origin, most of CD5+ DLBCL cases are predominantly non-GCB subtype. However, studies on the genetic variations of CD5+ DLBCL were barely reported. The purpose of this study is to delineate the molecular characteristics of CD5+ DLBCL.

Design: 24 CD5+ and 23 CD5- DLBCL cases in our center were collected with complete clinicopathological data. Total DNA from the formalin-fixed and paraffin-embedded samples was extracted for target sequencing, which covered the exon regions of 475 genes related to lymphoma. MYC, BCL-2 and BCL-6 rearrangements were detected by FISH. Genetic subtyping model reported by Schmitz et al. was used for further classification of our cases.

Results: CD5+ DLBCL had higher chromosome instability (CIN) (P=0.0331) and more copy number variations (CNV) (P=0.0377) than CD5- DLBCL. The incidence of MYD88, PIM1 and KMT2D mutations and CDKN2A deletion was higher in CD5+ DLBCL (P=0.0189, 0.0032, 0.0173 and 0.0496), while the incidence of DUSP2 and TET2 mutations was higher in CD5- DLBCL (P=0.0305 and 0.0496) (Figure 1, Table 1). By applying the genetics subtyping model which was published on N Engl J Med in 2018, we found that MCD, BN2, N1, EZB and Others subtypes accounted for 50.0%, 4.1%, 4.1%, 0% and 41.7% respectively in CD5+ DLBCL; while in CD5- DLBCL, the above subtypes accounted for 4.3%, 26.1%, 4.3%, 4.3% and 60.9% respectively. CD5+ DLBCL was predominantly MCD subtype (n=12, P=0.0007), while BN2 subtype was more common in CD5- cases (n=6, P=0.0479) (Figure 2).

Table 1. Significant mutations/SV/CNV in CD5+ and CD5- DLBCL cases.

Gene	CD5+ n=24	CD5- n=23	*P*
DUSP2	16.7% (4/24)	47.8% (11/23)	0.0305
MYD88	62.5% (15/24)	26.1% (6/23)	0.0189
PIM1	66.7% (16/24)	21.7% (5/23)	0.0032
KMT2D	41.7% (10/24)	8.7% (2/23)	0.0173
BCL6 SV	0% (0/24)	26.1% (6/23)	0.0094
TET2	0% (0/24)	17.4% (4/23)	0.0496
CDKN2A lost	23.8% (5/24)	0% (0/23)	0.0496

SV, structure variations; CNV, copy number variations

Figure 1 - 906

Figure 1

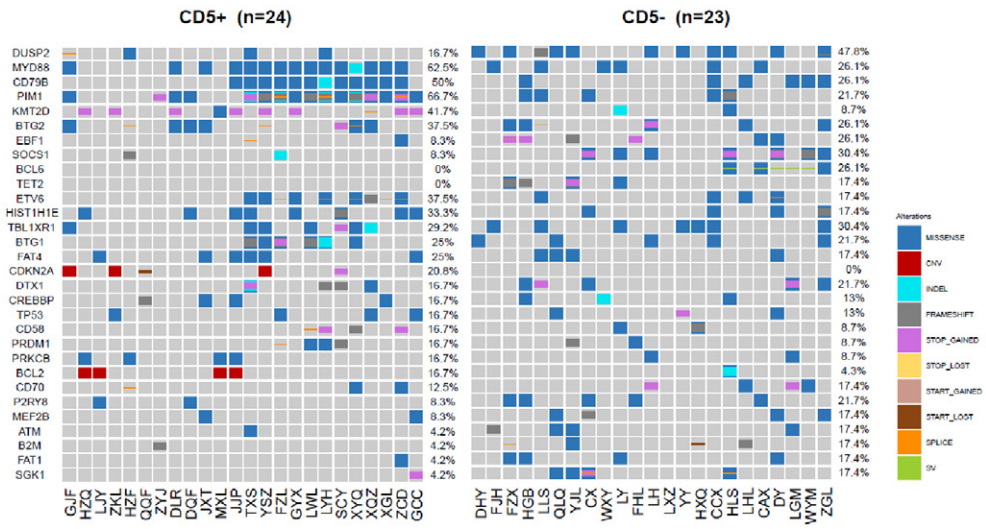

Figure 2 – 906

Figure 2

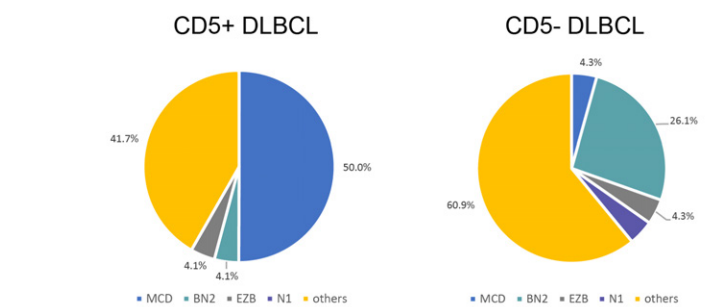

Conclusions: The molecular characteristics of CD5+ DLBCL are unique. MYD88, PIM1 and KMT2D were the most common mutations and 50% cases could be classified into MCD subtype. Identifying the genetic traits of CD5+ DLBCL is helpful for deeply understanding the pathogenesis and for further target therapy developing of this DLBCL subgroup.

907 NGS-Based Detection of Clonal TRG and TRB Rearrangements in Myelodysplastic Syndromes Patients and Correlative Immunophenotype: A Single Institution Experience

Xulei Liu[1], Zinnia Mai[2], Tatyana Sidorenko[2], Meenakshi Mehrotra[3], Shafinaz Hussein[4], Jane Houldsworth[2]
[1]Mount Sinai Health System, New York, NY, [2]Icahn School of Medicine at Mount Sinai, New York, NY, [3]Mount Sinai Medical Center, New York, NY, [4]Mount Sinai Hospital, New York, NY

Disclosures: Xulei Liu: None; Zinnia Mai: None; Tatyana Sidorenko: None; Meenakshi Mehrotra: None; Shafinaz Hussein: None; Jane Houldsworth: None

Background: Clonal expansions of T-cells are common in myelodysplastic syndrome (MDS) patients. Indeed, clonal immunophenotypically-defined T-cell large granular lymphocytes (T-LGL) have been speculated to impact hematopoiesis, potentially contributing to MDS development. Flow cytometric and *TRG*/*TRB* gene rearrangement analyses are routinely performed to assist in the diagnosis of such clonal T-cells. With the introduction of NGS-based methods to detect rearrangements, we sought to evaluate immunophenotypic alterations associated with clonal T-cell expansion in MDS patients.

Design: Extracted DNA from peripheral blood of 54 MDS cases was submitted to *TRG/TRB* gene rearrangement analysis by PCR with detection by polyacrylamide gel electrophoresis as part of routine care. NGS-based *TRG/TRB* assay and analysis (LymphoTrack [Invivoscribe]) was also performed on the same DNAs. Both assays had analytical sensitivities of 5%. Flow cytometric data within 3 months of *TCR* assessment was used, and the makers CD3, CD57, CD56, CD16, CD16/56, CD2, CD5, CD7, CD4 and CD8 were examined. The Wilcoxon rank-sum test was used to compare continuous variables and the Pearson's chi-squared test was used to compare categorical variables. All the statistical analyses were performed using R version 4.0.2.

Results: Of the 54 cases, 41 were positive for *TRG* and/or *TRB* rearrangement according to the gel-based method. However, by the NGS-based method, only 24 were found to be monoclonal/oligoclonal, and the remaining cases were polyclonal or has small clones of uncertain significance. Flow cytometric analyses showed the CD3+/CD57+ as a percentage of total cells or of total lymphocytes in those with NGS-based clonal *TCR* rearrangement was significantly higher than that in those without (Table 1). The percentage of T-cells expressing CD57 was also significantly higher in those exhibiting with a clonal *TRG* or *TRB* rearrangement. Atypical phenotypes were equally found, irrespective of *TCR* clonality.

Table 1. Comparison of characteristics between NGS-based Clonal T-Cell Expansion and Non-Clonal T-Cell Expansion

	Clonal T-Cell Expansion (N=24) Median (IQR)	Non-Clonal T-Cell Expansion (N=30) Median (IQR)	P value
Age	75 (65, 79)	78 (71, 82)	0.07
Gender Female Male	5 (21%) 19 (79%)	9 (31%) 21 (69%)	0.40
T Cells of Total Cells (%)	15.0 (11.0, 26.5)	14.0 (10.0, 18.4)	0.33
T Cells of Lymphocytes (%)	71.0 (65.2, 86.0)	72.0 (60.0, 81.0)	0.35
CD4:CD8 ratio	1.3 (1.1, 1.6)	2.2 (1.3, 3.9)	0.01
Natural Killer Cells of Total Cells (%)	2.4 (1.0, 4.0)	2.4 (1.6, 4.0)	0.89
Natural Killer Cells of Lymphocytes (%)	9.4 (6.0, 17.0)	11.5 (8.1, 20.3)	0.34
CD3+/CD57+ of Total Cells (%)	3.0 (2.2, 6.4)	1.2 (0.4, 3.0)	0.006
CD3+/CD57+ of Lymphocytes (%)	13.2 (9.8, 25.6)	5.8 (2.2, 12.2)	0.002
T Cells with CD57+ (%)	17.6 (14.0, 32.1)	8.7 (3.7, 16.6)	0.007
Atypical Phenotype Present Absent	3 (13%) 20 (87%)	1 (4%) 26 (96%)	0.23

N: number of cases

IQR: interquartile range

Conclusions: Overall, NGS-based assessment of *TCR* clonality in MDS patients resulted in fewer patients interpreted as having clonal T-cell expansions compared to gel-based detection. Samples displaying TCR-clonality as detected by NGS-based methods correlated with elevated proportion of CD3+/CD57+ T-cells. Follow up studies include increase of the dataset size and correlation of clonal T-cell expansions with clinical features and response to therapy.

908 Shorter Latencies in The Pediatric Therapy-Related Myeloid Neoplasms Highlight Their Differences from The Adult Counterparts

Yen-Chun Liu[1], Julia Geyer[2], Bryan Rea[3], Jeffery Klco[1]
[1]St. Jude Children's Research Hospital, Memphis, TN, [2]Weill Cornell Medicine, New York, NY, [3]University of Pittsburgh School of Medicine, Pittsburgh, PA

Disclosures: Yen-Chun Liu: None; Julia Geyer: None; Bryan Rea: None; Jeffery Klco: None

Background: Therapy-related myeloid neoplasm (tMN) in patients with prior cytotoxic therapies is a distinct entity for its adverse prognosis. Though tMN was thought as a complication of the treatment-induced DNA damage, the prevailing knowledge also underlines the importance of factors such as inherited cancer predisposition and clonal selection of CHIP (clonal hematopoiesis of indeterminate potential). Latencies of the tMNs usually fall between 1-10 years based on the adult data. Our recent study characterized the adult tMNs with unusually short and long latencies for their different biology and evaluated the contention to include them into the tMN entity. However, latencies of pediatric tMNs (ped tMNs) have not been well-characterized and it's unclear if we can apply the notion established in the adult tMNs to the pediatric lesions. We sought to characterize the latencies of ped tMNs in comparison with the adult tMNs considering their differences in the t-MN development.

Design: 123 ped tMN cases were retrieved from multiple institutions (n=85) and published series (n=38). Our recently published adult tMN cohort (n=196) was used as a comparison.

Results: In our ped tMN cohort (tMDS: tAML=51:72), the M:F ratio was 1.7:1. The median age was 13.7 yrs (1.2 to 27) at the diagnosis of t-MN and 8.7 yrs (0.5 to 21.9) at the time of primary malignancy. 77/123 tMNs had prior heme malignancies while 46/123 had histories of solid tumors. The median latency of 3 years (0.7 to 16.2) in ped tMNs was significantly shorter than that in the adult tMN ($p<0.01$). 90% of the ped tMNs (but only 62% of the adult tMNs) occurred within 7 yrs of the initial cytotoxic treatment. There were no significant differences between the latencies of the ped tMNs with primary heme malignancies and solid tumors. Latencies were not significantly different between the tMNs with (13/84) and without (71/84) likely pathogenic/pathogenic germline variants. There were no significant associations between different latencies and abnormalities such as del(7q), del(5q), complex karyotype, *KMT2A* or *RUNX1* rearrangement.

Conclusions: The shorter latency of the ped tMN in comparison with the adult tMN underscores their differences, likely due to the known low incidence of CHIP in children, the association between childhood cancers and inherited cancer predisposition, as well as the different spectrum of treatments for pediatric cancers. Caution should be exerted when applying the notions established in the adult studies to the ped tMNs.

909 From the Cell Up: Pairing Flow Cytometry and Deep Machine Learning to Accurately Classify Neoplastic B-Cell Populations to Aid in Diagnosis

Joseph Lownik[1], Serhan Alkan[2], Qin Huang[1], Sumire Kitahara[1]
[1]Cedars-Sinai Medical Center, Los Angeles, CA, [2]Cedars-Sinai Medical Center, Beverly Hills, CA

Disclosures: Joseph Lownik: None; Serhan Alkan: None; Qin Huang: None; Sumire Kitahara: None

Background: The analysis of flow cytometry data requires knowledge of normal and abnormal cell immunophenotypes to accurately gate and classify individual cells. This is classically done by an expert hematopathologist who, by human eye, visualizes and analyzes flow cytometry data in a 2-dimensional space. In contrast, machine learning is able to examine each cell in a high dimension space based on all parameters present in the panel. In this study, we applied immunophenotypic cell type classification by hematopathologists to a deep machine learning model to accurately predict both normal and malignant B-cell subsets.

Design: We created a machine learning training set using previously defined samples from patients without abnormal B-cell populations and patients with small B-lymphoproliferative disorders (BLPD). Flow cytometry files were from a single 10-color panel

(CD45, CD5, CD10, CD11c, CD19, CD20, CD22, CD23, sLambda, sKappa) primarily constructed to characterize B-cell populations with limited markers to characterize other WBC populations based on CD45, SSC & CD11c. Equal portions of all identified cell types were used to train the model using the random forest machine learning algorithm. This model was then used to predict cell types based off of all fluorescent markers as well as scatter parameters, with sensitivity and specificity as outcomes.

Results: Overall, the machine learning model had a >98% sensitivity and >99% specificity in cell type classification. The lowest sensitivity and specificity were seen in identification of monocytes and neutrophils due to the fact that this panel was designed to characterize B-cells and did not include sufficient markers to classify the former. As expected by the traditional algorithmic approach to identify and subclassify abnormal small BLPD, the machine learning model identified that CD20 and CD5 were the most important markers that distinguish abnormal from normal B-cell populations.

Table 1: Results from cell type classification using the Random Forest machine learning algorithm.

			Sensitivity	Specificity	PPV	NPV
CD19$^-$	**Non-B cells**	Granulocytes	0.987	0.999	0.998	0.999
		Monocytes	0.981	0.999	0.984	0.998
		T cell	0.998	0.999	0.995	0.999
		CD5$^-$ CD19$^-$ Lymphs	0.987	0.999	0.993	0.999
CD19$^+$	**Normal B cells**	sKappa$^+$	0.988	0.999	0.985	0.999
		sLambda$^+$	0.990	0.999	0.995	0.999
	Abnormal B cells	CD5$^-$ sKappa$^+$	0.984	0.999	0.969	0.999
		CD5$^-$ sLambda$^+$	0.979	0.999	0.986	0.999
		CD5$^-$ sLC$^-$	0.995	0.999	0.997	0.999
		CD5$^+$ CD20$^+$	0.991	0.997	0.977	0.999
		CD5$^+$ CD20$^-$ CD23$^+$	0.997	0.999	0.990	0.999
		CD5$^+$ CD20$^-$ CD23$^-$	0.995	0.999	0.989	0.999

Figure 1 - 909

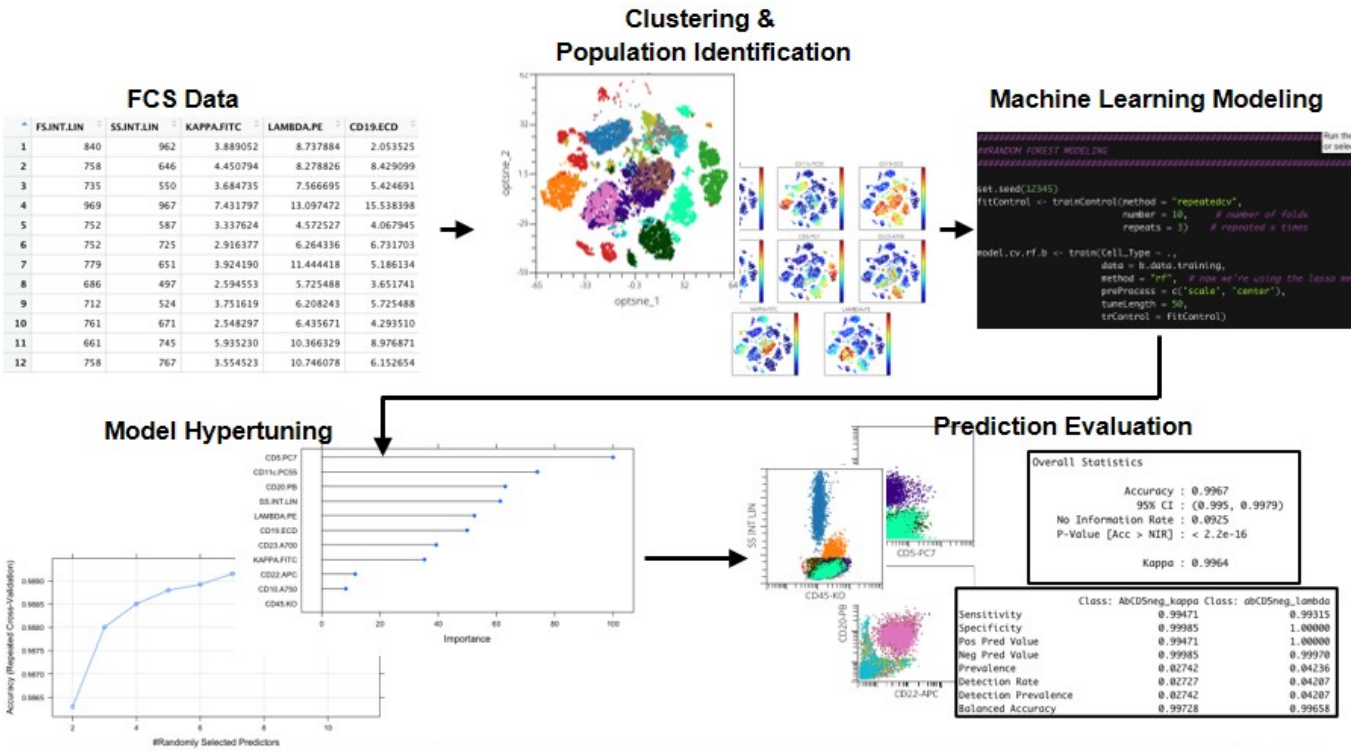

Figure 1: Workflow for deep machine learning model generation. FCS files with raw fluorescent data were initially clustered and gated to identify specific cell subsets. Cell identification with raw fluorescent data for each cell was then used to train a machine learning model using the Random Forest algorithm. The model was then optimized by hypertuning specific parameters of the model. The performance of the model was then evaluated based on overall accuracy in prediction as well as sensitivity and specificity for each individual cell population.

Conclusions: The deep learning model used in the study provided excellent sensitivity and specificity even on a relatively small training set comprising ~25,000 cells. Increasing the training set & including additional well-known immunophenotypic variations of the main BLPDs will likely increase the accuracy and applicability of the model. Machine learning automates the identification of cell subsets and has the potential to aid hematopathologists in identifying low incidence cell populations, such as in minimal residual disease detection.

910 Distinct Immunophenotypic Features of Chronic Myeloid Leukemia Blasts in Chronic Phase

Ly Luu[1], Seema Jabbar[2], Imran Hitto[1], Weina Chen[1], Franklin Fuda[1]
[1]UT Southwestern Medical Center, Dallas, TX, [2]Harlingen, TX

Disclosures: Ly Luu: None; Seema Jabbar: None; Imran Hitto: None; Weina Chen: None; Franklin Fuda: None

Background: Chronic myeloid leukemia (CML) is a clonal myeloproliferative neoplasm defined by left-shifted granulocytic hyperplasia and the fusion protein BCR-ABL1. In the chronic phase, the peripheral blood shows leukocytosis and neutrophilia at various stages of maturation including blasts. The 2016 WHO Classification states that there have been prior studies suggesting adverse prognosis with CD7 expression on CML blasts and does not report any other immunophenotypic data regarding the chronic phase CML blasts. The purpose of this study is to further examine and characterize the immunophenotypic features of CML blasts in the chronic phase.

Design: We searched our hematopathology database for chronic myeloid leukemia, BCR-ABL1- positive cases from 1/2015 to 1/2019. These cases were analyzed by 10-color flow cytometry (FC) with antibody panels directed toward evaluating myeloblasts (MBs). Doublets were excluded from the analysis. The immunophenotypic findings were compared to myeloblasts from other myeloproliferative neoplasms and a prior study performed at our institution.

Results: Eighteen cases (16 bone marrow, 2 peripheral blood, median age 50, 9 males, 9 female) were found with the diagnosis of chronic myeloid leukemia, positive BCR-ABL1 translocation and corresponding 10-color flow cytometric analysis. All 18 cases showed dim expression of CD7 in a subset of MBs with an average of 8.8% of MBs being positive (range 0.38-28%). 8/17 (47%) showed that these CD7(dim +) MBs were also CD13(dim+). 15/18 (83%) cases showed CD11b expression and 13/18 (72%) showed expression of CD56. Of 15 CML cases with CD11b(+) MBs, fourteen (14/15, 93%) showed a characteristic pattern where CD11b(+) MB were consistently CD56(-).

Figure 1 - 910

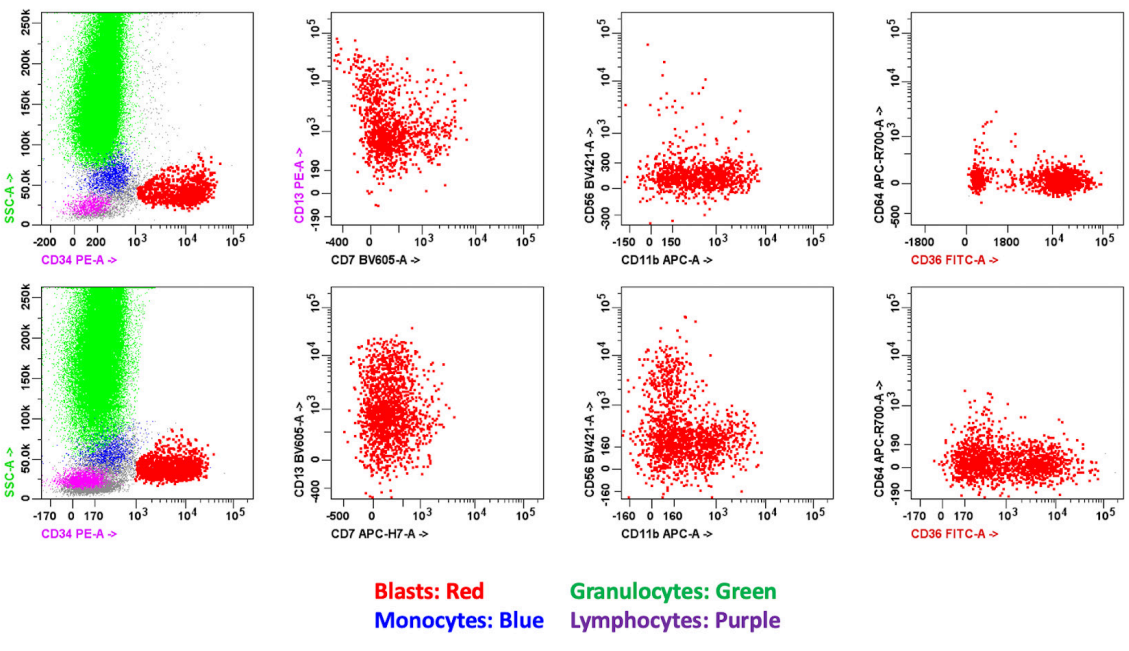

Conclusions: At our institution, we have reported that CD13(dim +) nonneoplastic myeloblasts express dim CD7 expression, similar to the expression pattern seen in less than half of the chronic phase CML blasts, indicating that CD7 expression alone on MBs may not be indicative of neoplasia. However, expression of CD11b and CD56 on MBs are more associated with neoplasia and a combination of these findings may suggest involvement by CML. This is the first study, to our knowledge, to report the distinct immunophenotypic features of CML blasts in the chronic phase.

911 Clinical, Pathologic and Genetic Findings in Acute Myeloid Leukemia with NF1 Mutation

Sameh Mahsoub[1], Robert Hasserjian[2], Weina Chen[1], Jeffrey Gagan[1], Yazan Madanat[1], Olga Weinberg[1]
[1]UT Southwestern Medical Center, Dallas, TX, [2]Massachusetts General Hospital, Harvard Medical School, Boston, MA

Disclosures: Sameh Mahsoub: None; Robert Hasserjian: None; Weina Chen: None; Jeffrey Gagan: None; Yazan Madanat: *Advisory Board Member*, Blueprint pharmaceutical, Stemline therapeutics, Taiho; *Consultant*, GERON; Olga Weinberg: None

Background: Acute myeloid leukemia (AML) is a malignancy of the stem cell/progenitors of the myeloid lineage and is the most common acute leukemia in adults. Although diagnosis can be straightforward; the identification of specific recurrent genetic mutations (e.g., *NPM1, FLT3-ITD, CEBPA*, etc.) have been associated with different clinical presentations, survivals, and overall prognosis. *Neurofibromin 1* gene *(NF1)* is a tumor suppressor gene involved in RAS-MAPK signaling pathway. *NF1* mutations in AML were not heavily studied as compared to other myeloid neoplasms (e.g., juvenile myelomonocytic leukemia). We aimed to study the features of de novo AML cases with normal karyotype associated with *NF1* mutation on overall survival, relapse rate, and other co-mutations commonly encountered in AML.

Design: 185 de novo AML cases from multiple large cancer centers were collected. Clinical, hematopathological, cytogenetic, and molecular data were reviewed. Next generation sequencing (NGS) was performed on all cases. Statistical analysis was done using GraphPad Prism 9.2.0. Survival analysis and unpaired t-test were used.

Results: (8/185, 4.3%) cases with de novo AML harbored mutated *NF1* (NF1+) by NGS. Patients presented at similar age (median 64.5 vs 60.0 years, respectively) with NF1+ and unmutated *NF1* (NF1-) AML (*P*=.62). Seven of 8 NF1+ cases showed normal karyotype compared to 144/177 NF1- AML. Median NF1+ variable allele frequency (VAF) was 38% with a range of 3-69%. Complete blood count and bone marrow parameters at presentations revealed no statistically significant differences (all have *P*>.05). Co-mutations in NF1+ cases included: *DNMT3A, TET2, & NPM1* (3/8) each; *ASXL1, BCOR, NRAS, & U2AF1* (2/8) each; *PHF6* (1/8, *P*=.0013), I*DH2, EZH2, FLT3, FLT3-ITD, CBL, PTPN11*, & *SRSF2* (1/8) each. Comparison of overall survival (OS) showed median OS of 12.5 and 36.8 months for NF1+ and NF1- AML, respectively (*P*=.05). (6/8) NF1+ had median relapse time of 3.9 and 40.7 months in NF1+ and NF1-, respectively. Median survival time to relapse after initial diagnosis was 7.4 and 25.8 months for NF1+ and NF1-, respectively (*P*=.031). Six out of 8 NF1+ had complete remission (CR) vs (150/177) of NF1- (*P*=.4).

	NF1+	NF1-	P value
Cases (number)	8	177	
Age (median)	64.5	60	0.6202
Male (%)	50	55	0.7428
Relapse Time (median)	7.4	25.8	0.0315
Relapse (%)	75	49.1	0.1543
Overall Survival (median)	12.5	35.4	0.061
Complete Remission	6	150	0.461
PHF6 co-mutation (number)	1/8	1/177	0.0013
WBC (x 10^9/L, mean)	10.25	41.5	0.1417
PB Blasts (%, mean)	18.63	36.19	0.1379
HGB (g/dL, mean)	9.963	9.249	0.4035
PLT (x 10^9/L, mean)	88.5	95.12	0.8204
BM Cellularity (%)	81.25	81.66	0.9534
BM Blasts (%, mean)	65.13	61.92	0.6884
Normal Karyotype (%)	12.5	18.6	0.6628
Bone Marrow Transplantation (%)	75	55.9	0.2895

Figure 1 - 911

Figure 1: NF1+ vs. NF1-

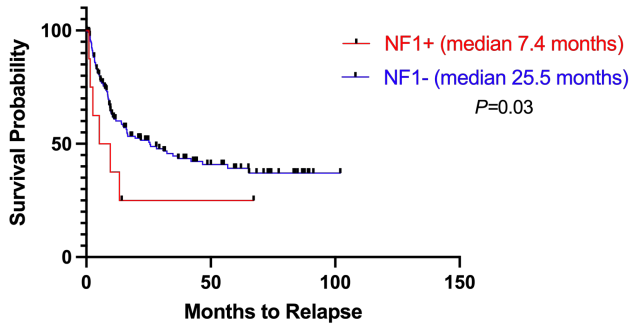

Figure 2 - 911

Figure 2: NF1+ vs. NF1-

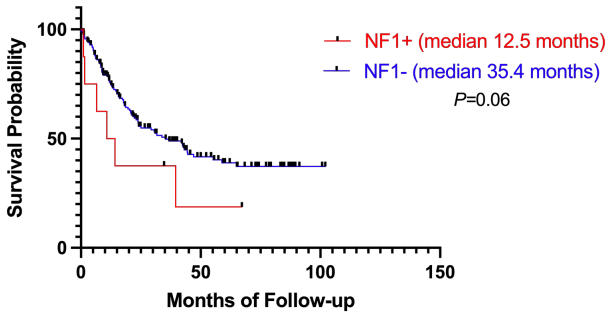

Conclusions: Our study indicates that *NF1* mutation in AML is uncommon and characterized by frequent co-mutation with *PHF6* and poor prognosis compared to the normal karyotype AML patients. Our findings suggest that this may represent a distinct entity and should be considered to have different clinical outcome.

912 EBV-positive Diffuse Large B-cell lymphomas of the CNS: A Report of 12 Cases

Brenda Mai[1], Andres Quesada[2], Wei Wang[3], Haval Ali[3], Ahmed Ahmed[3], Meenakshi Bhattacharjee[4], Wei Wang[2], Zhihong Hu[1]

[1]The University of Texas Health Science Center at Houston, Houston, TX, [2]The University of Texas MD Anderson Cancer Center, Houston, TX, [3]McGovern Medical School at UTHealth, The University of Texas Health Science Center at Houston, Houston, TX, [4]The University of Texas at Houston, Houston, TX

Disclosures: Brenda Mai: None; Andres Quesada: None; Wei Wang: None; Haval Ali: None; Ahmed: None; Meenakshi Bhattacharjee: None; Wei Wang: None; Zhihong Hu: None

Background: Epstein-Barr virus (EBV) is usually negative in primary central nervous system (CNS) lymphomas. CNS lymphomas with positive EBV were only rarely reported in the literature and their clinicopathologic features are not well defined.

Design: We retrospectively reviewed cases of CNS lymphomas in our institution during the period of 1/1/2010-7/16/2021. Patients' clinical information and pathologic findings were analyzed, including in situ hybridization (ISH) for EBV encoded small RNA (EBER) and EBV DNA in cerebrospinal fluid (CSF) by polymerase chain reaction (PCR) testing.

Results: There were 102 patients with a diagnosis of CNS diffuse large B-cell lymphomas (DLBCL). Of 33 patients with available EBV staining information, 12 (36.4%) cases were positive for EBER ISH. There were 4 women and 8 men with a median age of 41.0 years (range, 29.5-68.4). Among these 12 patients, 7 patients were human immunodeficiency virus (HIV)-positive, 2 patients had a history of renal transplantation, 1 patient had rheumatoid arthritis on immunosuppressants, and 1 patient had a history of subcutaneous T-cell lymphoma status post chemotherapy and high-dose methotrexate. The remaining one patient had no significant medical history. Histologic examination of all biopsies demonstrated large lymphoma cells with perivascular accentuation, similar to that of EBV-negative CNS DLBCL. EBER ISH showed diffuse and strong positivity in the lymphoma cells. Among 10 cases with available immunophenotypic information for evaluating cell of origin, all (100%) had a non-germinal center B-cell subtype. The detection of EBV DNA in CSF by PCR testing was positive in 4/9 (44.4%) patients. Nine patients received high-dose methotrexate including 6 of them with additional rituximab treatment. One patient received allogeneic stem cell transplant, and 2 HIV-positive patients had palliative therapy. The median follow-up was 2.6 months (range, 0.1 – 30.6) and at the last follow-up, all patients were alive and 2 HIV-positive patients were discharged to hospice care.

Conclusions: EBV-positive CNS lymphomas represent 36.4% of all DLBCL cases in our study with a male preponderance. Most of these EBV-positive CNS DLBCL cases occurred in immunocompromised patients, and their histology is similar to EBV-negative DLBCL of CNS. Our study indicates the necessity of performing EBER ISH on CNS lymphomas, especially in immunosuppressed patients.

913 Persistent NUP98 Rearrangement May Portend Poor Prognosis

Shikha Malhotra[1], Marietya Lauw[2], Brian Lockhart[3], Svetlana Yatsenko[4], Zhongxia Qi[2], Mary Ann West[5], Steven Swerdlow[6], Nathanael Bailey[7], Sara Monaghan[6], Vinodh Pillai[3], Linlin Wang[2], Nidhi Aggarwal[6]
[1]UPMC Presbyterian Hospital, Pittsburgh, PA, [2]University of California, San Francisco, San Francisco, CA, [3]Children's Hospital of Philadelphia, Philadelphia, PA, [4]University of Pittsburgh Medical Center, Pittsburgh, PA, [5]UPMC Magee-Womens Hospital, Pittsburgh, PA, [6]University of Pittsburgh School of Medicine, Pittsburgh, PA, [7]University of Pittsburgh, UPMC, Pittsburgh, PA

Disclosures: Shikha Malhotra: None; Marietya Lauw: None; Brian Lockhart: None; Svetlana Yatsenko: None; Zhongxia Qi: None; Mary Ann West: None; Steven Swerdlow: None; Nathanael Bailey: None; Sara Monaghan: None; Vinodh Pillai: None; Linlin Wang: None; Nidhi Aggarwal: None

Background: Gene rearrangements involving NUP98 (NUP98-r) are seen in a variety of hematologic malignancies, are enriched in pediatric leukemias and portend a poor outcome, requiring the early use of hematopoietic stem cell transplant. Since these rearrangements are often cryptic with >30 potential partners, break apart fluorescence in-situ hybridization (FISH) studies become the mainstay of follow up of these patients. Following detection of an unusual pediatric case of MPAL with persistence of *NUP98*-r post therapy (PMID-33784031), in the absence of morphological evidence of disease, we aimed to analyze the follow up of *NUP98*-r acute myeloid leukemia (AMLs) and mixed phenotype acute leukemia (MPALs) to determine the incidence of this phenomenon and its clinical implications.

Design: A total of 15 *NUP98*-r AML (n=13) and MPAL (n=2, B/myeloid) were reviewed from 3 institutes at diagnosis and follow up for bone marrow morphology, blast percentage, cytogenetic (including FISH) and molecular abnormalities, and overall clinical course.

Results: Patient age ranged from 1 day to 73 years with male:female ratio of 5:3. Three of these cases demonstrated a higher disease burden on cytogenetic studies than on morphology. These cases demonstrated progressive disease with subsequent progression or relapse (Table 1).

The first case was of a 13-year-old female with a cryptic t(5;11) and additional *NRAS* and *CEBPA* (monoallelic) mutations. After an initial fall in blast count and *NUP98*-r burden post therapy, FISH showed high level *NUP98*-r cells while morphology was negative (Fig. 1). The patient underwent stem cell transplant but had two recurrences/relapses, each of which was preceded by an elevation in *NUP98-r* cells by FISH studies. During her clinical course, she also developed additional genetic abnormalities and succumbed to her disease at 1.5 years from initial diagnosis.

In the second patient, the AML arose from a therapy related myeloid neoplasm with disproportionately high *NUP98*-r cells, within a brief period of 3 months.

The third patient demonstrated a del(5q) clone harboring an additional t(9;11), possibly representing a background dysplastic population. This patient had persistent disease at 5 month follow up marrow.

Age (Years)	13	59	72
Gender	F	M	F
Original Diagnosis	MPAL, B/Myeloid	tMN following Mantle Cell Lymphoma	tAML
Blast Percentage at Diagnosis	58	9	70
Mutation Analysis	NRAS, CEBPA	Initially negative. IDH1 and IDH2 mutations with transformation to AML.	Only TET2 mutation initially. Additional WT1 mutation at relapse.
Therapy and follow up	Induction I as per COG AAML1031 protocol with intrathecal Cytarabine. Induction II with cytarabine, mitoxantrone. Allo-MUDSCT received 6 months after diagnosis following MRD negative flow-cytometry. Patient relapsed 2 months after HSCT and received intrathecal cytarabine and palliative chemotherapy (maintenance azacitidine) for the same.	Treated for the t-MN with Vidaza. Subsequent t-AML treated with Fludarabine and high dose Cytosine induction chemotherapy. Re-induction for persistent circulating blasts (20%) at Day 16. Second re-induction (idarubicin/cytarabine) for persistent peripheral blasts (62%) at day 14.	tAML with t(9;11) and NUP98-r cells proportionate to blast percentage on morphology/FISH treated with BEAT AML study protocol. Relapse at 16 months from diagnosis with additional TET2 mutation, deletion 5q, and disproportionately high number of NUP98-r cells on FISH. Giltertinib started.
Outcome	Deceased 11 months after HSCT	Transformation to tAML within 3 months of diagnosis. Patient deceased 1.5 months after AML diagnosis.	Persistent disease at 5 months following relapse.

Figure 1 - 913

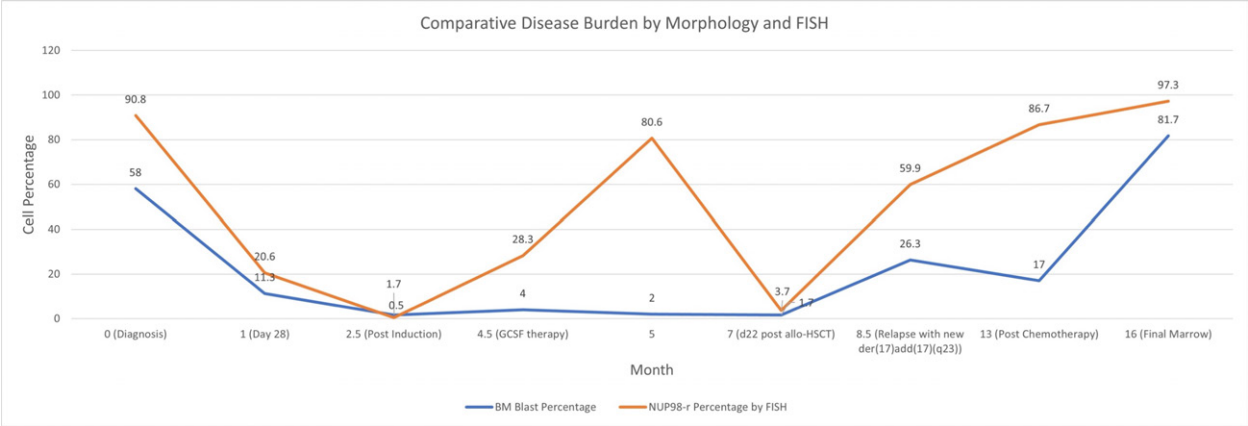

Conclusions: FISH/Cytogenetics may be better predictive of clinical course than morphology or flow cytometry in NUP98-r cases. Disproportionately high level of *NUP98*-r cells in the face of morphologic remission may suggest impending relapse or progression.

914 Novel Marker IRF8 Helps Differentiate Between CD30-Positive Large Cell Lymphomas

Daniel McQuaid[1], Sam Katz[1], Mina Xu[2]
[1]Yale School of Medicine, New Haven, CT, [2]Yale University, New Haven, CT

Disclosures: Daniel McQuaid: None; Sam Katz: None; Mina Xu: *Consultant*, Seattle Genetics, Pure Marrow, Blueprint Medicines

Background: Interferon regulatory factor 8 (IRF8) is a new biomarker shown to be positive in monocytic leukemias as well as in B cells. As a transcription factor, it plays a critical role in pre-B cell differentiation and induction of tolerance pathways, among other functions. Given the frequent diagnostic dilemma in CD30-positive large cell lymphomas that could resemble both Hodgkin lymphoma and anaplastic large cell lymphoma (ALCL), we sought to determine whether IRF8 can be useful in distinguishing between these neoplasms that require different treatment strategies.

Design: In this retrospective study, 74 cases of classic Hodgkin lymphoma (CHL) and 7 cases of nodular lymphocyte predominant Hodgkin lymphoma (NLPHL) on a tissue microarray (TMA), and 15 individual cases of ALK-negative ALCL were stained for IRF8. PAX5 immunostaining of the TMA was also performed and compared alongside since that marker is occasionally the only marker to help clinically differentiate between T and B cell lymphomas with anaplastic/Hodgkin-like cytology.

Results: All of the ALCLs were negative for IRF8 (100%) while all of the NLPHLs (100%) and 85% of the CHLs were positive for IRF8. There were 6 cases of CHL (8%) that were PAX5-negative but IRF8-positive. Conversely, there were 7 cases of CHL (10%) that were PAX5-positive but IRF8-negative. Total of 4 cases of CHL (6%) that were negative for both PAX5 and IRF8.

Classic Hodgkin Lymphoma

	PAX5 Positive	PAX5 Negative	Total
IRF8 Positive	55 (76%)	6 (8%)	61
IRF8 Negative	7 (10%)	4 (6%)	11

IRF8

Lymphoma Subtype	Negative	Positive	Total
Classical Hodgkin Lymphoma	11 (15%)	63 (85%)	74
Nodular Lymphocyte Predominant Hodgkin Lymphoma	0	7 (100%)	7

Figure 1 - 914

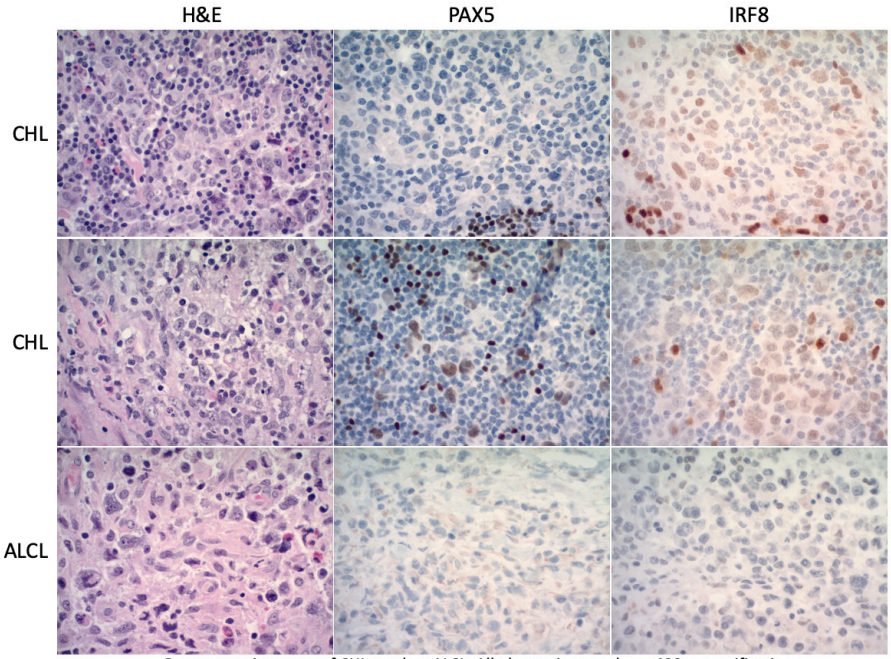

Representative cases of CHLs and an ALCL. All photomicrographs at 400x magnification.

Conclusions: There is significant morphologic and immunophenotypic (CD30-positive and CD45- and CD20-negative) overlap between CHL and ALCL. Since many ALCLs show downregulation of lineage specific T cell markers or are “null-cell” type, only PAX5 has been a reliable marker to differentiate between borderline cases. This is further confounded by positivity of PAX5 in some ALCLs due to amplification of PAX5. Based on recent discoveries of IRF8 function as well as performance as an immunostain, we tested this marker in human lymphoma samples and found that it aids in the discrimination between these tumors.

915 Flow Cytometry Forward Scatter as a Predictor of Large Cell Transformation in Follicular Lymphoma: A Retrospective Cyto-Heme Inter-Institutional Collaborative (CHIC) study

Joshua Menke[1], Linlin Wang[2], Yi Xie[2], Rama Yakubu[3], Ronald Balassanian[2], Annabel Frank[2], Srishti Gupta[4], Jason Kurzer[5], Steven Long[2], Yasodha Natkunam[5], Roberto Ruiz-Cordero[2], Kwun Wah Wen[2], Dita Gratzinger[6]
[1]Stanford Health Care, Stanford, CA, [2]University of California, San Francisco, San Francisco, CA, [3]UCSF Pathology, San Francisco, CA, [4]University of Virginia, Charlottesville, VA, [5]Stanford Medicine/Stanford University, Stanford, CA, [6]Stanford University Medical Center, Stanford, CA

Disclosures: Joshua Menke: None; Linlin Wang: None; Yi Xie: None; Rama Yakubu: None; Ronald Balassanian: None; Annabel Frank: None; Srishti Gupta: None; Jason Kurzer: None; Steven Long: None; Yasodha Natkunam: None; Roberto Ruiz-Cordero: None; Kwun Wah Wen: None; Dita Gratzinger: None

Background: Follicular lymphoma (FL) is typically an indolent, low-grade B-cell lymphoma, although a small subset of cases transform to large B-cell lymphoma. Detection of these rare transformation events requires close clinical follow up, imaging, and serial biopsies often with flow cytometry (FACS). Forward scatter (FSC) is studied on every event in all tubes by FACS and is known to correlate with cell size. We hypothesized that FSC could be used to predict large cell transformation in FL.

Design: All 127 patients had a history of FL and underwent 175 procedures, including 133 fine needle aspiration biopsies with or without core biopsy, 5 core biopsies alone, and 37 surgical biopsies to rule out transformation between 2012-2016. FACS was performed on all specimens at two academic FACS laboratories. Of the 175 specimens, 146 (83%) had flow plots available for review. FSC properties were used to draw a large cell gate that uniformly included monocytes and a small cell gate that included normal B-cells and T-cells in control samples. The percentage of lymphoma cells in the large and small cell gates were calculated as a percentage of total events. The percentage of large cells that represented all lymphoma cells was then derived. The ‘pROC’ package written in the R programming language was used to draw a receiver operator characteristic (ROC) curve, derive area under the curve, and determine optimal thresholds by Youden’s J statistic and closest top left methods.

Results: Area under the curve was 0.78 with 95% confidence interval of 0.69-0.86. Two distinct thresholds that optimized specificity and sensitivity were 0.36 (Youden method) and 0.25 (closest top left method); both are plotted on ROC curve in Figure 1. For the Youden method, the specificity was calculated as 81% and sensitivity as 69%. Negative predictive value was 85% and positive predictive value was 62%. The 19 false positives showed FL in biopsy, including only one FL grade 3A, 14 FL grade 1-2, and 4 FL that could not be graded.

Figure 1 - 915

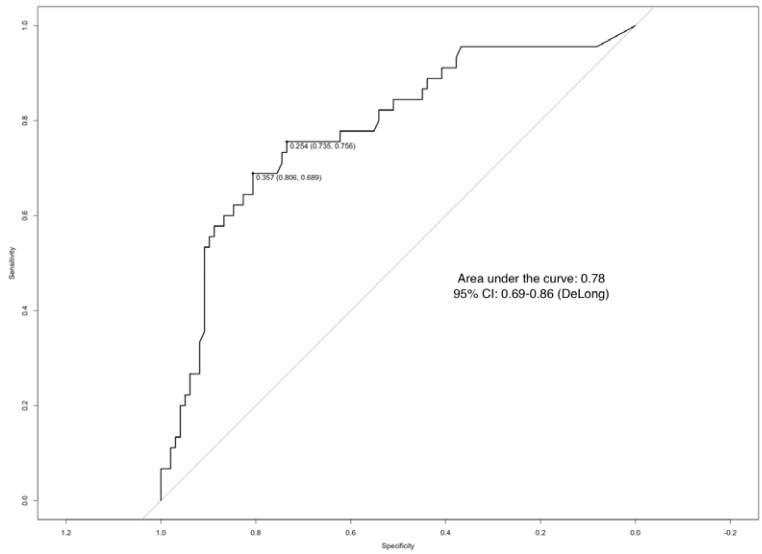

Conclusions: Statistical analysis of FSC in transformed FL cases demonstrated that a threshold of 36% large cells optimizes identification of the transformed subset while minimizing false positives per Youden J statistic. However, despite threshold optimization, multiple false positives still occurred when relying only on the FSC parameters by FACS. Therefore, correlation with intact tissue morphology is critical to prevent overcalling transformation.

916 Final Counts of Monoclonal Gammopathy of Renal Significance (MGRS) after Bone Marrow Biopsies (BMB) and Follow-up

Brandon Metcalf[1], James Zhiyan Huang[2], Wei Li[2], Hassan Kanaan[3], Ping Zhang[4]
[1]Oakland University William Beaumont School of Medicine, Rochester, MI, [2]William Beaumont Hospital, Royal Oak, MI, [3]Beaumont Health, Royal Oak, MI, [4]William Beaumont Hospital, Birmingham, MI

Disclosures: Brandon Metcalf: None; James Zhiyan Huang: None; Wei Li: None; Hassan Kanaan: None; Ping Zhang: None

Background: MGRS is a relatively new concept for patients with renal paraprotein deposition (RPD) (except monoclonal cast nephropathy) with no bone marrow confirmed diagnosis of malignancy or premalignancy (< 10% monoclonal plasma cells). This concept has been used as a reason for a nephrology consult for a bone marrow biopsy (BMB), therefore it is important to evaluate the outcome of MGRS tentatively diagnosed via renal biopsy and confirmed by BMB. This study's purpose was to identify what percentage of various subtypes of MGRS tentatively diagnosed via renal biopsy can be confirmed as MGRS by BMB and follow-up.

Design: In total, 124 renal biopsies with variants of RPD were identified at our center out of 3811 renal biopsies (3.3% of overall cases) over past 10 years. Biopsy cases with known Myeloma, B Cell Lymphoma or Monoclonal Cast Nephropathy were separated as a heavy burden group. The remaining biopsies with RPD were considered as tentative MGRS diagnoses. Their BMB and clinical indices were followed up to determine the percent that resulted in a confirmed MGRS diagnosis.

Results: Among the 124 renal paraprotein deposition cases, 43 cases (34.7%) were categorized to the heavy burden group (Figure). The remaining 81 cases with other variants of RPD were further divided into four categories based on the follow-up. Myeloma or Lymphoma were found in 34 cases (27.4%). Twelve outside consultation cases (10%) did not show follow-up biopsies as we were unable to obtain record access. BMB's diagnosed as nonmalignant (6 cases, 4.8%) or premalignant (29 cases, 23.4%)

were confirmed to be MGRS for a total of 35 cases (28.2%). Among the different categories of tentative MGRS, Monoclonal Light/Heavy Chain Deposition Diseases (L/HCDD) had the highest positivity rate for myeloma on the subsequent BMB (Table). Proliferative Glomerulonephritis with Monoclonal Immunoglobulin Deposition (PGNMID) had a high rate of nonmalignant or pre-malignant diagnosis by BMB. Monoclonal Amyloidosis had some nonmalignant and pre-malignant diagnoses after BMB although myeloma was associated with this renal entity (Table).

Different categories of RPD	Malignant	Nonmalignant	Premalignant	Confirmed MGRS
L/H CDD n = 19	15 (78.9%)	0	4 (21.1%)	4 (21.1%)
Amyloidosis n = 28	15 (53.6%)	1 (3.5%)	13 (42.9%)	14 (46.4%)
PGNMID n = 9	1 (11.1%)	4 (44.4%)	4 (44.4%)	8 (88.8%)
Proximal Tubulopathy n = 6	2 (33.3%)	1 (16.7%)	3 (50.0%)	4 (66.7%)
Cryoglobulin GN[1] n = 4	1 (25.0%)	0	3 (75.0%)	3 (75.0%)
Immunotactoid GN[1] n = 1	0	0	1 (100.0%)	1 (100.0%)
Fibrillary GN[1] n = 1	0	0	1 (100.0%)	1 (100.0%)

[1] GN: glomerulonephropathy

Figure 1 - 916

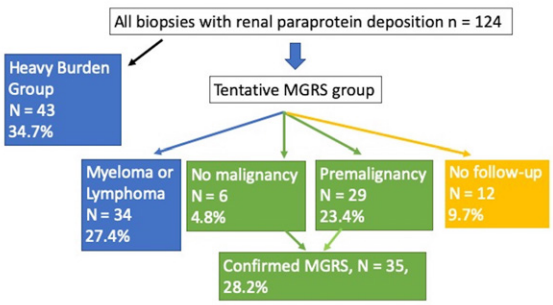

Conclusions: The data indicate that BMB is crucial for confirming a diagnosis of MGRS. The study also provides pathologists and clinicians with general expectations regarding the possible BMB outcome for the many variants of MGRS identified tentatively via renal biopsy.

917 The Evaluation of Blast Subsets Increases the Diagnostic Specificity for Myelodysplastic Syndrome by Flow Cytometry

Howard Meyerson[1], Manish Kumar[2]
[1]University Hospital Case Medical Center, Cleveland, OH, [2]Case Western Reserve University/University Hospitals Cleveland Medical Center, Cleveland, OH

Disclosures: Howard Meyerson: None; Manish Kumar: None

Background: We and others have used flow cytometric (FCM) parameters to predict for MDS. We have found CD177+ neutrophils in addition to the Ogata parameters (B cell progenitors percentage, blast percentage, low side scatter and CD45 blast expression) as sensitive and specific for MDS compared to age-matched cytopenic controls. However, false positive FCM analyses occur in roughly 10-15% of low-grade MDS cases mainly due to low B cell progenitor percentage in many cytopenic controls. We therefore examined whether blast subset parameters in addition to the B cell progenitor percentage could be utilized to enhance the specificity of FCM detection of MDS.

Design: 29 MDS cases (17 without excess blasts) and 27 cytopenic controls (negative by NGS, karyotype and morphology) were evaluated. Blast subsets were determined similar to that used by Shameli et. al (PMID 33369070). A total of 100,000 events were collected and CD34 cells were gated. CD34 subsets were enumerated based on 6 color analysis using a tube stained with CD71, CD371, CD38, CD34, CD19 and CD45. Percentage of CD34+ cells that were CD371+CD38+ (GM-like), CD71+CD371- (erythroid-like), CD71-CD38dim/negative (stem-like), CD19+ (B cell progenitor) and other (none of the above) were determined. Cut-offs were based on control samples and applied to the MDS cases. The percentage of cases showing 0, 1 or 2 or more abnormalities were tallied.

Results: Normal ranges were determined on control specimens as follows: %GM-like (16-45%), %erythroid-like (6-37%), %stem-like (5-37%) and %other (<37%). B cell progenitor cut-off used was <5%, as published in previous studies. 30% of the control specimens contained B cell progenitors <5% compared to 72% of MDS cases, p = 0.001. Blast subsets in the MDS cases more often demonstrated a significantly altered CD34 subset distribution compared to controls for all subsets except "other" (GM-like: 41.4% vs 0, p<0.001; erythroid-like 37.9% vs 0, p<0.001; stem-like 44.8% vs 4%, p<0.0001; other 3.4% vs 4%, ns). Two or more CD34 subsets were abnormally distributed in 65.5% of the MDS cases vs 3.7% of controls, p<0.001. Notably, 7/8 control cases with low B cell progenitors demonstrated a normal distribution of the other CD34 subsets. The PPV for MDS based only on abnormal CD34 subset distribution was 95% with a specificity of 96% in this data set.

Conclusions: FCM of blast subsets appears useful in the evaluation of MDS and reduces false positive rate due to low B cell progenitors in control samples.

918 Myeloid Neoplasms with Inv(3)/T(3;3): High-Grade Malignancies Best Considered Acute Myeloid Leukemia Irrespective of Blast Count

Rehab Mohamed[1], Jeffrey Vos[2], Jerome Givi[1], Cara Randall[2]
[1]West Virginia University School of Medicine, Morgantown, WV, [2]West Virginia University, Morgantown, WV

Disclosures: Rehab Mohamed: None; Jeffrey Vos: None; Jerome Givi: None; Cara Randall: None

Background: Inv(3)/t(3;3) is a recurrent cytogenetic abnormality identified in a relatively small subset of myeloid neoplasms which results in unregulated cellular proliferation due to overexpression of the MECOM gene (EVI1). Despite their aggressive clinical course and uniformly poor prognosis, these neoplasms are currently classified as either myelodysplastic syndrome (MDS) or acute myeloid leukemia (AML) based on the bone marrow and/or peripheral blood blast percentage.

Design: A retrospective review of cases from our tertiary academic center was performed to identify patients with MDS or AML with inv(3)/t(3;3) between 2006-2021. Only patients with available bone marrow biopsy and cytogenetic studies were included in this study. Patient demographics including age, sex, prior medical history, clinical status at diagnosis, subsequent therapy, and outcome were obtained via review of the electronic health record.

Results: Within the 15 year study period, 13 patients were identified with MDS or AML with inv(3)/t(3;3). The study group consisted of 8 males and 5 females, ranging from 40 to 84 years of age. Based on blast percentage, 4 patients (30.1%) were diagnosed with MDS while the remaining 9 patients (69.2%) were diagnosed with AML. Among the group of patients originally diagnosed with MDS, clinical presentation and initial peripheral blood blast percentage varied considerably. Patient #1 (66 year old male) presented with persistent thrombocytosis, an initial peripheral blood blast count of 2% and died of disease within 9 months of diagnosis. Patient #2 (84 year male) presented with thrombocytosis, leukopenia and 4% blasts, and showed progressive disease with a 15 month survival. The remaining 2 patients (60 year old male & 61 year old female) are currently alive with disease, 5 and 15 months following initial diagnosis respectively, but showed rapid progression to AML following their initial presentation. Finally, all cases initially diagnosed as AML showed a rapid clinical course with a median OS of 5 months.

Figure 1 - 918

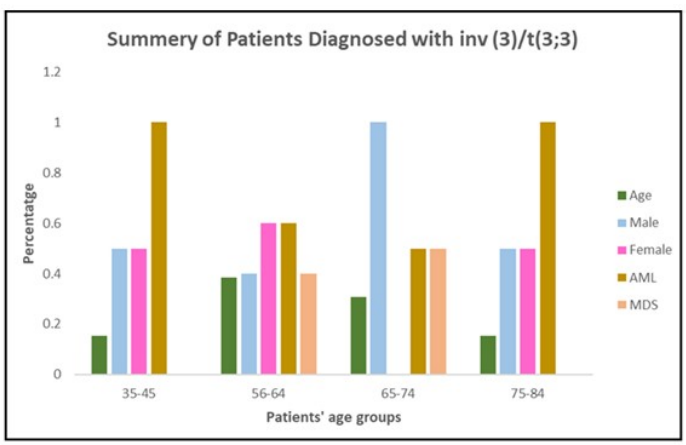

Conclusions: MDS with the inv(3)/t(3;3) uniformly showed an aggressive clinical course with poor OS. In particular, patients initially diagnosed with MDS showed rapid progression of their disease and similar OS as patients initially diagnosed with AML. These data offer further evidence that myeloid neoplasms harboring this recurrent cytogenetic abnormality should be diagnosed and treated as acute leukemia regardless of the presenting blast percentage.

919 NGS Clonality Assessment Shows that Many Synchronous or Metachronous PTLD Lesions are Clonally Distinct if EBV-Positive but Often Clonally Related if EBV-Negative

Erika Moore[1], Bijal Parikh[2], Vikas Dharnidharka[2], Dita Gratzinger[3], Steven Swerdlow[1], Marianna Ruzinova[2]
[1]University of Pittsburgh School of Medicine, Pittsburgh, PA, [2]Washington University School of Medicine, St. Louis, MO, [3]Stanford University Medical Center, Stanford, CA

Disclosures: Erika Moore: None; Bijal Parikh: *Speaker*, Cepheid; Vikas Dharnidharka: *Consultant*, Atara Bio, MedinCell; *Grant or Research Support*, CareDx; Dita Gratzinger: None; Steven Swerdlow: None; Marianna Ruzinova: None

Background: While prior studies have demonstrated that synchronous and metachronous lesions with post-transplant lymphoproliferative disorders (PTLD) may be clonally related or unrelated, they have been limited and have relied on low-resolution Southern blot and PCR technologies. In order to further address this issue, and to better understand disease progression in PTLD, clonality analysis using next generation sequencing (NGS) was utilized on a series of recurrent or multifocal polymorphic/monomorphic B-cell PTLD.

Design: 33 samples of recurrent or synchronous lesions with polymorphic or monomorphic B-cell PTLD with available paraffin embedded material from 14 patients were identified from a multi-institutional clinicopathologic study of viral genomes in PTLD. EBV status was assessed by EBER in situ hybridization. DNA was extracted from formalin fixed paraffin embedded tissue for IGH clonality studies and analyzed utilizing the LymphoTrack® IGH FR2/3 Assay-S5/PGM™ reagents (Invivoscribe Technologies). NGS was performed on a ThermoFisher Scientific Ion Torrent S5™ sequencer. The LymphoTrack® Software-S5/PGM™ Version 2.4.5 was used to analyze the IGH rearrangement sequences and relative proportion of the sequences was determined as a percentage of total sequencing reads. The results were correlated with the clinicopathologic findings.

Results: The clinical information and molecular findings are shown in Table 1. Six patients had recurrent PTLD following remission and 8 had synchronous or metachronous PTLD without intervening remission. Molecular analysis revealed that among the evaluable cases, 4 patients had clonally-related PTLD (3 EBV $^{-}$), while 6 patients had clonally-unrelated PTLD (all EBV^{+}). Two patients with >2 samples had both clonally-related and clonally-unrelated lesions. In our cohort, recurrent cases were an even mix of EBV^{+} and EBV^{-} lesions, while multifocal samples were predominantly EBV^{+}.

Case No.	Age at 1st Dx/ Gender	Transplant Type	PTLD Site	Time from 1st Dx (months)	Histology	EBER Result	IGH Sequencing	Initial Treatment	Clinical Follow-Up
Remission Between PTLD Occurrences									
1	9/M	Heart and lung	Cecal polyp	11	M-PTLD, DLBCL	Pos	C	Decreased immunosuppression	Remission
			Left neck lymph node		P-PTLD	Pos	C (different clone)		
2	39/M	Bilateral lung	Left tongue base	17	M-PTLD, DLBCL	Pos	C	Rituximab, systemic chemotherapy, & radiation	Remission
			Esophagus		M-PTLD, DLBCL	Pos	C (different clone)		
3	17/M	Heart	Jejunum	7	M-PTLD, Burkitt	Pos	C	Rituximab, cytoxan, & methylprednisone	Deceased
			Mediastinum		M-PTLD, Burkitt	Pos	C (same clone)		
			Abdominal wall	152	M-PTLD, High grade B-cell lymphoma	Neg	C (different clone)		
4	52/M	Renal, Pancreas	Right axillary lymph node	18	M-PTLD, DLBCL	Neg	C	Rituximab, systemic chemotherapy	Deceased
			Retroperitoneum		M-PTLD, DLBCL	Not done	C (same clone)		
5	12/F	Heart	Omentum	10	M-PTLD, plasmacytoma	Neg	C	Rituximab, cytoxan, & methylprednisone	Remission
			Small intestine		M-PTLD, plasmacytoma	Neg	C (same clone)		
6	17/F	Heart	Right pelvic mass	20	M-PTLD, DLBCL	Neg	P*	Rituximab, cytoxan, & methylprednisone	Deceased
			Left ovary		M-PTLD, DLBCL	Neg	P*		
Simultaneous/No Remission Between PTLD Occurrences									
7	61/F	Renal	Right inguinal lymph node	22	Difficult to classify with plasmacytic features	Pos	C	Rituximab & systemic chemo-therapy	Remission
			Left lower lung lobe		M-PTLD, DLBCL	Pos	C (different clone)		

8	12/M	Heart	Spleen	0.75	M-PTLD, DLBCL	Pos	C	Decreased immunosuppression, Rituximab	Deceased
			Lung		P-PTLD	Pos	C (different clone)		
9	54/F	Liver	Tonsil	0.25	M-PTLD, DLBCL	Pos	C	Decreased immunosuppression, Rituximab	Remission
			Tonsil (deeper biopsy)		M-PTLD, DLBCL	Pos	C (different clone)		
10	4/M	Bilateral lung	Mesentery	2	P-PTLD	Pos	C	Rituximab, cytoxan, & methylprednisone	Deceased
			Liver		P-PTLD with increased large cells	Pos	C (different clone)		
11	0.5/M	Heart	Left lower lung lobe		M-PTLD, DLBCL	Pos	C	Rituximab, cytoxan, & methylprednisone	Deceased
			Hilar lymph node	0	M-PTLD, DLBCL	Pos	P*		
			Spleen	0	M-PTLD, DLBCL	Pos	P		
			Liver, right lobe	0	M-PTLD, DLBCL	Pos	C (different clone from lung)		
			Right kidney	0	M-PTLD, DLBCL	Pos	C (same clone as liver)		
12	16/M	Heart	Inguinal lymph node	1.5	P-PTLD	Pos	C	Rituximab, cytoxan, & prednisone	Deceased
			Small intestine		M-PTLD, DLBCL	Pos	C (same clone)		
13	20/M	Heart	Peritoneal implant	7	M-PTLD, DLBCL	Neg	C	Rituximab & systemic chemotherapy	Deceased
			Abdominal nodule		M-PTLD, DLBCL	Neg	C (same clone)		
			Right pelvic sidewall mass	9	M-PTLD, DLBCL	Neg	C (same clone)		
14	6/F	Small intestine	Small intestine	0.5	M-PTLD, DLBCL	Pos	C	Rituximab	Remission
			Colon		M-PTLD, DLBCL	Pos	Failed		
	* One framework was polyclonal, the other framework failed								
	C = clonal, P = polyclonal								

Conclusions: NGS clonality studies reveal that patients with >1 PTLD lesion often, but not always, demonstrate clonally unrelated lesions, when they are all EBV$^+$, whether these lesions are seeming relapses or present without intervening remissions. Recurrent or multiple EBV$^-$ lesions appear to more often represent clonally related lesions, the expectation with lymphomas in immunocompetent hosts. Better understanding of clonal relationship in synchronous or metachronous PTLD cases may eventually lead to different therapeutic approaches in EBV$^+$ and EBV$^-$ lesions.

920 Higher Expression of CD44 in De Novo Diffuse Large B-cell Lymphoma Than in Richter Syndrome

Charline Moulin[1], Sébastien Hergalant[1], Romain Piucco[1], Romain Morizot[1], Christine Carapito[1], Luc-Matthieu Fornecker[2], Pierre Feugier[1], Julien Broseus[1], Herve Sartelet[1]
[1]Nancy University Hospital, Nancy, France, [2]Hôpitaux Universitaires de Strasbourg, Strasbourg, France

Disclosures: Charline Moulin: None; Sébastien Hergalant: None; Romain Piucco: None; Romain Morizot: None; Christine Carapito: None; Luc-Matthieu Fornecker: None; Pierre Feugier: None; Julien Broseus: None; Herve Sartelet: None

Background: A subset of patients with chronic lymphocytic leukaemia will experience transformation into Richter syndrome (RS), usually a diffuse large B–cell lymphoma (DLBCL). Clonal relationship based on IGHV analysis can determine a true RS transformation. Separating de novo DLBCL and RS is essential because novo DLBCL have a significantly better prognosis.

The aim of this study is to find a differential expression of proteins in RS and de novo DLBCL.

Design: The study comprised a total of 44 samples, specifically, 18 RS and 26 de novo DLBCL of the non-GCB type. Among the RS, 8 were clonally related, 2 were clonally unrelated and for 8 no information was available regarding the clonal relationship. Initial proteomic screening analysis was processed through liquid chromatography coupled with tandem mass spectrometry (LC-MS/MS). Among this 44 samples, 20 (10 RS and 10 de novo DLBCL were analyzed by immunohistochemistry in order to evaluate the expression of CD44 and PKC-β. H-score was calculated with the semi quantitative evaluation of percentage of positive PKC-β cells multiplied by the weighted intensity of stain. All statistical analyses were performed using Student's t-test. $p < 0.05$ was considered statistically significant.

Results: LC-MS/MS proteomic study identified a panel of proteins differentially expressed between RS and de novo DLBCLs (FDR < 0.05), including CD44 (which was comparatively underexpressed in RS) and PKC-β (which was comparatively overexpressed in RS). The immunohistochemical study confirmed that CD44 is significant higher expressed in de novo DLBCL than in RS ($p< 0.002$). However, the PKC-β is higher expression in RS but the difference is not significant

Conclusions: RS has a very poor prognosis and should not be confused with de novo DLBCL. This study demonstrated the interest of CD44 to immunophenotically distinguish RS from de novo DLBCL.

921 GeneXpert MTB/RIF Assay Compared with Non-molecular Methods on Fine Needle Aspiration Samples for Diagnosis of Tuberculous Lymphadenitis at University Teaching Hospital of Kigali (CHUK)

Louise Munezero[1], Emile Musoni[2], Annette Uwineza[2], Claude Muvunyi[1], Belson Rugwizangoga[2]
[1]University of Rwanda, Kigali, Rwanda, [2]University of Rwanda/CHUK, Kigali, Rwanda

Disclosures: Louise Munezero: None; Emile Musoni: None; Annette Uwineza: None; Claude Muvunyi: None; Belson Rugwizangoga: None

Background: Tuberculous lymphadenitis is one of the most common form of Extra-Pulmonary Tuberculosis (EPTB) whose diagnosis still faces many challenges. The commonly used conventional methods like auramine stain generally has a low sensitivity and specificity. The gold standard culture takes long time to grow, delaying the treatment. Recently, WHO recommended GeneXpert to be used as the initial diagnostic test of EPTB and there are limited data about GeneXpert test on fine needle aspiration samples. The present study aimed to evaluate the diagnostic performance of GeneXpert MTB/RIF assay and compare it with auramine and combined auramine/GeneXpert tests on fine needle aspiration samples

Design: For each patient, Fine Needle Aspiration was performed and the aspirated material was used to prepare slides for cytomorphology and auramine O stain. The needle was rinsed by normal saline to have at least 4ml to process for GeneXpert and culture on Lowenstein-Jensen medium. Culture was considered as gold standard as well as composite reference standard (culture and/ or auramine positive). Analysis was done by SPSS version 27.0, Graph Pad Prism version 9 and MedCalc statistical software. Chi-square, Fisher's exact, odd ratio, Cohen's kappa coefficient, positive/negative likelihood ratio and receiver operator characteristic (ROC) with area under the curve (AUC) were used accordingly, *p* value<0.05 was considered significant.

Results: Taking culture as gold standard, the sensitivity, specificity, PPV and NPV of GeneXpert taking culture as gold standard were 100%, 88.4%, 54.5% and 100% respectively. Considering composite reference standard (culture and/ or auramine positive) specificity and PPV were improved significantly and the values of sensitivity, specificity, PPV as well as NPV were as follow: 94.7%, 94.9%, 81.8% and 98.7%. The GeneXpert showed the excellent accuracy with AUC of 0.942, followed by combined auramine/GeneXpert (AUC: 0.936; excellent accuracy) and auramine with AUC of 0.787 (fair accuracy), p <0.001. This has been supported by the value of likelihood ratios where GeneXpert showed a higher LR+ of 8.620 than combined auramine/GeneXpert (8.196) and auramine (7.172). The values of LR- are 0, 0.367 and 0 for GeneXpert, auramine and combined auramine/GeneXpert respectively. During this study there was no rifampicin resistance detected by the GeneXpert MTB/RIF assay.

Figure 1 - 921

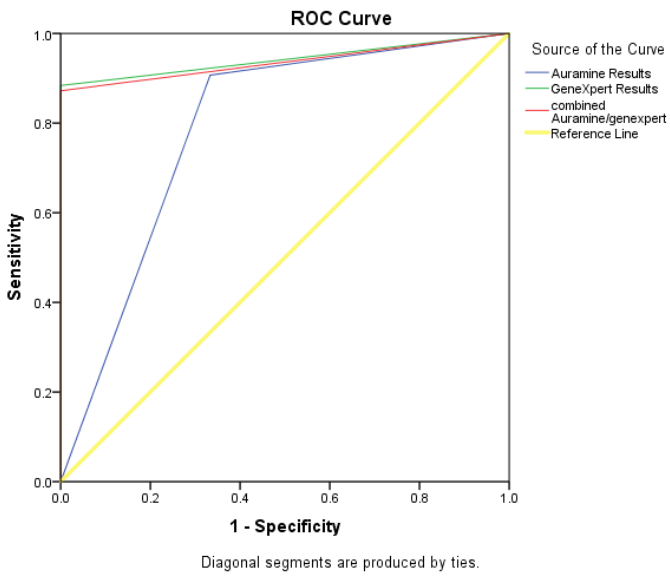

Conclusions: GeneXpert MTB/RIF assay is more accurate than both combined Auramine/GeneXpert and auramine in diagnosis of TBL on fine needle aspiration samples. The implementation of GeneXpert may improve early and accurate diagnosis of TBL and guide for proper treatment.

922 High Ki67 Proliferative Index in Follicular Lymphoma Predicts Treatment Response to Immunochemotherapy-Based Treatment Regimens

Meredith Nichols[1], Sarah Ondrejka[1], Lisa Durkin[1], Brian Hill[1], Eric Hsi[2]
[1]Cleveland Clinic, Cleveland, OH, [2]Wake Forest Baptist Health, Winston-Salem, NC

Disclosures: Meredith Nichols: None; Sarah Ondrejka: None; Lisa Durkin: None; Brian Hill: *Consultant*, Genentech; *Primary Investigator*, Genentech; Eric Hsi: *Consultant*, Loxo, Seattle Genetics, Cytomx; *Grant or Research Support*, Abbvie, Eli Lilly

Background: Follicular lymphoma (FL) is an indolent B cell lymphoma with variable treatment options and clinical course. Prognostic tools such as FL International Prognostic Index (FLIPI) have been developed, but additional predictive and prognostic biomarkers are needed. A recent study suggested that interfollicular staining patterns of CD10, BCL6, and high follicular Ki67 are associated with poor outcome in FL patients treated with chemotherapy-free regimens. We aimed to explore the utility of CD10, BCL6, and Ki67 staining patterns in predicting progression free and overall survival (PFS, OS) in patients treated with immunochemotherapy.

Design: Archival cases of newly diagnosed FL were reviewed from 2009 to 2016. Clinical data (FLIPI score, treatment, progression, PFS and OS) were reviewed. Immunostaining was performed for CD10, BCL6 and Ki67. Interfollicular staining (>10% of cells) for CD10 and BCL6 as well as follicular Ki67 positivity (>30%) were scored for each case (Figure 1). Data were analyzed using Cox proportional hazard (CPH) analysis.

Results: 90 patients (43 M, 47 F; median age 60.5 years) treated with immunochemotherapy within the first 6 months of diagnosis were identified. 58 patients received bendamustine-rituximab (BR), and 32 patients received R-CHOP. FL was predominately low grade (79 grade 1-2, 11 grade 3A). Median follow-up for PFS and OS was 59 and 69 months in the BR group and 51 and 87 months in the RCHOP group. 9 patients had a high FLIPI score (4-5). 76 had low to intermediate FLIPI scores. Univariate CPH analysis showed no difference in PFS or OS stratified by treatment regimen; thus, BR and RCHOP patients were combined for further analysis. High FLIPI was associated with shorter OS but not PFS. Interfollicular CD10 and BCL6 staining was not associated with PFS or OS. However, univariate CPH modeling showed high Ki67 was associated with longer PFS but not OS (Figure 2).

Figure 1 - 922

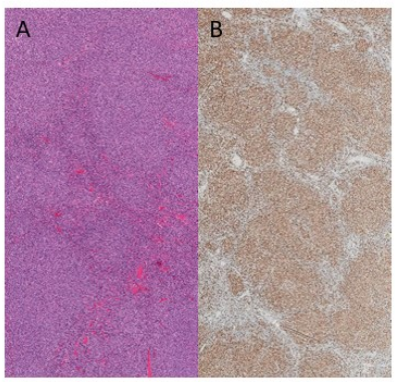

Figure 1: Representative photomicrographs at 2x magnification of the H&E (A) and Ki67 (B) from a case with high follicular staining for Ki67.

Figure 2 - 922

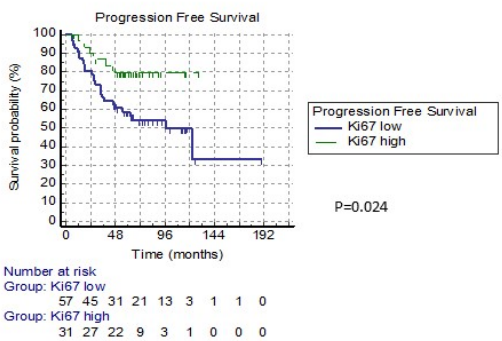

Figure 2: High follicular Ki67 is associated with decreased progression free survival in patients treated with immunochemotherapy.

Conclusions: In FL patients treated with immunochemotherapy, FLIPI score remains the main driver of OS. Interfollicular positivity for CD10 and BCL6 is not associated with PFS in patients treated with chemoimmunotherapy regimens in contrast to previous studies with patients receiving chemotherapy-free regimens. Follicular Ki67 >30% is associated with longer PFS. This may be due to the effects of chemotherapy on highly proliferative cells. These studies highlight the importance of therapy-specific prognostic factors. Highly proliferative low grade FL may benefit from cytotoxic treatment strategies.

923 Prognostic Impact of 8q24/MYC Rearrangement in Myeloma in the Era of Novel Therapy

Okechukwu Nwogbo[1], Shimin Hu[1], Suyang Hao[2], Shaoying Li[1], Jie Xu[1], C. Cameron Yin[1], Carlos Bueso-Ramos[1], Guilin Tang[1], L. Jeffrey Medeiros[1], Pei Lin[1]
[1]The University of Texas MD Anderson Cancer Center, Houston, TX, [2]Houston Methodist Hospital, Houston, TX

Disclosures: Okechukwu Nwogbo: None; Shimin Hu: None; Suyang Hao: None; Shaoying Li: None; Jie Xu: None; C. Cameron Yin: None; Carlos Bueso-Ramos: None; Guilin Tang: None; L. Jeffrey Medeiros: None; Pei Lin: None

Background: Novel therapies have markedly improved the overall survival (OS) of myeloma patients with standard risk disease. *MYC* rearrangement (*MYC*-R) is a known adverse marker in most B cell lymphomas, but its prognostic impact in myeloma is controversial. Currently, *MYC*-R is not part of the revised international staging system and routine testing by fluorescence in situ hybridization (FISH) is not required. We reviewed a large series of myeloma cases carrying 8q24/*MYC*-R to better understand its prognostic impact.

Design: Cases of myeloma with 8q24/*MYC*-R were retrieved from our database from July 1998 through July 2021. Cases identified before January 2021 were all assessed by karyotyping first and routine FISH testing for *MYC-R* was performed on CD138 enriched plasma cells in 2021. The clinicopathological features are reviewed.

Results: The study group included 122 men and 70 women with median age of 65 years (range 20-94 years). 8q24/*MYC*-R was detected at initial diagnosis in 120 patients and at relapse or during follow up in 72 patients. *MYC*-R was detected by FISH alone in 23; the remaining 169 (88%) cases had an abnormal 8q24 usually detected as part of a complex karyotype (n=164). In 73/175 (42%) cases, the 8q24/*MYC* was juxtaposed to 14q32 (n=33), 2p12 (n=15) or 22q11 (n=25); presumably loci of *IGH, IGK or IGL* genes, respectively. The remaining cases involved a wide range of chromosomal loci. *MYC*-R occurred with *TP53* deletion (n=39/95, 41%), *CKS1B* gain/amp (n= 71/91, 78%), *CCND1-IGH* (n=39/130, 30%) respectively. Morphologically, the neoplastic cells showed mature to immature cytology. All patients were treated with proteasome inhibitors and 120/192 (63%) also underwent stem cell transplant. Follow up (FU) ranged from 0.1 to 278.5 mos (median: 33 mos). At last FU, 122/192 (63%) patients had died and 52 (27%) were alive with a median OS of 52 mos. The median interval from detection of 8q24/*MYC*-R to death was 9.4 (range 0.2-120); however, 52 patients survived >36 mos, including 11 long-term survivors (40.5-278.5, median 70.5 mos).

Conclusions: 8q24/*MYC*-R can occur at initial diagnosis or relapse, and commonly involves non-*IG* loci. In most patients, 8q24/*MYC*-R was marked by rapid disease progression and demise, but a small subset of patients survived beyond 3 yrs. This highly variable outcome suggests that the impact of *MYC*-R is nuanced and more studies are needed.

924 Myocyte Enhancer Factor 2B is Consistently Expressed in Neoplastic Cells of Nodular-Lymphocyte Predominant Hodgkin Lymphoma and is Absent in Hodgkin/Reed-Sternberg Cells of Classic Hodgkin Lymphoma: A Paraffin Immunohistochemical Study Across Hodgkin and Non-Hodgkin B-cell Lymphoma Subtypes

Olumide Odeyemi[1], Rebecca Kunak[2], Kaitlyn Nielson[3], Mohammad Vasef[3]
[1]Stanford Pathology, Stanford, CA, [2]Spectrum Health, Grand Rapids, MI, [3]University of New Mexico, Albuquerque, NM

Disclosures: Olumide Odeyemi: None; Rebecca Kunak: None; Kaitlyn Nielson: None; Mohammad Vasef: None

Background: Myocyte enhancer factor 2B (MEF2B) is a transcriptional activator of a variety of genes and is particularly known to upregulate the *BCL6* proto-oncogene. By immunoperoxidase staining, the expression of MEF2B is closely related to that of the germinal center markers BCL6 and CD10 in follicular lymphoma (FL), Burkitt lymphoma (BL), and diffuse large B-cell lymphoma (DLBCL), germinal center (GCB) subtype. MEF2B positivity has also been reported in a variety of other types of B-cell lymphomas, including nodular lymphocyte predominant Hodgkin lymphoma (NLPHL), mantle cell lymphoma and DLBCL, non-GCB type. Overall, studies evaluating MEF2B expression in a variety of hematolymphoid neoplasms remain limited.

Design: De-identified tissue blocks and tissue microarrays (TMAs) containing 180 cases of various hematolymphoid neoplasms, were stained with MEF2B antibody. Diagnostic entities evaluated were FL, DLBCL, GCB subtype, DLBCL, non-GCB subtype, NLPHL, classic Hodgkin lymphoma (CHL), marginal zone lymphoma (MZL), mantle cell lymphoma (MCL), chronic lymphocytic leukemia/small lymphocytic lymphoma (CLL/SLL), lymphoblastic leukemia/lymphoma, hairy cell leukemia (HCL), plasma cell neoplasm (PCN), and blastic plasmacytoid dendritic cell neoplasm (BPDCN). MEF2B showed strong nuclear expression in all positive cases.

Results: MEF2B expression was positive in all evaluated cases of DLBCL, GCB type (9/9), nodal FL (7/7), and NLPHL (19/19). MEF2B positivity was also detected in a subset of FL in decalcified bone marrow core biopsies (14/29), MCL (4/6), DLBCL, ABC type (5/6), and PCN (4/7). MZL cases were predominantly MEF2B-negative, with only 4 of 33 cases expressing the marker. MEF2B was negative in all cases of CHL (0/45), CLL/SLL (0/7), HCL (0/5), lymphoblastic leukemia/lymphoma (0/5), and BPDCN (0/2).

Figure 1 - 924

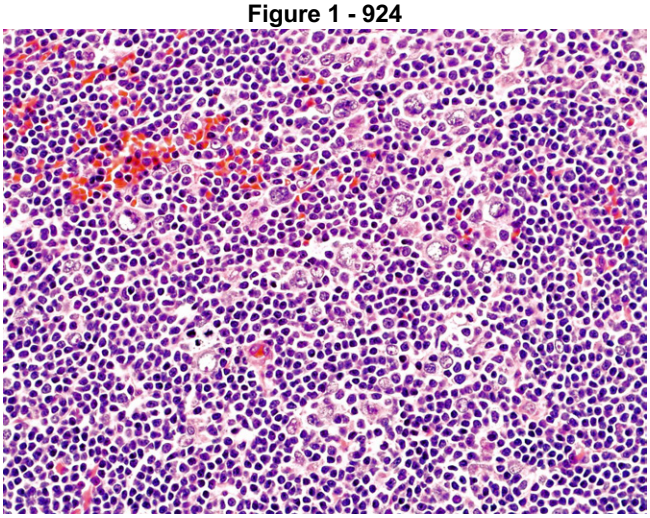

Figure 2 - 924

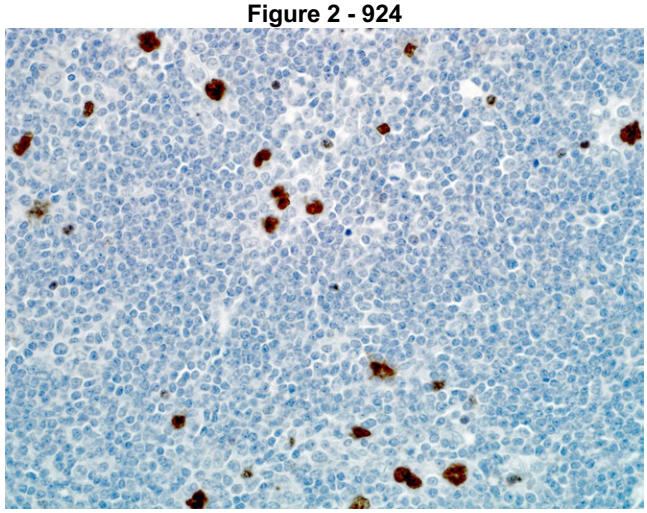

Conclusions: MEF2B positivity in all cases of FL and DLBCL, GCB subtype is consistent with its typical expression profile in germinal center B-cell neoplasms. The consistent expression of MEF2B in NLPHL, along with consistent negative expression in CHL, is especially a key finding that highlights further usefulness of the antibody, in challenging cases, for differentiating between the two disparate types of Hodgkin lymphoma.

925 Routine Evaluation of Minimal Residual Disease in Multiple Myeloma by Next-Generation Flow Cytometry Consistently Detects Abnormal Plasma Cell Clones with 10e-5-10e-6 Sensitivity: A Single Institution Analysis of ~ 7,000 Clinical Cases

Horatiu Olteanu[1], Gregory Otteson[1], Min Shi[1], Dragan Jevremovic[1]
[1]Mayo Clinic, Rochester, MN

Disclosures: Horatiu Olteanu: None; Gregory Otteson: None; Min Shi: None; Dragan Jevremovic: None

Background: Minimal residual disease (MRD) assessment in multiple myeloma (MM) has prognostic and therapeutic implications. The 2016 International Myeloma Working Group consensus recommendations include highly sensitive and specific methods, such as multi-parameter flow cytometry (mpFC) and next generation sequencing as disease-monitoring modalities. Both methods were found able to detect one abnormal plasma cell (PC) in 10^5–10^6 cells. Due to the complexity of establishing such assays in the clinical laboratory, it may not be feasible to achieve a sensitivity of 10^{-6} or lower in the routine practice. Here, we present our experience with the EuroFlow high-sensitivity FC assay, as derived from a large volume of in-house and reference cases. We also highlight assay performance characteristics, including stability, precision and accuracy.

Design: 6,911 consecutive cases (1,971 in-house; 4,940 reference) were evaluated. FC was performed with the standardized 2-tube EuroFlow MM MRD assay. Up to 10 million events were acquired on FACSCanto II (BD Biosciences) cytometers equipped with FACSDiva software, to detect a 20-event abnormal PC cluster. Data analysis was performed in Infinicyt (Cytognos).

Results: MRD was detected in 2,935 cases (42.5%), with a median of 0.0026% abnormal PCs for in-house cases, and 0.0214% for reference cases, respectively. Of these, 1,045 (15.1%) showed MRD in the 10^{-4}–10^{-5} range, while 308 (4.5%) demonstrated $<10^{-5}$ abnormal PCs. Specimen stability was validated up to 72 hours, and the assay was shown to be highly precise, with intra/interassay %CV<25% near the validated limit of detection. Accuracy comparison with an FDA-approved commercial molecular assay (ClonoSEQ, Adaptive Biotechnologies) demonstrated 100% concordance for positive cases by FC (n=20) at a 2 x 10^{-6} MRD cut-off.

Conclusions: Our data from a large cohort of clinical cases confirms the very high detection sensitivity of mpFC in the routine evaluation of MM patients. From an operational standpoint, FC and molecular MRD assays may be employed essentially interchangeable by individual laboratories, based on other practical considerations, such instrumentation, specimen volume, and available local expertise. Advantages of FC include fast turnaround time, no prior requirement of a diagnostic specimen, and lower overall cost. The latter is also achieved by using an algorithmic approach that reflexes MRD testing only to cases that are negative by other, less sensitive, modalities.

926 Clinicopathologic Characteristics of High Grade B-cell Lymphomas with t(3;8)(q27;q24) BCL6/MYC

Anna Owczarczyk[1], Russell Ryan[1], Noah Brown[1], Joo Song[2], Pamela Skrabek[3], Anamarija Perry[1]
[1]University of Michigan, Ann Arbor, MI, [2]City of Hope Medical Center, Duarte, CA, [3]CancerCare Manitoba, Winnipeg, Canada

Disclosures: Anna Owczarczyk: None; Russell Ryan: None; Noah Brown: None; Joo Song: None; Pamela Skrabek: *Consultant*, Novartis; Anamarija Perry: None

Background: High grade B-cell lymphomas (HGBCL) with t(3;8)(q27;q24) *BCL6/MYC* are rare and likely underrecognized, as they are often classified with lymphomas bearing separate *MYC* and *BCL6* rearrangements in routine practice (produce identical break-part fluorescent in-situ hybridization (FISH) results). Furthermore, the prognostic significance of this rearrangement remains unclear given the scarcity of reported cases. The aim of this study was to evaluate the clinical, pathologic, and cytogenetic characteristics of HGBCLs with t(3;8)(q27;q24) *BCL6/MYC*.

Design: A cohort of 10 patients with HGBCLs with t(3;8)(q27;q24) was identified through multi-institutional retrospective searches of pathology databases from 2000-2021. Available tissue was immunohistochemically stained (CD20, CD3, CD10, BCL6, MUM1, C-MYC, BCL2) and FISH studies for *MYC*, *BCL6*, and *BCL2* rearrangements (*MYC* and *BCL6* break-apart, BCL2-IGH dual-fusion) were performed. FISH analysis using a t(3;8)(q27;q24)-custom dual-fusion probe was performed on cases that were found to have *MYC* and *BCL6* rearrangements. If available, clinical information was retrieved from medical records.

Results: Clinicopathologic and cytogenetic characteristics of 10 patients are summarized in Table 1. There were three females and seven males, with a median age of 63 years (range 41-77 years). Clinical stage was available in six patients, and all had high-stage disease (III/IV). Patients were treated with various therapeutic protocols, and many had several lines of chemotherapy. Median follow up was 23 months. Most patients died of disease and only two achieved complete remission. Morphologically, the lymphomas ranged from large cells with prominent nucleoli to medium-sized cells with fine chromatin. Most cases (5/6 tested) demonstrated a *BCL2* rearrangement in addition to t(3;8)(q27;q24). Of the available tested cases, all were positive for CD10 and BCL6. Ki67 was variable, ranging from 40% to > 95%.

Table 1. Clinicopathologic and cytogenetic characteristics of high-grade B-cell lymphomas with t(3;8)(q27;q24) *BCL6/MYC*

	Age/gender	Clinical Stage	Follow-up (months)	Outcome	CD10 IHC	BCL6 IHC	MUM1 IHC	Ki67	*BCL6/MYC* FISH	*BCL2* FISH
Case 1	77/F	NA	NA	NA	NA	NA	NA	N/A	+	NA
Case 2	74/F	NA	115	DOD	+	+	NA	60%	+	NA
Case 3	75/F	IIB	5	DOD	+	NA	NA	70%	+	NA
Case 4	63/M	IIIB	16	DOD	+	+	NA	50%	+	NA
Case 5	53/F	IVBE	89	CR	+	NA	NA	40%	+	--
Case 6	59/F	NA	NA	NA	+	+	--	>50%	+	+
Case 7	41/F	NA	12	DOD	+	+	--	70%	+	+
Case 8	77/F	IVA	29	CR	+	+	--	>90%	+	+
Case 9	56/M	IVE	< 2	PR	+	+	--	>95%	+	+
Case 10	63/M	IIIB	< 12	DOD	+	+	--	80%	+	+

Abbreviations: CR, complete remission; DOD, died of disease; NA, not available; PR, partial remission; +, positive; --, negative; FISH, fluorescence in situ hybridization; IHC, immunohistochemistry.

Conclusions: Our study shows that most HGBCLs with t(3;8)(q27;q24) *BCL6/MYC* also have a *BCL2* rearrangement. Clinically, these are aggressive lymphomas, with most patients responding poorly to therapy and dying of disease within one to two years. Two patients in our study achieved complete remission, one with a *BCL2* rearrangement and one without. Prognostic significance of an isolated t(3;8)(q27;q24) remains uncertain. Larger cohorts are needed to further investigate if these lymphomas truly behave aggressively or if they have a more favorable prognosis.

927 Spectrum of Pathologic Findings and Clonal Evolution in RUNX1 Familial Platelet Disorder with Propensity for Myeloid Malignancy

Neval Ozkaya[1], Lea Cunningham[2], Matthew Merguerian[3], Seila De Leon[3], Nisha Patel[3], Alina Dulau Florea[4], Raul Braylan[3], Paul Liu[3], Katherine Calvo[3]
[1]National Cancer Institute, Bethesda, MD, [2]National Cancer Institute, National Institutes of Health, Bethesda, MD, [3]National Institutes of Health, Bethesda, MD, [4]Clinical Center, National Institutes of Health, Bethesda, MD

Disclosures: Neval Ozkaya: None; Lea Cunningham: None; Matthew Merguerian: None; Seila De Leon: None; Nisha Patel: None; Alina Dulau Florea: None; Raul Braylan: None; Paul Liu: None; Katherine Calvo: None

Background: The *RUNX1* Familial Platelet Disorder with Associated Myeloid Malignancy (*RUNX1* FPDMM) is a rare autosomal dominant cancer predisposition syndrome. The lifetime risk of developing hematopoietic malignancies (HM) is 30–40%, often MDS/AML. Understanding the baseline spectrum of bone marrow morphology, genetic findings, and temporal disease progression is critical to ensure diagnostic accuracy and develop criteria to recognize the onset of HM.

Design: We analyzed the clinicopathologic and genetic findings of 36 patients; 24 adult and 12 pediatric.

Results: 30 patients did not develop HM over a 24-month period; 6 patients developed or had history of HM including 1 AML; 1 CMML, 1 MDS, 1 T-ALL, and 2 plasma cell neoplasm, both positive for CD20. Development of myeloid HM was associated with acquired genetic alterations, additional cytopenia, two or more dysplastic lineages, and/or increased blasts. Peripheral blood abnormalities including thrombocytopenia (78%), abnormal MPV for age (39%), anemia (22%), and eosinophilia (25%) were present at initial evaluation. All 36 patients showed baseline bone marrow abnormalities: low-for-age cellularity (49%), high-for-age cellularity (8%), megakaryocytic atypia (89%) ranging from mild to moderate with features of dysmegakaryopoiesis, dysplastic erythroid and myeloid lineages (8%), eosinophilia (39%), and low to absent B-cell precursors (14%).

Twelve different *RUNX1* mutations were identified, most commonly in the RUNT homology domain. In 76% of patients, *RUNX1* mutation was the only genetic finding. Molecular analysis identified clonality in 24% of patients. Mutations in *BCOR*, *NRAS*, and *TET2* were identified in patients without progression to HM. Patients with HM harbored mutations in genes affecting signaling (*JAK2*, *NRAS*), tumor suppressors (*PHF6*), cellular metabolism (*IDH1*), chromatin-spliceosome machinery (*SF3B1*), and epigenetic regulators (*BCOR*, *EZH2*).

Of the clinically stable patients with isolated thrombocytopenia, normal karyotype, and no acquired clonal genetic alterations, all but one had megakaryocytic atypia.

Conclusions: Given the frequency of baseline megakaryocytic atypia which could be misinterpreted as MDS, separate diagnostic criteria for MDS in *RUNX1* FDPMM is proposed including at least 2/3 of the following: acquired pathogenic genetic alterations, dysplasia in 2 or more lineages, and/or additional non-platelet cytopenia; or increased blasts (5-19%). Acquired genetic alterations may be harbingers of progression to HM in *RUNX1* FDPMM.

928 Discrepant Post Induction Morphology and FISH Findings in Core Binding Factor Acute Myeloid Leukemia: A Diagnostic Pitfall with Clinical Implication

Erik Pearson[1], Juehua Gao[1], Qing Chen[2], Barina Aqil[2], Xinyan Lu[2], Yi-Hua Chen[1]
[1]Northwestern Memorial Hospital, Chicago, IL, [2]Northwestern University Feinberg School of Medicine, Chicago, IL

Disclosures: Erik Pearson: None; Juehua Gao: None; Qing Chen: None; Barina Aqil: None; Xinyan Lu: None; Yi-Hua Chen: None

Background: Acute myeloid leukemia (AML) with inv(16)/t(16;16) or t(8;21) are referred to as core binding factor AML (CBF-AML). These rearrangements disrupt the genes encoding CBF subunits that play a critical role in hematopoiesis. Detection of the cytogenetic abnormalities is diagnostic even when the bone marrow (BM) blast count is <20%. In our practice, we have observed an unusual phenomenon that occurred most frequently in CBF-AML, i.e., increased blasts up to 15% in post-induction BM but negative FISH/cytogenetic results. Evaluation of post-therapy BM has significant clinical impact as reinduction may be indicated.

Design: Patients diagnosed with AML with inv(16)/t(16;16) or t(8;21) from 2010-2020 in our institution were searched from the database. The morphologic findings and ancillary studies in the diagnostic, post-induction and follow-up BMs were reviewed.

Results: A total of 46 patients with CBF-AML were identified including 33 with inv(16)/t(16;16) and 13 with t(8;21). The post-induction BM showed that 17 of 46 (37%) patients had blasts ≥ 5% (up to 15%), but FISH/cytogenetics were negative. The blasts ranged from 5%, 5-10%, to >10% in 11 (65.0%), 5 (29.4%) and 2 (11.8%) cases, respectively. Based on the morphology alone, 3 cases (blasts: 5-10%; 10%; 15%) were considered as residual AML, 2 as low-level residual AML, 5 suspicious for residual AML, 4 unclear (regeneration vs residual AML), and 3 favoring regeneration. None of the patients received reinduction owing to the rapid FISH results. Follow-up BM biopsies revealed resolution of increased blasts and negative FISH results in all 17 patients. Review of therapy history showed that only 2 patients received a FLAG-GO regimen which contains G-CSF, and the remaining patients received conventional chemotherapy.

Conclusions: Our study revealed an unusual phenomenon of a high frequency of increased blasts but negative FISH/cytogenetic results in post-induction BMs in patients with CBF-AML. Our series showed that all of these patients were confirmed to be negative for residual AML on the repeat BM biopsies. The elevated blast count poses diagnostic challenges in post-therapy BM, and FISH/cytogenetic studies are crucial for an accurate diagnosis in patients with CBF-AML. CBF-AML has a favorable prognosis, and recognizing this phenomenon is critical to prevent unnecessary reinduction chemotherapy.

929 Recurrent SETD2 Mutations in T-Cell Large Granular Lymphocytic Leukemia

R. Plowman[1], Jingwei Li[2], Frank Mason[1], R. Lindsley[3], Emily Mason[1], Annette Kim[2]
[1]Vanderbilt University Medical Center, Nashville, TN, [2]Brigham and Women's Hospital, Boston, MA, [3]Dana-Farber Cancer Institute, Boston, MA

Disclosures: R. Plowman: None; Jingwei Li: None; Frank Mason: None; R. Lindsley: None; Emily Mason: None; Annette Kim: None

Background: T-cell large granular lymphocytic leukemia (T-LGLL) is a neoplasm of T-LGLs associated with neutropenia and mutations in *STAT3* (up to 70%) and *STAT5B* (<5%) as well as other rarely reported variants in components of the STAT3 (*PTPRT)* and T-cell activation *(BCL11B*, *SLIT2*, *NRP1*) pathways. *SETD2* mutations have not been previously described in T-LGLL. SETD2 is a histone methyltransferase that acts as a tumor suppressor through roles in transcriptional regulation and chromosome stability. *SETD2* mutations occur recurrently in T-cell lymphomas, particularly of g/d phenotype, including 90% of monomorphic epitheliotropic intestinal T-cell lymphoma and 30% of hepatosplenic T-cell lymphoma (HSTL), both of which also often harbor *STAT3/5B* mutations. The role of *SETD2* mutations in T-LGLL is unclear.

Design: Next generation sequencing was performed as a part of clinical care using a 95-gene amplicon-based or 88-gene hybrid capture-based hematologic neoplasm gene panel. Cases were selected from the Hematologic Malignancy Data Repository (HMDR) with IRB approval. Clinicopathologic data was collected. T-cell receptor gene rearrangement studies (TCR) were performed using BIOMED-2 primers.

Results: 133 T-LGLL cases were identified in the HMDR, in which 5 *SETD2* mutations were identified in 4 patients (4/133, 3%), including 3 females and 1 male (Table 1). 3 patients were diagnosed with T-LGLL; 1 was diagnosed with T-LGLL vs. HSTL. The median age at diagnosis was 66.5 yrs (range 49-91 yrs). All patients had absolute neutropenia at diagnosis. 3/4 patients were alive at last follow-up. *SETD2* mutations co-occurred with *STAT3* mutations in 3 cases and with a *STAT5B* mutation in 1 case. *SETD2* VAFs were similar to or smaller than *STAT3*/*5B* VAFs in all cases. Definitive clonal architecture was uncertain, but, as *SETD2* is not recurrently mutated in clonal hematopoiesis, it is likely that the *STAT3/5B* and *SETD2* mutations co-occurred in the T-cell clone. TCR studies showed clonal patterns in all 4 cases. The aberrant T-cell populations were composed of a/b T-cells in 3/4 cases and g/d T-cells in 1 case.

Case ID	Age (yrs)	Sex	TCR	Gene	Mutation	VAF	T-cell phenotype
1	74	Female	Clonal	SETD2	c.607_608delTC (p.S203Ifs*33)	1.8%	Alpha/beta
				STAT3	c.1982A>T (p.D661V)	3.1%	
				STAT3	c.1919A>T (p.Y640F)	2.5%	
				DNMT3A	c.742C>T (p.Q248*)	2.2%	
2	91	Female	Clonal	SETD2	c.1366C>T p.R456*	12.0%	Alpha/beta
				STAT3	c.1981G>T p.D661Y	18.3%	
				TET2	c.1999_2000insTG p.H667fs*	15.7%	
3	59	Male	Clonal	SETD2	c.6477_6481delCCCGC (p.P2160Sfs*22)	1.3%	Alpha/beta
				STAT3	c.1981G>T (p.D661Y)	15.8%	
				STAT3	c.1919A>T (p.Y640F)	7.1%	
				STAT3	c.1982A>T (p.D661V)	0.9%	
4	49	Female	Clonal	SETD2	c.5974_5975delAG (p.S1992*)	6.3%	Gamma/delta
				SETD2	c.7523_7533+8delTGGCTCGCAAGGTACTCCC (SPLICE)	2.6%	
				STAT5B	c.1924A>C (p.N642H)	4.8%	

Conclusions: We report, for the first time, the finding of recurrent *SETD2* mutations in T-LGLL. Downregulation of *SETD2* can skew T-cells toward a g/d fate, and *SETD2* mutations promote cell proliferation in HSTL. Cell-type specific epigenetic landscapes may contribute to the common co-occurrence of *STAT3/5b* and *SETD2* mutations in g/d T-cell neoplasms and herein we demonstrate a similar phenomenon in a/b T-LGLL as well.

930 Defining an Optimal Donor Chimerism Threshold for the Use of Next Generation Sequencing in Monitoring Genetically Measurable Residual Disease Post-Allogenic Stem Cell Transplant

Christian Puzo[1], Christopher Tormey[1], Alexa Siddon[1]
[1]*Yale School of Medicine, New Haven, CT*

Disclosures: Christian Puzo: None; Christopher Tormey: None; Alexa Siddon: None

Background: The use of Next Generation Sequencing (NGS) to detect genetically measurable residual disease (gMRD), the reappearance of molecular mutations following allogenic stem cell transplant (aSCT), has recently been proposed. Theoretically, at high levels of donor cell engraftment, no malignant cells may be present to detect gMRD. Thus, the use of chimerism testing to monitor donor cell engraftment offers a practical means to guide decision making on NGS testing. The current investigation sought to determine an optimal chimerism threshold for which NGS would be appropriate to detect gMRD.

Design: A retrospective review was undertaken for all patients who had an NGS panel performed between 2016 and 2020 (N= 1282). Patients were included if they possessed at least one NGS panel both before and after aSCT, as well as, a pathogenic mutation; repeat NGS panels for a given patient following aSCT were considered as independent samples (total N= 155). Donor chimerism values were computed either via the analysis of short tandem repeats using PCR or sex chromosome analysis via FISH cytogenetics. Binomial logistic regression was employed to detect the relationship between donor chimerism and gMRD post-aSCT. Receiver operator curves and a Youden Index were computed to determine the optimal chimerism threshold for which gMRD would not be detected.

Results: One hundred and fifty-five samples were assessed, which comprised of 99 males and 56 females with an average age at transplant of 61.1 (SD= 9.4). The sample consisted of 104 AML, 41 MDS, 6 MF, 1 CMML, and 3 ALL patients. Logistic regression analysis revealed that donor chimerism (OR= 0.66, $p < 0.001$), age at transplant (OR= 1.12, $p < 0.05$), and presence of a known Clonal Hematopoiesis of Indeterminate Potential mutation (OR= 0.04, $p < 0.01$) prior to transplant were significant predictors of gMRD following aSCT. ROC for this model (AUC= 0.976) was found not to be significantly different from an ROC curve including donor chimerism only (AUC= .949, p= 0.08) via Delong's Test for Two Correlated ROC Curves. Youden Index calculation indicated that an optimal chimerism cutoff for the donor chimerism only model is 92.5% (sensitivity= 89.6, specificity= 93.5).

Table 1. Chimerism thresholds with associated sensitivities and specificities

Chimerism Threshold	Sensitivity	Specificity
99.25	100	27.1
98.25	97.9	46.7
97.25	93.8	57.9
96.50	91.7	75.7
95.50	89.6	82.2
94.50	89.6	85.0
93.50	89.6	87.9
92.50	89.6	93.5
91.50	87.5	94.4
90.50	81.2	96.3

Figure 1 - 930

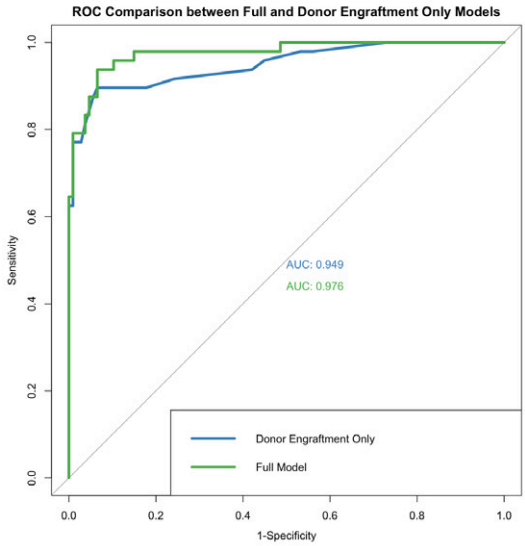

Figure 1. ROC predicting the presence of gMRD for patients post-aSCT for both the full regression and donor engraftment only models

Conclusions: Our results support forgoing NGS to detect gMRD in patients post-aSCT when donor chimerism values are above 92.5%. While this threshold cannot guarantee complete lack of gMRD, it may aid clinician decision making when considering a patient's entire clinical picture.

931 Clinicopathologic and Cytogenetic Features of Blastoid High-grade B-cell Lymphoma

Lianqun Qiu[1], Mahsa Khanlari[2], Guilin Tang[1], Jie Xu[1], Pei Lin[1], Joseph Khoury[1], Sergej Konoplev[1], Sofia Garces[1], Sa Wang[1], Wei Wang[1], L. Jeffrey Medeiros[1], Shaoying Li[1]
[1]The University of Texas MD Anderson Cancer Center, Houston, TX, [2]St. Jude Children's Hospital, Memphis, TN

Disclosures: Lianqun Qiu: None; Mahsa Khanlari: None; Guilin Tang: None; Jie Xu: None; Pei Lin: None; Joseph Khoury: None; Sergej Konoplev: None; Sofia Garces: None; Sa Wang: None; Wei Wang: None; L. Jeffrey Medeiros: None; Shaoying Li: None

Background: High-grade B-cell lymphoma (HGBL) is a heterogeneous disease category, including HGBL with *MYC, BCL2*, and/or *BCL6* rearrangements (double/triple hit lymphoma, D/THL) and HGBL, not otherwise specified (NOS). A small subset of HGBL cases show blastoid morphology (blastoid-HGBL) and are poorly understood.

Design: Patients diagnosed with blastoid-HGBL over 11 years (2010-2021) were included. The clinicopathologic and cytogenetic characteristics of these cases were reviewed.

Results: The cohort included 99 cases of blastoid-HGBL: 51 HGBL-NOS with 20 had *MYC* rearrangement (*MYC*-R), and 48 D/THL which were further classified as *MYC*/*BCL2* DHL (n=27), *MYC*/*BCL6* DHL (n=5) and THL (n=16). Most patients presented with an elevated serum LDH (83%), stage III-IV disease (87%), extranodal involvement (67%), and a high-risk International Prognostic Index (IPI) score (78%). Bone marrow involvement was seen in 46% of patients, and central nervous system involvement was observed in 18% of patients evaluated. 28 patients (27%) had a history of lymphoma, of which 70% were follicular lymphoma. The blastoid B-cells were frequently positive for CD10 (82%), CD38 (96%), BCL-2 (82%), BCL-6 (77%) and MYC (84%). CD45 expression was variable; 71% of cases had intensity similar to lymphocytes, and in 29% of cases CD45 was dim positive or negative. TdT was expressed in 24% of examined cases, 13% in HGBL-NOS and 32% in D/THL. The clinicopathologic features were similar between HGBL-NOS and D/THL, except that HGBL-NOS had less frequent bright CD38 (53% vs 74%, *P*=0.06) and BCL-2 positivity (69% vs 96%, *P*=0.001), and more often were CD20 positive (82% vs 61%, *P*=0.05). A complex karyotype was identified in 87% of HGBL-NOS and 100% of DHL (p=0.22). Compared to HGBL-NOS patients, patients with D/THL had a poorer initial response to chemotherapy with lower complete remission rates (29% vs 53%, *P*=0.05). However, the median overall survival (OS) was similar between the two groups,15.0 months in patients with HGBL-NOS vs 16.8 months in patients with DHL (p=0.58). *MYC*-R was associated with significant worse OS within the HGBL-NOS group (p=0.002) or all blastoid-HGBL (p=0.009).

Conclusions: Patients with HGBL-NOS and those with D/THL showed very similar clinicopathologic and cytogenetic features. There were some immunophenotypic differences. TdT was expressed in 24% of blastoid-HGBL. Blastoid-HGBL is a highly aggressive B cell lymphoma with a poor prognosis that is commonly associated with *MYC* rearrangement.

932 DUSP22-Rearrangement is Associated with Younger Age, Unique Immunophenotype, and Minimal expression of PD-L1 and pSTAT3, but not Prognosis in Patients with Systemic ALK-Negative Anaplastic Large Cell Lymphoma

Lianqun Qiu[1], Guilin Tang[1], Shaoying Li[1], Pei Lin[1], Sa Wang[1], Sergej Konoplev[1], Roberto Miranda[1], Swami Iyer[1], Wei Wang[1], L. Jeffrey Medeiros[1], Jie Xu[1]
[1]*The University of Texas MD Anderson Cancer Center, Houston, TX*

Disclosures: Lianqun Qiu: None; Guilin Tang: None; Shaoying Li: None; Pei Lin: None; Sa Wang: None; Sergej Konoplev: None; Roberto Miranda: None; Swami Iyer: *Grant or Research Support*, Merck, Seagen, Acrotech, Rhizen, Crisprx, legend; Wei Wang: None; L. Jeffrey Medeiros: None; Jie Xu: None

Background: ALK-negative (neg) anaplastic large cell lymphoma (ALCL) is a heterogeneous entity. About 30% of ALK-neg ALCL cases have *DUSP22*-rearrangement (*DUSP22*-R) which has been reported to be associated with a favorable outcome [5-year overall survival (OS) of 90%]. However, a recent study reported that patients with *DUSP22*-R ALK-neg ALCL had a poorer prognosis (5-year OS of 40%) than what was reported initially.

Design: We identified 80 patients with systemic ALK-neg ALCL at our institution between January 2007 and December 2020 with *DUSP22* status evaluated by FISH. The clinicopathologic features and outcomes were compared between patients with and without *DUSP22*-R. Differences between these two groups were evaluated using Fisher's exact test. OS was analyzed using the Kaplan-Meier method followed by log-rank test.

Results: Twenty-two (28%) patients with systemic ALK-neg ALCL had *DUSP22*-R. Patients with *DUSP22*-R were younger than patients with *DUSP22*-nonrearranged (*DUSP22*-NR) ALK-neg ALCL (median 52 years vs 61 years, $p = 0.04$). There were no significant differences in other clinical features (such as gender, nodal and extra-nodal involvement, stage, B symptoms, IPI, initial treatment and complete response rate) between these two groups (all $p > 0.05$). Immunophenotypically, *DUSP22*-R neoplasms were more often positive for CD8 (28% vs 7%, $p = 0.04$), CD15 (88% vs 16%, $p = 0.0003$), and tended to have a lower frequency of EMA expression (20% vs 57%, $p = 0.067$). All tested *DUSP22*-R cases were negative for granzyme B, in contrast to 63% of *DUSP22*-NR cases being positive ($p < 0.001$). The *DUSP22*-R group showed minimal positivity for PD-L1 and pSTAT3, significantly lower than the *DUSP22*-NR group (3% vs 26%, $p = 0.01$; 2% vs 36%, $p = 0.02$, respectively). The OS of patients with *DUSP22*-R was similar to that of patients with *DUSP22*-NR neoplasms (median 22 months vs 31 months, $p = 0.64$), but was significantly shorter than patients with ALK+ ALCL (median 22 months vs undefined, $p = 0.009$).

Conclusions: These data show that systemic *DUSP22*-R ALK-neg ALCL is characterized by younger patient age, a higher frequency of CD8 and CD15 expression, and a lack of granzyme B positivity. *DUSP22*-R ALK-neg ALCL cases have very minimal PD-L1 expression, likely due to minimal STAT3 activation, suggesting these patients may not be candidates for PD-1 blockade immunotherapy. In addition, our data show that *DUSP22*-R is not a prognostic factor in patients with systemic ALK-neg ALCL.

933 Somatic U2AF1 Mutations Involving Codons Q157 and S34 are Associated with Distinct Clinical and Molecular Characteristics but Similar Outcomes in Patients with Myelodysplastic Syndrome

Lianqun Qiu[1], Guillermo Garcia-Manero[1], Guillermo Montalban-Bravo[1], Hui Yang[1], Zhenya Tang[1], Keyur Patel[1], Sanam Loghavi[1], Chi Young Ok[1], Carlos Bueso-Ramos[1], L. Jeffrey Medeiros[1], Rashmi Kanagal-Shamanna[1]
[1]*The University of Texas MD Anderson Cancer Center, Houston, TX*

Disclosures: Lianqun Qiu: None; Guillermo Garcia-Manero: None; Guillermo Montalban-Bravo: None; Hui Yang: None; Zhenya Tang: None; Keyur Patel: *Consultant*, Astellas Pharma, Novartis Pharmaceutical Corporation; Sanam Loghavi: None; Chi Young Ok: None; Carlos Bueso-Ramos: None; L. Jeffrey Medeiros: None; Rashmi Kanagal-Shamanna: None

Background: *U2AF1* mutations in myelodysplastic syndromes (MDS) often involve codons, Q157 and S34, and result in distinct RNA splicing alterations. However, the impact of these mutations on clinic-pathologic features and outcomes is not well characterized, which were the goal of this study.

Design: We selected all newly diagnosed MDS patients (pts) with *U2AF1* mutations detected in baseline bone marrow (BM) specimens using an 81-gene NGS panel. Clinicopathological characteristics were reviewed retrospectively and compared between the two mutant groups.

Results: There were 66 *U2AF1* mutated MDS pts [55 men, 11 women; median age: 69 yrs (45-86)]. *U2AF1* S34F/Y mutations [MDS^{S34}] (n=33, 50%;) were more frequent than Q157 [MDS^{Q157}] (n=29, 44%;). Four had mutations involving R156, duplication and splice site mutation.

Compared with MDS^{Q157}, MDS^{S34} pts showed a higher frequency of absolute neutropenia (27% vs 7%, *P*=0.048), and a trend for lower median platelet count (61 vs 69 $\times 10^9$/L, *P*=0.082). There were no differences in age, hemoglobin level, PB blasts, WHO categories, and %ring sideroblasts. BM from MDS^{S34} pts showed a higher median cellularity (75% vs 55%, *P*=0.008), without any significant differences in BM blast% and frequencies of morphologic dysplasia. Per IPSS-R, a higher proportion of MDS^{S34} pts had high/very-high risk (52% vs. 28%; p=0.015) compared with MDS^{Q157}.

By conventional karyotype, del(20q) was seen more frequently present in MDS^{S34} (31% vs 4%; p=0.024) with no differences in other abnormalities. By NGS, additional gene mutations included *ASXL1* (n=23, 37%), *TET2* (n=22, 35%), *DNMT3A* (n=13, 21%) *TP53* (n=12, 19%), *RUNX1* (n=10, 16%), *BCOR* (n=9, 15%) and *SETBP1* (11%; n=5). MDS^{Q157} showed enrichment in *ASXL1* mutations (66% vs 12%, *P*<0.001). In contrast, MDS^{S34} showed a higher frequency of *DNMT3A* (33% vs 7%, *P*=0.013) and *BCOR* (24% vs. 3%; p=0.029) mutations. The median VAFs of MDS^{Q157} and MDS^{S34} were not significantly different (31% vs. 35%; *P*=0.06).

Forty (83%) pts were treated with hypomethylating agents. The median overall survival (OS) was 20 months. Despite differences in R-IPSS and mutational profiles, there was no difference in median OS between the two groups (51 vs. not reached; p=0.54). Concurrent *BCOR* mutation was associated with improved OS, especially within MDS^{S34}, although the difference was not significant (46 vs. 36 mo, p=NS).

	MDS with *U2AF1* Q157 Q157P (n=24) Q157R (n=5)	**MDS with *U2AF1* S34** S34F (n=28) S34Y (n=4) S34F & S34Y (n=1)	**p-value**
Age	69 (51-86)	69 (45-81)	0.499
PB findings			
WBC (x10^9/L)	3.3 (1-10)	3.2 (1-12)	0.989
ANC (< 0.8 x10^9/L)	7% (2/29)	27% (9/33)	**0.048**
Hgb g/dL	9.3 (6-14)	9 (5-14)	0.215
Platelet (x10^9/L)	69 (13-431)	61 (14-277)	0.082
PB Blasts%	0 (0-16%)	0 (0-27%)	0.849
BM findings			
BM blasts%	4 (0-30)	5 (1-25)	0.734
Cellularity	55 (10-100)	75 (20-100)	**0.008**
Ring sideroblasts%	3 (0-60)	6 (0-55)	0.963
IPSS-R			
High/ Very high	28% (8/29)	52% (17/33)	**0.015**
Intermediate	31% (9/29)	30% (10/33)	
Very Low/ Low	41% (12/29)	18% (6/33)	
Cytogenetics			
Diploid karyotype	45% (13/29)	30% (10/33)	0.296
Complex karyotype	17% (5/29)	21% (7/33)	0.756
Del(20q)	4% (1/24)	31% (8/26)	**0.024**
NGS findings			
***U2AF1* VAF**	31% (3.4-43.0)	35% (2.7-68.5)	0.06
ASXL1	66% (19/29)	12% (4/33)	**<0.001**
TET2	24% (7/29)	46% (15/33)	0.112
DNMT3A	7% (2/29)	33% (11/33)	**0.013**
TP53	24% (7/29)	15% (5/33)	0.522
SETBP1	17% (5/29)	6% (2/33)	0.237
RUNX1	21% (6/29)	12% (4/33)	0.493
BCOR	3% (1/29)	24% (8/33)	**0.029**

Data are presented as median values with ranges in parentheses, unless otherwise indicated.

Conclusions: *U2AF1* mutations at Q157 and S34 sites in MDS show distinct clinical features and mutational landscapes but similar outcomes.

934 Intracellular Cytokine Profiling by High-Dimensional Flow Cytometry Demonstrates Highly Augmented Cytotoxicity and Overly Activated NK cells in COVID-19 Patients

Josean Ramos[1], Barina Aqil[2], Yi-Hua Chen[3], Estefany Guzman[1], Nabeel Yaseen[2], Juehua Gao[3], Qing Chen[2], Suchitra Swaminathan[1]

[1]Feinberg School of Medicine/Northwestern University, Chicago, IL, [2]Northwestern University Feinberg School of Medicine, Chicago, IL, [3]Northwestern Memorial Hospital, Chicago, IL

Disclosures: Josean Ramos: None; Barina Aqil: None; Yi-Hua Chen: None; Estefany Guzman: None; Nabeel Yaseen: None; Juehua Gao: None; Qing Chen: None; Suchitra Swaminathan: None

Background: COVID-19 pandemic has caused more than 4.7 million deaths worldwide to date and still continues globally unabated. Numerous studies have linked the mortality in COVID-19 to aggressive immune response and cytokine storm. However, little is known about the cytokine profiles of individual immune cells that are directly involved in tissue damage. Here we investigate intracellular cytokines in individual T and NK cells of COVID-19 patients.

Design: We studied 50 blood samples from 22 COVID-19 patients, 4 with mild, 6 moderate and 12 severe disease. There were 6 healthy controls. We performed high-dimensional 30-color spectral flow cytometry to characterize the immune cell subsets. For cytokine study, cells were stimulated for 6 hours, and stained for surface antigens and intracellular cytokines (IL1b, IL2, IL4, IL6, IL8, IL10, IL12, IL17a, IL21, INFg, GnzB, TNFa, and GMCSF). Data ware acquired on FACSymphony 50-parameter analyzer and analysis performed using FlowJo.

Results: Our studies revealed significant differences in lymphocyte cytokine profiles between COVID+ and healthy controls (Fig 1). CD4+ and CD8+ T-cells exhibited increased percentages of IL2+ and IFNg+ cells, indicating a shift towards Th1 reaction. Granzyme B is highly upregulated in all T and NK cell subsets, demonstrating highly armed cytotoxic cells in COVID patients. The most prominent changes were noted in NK cells, 7 cytokines were highly expressed, most are proinflammatory cytokines. Of particular interest are IL-21 and GMCSF, both are known to play important roles in inflammatory cell recruitment, activation and renewal, which can lead to augmented tissue inflammation and injury. These changes were already evident in patients with mild disease, but there is heightened cytokine production in severe cases.

Figure 1 - 934

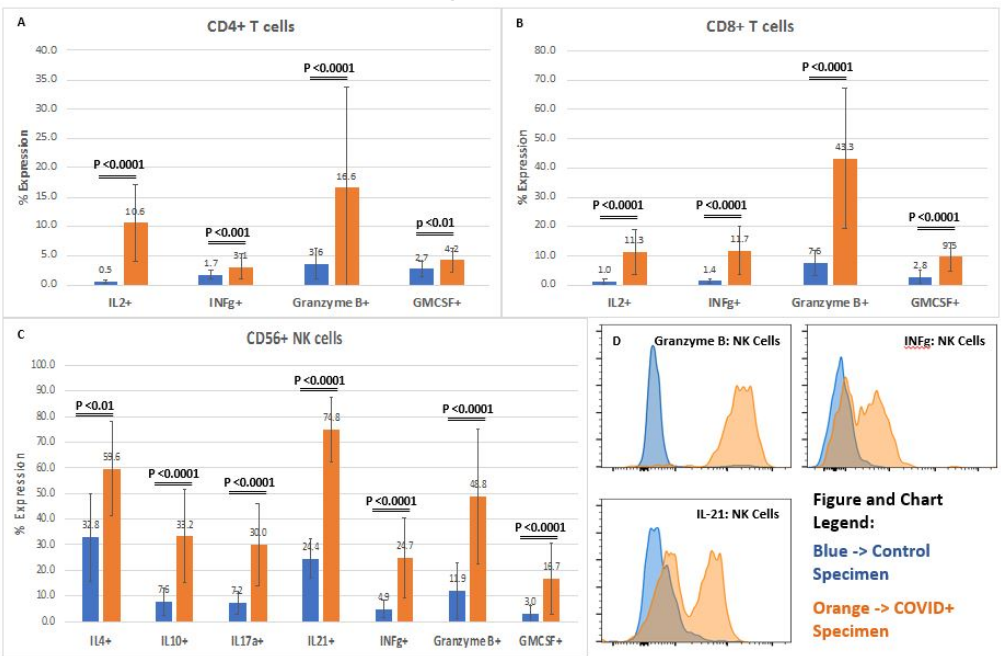

Figure 1: Flow cytometric evaluation of intracellular cytokines in response to PMA+ Ionomycin+ Lipopolysaccharide stimulation in T cells and NK Cells from COVID-19+ patients in comparison to normal controls. Representative mean cytokine expression profile in **(A)** CD4+ T cells, **(B)** CD8+ T cells and **(C)** CD56+ NK cells, comparing normal controls (n=6) to COVID-19+ patients (n=50). **(D)** Representative histogram overlays showing Granzyme B, Interferon-gamma and IL-21 expressions in COVID-19+ patient sample (orange) compared to normal control (blue).

Conclusions: Using high-dimensional flow cytometry we demonstrated for the first time significantly increased production of multiple proinflammatory cytokines and cytotoxic molecules in individual T and NK cells of COVID-19 patients. NK cells are most drastically activated. It is conceivable that when recruited to the target tissue such as lung, these highly primed cells will play a major role in tissue injury and ultimately organ failure via their direct cytotoxicity and cytokine secretion. This is consistent with previous reports of increased NK cells in the COVID lungs. Analysis of NK cell cytokine profiles may serve to predict disease progression, and reveal new targets for immune-therapy for severe COVID patients.

935 Large B-cell Lymphoma with IRF4 gene rearrangement: A Clinico-pathological Study of 8 cases

Shruti Rao[1], Tanuja Shet[2], Sumeet Gujral[2], Hasmukh Jain[2], Gaurav Narula[2], Manju Sengar[3], Sridhar Epari[1]
[1]Tata Memorial Centre, Mumbai, India, [2]Tata Memorial Hospital, Mumbai, India, [3]Tata Memorial Hospital

Disclosures: Shruti Rao: None; Tanuja Shet: None; Sumeet Gujral: None; Hasmukh Jain: None; Gaurav Narula: None; Manju Sengar: None; Sridhar Epari: None

Background: Rearrangement involving *IRF4* gene is a recently described provisional entity with a peculiar clinico-pathological presentation. It poses a diagnostic challenge due to considerable clinical and morphological overlap with Pediatric-type follicular lymphoma and Diffuse Large B-cell lymphoma.

Design: We retrospectively examined the medical records (including patient history, H&E stained slides review with immunohistochemistry and FISH) of eight patients of LBCL with IRF4 rearrangement diagnosed in a tertiary cancer care hospital during Jan. 2016 to Jun. 2020.

Results: Eight cases were identified with an age range of 7-74 years. The patients predominantly presented with head and neck disease. All cases presented with localized disease (Ann Arbour stage I and II). Baseline serum Lactate Dehydrogenase (LDH) and albumin levels ranged from 150-266U/L and 3.4-5.1gm/dl respectively. Histomorphology showed nodular/diffuse architecture with diffuse strong immunopositivity for multiple myeloma oncogene 1 (MUM1) along with co-positivity for BCL6. CD10 and MUM1 co-positivity was noted only in 50% cases. MIB-1 labeling index was high in all the cases. *IRF4* gene rearrangement was evaluated by IRF4,
DUSP22 dual-colored break-apart FISH probe. All the patients were treated with Rituximab based chemotherapy and 71.4% cases attained complete response on follow up.

Features	Case1	Case 2	Case 3	Case 4	Case 5	Case 6	Case 7	Case 8
Age (years)	12	19	15	74	18	7	31	25
Sex	Male	Male	Male	Male	Female	Male	Female	Male
Stage	I	II	I	I	I	II	I	I
Site	Inguinal	Nasopharynx	Tonsil	Tonsil	Nasopharynx	Tonsil	Cervical node	Tonsil
B symptoms	Absent	Absent	Absent	Absent	Absent	Absent	Absent	Absent
Age adjusted IPI	Low risk	Low-Intermediate risk	Low risk	Low risk	Low risk	NA	Low risk	Low risk
ECOG status	0	1	1	1	0	NA	1	0
Size (cm)	5.0	5.5	2.0	2.0	5.1	6.0	4.0	2.7
S.LDH (U/L)	266	248	159	181	150	NA	213	219
S.Albumin(g/dl)	50	5.1	5.0	3.8	3.9	3.4	4.1	4.4
Bone marrow involvement	Absent	Absent	Absent	Absent	Absent	Absent	Absent	NA
Histology	HGBCL	DLBCL	DLBCL	DLBCL	HGBCL	DLBCL	DLBCL	HGBCL
MUM1	+	+	+	+	+	+	+	+
CD 20	+	+	+	+	+	+	+	+
CD 10	+	-	+	-	+	-	-	+
BCL6	+	+	+	+	+	+	+	+
BCL2	-	+	+	-	-	+	-	+
cmyc (%)	20	NA	NA	NA	10-15	-	NA	50-60
MIB-1 (%)	90-95	60-65	95-100	50-60	80-90	80-90	80-90	80-90
Hans Subtype	GCB	nGCB	GCB	nGCB	GCB	nGCB	nGCB	GCB
IRF4 FISH Splits (%)	+ (95)	+ (87)	+ (35)	+ (18)	+ (69)	+ (27)	+ (20)	+ (56)
Rx	RGMALL	RGMALL + IFRT	RGMALL	NA	RCHOP + IFRT	RCOP	RCHOP	RCHOP
Response	CMR	CMR	CMR	NA	CMR	Partial	CMR	On Rx

Conclusions: LBCL with *IRF4* rearrangement is a distinct entity with usually localized-stage disease. Immunohistochemical staining for MUM1 (diffuse) along with co-expression of BCL6, with or without CD10 expression with a characteristic morphology may be a pathological clue to the diagnosis. Identification of these cases is of essence as they carry excellent prognosis.

936 Digital Spatial Profiling Reveals Spatial Heterogeneity in Nodular Lymphocyte-Predominant Hodgkin Lymphoma

Rebecca Rojansky[1], Sheren Younes[2], Ajay Subramanian[3], Michael Binkley[3], Yasodha Natkunam[3]
[1]Stanford Hospital and Clinics, Stanford, CA, [2]Stanford Pathology, Stanford, CA, [3]Stanford Medicine/Stanford University, Stanford, CA

Disclosures: Rebecca Rojansky: None; Sheren Younes: None; Ajay Subramanian: None; Michael Binkley: None; Yasodha Natkunam: None

Background: Nodular lymphocyte-predominant Hodgkin lymphoma (NLPHL) typically confers a good prognosis, however variant growth patterns correlate with recurrence and progression to T-cell and histiocyte-rich large B-cell lymphoma (THRLBCL) or diffuse large B-cell lymphoma. Variant NLPHL and de novo THRLBCL can be challenging to distinguish and the changes responsible for the altered growth characteristics of variant NLPHL are poorly understood. We hypothesize that spatial characterization of the tumor microenvironment may reveal insights into the biological differences between NLPHL variants and THRLBCL.

Design: Spatially indexed transcript profiling (GeoMx digital spatial profiling) was performed on 12 regions of interest (ROIs) for each of four cases of NLPHL (predominantly patterns A, C, D, and E respectively), one case of reactive follicular hyperplasia (RFH), and one case of THRLBCL. Expression data was collected for 1812 genes. Cell type abundances were calculated by CIBERSORT analysis. Corresponding H&E sections for each sample and each region of interest were evaluated morphologically.

Results: Cell type deconvolution (Figure 1) shows a relative increase in macrophages and activated T cells in variant patterns D, E, and THRLBCL ($p < 0.001$). Reactive follicular hyperplasia (RFH) and NLPHL pattern C show a significant component of naïve CD4-positive T-cells whereas follicular helper T-cells are prominent in other NLPHL variants and diminished in variant pattern C. B-cells are reduced in THRLBCL and NLPHL patterns D and E but not in patterns A and C. By hierarchical clustering (Figure 2) NLPHL cases show distinctly different gene expression than both RFH germinal centers and THRLBCL. Additionally, NLPHL variant patterns each segregate into independent clusters.

Figure 1 - 936

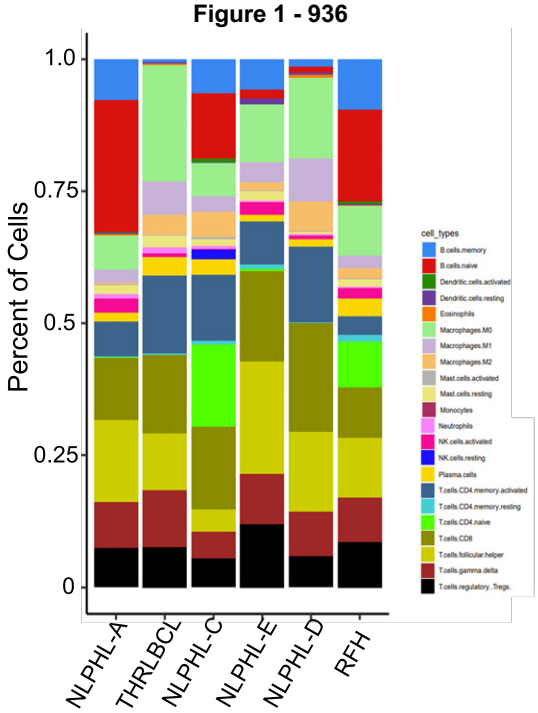

Figure 1. Cell type distribution by CIBERSORT analysis. Cell type distribution averaged over 12 ROIs for each sample. Only reactive follicular hyperplasia (RFH) and NLPHL variant pattern C show a significant component of naïve CD4 positive T-cells ($p < 0.001$). B-cell populations are reduced in THRLBCL and NLPHL variant patterns D and E but not in NLPHL variant patterns A and C ($p<0.001$). M0 macrophages are markedly increased in THRLBCL and NLPHL variant patterns D and E ($p<0.001$).

Figure 2 – 936

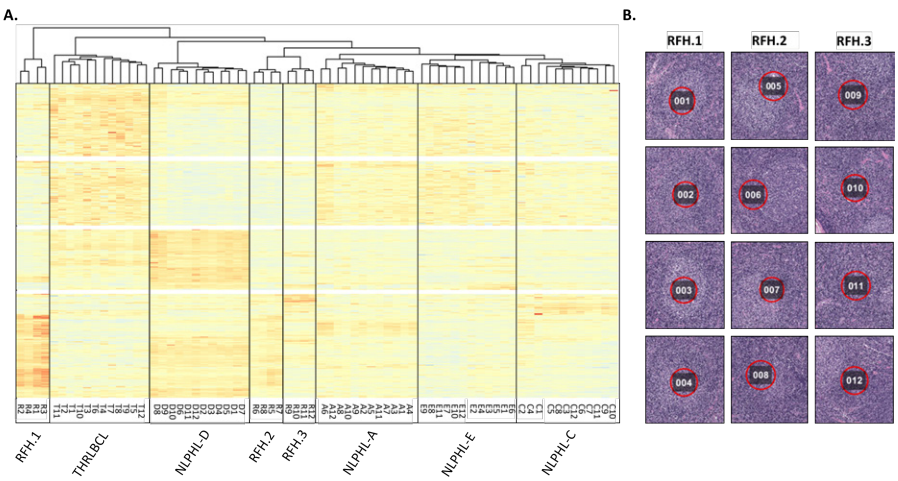

Figure 2. Hierarchical relationship of NLPHL variants. A) Hierarchical clustering of gene expression profiles for 72 regions of interest (ROIs) across six cases: reactive follicular hyperplasia (RFH), T-cell and histiocyte-rich large B-cell lymphoma (THRLBCL), Nodular lymphocyte-predominant Hodgkin lymphoma (NLPHL) classical pattern A (NLPHL-A), NLPHL pattern C (NLPHL-C), NLPHL pattern D (NLPHL-D), and NLPHL pattern E (NLPHL-E). Black boxes highlight biologically distinct clusters. B) Locations of RFH ROIs (red circles) within clusters 1, 2, and 3 corresponding to germinal centers (RFH.1), mantle zones (RFH.2), and extrafollicular areas (RFH.3).

Conclusions: Gene expression data corroborates the distinctions between variant patterns of NLPHL and demonstrates transcriptional relationships between variants. Calculated cell type deconvolution from transcriptomic data corroborates morphologic characterization of NLPHL variants and hierarchical clustering shows spatial heterogeneity in the tumor microenvironment. We find that extrafollicular areas of RFH cluster more closely with NLPHL, consistent with the T-cell rich nature of this neoplasm. These findings support the utility of digital spatial profiling in characterizing the tumor microenvironment of NLPHL.

937 DLBCL Presenting in Leukemic Phase is Frequently "Double-hit" and is Germinal Center in Origin

Ziver Sahin[1], Jinglan Liu[1], Mariam Ghafoor[1], Jerald Gong[2], Guldeep Uppal[3]
[1]Thomas Jefferson University Hospital, Philadelphia, PA, [2]Thomas Jefferson University, Philadelphia, PA, [3]Sidney Kimmel Medical College, Thomas Jefferson University, Philadelphia, PA

Disclosures: Ziver Sahin: None; Jinglan Liu: *Employee*, Thomas Jefferson University; Mariam Ghafoor: None; Jerald Gong: None; Guldeep Uppal: None

Background: Leukemic phase presentation is a well-established feature of some lymphomas; however, it is very unlikely for diffuse large B cell lymphoma (DLBCL) to initially present in leukemic phase. Only a few cases have been published so far. We report clinicopathological features of 6 cases of DLBCL primarily presenting in leukemic phase (DLBCL-LP) to our institution.

Design: This was a retrospective evaluation of 6 cases that we came across in the past 5 years. All cases were evaluated for the following set of markers by immunohistochemistry and/or flow cytometry : CD45, CD3, CD5, CD10, CD19, CD20, CD22, CD30, CD34, CD79a, surface light chains kappa & lambda, BCL-2, BCL-6, MUM-1, c-MYC, Ki-67, p53, PD-L1, TdT, and MPO. FISH and cytogenetic studies were available in all cases. Next-generation-sequencing (NGS) studies are pending at the time of abstract submission.

Results: All of the patients showed bone marrow involvement and 5 showed PB involvement (table 1). 5 of 6 patients were started on the aggressive chemotherapy (table 1); 2 of them developed tumor lysis syndrome; while 1 patient died before the initiation of chemotherapy. All patients showed very poor prognosis. 4 patients died before 7 months following their initial diagnosis (range 1-7 months). The other 2 patients were discharged to rehabilitation center and lost to follow up .

PB showed abnormal circulating blastoid cells in 5 cases (Fig. 1). The BM core biopsy showed diffuse interstitial infiltration as well as sheets of medium to large size cells with vesicular nuclei, variably prominent nuclei, and scant to moderate cytoplasm (Fig. 1). Three cases showed significant tumor necrosis. All cases showed uniform expression of CD10 (100%) and stained positive for at least 2 B- cell markers (Table 1). FISH studies revealed had rearrangement of *MYC* and *BCL2* genes ("double- hit") 4 cases, 1 patient had *MYC* deletion and extra copy *of BCL2* genes and 1 patient did not show any FISH abnormalities. Four cases showed complex karyotype while the chromosomes were normal in 2 cases.

Patients:	P1	P2	P3	P4	P5	P6
Age	51	41	75	58	75	74
Sex	F	F	M	M	M	M
Treatment	R-EPOCH + BOCE	REPOCH	EPOCH	Hyper-CVAD* MTX (IT) CHOP-R	None	CHOP Ara-C (IT)
Tumor lysis syndrome	No	yes	no	yes	no	No
PB involvement	yes	yes	yes	Yes	Yes	no
BM involvement	yes	yes	yes	yes	yes	yes
CNS involvement	No	yes	no	no	no	no
other organ/system involvement	LN	breast mass	LN	N/A	STM, PF	Stomach Ulcer
Diagnosis to death time (months)	**lost to f/u after 10 mo	7	1	3	1	**lost to f/u after 1 mo
CD45	+ (mod)	+ (dim)	+ (mod)	+ (dim)	+ (mod)	+ (mod)
CD19	+(dim)	+	+	+	+	+
CD20	+	-	+	+	+	+
CD22	+	-	+ (dim)	+	+	+
CD10	+	+	+	+	+	+
BCL6	+	-	-	-	-	+
MUM1	-	-	-	-	-	-
MYC	+	-	+	+	+	+
BCL2	+	+	+	-	+	+
EBER	-	-	-	-	-	-
PDL1	-	-	-	-	-	-
P53	+	-	-	+	-	-
CD5	-	-	-	-	-	-
CD34	-	-	-	-	-	-
TdT	-	-	-	-	-	-
sIg light chain	K	-	K	K	-	L
Ki-67	80%	20-30%	80%	>95%	70%	90%

BM: Bone marrow, LN: lymph node, PF: pleural fluid, IT:intrathecal, MTX: Methotrexate, PB: peripheral blood, CNS: central nervous system, STM: soft tissue mass, sIg: surface immunoglobulin,
*Patient P5 was initially started on Hyper-CVAD and intrathecal MTX but did not tolerate the therapy and switched to CHOP-R
** Lost F/U: Lost to follow up

Figure 1 - 937

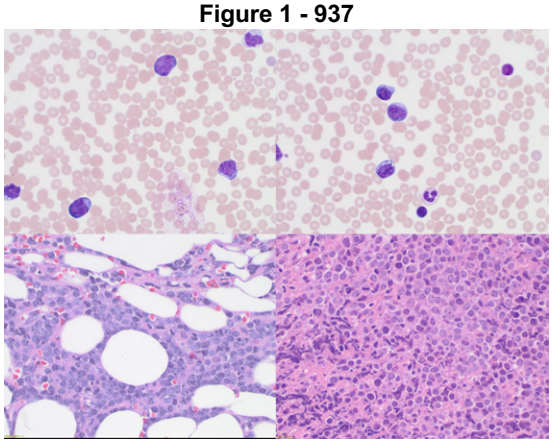

Figure 2 - 937

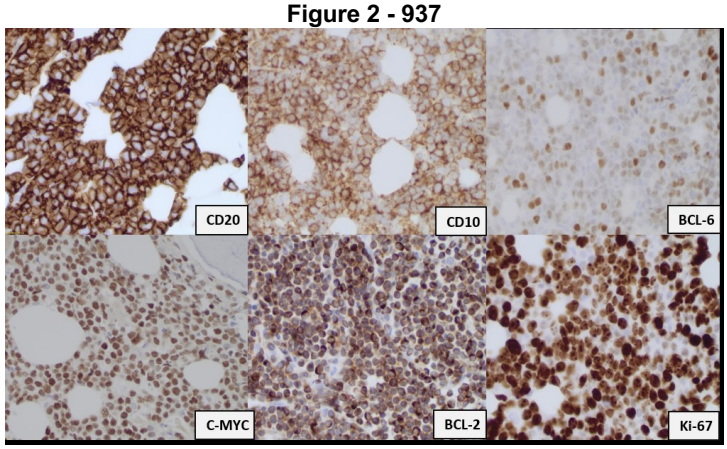

Conclusions: We are presenting a mini case series of 6 cases of DLBCL in leukemic phase at the time of initial presentation. This is rare phenomenon and can be confused with acute leukemia. Our study cases showed germinal center origin with CD10 expression (100%), high clinical stage, aggressive clinical course and frequent rearrangement of *MYC* and *BCL*-2 ("double-hit"). It is possible that this sub-group represents a distinct entity of aggressive B-cell neoplasms.

938 Flow Cytometry and Immunohistochemistry Assessment of PD1 Expression in T Cell Lymphomas/Leukemias

Ziver Sahin[1], Guldeep Uppal[2], Jerald Gong[3]
[1]Thomas Jefferson University Hospital, Philadelphia, PA, [2]Sidney Kimmel Medical College, Thomas Jefferson University, Philadelphia, PA, [3]Thomas Jefferson University, Philadelphia, PA

Disclosures: Ziver Sahin: None; Guldeep Uppal: None; Jerald Gong: None

Background: PD1 expression is a characteristic feature of peripheral T-cell lymphoma of follicular T-cell origin. Its expression is less clear in other types of T-cell lymphomas/leukemias (TCL). We assessed PD1 expression using two methodologies, flow cytometry (FC) and immunohistochemistry (IHC), in a series of various categories of TCL including both follicular T-cell and non-follicular T-cell origins.

Design: Twenty-five cases were identified in our pathology archives dated between January 2019 to June 2020. IHC was performed using PD1 antibody (NAT105 Clone, Sigma Aldrich) with the condition per manufacturer's recommendation. IHC intensity was scored as follows: "0" for no staining, "1+" for faint staining, "2+" for medium staining, and "3+" for strong staining. The percentages of the positive cells in the neoplastic cells were determined in 5% increments. FC for PD1 was assessed using PD1 antibody without dilution (EH12.1 Clone, Becton Dickinson) and data were analyzed using Kaluza Software (Beckman Coulter). The neoplastic cells were selectively gated using various gating strategies and the mean fluorescence intensities (MFI) of PD1 were calculated. In addition, the percentages of positive cells were determined based on the internal negative controls. We used ggpubr package in R studio software to calculate and plot Pearson correlation coefficient (PCC) between the PD1 percentage by IHC and FC; and PCC between PD1 IHC intensity score and MFI value.

Results: Of the 25 cases included, the median age is 64 (range 10-87) and male to female ratio is 1.5 (15:10). By IHC, 12 out of 25 (48%) cases showed no staining (score 0); 4 cases showed weak staining (1+), 5 cases showed medium staining (2+), and 4 cases showed strong staining (3+). By FC, 10 cases showed no PD1 expression, 2 cases showed weak signal, 10 cases showed moderate signal, and 5 cases showed bright signal. There was strong correlation between PD1 expression by IHC and FC (r=0.74) and between PD1 IHC intensity and FC MFI in PD1+ neoplastic cells (r=0.71). One case of PTCL, FHT showed discrepant result with PD1 expression detected only by FC (P9).

Table 1. PD1 expression in TCLs by IHC and FL

Patient	Diagnosis	PD1 IHC %	PD1 IHC score	PD1+ neoplastic cells %	MFI value
P1	AITL	100	3+	100	2112.43
P2	AITL	80	2+	95	1780.11
P3	ALCL	0	0	0	149.5
P4	ALCL	0	0	58	1328.64
P5	ALCL	0	0	2	267.97
P6	ATLL	50	3+	10	661.16
P7	ATLL	0	0	0	448.08
P8	MEITCL	0	0	0	101.15
P9	PTCL, FHT	0	0	73	1520.67
P10	PTCL, FHT	70	2+	86	2395.13
P11	PTCL, FHT	70	1+	66	1287.91
P12	PTCL, FHT	100	2+	85	2109.85
P13	PTCL, FHT	50	3+	82	2117.96
P14	PTCL, NOS	10	1+	2	292.08
P15	PTCL, NOS	0	0	1	142.18
P16	PTCL, NOS	50	3+	12	756.78
P17	T-ALL	0	0	0	314.19
P18	T-ALL	50	1+	95	2862.35
P19	T-ALL	0	0	0	89.24
P20	T-LGL	0	0	2	430.89
P21	T-LGL	100	2+	72	4876.61
P22	T-LGL	0	0	60	567.93
P23	T-LGL	0	0	0	114.84
P24	T-LPD	50	1+	49	395.85
P25	T-PL	100	2+	77	1397.94

Flow signal intensity: negative (MFI<500); weak (MFI 501-1000); moderate (10001-3000); strong (>3000)
AITL: Angioimmunoblastic T cell lymphoma; ALCL: Anaplastic large cell lymphoma; ATLL: Adult T cell leukemia/lymphoma; MEITCL: Monomorphic epitheliotropic intestinal T-cell lymphoma; PTCL-FHT: Peripheral T cell lymphoma – Follicular T cell type; PTCL, NOS: Peripheral T cell lymphoma – Not otherwise specified; T-ALL: T-cell acute lymphoblastic leukemia; T-LGL: T-cell Large Granular Lymphocytic Leukemia; T-LPD: T-cell lymphoproliferative disorder; T-PL: T-cell prolymphocytic leukemia; MFI: Mean fluorescent intensity

Conclusions: PD1 was consistently expressed in T-cell lymphomas of follicular T-cell origin (AITL, PTCL, FTC). Additionally, PD1 expression was also found in nearly all other types of TCL including ATLL, ALCL, PTCL-NOS, T-ALL, T-LGL, and T-PL, with variable frequencies. Although PD1 and IHC were generally comparable, in rare cases of TCLs, FC was more sensitive than IHC in detecting PD1.

939 Distinct Clinicopathologic Features of NUP98 Rearranged/Altered Acute Leukemia: A Single Institution Experience

Sujata Sajjan[1], Estelle Oertling[1], Franklin Fuda[1], Jeffrey Gagan[1], Prasad Koduru[1], Rolando Garcia[1], Kathleen Wilson[1], Olga Weinberg[1], Mingyi Chen[1], Jesse Jaso[1], Weina Chen[1]
[1]UT Southwestern Medical Center, Dallas, TX

Disclosures: Sujata Sajjan: None; Estelle Oertling: None; Franklin Fuda: None; Jeffrey Gagan: None; Prasad Koduru: None; Rolando Garcia: None; Kathleen Wilson: None; Olga Weinberg: None; Mingyi Chen: None; Jesse Jaso: None; Weina Chen: None

Background: *NUP98* (Nucleoporin 98) rearrangements are rare and have been reported in hematolymphoid malignancies, including acute leukemia, with a poor prognosis. This study further explores clinicopathologic features of *NUP98* rearranged/altered acute leukemia.

Design: Four cases with *NUP98* rearrangement/alterations (2 males, 2 females, median age 13) were identified (2019-2021) by cytogenetic/FISH (fluorescence in situ hybridization) and/or NGS (next generation sequencing by >1,300 gene panel). A CytoCell *NUP98* break-apart probe was used to evaluate the *NUP98* alterations. Immunophenotypic analysis was performed by 10-color flow cytometry. Clinicopathological and cytogenetic/molecular features were examined.

Results: All cases were *de novo*, newly diagnosed leukemia (Table 1). Cases 1, 2, and 4 had *NUP98* rearrangement whereas case 3 had apparent *NUP98* 3'-end deletion by FISH but NGS identified only the fusion of cytogenetically cryptic inv(16)/*CBFA2T3-GLIS2*; the latter case was acute myeloid leukemia (AML) with an unusual immunophenotype (IP) of $CD34^{+}$/$HLA\text{-}DR^{-}$

/CD56$^{bright+}$ and complex karyotype. Cases 1 and 2 were AML with an IP of CD34^{+}/HLA-DR^{+}/CD56^{-}, normal karyotype, and cryptic t(5;11)/*NUP98-NSD1* fusion and *FLT3*-ITD. Case 4 was acute leukemia of ambiguous lineage, not otherwise specified (ALAL-NOS) with a rare IP of expressing myeloid, B-cell, and T-cell antigens but lacking MPO, CD3 or strong CD19 (or strong CD22 or CD79a), blasts resembling lymphoblasts by morphology, complex karyotype, cryptic t(11;19)(*NUP98-MLLT1*), and mutations in *NF1, BCOR*, and *KMT2D*. Three patients (3/3, 100%) had minimal residual disease at day 29 bone marrow. With a median follow-up of 8 months (3 to 22 months), 2/4 patients had relapse and 3/4 patients were alive.

Table 1. Clinicopathological and genetic/molecular features of acute leukemia with *NUP98* rearrangements/alterations

Patient #:	1	2	3	4	ClinicoPath Summary
Age/Gender	6/F	34/F	5/M	20/M	median 13 year (5-34), 2M/2F
WBC (K/uL)	15	9.2	24	2.3	median 12 (2.3-24)
Hgb (g/dL)	9.2	8.5	8.7	9.6	median 9.0 (8.0-9.6)
PLT (K/uL)	145	117	89	82	median 103 (82-145)
Blast% (PB)	41	39	12	2.0	median 26 (2.0-41)
Blast% (BM)	57	24	38	52	median 45 (24-51)
Immunophenotype CD34/HLA-DR/CD56	+/+/-	+/+/-	+/-/+	-/+/-	CD34+/-: 3/1, HLA-DR+/-:3/1, CD56+/-: 1/3
Diagnosis (*de novo*, new)	AML	AML	AML	ALAL, NOS	AML: 3/4 (75%), ALAL: 1/4 (25%)
Residual disease (FC day 29) neoplastic blast %	0.9	ND	1.1	2.0	Residual at 29 days: 3/3 (100%)
Relapse (months after diagnosis)	No	Yes (7.6)	Yes (7.7)	No	Relapse: 2/4 (50%)
Alive (A)/Dead(D) (f/u month)	A (5.6)	D (22)	A (10, hospice care)	A (3.3)	Alive/Dead: 3/1 (median f/u: 8 months)
Cytogenetics	Normal	Normal	Abnormal	Abnormal	Normal: 2/4 (50%)
	46XX	46XX	46XY	46XY	
			add(11p)	del(6p)	
			del(13q)	t(7;9)	
			t(18;21)	del(12p)	
FISH	*NUP98* 3'-end deletion	ND	*NUP98* 3'-end deletion	*NUP98* 3'-end deletion	
Molecular (mutations/alterations)					
NUP98-NSD1					Nuclear transport; Histone methylation
NUP98-MLLT1					Nuclear transport; Transcription regulator
CBFA2T3-GLIS2					Transcription repressor; Transcription regulator
FLT3-ITD					Signaling
NF1					
ARID2					Chromatin modifier
MYCN					Transcription factor
BCOR					Transcription repressor
KMT2D					DNA methylation
U2AF1					Splicing
chr12q					Deletion transcription factor *ETV6*
chr17q					Copy loss of *NF1* and *SUZ12*
chr6q					Loss, uncertain significance

Key	
FC, flow cytometry	Fusion
ND, not done	Duplication
ALAL, NOS, acute leukemia of ambiguous lineage, not otherwise specified	Missense
FC day 29, residual disease detection by FC (0.01% sensitivity)	Nonsense
f/u: follow up, month	Frameshift
	Deletion
	No mutation

Conclusions: Our results demonstrated a spectrum of cytogenetically cryptic *NUP98* rearranged acute leukemia in children and young adults with poor prognosis, co-operation between *NUP98-NSD1* fusion and *FLT3*-ITD in AML whereas novel *NUP98-MLLT1* fusion and other gene mutations in ALAL-NOS. Importantly, caution is required in interpreting FISH result of the *NUP98* probe and abnormal finding to be confirmed by NGS study. Remarkably, our case with apparently false *NUP98* alteration exhibited the characteristic feature of a rare subtype of pediatric AML carrying a cytogenetically cryptic *CBFA2T3-GLIS2* fusion: a peculiar immunophenotype and dismal prognosis.

940 Extranodal Follicular Lymphoma Is Immunophenotypically Comparable to Nodal Counterpart but with a Better Outcome

Ali Sakhdari[1], Jan Delabie[2], Helia Hatam Tehrani[3]
[1]University Health Network, University of Toronto, Toronto, Canada, [2]University of Toronto, University Health Network, Toronto, Canada, [3]Laboratory Medicine Program, Toronto General Hospital/University Health Network, Toronto, Canada

Disclosures: Ali Sakhdari: None; Jan Delabie: None; Helia Hatam Tehrani: None

Background: Follicular lymphoma (FL) is the most common indolent lymphoma with most patients experience prolonged survival in the current treatment era. Treatment is guided based on disease stage and whether the patient presents symptoms. While most

FL presents with extensive nodal disease, a substantial subset presents mainly outside the lymph nodes, referred to as extranodal FL (enFL). Here we aimed to evaluate a large cohort of FL patients based on their initial presentation in nodal (nFL) or extra-nodal (enFL) *sites* to explore any clinical, immunophenotypic, genetic or survival differences between nFL and enFL.

Design: Patients with a diagnosis of untreated FL grades 1 to 3A (n=488) were selected for this study from the archives of the University Health Network (UHN) and divided into two groups of nFL (n=383; 78%) and enFL (n=105; 22%) based on the initial site(s) of presentation. We compared these two groups in the following categories: clinical, histologic, immunophenotypic, genetic and outcome.

Results: Extra-nodal FL was more common in older patients (≥60 years; *p*=0.047) and in women (*p*=0.015) and was more likely to be of a lower stage (*p*=0.0001), or to have a lower FLIPI score (*p*=0.0014). There was no significant difference in terms of tumor grade, immunophenotype, and presence of *BCL2/*IgH translocation (*p*=ns). Both nFL and enFL were similar in their immunophenotypes (table 1) for pan B-cell and germinal center biomarkers. A total of 487 patients had available survival data with a median survival interval of 5.8 years (range, 0.1 – 24.6 years). nFL showed a worse disease-specific survival (DSS; *p*=0.053) than enFL, while the overall survival (OS) and progression-free survival were not significantly different (figure 1). In multivariate analysis considering age, tumor stage and FLIPI score, this survival difference for site/location of FL become more significant (*p*=0.023).

	nFL, N (%)	enFL N (%)	*P* value
Patients	383 (78)	105 (22)	NA
Gender			**0.015**
Male	216 (56)	45 (43)	
Female	167 (44)	60 (57)	
Age, y			**0.028**
Median (range)			
<60	200 (52)	42 (40)	
≥60	183 (48)	63 (60)	
Stage			**0.0001**
I/II	190 (49)	78 (75)	
III/IV	193 (51)	26 (25)	
FLIPI			**0.0014**
Low/ Intermediate	266 (72)	84 (88)	
High	105 (28)	12 (12)	
Grade			0.76
I/II	302 (82)	79 (84)	
IIIA	67 (12)	15 (16)	
Biomarkers			
CD10+	86/95 (91)	14/15 (93)	1.00
BCL6+	92/93 (99)	15/15 (100)	1.00
BCL2+	86/90 (96)	13/14 (93)	1.00
CD5+	0/75 (0)	1/10 (10)	0.12
CD23+	19/58 (33)	2/9 (22)	0.71
t(14;18)+	100/194 (52)	25/50 (50)	1.00

Figure 1 - 940

A

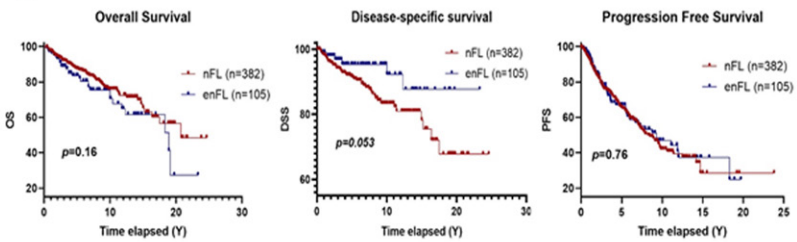

B

Multivariable Model		
Variable	HR, 95% CI	*p*-value
Site	0.340 (0.134 - 0.864)	**0.023**
Age	2.145 (1.219 - 3.775)	0.008
Stage	1.679 (0.935 – 3.014)	0.083
FLIPI score	0.729 (0.406 – 1.310)	0.291

Conclusions: Both nFL and enFL are immunophenotypically similar with only minor differences. Demographically, extranodal follicular lymphoma is more common in females and patients over 60 years old. While there was no difference in overall and progression-free survival between nFL and enFL, disease-specific survival is better in enFL.

941 Follicular Lymphoma (FL) of Lower Female Genital Tract (LFGT): Evidence for a Relationship to Primary Cutaneous Follicle Center Lymphoma (PCFCL)

Annapurna Saksena[1], Ashish Jain[2], Svetlana Pack[1], Jung Kim[3], Ina Lee[3], Manoj Tyagi[3], Liqiang Xi[4], Stefania Pittaluga[5], Mark Raffeld[6], Elaine Jaffe[4]

[1]National Institutes of Health, Bethesda, MD, [2]Center for Cancer Research, National Cancer Institute, National Institutes of Health, Bethesda, MD, [3]Center for Cancer Research, National Cancer Institute, Bethesda, MD, [4]National Cancer Institute, National Institutes of Health, Bethesda, MD, [5]National Institutes of Health, Washington, DC, [6]National Cancer Institute, Bethesda, MD

Disclosures: Annapurna Saksena: None; Ashish Jain: None; Svetlana Pack: None; Jung Kim: None; Ina Lee: None; Manoj Tyagi: None; Liqiang Xi: None; Stefania Pittaluga: None; Mark Raffeld: None; Elaine Jaffe: None

Background: PCFCL has been distinguished from nodal FL based on the absence of *BCL2*-rearrangement (BCL-R) and the tendency to remain confined to the skin without dissemination. The nature of other extranodal FCL, including those of the LFGT, is not well defined.

Design: We searched for cases of FL involving the LFGT from 01/01/2000 to 02/17/2021. Cases were evaluated using an immunohistochemical (IHC) panel for B-cell lymphoma and examined using the TSO-500 Oncology Gene panel by NGS. In addition, FISH for BCL2 rearrangement was performed.

Results: Fourteen cases (Table 1) (7 cervix, 4 vagina, and 3 cervix and vagina) were identified. The median age at diagnosis was 40.5 years. 9 presented with symptomatic mass lesions; 5 cases were identified as incidental findings on surgical specimens. All patients had localized disease, negative for marrow involvement. 3/9 (33%) cases had B-symptoms. 7/14 (50%) of cases had diffuse growth pattern. Large centrocytes were a prominent feature, admixed with other follicle center (FC) cells. All cases were positive for CD20 and BCL6. Other IHC showed CD10+ in 3/14 (21%); BCL2+ in 2/14 (14%) cases. CD21 was focally positive - 4/7 (57%) cases. PCR for IGR confirmed clonality in 8/10 (80%) cases. FISH for *BCL2*-R was negative in 10/11 (91%). NGS (Figure 1) performed in 9 patients, revealed recurrent mutations in *TNRFSF14* (5/9, 55.5%), *B2M* (4/9, 44.4%), *XIAP* (3/9, 33.3%), *SOCS1*(2/9, 22.2%) similar to PCFCL. No case had *CREBBP* or *KMT2D* mutations as seen in nodal FL. Few cases showed mutations in other chromatin-modifying genes including *EZH2* (1/9,11.1%), *HIST1H2BD* (1/9,11.1%), *SETD2* (1/9, 11.1%) and *TET2* (1/9, 11.1%). Median follow-up period (10/14) was 7 years (range-0.5-20 years) with a 5-year relapse-free survival of 85% (Figure 1) and a 100% overall survival. None of the patients had progressive disease with durable complete remission following surgical resection (3/10 evaluable cases), brachytherapy (1/10), systemic chemo-immunotherapy (6/10), and additional consolidative radiation therapy (2/10).

Case no	Age (years)	Anatomic site	Pattern	BCL-6 IHC	BCL-2 IHC	IG PCR Clonality	*BCL2* FISH
1	44	C	F & D	BCL-6	BCL-2	Clonal	Neg
2	43	C	D	Pos	Neg	Clonal	Neg
3	44	V	D	Pos(subset)	Neg	Clonal	Neg
4	40	C & V	D	Pos	Pos(focal)	Clonal	Neg
5	36	C	F & D	Pos	Neg	Clonal	Neg
6	36	C & V	D	Pos	Neg	Polyclonal	Neg
7	31	C & V	D	Pos	Neg	Clonal*	Neg
8	48	C	D	Pos	Neg	Indeterminate**	Neg
9	36	V	F	Pos	Neg	Clonal	Neg
10	41	C	D	ND	Neg	Clonal	Neg
11	53	V	F &D	Pos	Neg	No Amp	Pos
12	46	C	D	Pos	Neg	ND	ND
13	40	V	D	Pos(partial)	Neg	ND	ND
14	37	C	F	Pos	Neg	ND	ND

ND= not done, Pos=positive, Neg=negative, * peak in only one Light chain tube, ** suspicions peak in one light chain tube, No Amp=no amplification, F=follicular, D=diffuse/predominantly diffuse, F & D =follicular and diffuse, C= cervix, V=vagina, C and V= cervix and vagina

Figure 1 - 941

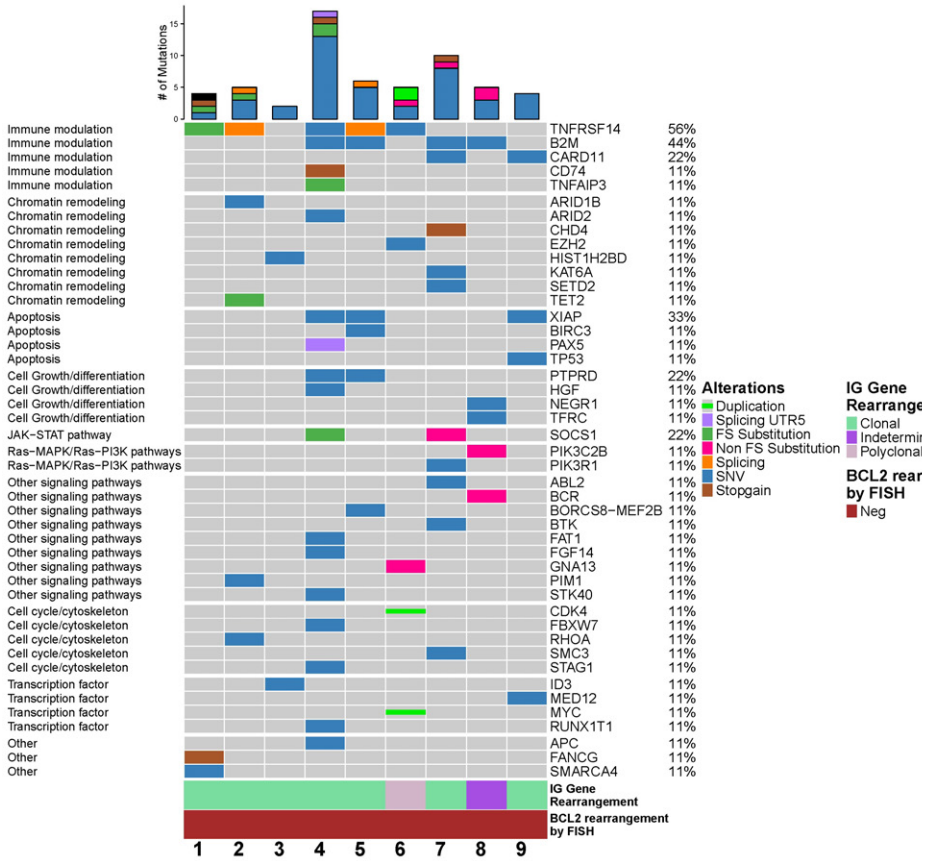

Figure 2 - 941

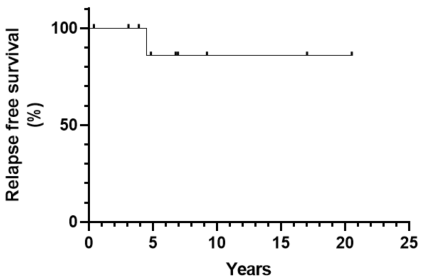

Conclusions: FL of the LFGT is similar to PCFCL and distinct from nodal FL, with localized disease and indolent course. Despite the frequent presence of large FC cells (centrocytes and centroblasts), it has a low risk of dissemination and excellent prognosis.

942 Increased Expression of Immune Checkpoint Regulators LAG3 and CD70 in the Tumor Cells and Microenvironment in Immunodeficiency Associated Lymphoproliferative Disorders

Sandra Sanchez[1], Luis Veloza Cabrera[2], Christos Masaoutis[3], Marco Buehler[1], Inmaculada Ribera[4], Anna Sellares[1], Cristina Arnaldos Pérez[1], Carlos Castillo Giron[1], Gerard Frigola[4], Jose Guerrero Pineda[5], Ricardo Lopez del Campo[1], Manel Juan[5], Pedro Jares[4], Lazaros Lekakis[6], Juan Ramos[6], Patricia Balsas[1], Virginia Amador[1], Josep Antoni Bombi[7], Aurea Mira[1], Olga Balagué[5], Antonio Martinez[1]

[1]Hospital Clinic-IDIBAPS, University of Barcelona, Barcelona, Spain, [2]CHUV and University of Lausanne, Lausanne, Switzerland, [3]National and Kapodistrian University of Athens, Athens, Greece, [4]Hospital Clinic, Barcelona, Spain, [5]Hospital Clinic, University of Barcelona, Barcelona, Spain, [6]University of Miami Miller School of Medicine, Sylvester Cancer Center, Miami, FL, [7]Hospital Clínic de Barcelona, Spain

Disclosures: Sandra Sanchez: None; Luis Veloza Cabrera: None; Christos Masaoutis: None; Marco Buehler: None; Inmaculada Ribera: None; Anna Sellares: None; Cristina Arnaldos Pérez: None; Carlos Castillo Giron: None; Gerard Frigola: None; Jose Guerrero Pineda: None; Ricardo Lopez del Campo: None; Manel Juan: None; Pedro Jares: None; Lazaros Lekakis: None; Juan Ramos: None; Patricia Balsas: None; Virginia Amador: None; Josep Antoni Bombi: None; Aurea Mira: None; Olga Balagué: None; Antonio Martinez: None

Background: Immune checkpoint regulators (ICR) regulate T-cells in the tumor microenvironment (TME). Checkpoint inhibitors promote anti-tumor immune responses and have improved prognosis of many cancers. LAG-3 is an ICR on T-cells and its inhibition in melanoma has shown synergy with PD-1 inhibition. CD70 is expressed on the malignant cells (TC) of many lymphoid malignancies but rarely on normal lymphocytes. The expression of CD70 and LAG-3 on TME and TC and its relation to EBV infection has not been characterized in IA-LD.

Design: We examined by IHC expression of CD70 and LAG3 in TC and TME cells in 33 FFPE tissue specimens of IA-LD: PTLD EBV+DLBCL (10), PTLD EBV-DLBCL (2), polymorphic PTLD (4/5 EBV+), HIV+DLBCL (7/12 EBV+), and EBV+DLBCL, NOS (4) as a control (Figure 1). We studied the expression of mRNA by using a mRNA protection assay with the HTG EdgeSeq Precision Immuno-Oncology Panel in 16 cases.

Results: Although no differences in mRNA expression were observed between LAG3 and CD70 in (all cases), LAG3 expression was mainly observed in TME cells and CD70 was observed in both TME and TC. LAG3+ expression in TME was observed in 24% PTLD EVB+DLBCL and 21% EBV+HIV+DLBCL and only 12% EBV+DLBCL, NOS ($p<0.04$). LAG3 was largely negative in TC in all cases. Only 6% PTLD EVB-DLBCL, 6% EBV+HIV+DLBCL were positive in TC and none of EBV+DLBCL, NOS ($p<0.04$). CD70 expression was found on TME cells in 33% PTLD EVB+DLBCL, 12% PTLD EVB-DLBCL, 21% EBV+HIV+DLBCL and 12% EBV+ DLBCL, NOS ($p<0.04$). Expression on TC was found in 36% PTLD EVB+DLBCL, 12% PTLD EBV-DLBCL, 21% EBV+ HIV+DLBCL and 12% EBV+ DLBCL, NOS($p<0.04$). Regarding EBV expression, overall 57% of LAG3+ cases and 66% of CD70+ cases in TME were EBV+ vs 15% each in EBV negative. In TC, we did not observe differences among EBV positive and negative cases for LAG3 but 70% of CD70 positive cases were EBV positive.

Figure 1 - 942

LAG3 and CD70 immunotherapeutic target

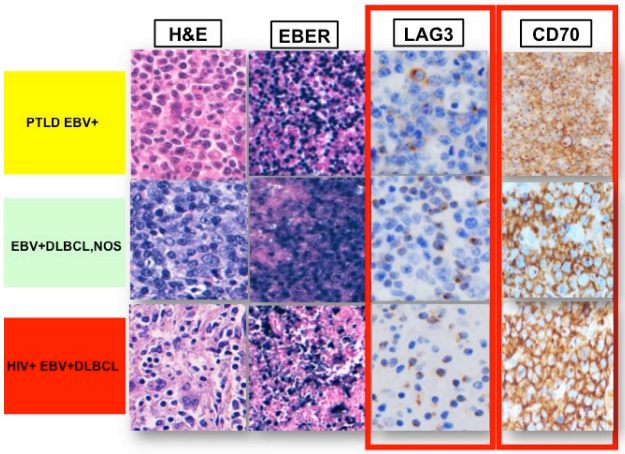

Conclusions: LAG3 and CD70 are expressed in IA-LD. Although CD70 is highly expressed in TC and TME, LAG3 is mainly expressed in TME. EBV infection is associated with high expression of CD70 and LAG3 in TME. Expression of CD70 in TC seems to be also related to viral infection. The lack of differences between LAG3 and CD70 at mRNA levels seems to indicate a post transcriptional regulation of gene expression that is commonly seen in other immune regulators. The expression of those ICR provide a rational for targeting CD70 and LAG3 inhibitors in EBV+ IA-LD as is used in other tumors.

943 Morphologic Features of Peripheral Blood Smears in COVID-19 Infection

Virian Serei[1], Lauri Goodell[1], Jina Salim[2], Lizabeth Bevilacqua[2], Gratian Salaru[1], Payal Sojitra[1]
[1]Rutgers Robert Wood Johnson Medical School, New Brunswick, NJ, [2]Rutgers Robert Wood Johnson University Hospital, New Brunswick, NJ

Disclosures: Virian Serei: *Stock Ownership*, Pfizer; Lauri Goodell: *Stock Ownership*, Johnson and Johnson; Jina Salim: None; Lizabeth Bevilacqua: None; Gratian Salaru: None; Payal Sojitra: None

Background: At the end of 2019, severe acute respiratory syndrome coronavirus 2 (SARS-CoV-2) emerged as a novel coronavirus responsible for causing the global coronavirus disease 19 (COVID-19) pandemic. Symptoms range from asymptomatic to severe respiratory symptoms. SARS-CoV-2 infection is well known to be associated with immune dysregulation and hematologic aberrancies. Few studies have reviewed peripheral blood smears abnormalities from COVID-19 patients. In this study, we aimed to characterize the morphologic features of peripheral blood smears from COVID-19 patients.

Design: Hospitalized patients with PCR-confirmed COVID-19 infection were identified. Complete Blood Count (CBC) data, clinical findings, and peripheral blood morphology were compared to control patients with confirmed negative COVID-19 PCR.

Results: Twelve PCR confirmed covid 19 positive patients (male- 9, female- 3) with an age range 38 to 95 were compared to 11 control patients PCR-negative for COVID-19. Most patients presented with fever or respiratory symptoms. Among the COVID-19 positive patients absolute lymphopenia was seen in 9/12 patients. Absolute monocytosis was seen in 2/12 and monocytopenia was seen in 3/12 cases. Interestingly, large, activated monocytes with abundant gray-blue cytoplasm with prominent cytoplasmic vacuoles were seen in all the COVID-19 positive patents (see fig. 1 D-F) as compared to normal controls. These activated monocytes consist of 1-11% of leukocytes, with absolute counts ranging from 0.12-0.69 x 10^3/microliter. Other morphologic findings found in peripheral blood smears include plasmacytoid and atypical lymphocytes (Fig 1A-C), as well as neutrophils with pseudo-Pelger-Huet nuclei (Fig 1G-I). 10/12 patients with COVID-19 infection were unvaccinated; differences between peripheral blood smears from vaccinated and unvaccinated patients were not seen. All patients recovered upon follow up.

Figure 1 - 943

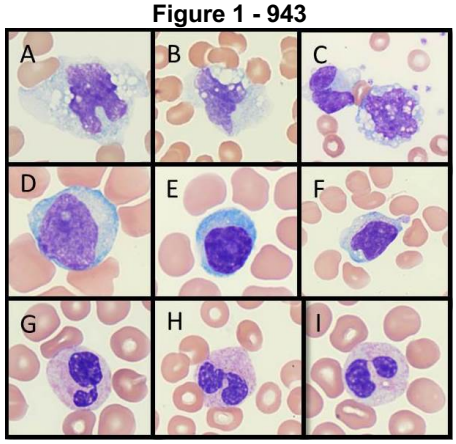

Conclusions: In conclusion, activated monocytes with distinct morphology are present in varying numbers in the peripheral blood from hospitalized COVID-19 patients. These activated monocytes are not present in non-COVID-19 patients. These findings are consistent with those found in previous studies. Some of these studies have shown the presence of activated monocytes may indicate favorable outcomes.

944 HIV-Associated Hodgkin Lymphoma Has Increased CD8 T-Cells and NK Cells in the Tumor Microenvironment

Venkata Rakesh Sethapati[1], Parastou Tizro[2], Mary Nwangwu[3], Wendy Cozen[4], Jose Aparicio[5], Imran Siddiqi[6], Dennis Weisenburger[3], Wing Chan[3], Alex Herrera[3], Joo Song[3]

[1]City of Hope Medical Center, Duarte, CA, [2]City of Hope Cancer Center, Duarte, CA, [3]City of Hope National Medical Center, Duarte, CA, [4]USC Norris Comprehensive Cancer Center, Los Angeles, CA, [5]Keck School of Medicine of USC, Los Angeles, CA, [6]University of Southern California, Keck School of Medicine of USC, Los Angeles, CA

Disclosures: Venkata Rakesh Sethapati: None; Parastou Tizro: None; Mary Nwangwu: None; Wendy Cozen: None; Jose Aparicio: None; Imran Siddiqi: None; Dennis Weisenburger: None; Wing Chan: None; Alex Herrera: None; Joo Song: None

Background: The tumor microenvironment (TME) in classical Hodgkin lymphoma (CHL) is important and allows the Hodgkin cells to proliferate and evade the immune system. Studies have shown that the CHL TME is rich in T cells and PDL1+ tumor associated macrophages which facilitates for the sensitivity to checkpoint blockade. HIV-associated CHL (HIV-CHL) is frequently Epstein-Barr virus (EBV) positive and its TME has been less investigated.

Design: We created a tumor microarray (TMA) with cases diagnosed as CHL, nodular sclerosis subtype (CHL-NS) (N=34), that were cured by first-line therapy with ABVD and 5 cases of HIV-CHL. Routine immunohistochemical stains for CHL were performed on the diagnostic cases (e.g. CD20, PAX5, CD30, CD15, EBER-ISH). Multispectral immunofluorescence (mIF) was performed on the TMA using the Opal 7 kit and two antibody panels (1: CD3, CD8, CD4, PD1, CD30, DAPI; 2: PAX5, CD163, CD79a, PD-L1, CD56, CD30, DAPI), and the slides were scanned with the Vectra spectral imaging system and analyzed using InForm software. Logistic regression analysis was performed using multiple parameters (nearest neighbor analysis, T cell subset densities, etc). The student t-test was performed for comparisons and p values <0.05 were considered statistically significant.

Results: Four out of the 5 cases of HIV-CHL were positive for EBV by EBER-ISH, and the density of CD8+PD1- T-cells and NK cells was significantly higher compared to the CHL-NS (p<0.0001, p=0.04, respectively). There was also a higher number of PDL1+ macrophages in HIV-CHL compared to CHL-NS (228 vs 88 cells/mm^2, P=0.056). The density of CD4+ T cells was higher in CHL-NS compared to the HIV-CHL cases (P=0.09).

Figure 1 - 944

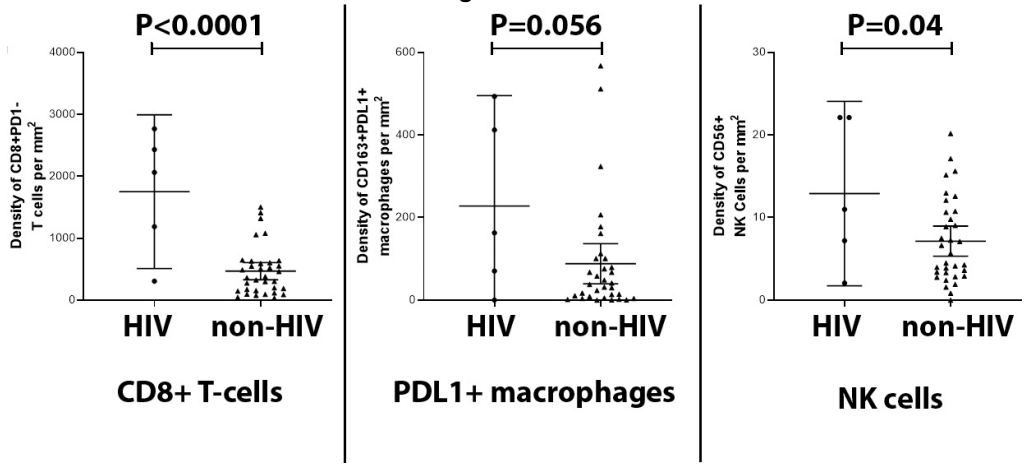

Conclusions: Using mIF, we found that HIV-CHL has a different TME compared to CHL-NS, with a higher proportion of CD8+ T-cells and NK cells. The EBV-infected Hodgkin cells in HIV-CHL likely promote a TME with a higher proportion of PDL1+ macrophages and CD8+ T-cells. These findings can be informative for therapeutic targeting of the TME in Hodgkin lymphoma particularly with immune checkpoint inhibitors. Additional studies will be needed to confirm these findings.

945 The Presence of Chronic Lymphocytic Leukemia Milieu Does not Change Survival of Large B-cell Lymphoma Richter Transformation

Min Shi[1], Kari Rabe[1], Rong He[1], Ji Yuan[1], Yucai Wang[1], Sameer Parikh[1], Wei Ding[1]
[1]Mayo Clinic, Rochester, MN

Disclosures: Min Shi: None; Kari Rabe: None; Rong He: None; Ji Yuan: None; Yucai Wang: *Primary Investigator*, Incyte, InnoCare, LOXO Oncology, Novartis, Genentech, MorphoSys; *Advisory Board Member*, Eli Lilly, TG Therapeutics, LOXO Oncology, Incyte; Sameer Parikh: *Grant or Research Support*, Pharmacyclics, AstraZeneca, Janssen, TG Therapeutics, Merck, AbbVie, Ascentage Pharma; *Advisory Board Member*, AstraZeneca, Pharamcyclics, Genentech, GlaxoSmithKline, Adaptive Biotechnologies, AbbVie; Wei Ding: *Grant or Research Support*, Merck, AstraZeneca, DTRM Pharma, OCTA Pharma, AbbVie, BeiGene; *Advisory Board Member*, BeiGene, Alexion, Merck

Background: Progression of chronic lymphocytic leukemia (CLL) to large B-cell lymphoma (LBCL), is defined as Richter transformation (RT). Pathologically, LBCL is often intermixed with CLL in the same anatomic site (referred to as LBCL-composite), although there is a subset of patients where the specimen consists of LBCL without CLL (LBCL-sole). It is unknown whether the CLL milieu could affect the behavior of LBCL. Herein, we report the clinicopathologic features of the two groups.

Design: CLL patients with biopsy-proven LBCL were identified from the Mayo Clinic CLL Database retrospectively. Clinicopathological data were collected, and the biopsy slides were re-reviewed by at least one hematopathologist, who were blinded to the outcomes of patients. Clonal relationship was defined as the presence of concordant clonal immunoglobulin gene rearrangement patterns or the same cytogenetic abnormalities between CLL and LBCL.

Results: A total of 115 patients consisting of 55 LBCL-composite and 60 LBCL-sole were included in this study. The median age at RT was 70 (30-85) years with 88 (77%) males. Of the 24 patients where clonal relationship was tested, 20 were clonally related to the underlying CLL (13/14 LBCL-composite, 7/10 LBCL-sole, p=0.27). Not all LBCL maintained typical CLL immunophenotype - a subset of LBCL cases showed CLL antigen expression such as CD5 (53%), CD23 (54%), MUM-1 (65%), and BCL2 (82%). Some LBCLs also expressed EBER (17%), CD10 (17%), BCL6 (48%), MYC (75%), and PD-1 (79%), which are not typically seen in CLL. 35/48 (73%) of LBCL-composite cases showed CD5 expression on large B cells, which was significantly more than those with

LBCL-sole (16/48, 33%, p<0.001). LBCL-composite also had higher CD23 expression (31/48, 65%) compared to 18/43 (42%) of LBCL-sole (p=0.03). Other antigen expressions were comparable between the two groups. While comparing the clinical features between the two groups, median platelet counts were significantly different (LBCL-composite 126 x 10^9/L vs LBCL-sole 156 x 10^9/L; p=0.01), while age, gender, LDH, CLL FISH, *TP53* and *IGHV* status, CLL to RT interval, and CLL therapies before RT development (including novel agents), were similar (Table 1). The median overall survival from RT was 1.0 year in both LBCL-composite and LBCL-sole groups (p=0.84) (Figure 1).

Table 1. The clinical features among RT patients with LBCL-composite and LBCL-sole.

	LBCL-composite (N=55)	LBCL-sole (N=60)	Total (N=115)	p value
CLL dx age				0.924[1]
Median	63.5	61.3	62.3	
Range	(40.9-82.4)	(21.9-85.0)	(21.9-85.0)	
RT dx age				0.920[1]
Median	69.8	69.9	69.8	
Range	(41.3-83.7)	(29.9-85.0)	(29.9-85.0)	
gender				0.969[2]
female	13 (23.6%)	14 (23.3%)	27 (23.5%)	
male	42 (76.4%)	46 (76.7%)	88 (76.5%)	
Lactate Dehydrogenase (U/L) closest to diagnosis at any time point				0.961[1]
Median	301.0	277.0	290.0	
Range	(150.0-3590.0)	(109.0-3838.0)	(109.0-3838.0)	
Platelet Count (x10(9)/L) closest to diagnosis at any time point				0.014[1]
Median	126.0	156.5	148.0	
Range	(17.0-671.0)	(31.0-569.0)	(17.0-671.0)	
FISH category				
Missing	15	27	42	
0=None detected	11 (27.5%)	9 (27.3%)	20 (27.4%)	
2=13q-	14 (35.0%)	10 (30.3%)	24 (32.9%)	
3=trisomy 12	4 (10.0%)	2 (6.1%)	6 (8.2%)	
4=11q-	4 (10.0%)	3 (9.1%)	7 (9.6%)	
5=17p-	7 (17.5%)	9 (27.3%)	16 (21.9%)	
FISH 3-level				0.719[2]
Missing	15	27	42	
0=FISH 2: 13q	14 (35.0%)	10 (30.3%)	24 (32.9%)	
1=FISH 0,3: None detected, tri 12	15 (37.5%)	11 (33.3%)	26 (35.6%)	
2=FISH 4,5: 11q, 17p	11 (27.5%)	12 (36.4%)	23 (31.5%)	
Prior TP53 Result				0.954[2]
Normal	11 (61.1%)	6 (60.0%)	17 (60.7%)	
Abnormal	7 (38.9%)	4 (40.0%)	11 (39.3%)	
IGHV mutation status				0.217[2]
0=Mutated	9 (23.1%)	12 (36.4%)	21 (29.2%)	
1=Unmutated	30 (76.9%)	21 (63.6%)	51 (70.8%)	
CLL to RT, years				0.758[1]
Median	4.5	5.1	4.7	
Range	(0.0-34.5)	(0.0-32.8)	(0.0-34.5)	
Any prior CLL tx				0.388[2]
0=No	16 (29.1%)	22 (36.7%)	38 (33.0%)	
1=Yes	39 (70.9%)	38 (63.3%)	77 (67.0%)	
Number prior lines of CLL tx				0.847[1]
Median	1.0	2.0	1.0	
Range	(0.0-13.0)	(0.0-6.0)	(0.0-13.0)	

Any prior novel agent CLL tx				0.820[2]	
0=No	44 (80.0%)	49 (81.7%)	93 (80.9%)		
1=Yes	11 (20.0%)	11 (18.3%)	22 (19.1%)		
Number prior lines of novel agent CLL tx				0.806[1]	
Mean (SD)	0.3 (0.6)	0.3 (0.6)	0.3 (0.6)		
Median	0.0	0.0	0.0		
Range	(0.0-2.0)	(0.0-3.0)	(0.0-3.0)		
MYC rearrangement				0.076[2]	
Missing	32	30	62		
0=Negative	19 (82.6%)	18 (60.0%)	37 (69.8%)		
1=Positive	4 (17.4%)	12 (40.0%)	16 (30.2%)		
BCL2 rearrangement				0.144[3]	
Missing	46	41	87		
0=Negative	9 (100.0%)	14 (73.7%)	23 (82.1%)		
1=Positive	0 (0.0%)	5 (26.3%)	5 (17.9%)		
BCL6 rearrangement				0.234[3]	
Missing	46	41	87		
0=Negative	7 (77.8%)	18 (94.7%)	25 (89.3%)		
1=Positive	2 (22.2%)	1 (5.3%)	3 (10.7%)		
[1]Kruskal Wallis [2]Chi-Square [3]Fisher Exact					

Figure 1 - 945

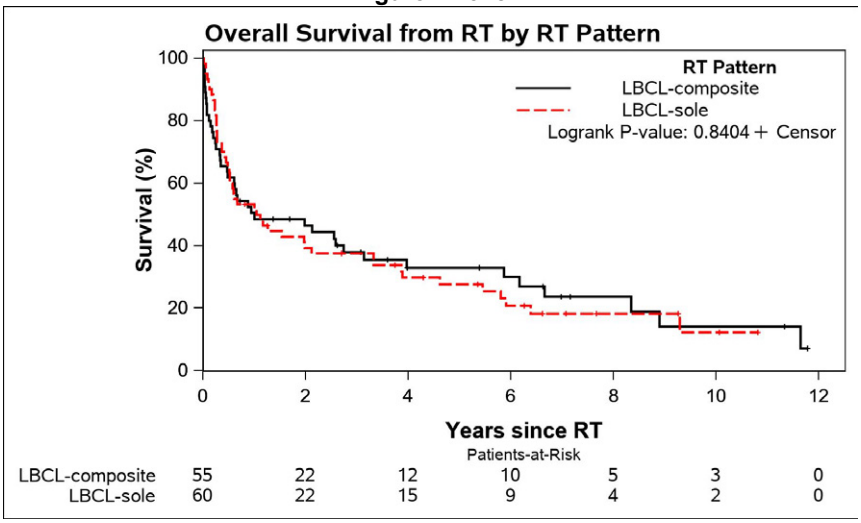

Conclusions: LBCL often showed different immunophenotype from CLL. Patients with LBCL-composite had more frequent expression of CD5 and CD23 compared to patients with LBCL-sole, while overall survival and other clinicopathologic features including clonal relationship were comparable between the two groups. This finding further argues against using CD5 and CD23 as surrogate markers for Richter transformation.

946 IDH1-mutant CMML is Associated with More Aggressive Disease Relative to IDH2-mutant CMML

Amy Song[1], Ismail Elbaz Younes[2], Mohammad Hussaini[3]
[1]Rutgers New Jersey Medical School/Rutgers University, Newark, NJ, [2]H. Lee Moffitt Cancer Center & Research Institute, University of South Florida, Tampa, FL, [3]H. Lee Moffitt Cancer Center & Research Institute, Tampa, FL

Disclosures: Amy Song: None; Ismail Elbaz Younes: None; Mohammad Hussaini: None

Background: Previous studies have found that isocitrate dehydrogenase 1 and 2 (*IDH1* and *IDH2*) mutations are uncommon in chronic myelomonocytic leukemia (CMML), a clonal myeloproliferative neoplasm capable of transformation into acute myeloid leukemia (AML). Although they are presumed to be acquired early in CMML, few studies have explored the impact

of *IDH1/2* mutation on CMML disease trajectory. In particular, this study investigates overall survival (OS), cytogenetics, and disease course in CMML patients with *IDH1* versus *IDH2* mutations.

Design: In this study, we searched ~ 6800 patients with next-generation sequencing (NGS) data to identified 26 patients an initial diagnosis of CMML and with *IDH1* or *IDH2* mutations. Final diagnosis and cytogenetics were collected by retrospective chart review. Two tailed t-tests and Fischer's exact test were used to compare differences in OS and disease progression.

Results: Of the 26 patients with an initial diagnosis of CMML, 10 patients (38%) were *IDH1*- positive and 16 patients (62%) were *IDH2*-positive. No patients had concurrent *IDH1* and *IDH2* mutations. Among patients who were *IDH1*-positive, 8 patients (80%) transformed to AML while 7 *IDH2*-positive patients (44%) underwent transformation to AML (p=0.109). *IDH1*-positive patients had poorer cytogenetics (70%) than *IDH2*-positive patients (31%, p=0.105). CMML-0 or CMML-1 were considered low grade disease and those with CMML-2 or AML were classified as high grade disease. A significantly greater proportion of *IDH1*-positive CMML patients (100%) developed high grade disease (CMML-2 or AML) than *IDH2*-positive CMML patient (44%, p =0.0039). The median overall survival (OS) of *IDH1*-positive patients was 3.02 months, while that of *IDH2* mutated patients was 10.0 months (p =0.441). Commonly co-mutated genes included *SRSF2, TET2, ASXL1, RUNX1*, and *CBL*.

Conclusions: Our study found that *IDH1*-positive CMML patients with the *IDH1* mutation are more likely to develop high grade disease (p=0.0039) and show a trend for poorer cytogenetics and worse overall survival relative to those with *IDH2* mutation. CMML patients who are *IDH1*-positive may require closer surveillance and more aggressive treatment to prevent progression to high grade disease.

947 HIV-associated Follicular Lymphoma (HIV-FL): A Rare Entity with Poor Prognosis

Kran Suknuntha[1], Tayler van den Akker[1], Wayne Tam[2], Zhengming Chen[2], Susan Mathew[2], Ethel Cesarman[3], Amy Chadburn[3]
[1]New York-Presbyterian/Weill Cornell Medicine, New York, NY, [2]Weill Cornell Medicine, New York, NY, [3]Weill Cornell Medical College, New York, NY

Disclosures: Kran Suknuntha: None; Tayler van den Akker: None; Wayne Tam: None; Zhengming Chen: None; Susan Mathew: None; Ethel Cesarman: None; Amy Chadburn: None

Background: Diffuse large B cell lymphoma (DLBCL) is the most common B cell non-Hodgkin lymphoma (B-NHL) in both HIV positive (HIV+) and HIV-negative patients. Follicular lymphoma (FL) is the second most common B-NHL in HIV-negative individuals but is rarely diagnosed in HIV+ patients. Whether HIV-FL, a non-AIDS defining lymphoma, is similar or different to FL in HIV-negative individuals is not clear. Here we report on the clinicopathologic features of 8 HIV-FL in comparison to HIV-negative FL.

Design: Eight HIV+ patients with FL (HIV-FL; 18 samples; 1-4 bx/pt; all men; 1997-2020) were identified and compared to all 27 newly diagnosed FL in HIV-negative patients (2010 and 2011). The pathology reports and medical records of both patient groups and the H+E sections of the HIV-FLs were reviewed. Statistical analysis was performed using Fishers exact test and Wilcoxon Rank-sum test. Survival analysis was done by the Kaplan-Meier method.

Results: The initial HIV-FL lymph node biopsies (50% grade 1/2, 38% grade 3A/3B, 12% unknown) were post-combined anti-retroviral therapy (cART), with 7 (88%) diagnosed after January 2003. 7 cases were CD10+ and/or BCL6+, 1 was only BCL6+. By flow cytometry 1 case was kappa and 4 were lambda light chain positive. BCL2 expression was seen in 6/7 HIV-FL cases tested; the BCL2 negative case was grade 3A, IGH rearranged. FISH showed an IGH-BCL2 rearrangement in 4 tested cases. All 5 cases examined for EBV (EBER ISH) were negative. Clinical information was available for 7 patients. At diagnosis five patients were on cART (1 was non-compliant); 2 started cART with chemotherapy. Six patients had CD4 counts between 299-780/uL, LDH <300 U/L and no B symptoms; 4 had an undetectable HIV viral load. One patient had Kaposi sarcoma (KS). Six patients (85%) had stage III/IV disease. Two patients had low, 3 had intermediate and 2 had high FLIPI scores. Five (63%) HIV-FL patients had recurrent disease. Three patients died of disease, including the 2 with high FLIPI (one who developed DLBCL) and 1 with low FLIPI scores (54, 54, 56 mo). Two patients developed CMV infection and 1 KS after treatment. One patient is alive with disease (111 mo) and 3 are in remission (14, 29, 222 mo).

Features of HIV-FL Compared to HIV-negative FL			
Variable	**HIV+**	**HIV-negative**	**p value**
Age (years)	53	60	0.10
Sex (M:F)	8:0	14:13	0.02
Grade 3 vs. Grade 1/2	43%	15%	0.15
Stage 3/4 vs. Stage 1/2	85%	65%	0.60
Transformed to DLBCL	12.5%	18.5%	1.00

Figure 1 - 947

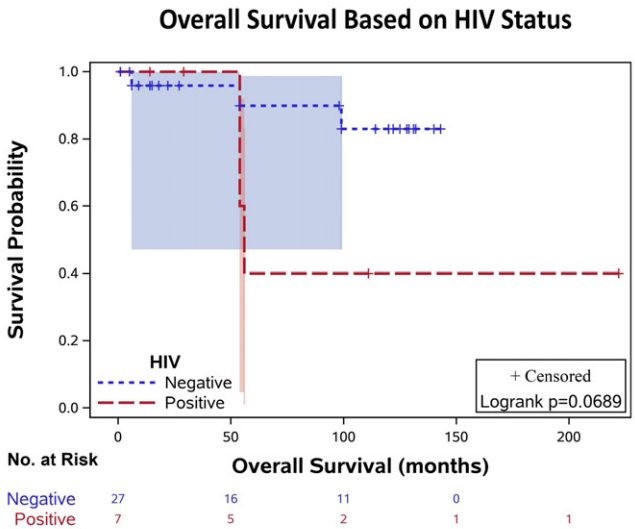

Conclusions: In comparison to HIV-negative FL, where the disease occurs equally in men and women, HIV-FL preferentially occurs in men. Although patient age, lymphoma grade, disease stage and rate of transformation to DLBCL are not significantly different between the two groups, the survival of patients with HIV-FL is relatively poor (only borderline significant due to the small sample size; 5-year survival rate: 40.0% vs. 89.6%, p=0.069). These findings suggest that HIV dysregulation of the immune system, even in the setting of cART, impact survival of HIV+ patients with relatively indolent lymphomas.

948 Targeted Next-Generation Sequencing Reveals Increased Incidence of Somatic Myeloid Mutations in Pediatric Systemic Mastocytosis Compared to Pediatric Cutaneous Mastocytosis

Xiaoping Sun[1], Melody Carter[2], Dean Metcalfe[3], Irina Maric[4]
[1]Clinical Center, National Institutes of Health, Bethesda, MD, [2]National Institute of Allergy and Infectious Diseases, National Institutes of Health, Bethesda, MD, [3]National Institute of Allergy and Infectious Diseases, Bethesda, MD, [4]National Institutes of Health, Bethesda, MD

Disclosures: Xiaoping Sun: None; Melody Carter: None; Dean Metcalfe: None; Irina Maric: None

Background: Mastocytosis is a clonal disease characterized by the presence of excessive numbers of mast cells in the skin and internal organs. Mastocytosis may present with varied clinical manifestations. Children are primarily represented on the benign end of the disease spectrum, often with disease limited to the skin. Children may also have systemic disease, most often associated with the somatic mutation in *KIT* D816V, presenting as early as infancy. Studies investigating the presence of additional somatic myeloid mutations in pediatric systemic disease have not been reported.

Design: We studied 49 patients with cutaneous and systemic variants of pediatric-onset mastocytosis enrolled into NIH clinical protocols. All patients underwent a peripheral blood molecular analysis by allele-specific *KIT* D816V qPCR and targeted next-generation sequencing using the Qiagen Human Myeloid Neoplasms Panel.

Results: 13 pediatric patients were diagnosed with only maculopapular cutaneous mastocytosis (MPCM), 5 with diffuse cutaneous mastocytosis (DCM) and 31 with indolent systemic mastocytosis (ISM). 26/31 patients with ISM carried the *KIT* D816V mutation, and 2/31 carried the *KIT* D816Y mutation. No patients with cutaneous variants of mastocytosis were *KIT* D816V positive. One patient with MPCM carried the *KIT* N822H mutation and one DCM patient showed *KIT* D419del. 6/31 (20%) of ISM patients also

carried *KIT* M541L (VAF 50% or 100%, consistent with germline variant). In addition, 11/31 (35%) of pediatric patients with ISM carried additional myeloid mutations, compared to 0/18 patients with cutaneous disease only. The most prevalent mutations were *RUNX1 L29S* and *TET2* (each detected in 3 ISM patients). All *RUNX1* positive patients had VAF of 50%, consistent with a germline variant. Somatic mutations in *JAK2, CBL, EZH2, MET, MPL, BRAF,* and *RAD50* were each detected in a different single ISM patient. No patient had clinicopathologic evidence of advanced/associated myeloid disease. Somatic mutations in *ASXL1* and *SRSF2*, associated with advanced systemic mastocytosis in adults, were not detected in any pediatric patients.

Conclusions: In addition to mutations within *KIT* codon 816, more than a third (35%) of pediatric patients with ISM were found to have additional somatic myeloid mutations. No somatic myeloid mutations were detected in pediatric patients with cutaneous mastocytosis only.

949 Clinicopathologic Spectrum of Co-existing JAK2 V617F and ASXL1 Mutation in Myeloproliferative Neoplasms: A Single Institute Experience

Sami Talibi[1], Andrea Ferreira-Gonzalez[2], Rajeswari Jayakumar[1]
[1]Virginia Commonwealth University Health System, Richmond, VA, [2]Virginia Commonwealth University, Richmond, VA

Disclosures: Sami Talibi: None; Andrea Ferreira-Gonzalez: None; Rajeswari Jayakumar: None

Background: *JAK2* V617F is the most common mutation identified in myeloproliferative neoplasms (MPN). Additional mutations in epigenetic modifier genes are often present in these cases. Although co-existing *ASXL1* mutations are known to be associated with poor prognosis, the clinicopathologic features of these cases are not well characterized.

Design: We reviewed the next generation sequencing data of MPNs in our institution from September 2019 to September 2021 and recorded the mutation spectrum of these cases. We reviewed the peripheral blood and bone marrow morphology, cytogenetic features and clinical parameters of the cases with co-existing *JAK2* V617F and *ASXL1* mutation.

Results: Of the 31 cases with *JAK2* V617F positive MPN, 14(45.2%) had co-existing *ASXL1* mutation. There were 3 females and 9 males with a median age of 71(range 61 to 80 years). Most common initial presentation was leukocytosis along with a cytopenia, especially anemia. 7 patients (50%) had previous history of other malignancies (Breast carcinoma, prostate cancer, lung adenocarcinoma and hepatocellular carcinoma) including 3 cases with lymphomas (DLBCL,CLL/SLL and splenic marginal zone B-cell lymphoma). 8 Cases (57%) presented with moderate to severe (MF 2-3) myelofibrosis; 1 case with pre fibrotic stage of myelofibrosis and 3 cases with other MPNs that eventually progressed to myelofibrosis. One patient with CML developed *JAK2* and *ASXL1* mutation a decade after allogenic stem cell transplant. 3(21.4%) cases presented with increased blast counts consistent with blast phase of myelofibrosis. 8 out of 14 cases featured markedly hypercellular marrow, and of the remainder 2 were markedly hypocellular. All patients have at least one additional mutation, with TET2 being the most frequent (5/14, 36%). Other mutations include NRAS (19%), U2AF1 (21%) and GATA2 (14.3%). Most cases had normal cytogenetics. One patient had gains in chromosome 1 and 8 and one had loss of CFMB locus in chromosome 16. Patients treated with hydroxyurea/Jakafi (6/14, 43%) or hematopoietic stem cell transplantation (2/14, 14.3%) fared poorly with little resolution of myelofibrosis or the neoplasm. One patient died rapidly, the remaining 13 had continuing marrow abnormalities.

Conclusions: *JAK2* and *ASXL1* mutated MPN often present with or rapidly develop myelofibrosis and are prone to progress to blast phase. They frequently show hypercellular bone marrows and respond poorly to treatment with hydroxyurea/Jakafi as well as stem cell transplant.

950 Therapy-Related Myeloid Neoplasms with Normal Karyotype Show distinct Genomic and Clinical Characteristics compared to their Counterparts with Abnormal Karyotype

Hamza Tariq[1], Liron Barnea Slonim[1], Mir Alikhan[2], Irene Helenowski[1], Hui Zhang[1], Amir Behdad[1]
[1]Northwestern University Feinberg School of Medicine, Chicago, IL, [2]NorthShore University HealthSystem, Evanston, IL

Disclosures: Hamza Tariq: None; Liron Barnea Slonim: None; Mir Alikhan: None; Irene Helenowski: None; Hui Zhang: None; Amir Behdad: None

Background: Therapy-related myeloid neoplasms (t-MNs), a complication of treatment with cytotoxic chemotherapy and/or radiation therapy, are characterized by poor clinical outcomes. Majority of t-MNs show chromosomal abnormalities associated with

MDS or *KMT2A* rearrangements. However, a small number of cases show normal karyotype (NK) and their clinical characteristics & mutational profile remain less studied. This study aims to investigate the genomic landscape and clinical features of t-MN with NK, and to compare with those of t-MN with abnormal karyotype (AK).

Design: We studied patients diagnosed with t-MN at 3 institutions between 01/2016 & 03/2021. Clinical information, results of cytogenetics, FISH & NGS were collected. Mutational profile, survival, and time to progression were compared between NK and AK cases.

Results: A total of 204 patients with t-MN were identified including 158 with AK (71 AML & 87 MDS or MDS/MPN) and 46 with NK (23 AML & 23 MDS or MDS/MPN). Most common mutations in NK t-MNs were *TET2*(41%), *ASXL1*(31%), *SRSF2*(28%), *RUNX1*(26%), *NPM1*(15%) & *STAG2*(13%) while AK t-MNs were enriched for *TP53* mutations (51%) (Table1). 69.5% of NK t-MNs had at least 1 mutation in DTA genes (*DNMT3A, TET2, ASXL1*) & 43.4% in spliceosome genes (*SRSF2, U2AF1, ZRSR2, SF3B1*). 3 patterns of mutations in NK t-MN included: **1**-a combination of mutations in DTA with spliceosome genes and/or *RUNX1 & STAG2* (50%), **2**-*NPM1* mutations with other co-mutated genes (15.2%) & **3**-isolated *TP53* mutation (6.5%). T-MNs with AK showed significantly lower OS than NK (23 vs 10 months;p=0.0094) (Figure1A). Within the MDS+MDS/MPN & AML subgroups, cases with AK showed lower OS compared to NK but did not reach a statistical significance (p=0.06&0.14) (Fig1B&C). Time to progression to AML from MDS was not different between the 2 groups (p=0.38) (Fig1D).

Mutation	AK cases N=158	NK Count N=46	p-value
ASXL1	13 (8.28%)	14 (30.43%)	0.0003
BCOR	2 (1.27%	4 (8.7%)	0.0246
CBL	2 (1.27%)	2 (4.35%)	0.2216
CEBPA	2 (1.27%)	3 (6.52%)	0.0779
DNMT3A	20 (12.74%)	7 (15.22%)	0.6289
EZH2	5 (3.18%)	1 (2.17%)	0.9999
FLT3	2 (1.27%)	6 (13.04%)	0.002
GATA2	1 (0.64%)	1 (2.17%)	0.4027
IDH1	2 (1.27%)	3 (6.52%)	0.0779
IDH2	2 (1.27%)	3 (6.52%)	0.0779
JAK2	2 (1.27%)	3 (6.52%)	0.0779
KRAS	4 (2.55%)	1 (2.17%)	0.9999
MPL	3 (1.91%)	1 (2.17%)	0.9999
NF1	3 (1.91%)	1 (2.17%)	0.9999
NPM1	1 (0.64%)	7 (15.22%)	0.0001
NRAS	7 (4.46%)	1 (2.17%)	0.6858
PHF6	1 (0.64%)	4 (8.7%)	0.0099
PTPN11	6 (3.82%)	2 (4.35%)	0.9999
RUNX1	19 (12.1%)	12 (26.09%)	0.0336
SETBP1	4 (2.55%)	2 (4.35%)	0.6199
SF3B1	3 (1.91%)	2 (4.35%)	0.3174
SH2B3	3 (1.91%)	2 (4.35%)	0.3174
SRSF2	8 (5.1%)	13 (28.26%)	<0.0001
STAG2	4 (2.55%)	6 (13.04%)	0.0102
TET2	17 (10.83%)	19 (41.3%)	<0.0001
TP53	80 (50.96%)	3 (6.52%)	<0.0001
U2AF1	9 (5.73%)	4 (8.7%)	0.4965
ZRSR2	1 (0.64%)	3 (6.52%)	0.0371

Figure 1 - 950

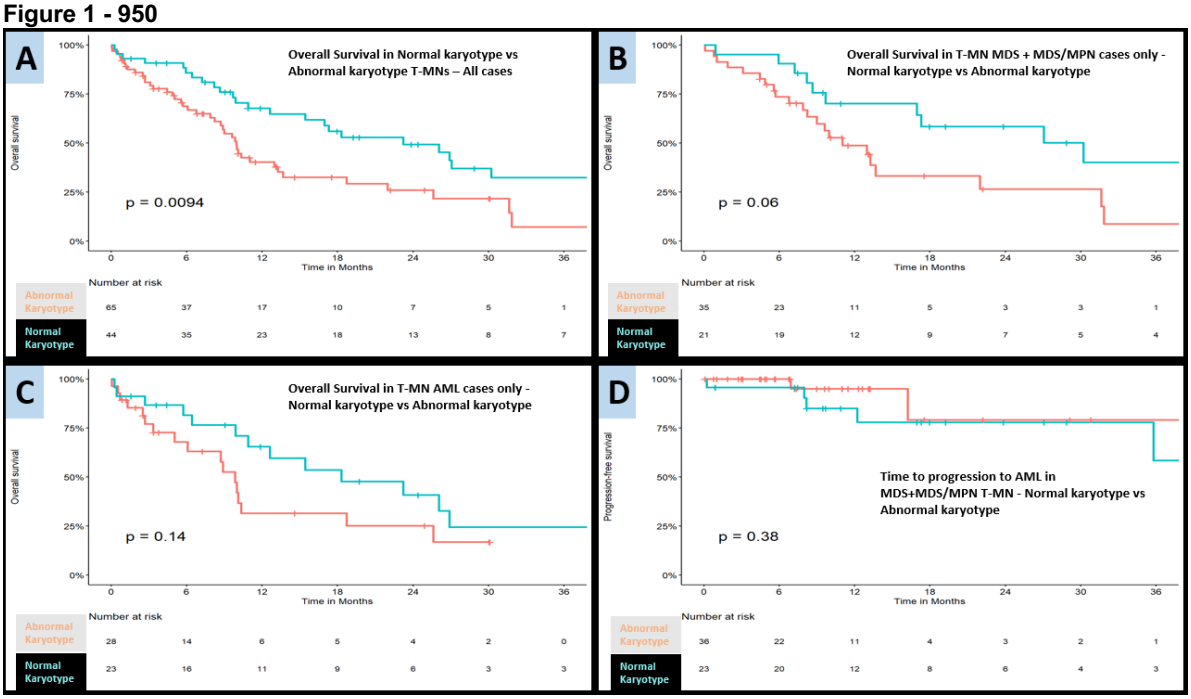

Figure 2 – 950

Figure 2: Clinical Characteristics of the Cohort

	AK* (67)	NK (46)
Age at diagnosis (Median, range)	67.4 (21.2 to 84.6)	72.0 (48.0 to 89.0)
Gender		
Female: n (%)	30 (44.8%)	25 (54.3%)
Male: n (%)	37 (55.2%)	21 (45.7%)
Diagnosis at Onset		
AML (%)	44.94	50.0
MDS (%)	52.53	41.3
MDS/MPN (%)	2.53	8.70
Type of cytotoxic therapy		
Chemotherapy (%)	83.58	56.52
Ionizing radiation therapy (XRT)(%)	5.97	30.43
Chemotherapy + XRT (%)	10.45	13.05
Type of chemotherapy used		
Alkylating agents (%)	11.94	15.22
Topoisomerase II inhibitors (%)	10.44	6.53
Others** (%)	4.48	4.34
Combination chemotherapy regimens (%)	67.17	43.48
Latency * in years (mean; range)**	8.54; 0.70 – 28.32	9.28; 0.81 – 35.35
Progression from MDS or MDS/MPN to AML (%)	23.01%	22.71%
Interval to progression to AML in years (mean; range)	1.2; 0.4 – 2.5	1.1; 0.5 – 3.0

*** Clinical information was available only for 67/158 of AK t-MNs**
** Includes antimetabolites such as thiopurines, mycophenolate mofetil, and fludarabine, and anti-tubulin agents such as vincristine, vinblastine, vindesine, paclitaxel, and docetaxel
***Time from initiation of cytotoxic therapy to the diagnosis of t-MN

Conclusions: In one of the largest series to date we describe the mutational landscape of t-MN with NK, highlighting frequent mutations in DTA genes often combined with mutations in spliceosome, *RUNX1*, & cohesion genes. This is in contrast to t-MNs

with AK that have frequent *TP53* mutations and a lower percentage of myeloid-related gene mutations. These findings highlight a likely stepwise mutagenesis in NK t-MN and the potential need for screening for DTA & spliceosome mutations before treatment of preceding malignancy. NK t-MNs show better survival compared to their AK counterparts. We propose a separate category of t-MNs with NK given their distinct mutational and clinical profile.

951 TP53-mutated Acute Myeloid Leukemia with Myelodysplasia-Related Changes and Therapy-Related Acute Myeloid Leukemia Have Comparable TP53 Mutational Signature and Clinical Features

Mehrnoosh Tashakori[1], Kadia Tapan[2], Sanam Loghavi[2], Zhenya Tang[2], Mark Routbort[2], Farhad Ravandi-Kashani[2], Joseph Khoury[2]
[1]University of Minnesota, Minneapolis, MN, [2]The University of Texas MD Anderson Cancer Center, Houston, TX

Disclosures: Mehrnoosh Tashakori: None; Kadia Tapan: None; Sanam Loghavi: None; Zhenya Tang: None; Mark Routbort: None; Farhad Ravandi-Kashani: None; Joseph Khoury: None

Background: Acute myeloid leukemia (AML) with myelodysplasia-related changes (AML-MRC) and therapy-related AML (t-AML) are distinct disease subtypes that share a high frequency of *TP53* mutations (*TP53*mut). Given their different leukemogenic evolutionary factors, we aimed to compare the *TP53* mutational signature and clinical features across *TP53*-mutated AML-MRC and t-AML.

Design: We identified patients diagnosed with AML-MRC or t-AML with *TP53*mut seen at our institution who had not received AML therapy. Mutation analysis was performed using next-generation sequencing. Copy number loss (CNL) was determined by fluorescence *in situ* hybridization using a probe set specific for the *TP53* gene locus and/or array-based comparative genomic hybridization.

Results: The study group included 233 patients; 167 (71.7%) with AML-MRC and 66 (28.3%) with t-AML. Both groups had comparable clinical findings and overall survival. In both groups, the majority of patients had complex karyotype: AML-MRC, 94.6%; t-AML, 89.3%. Myelodysplasia-related cytogenetic abnormalities were also similar in incidence: AML-MRC, 86.7%; t-AML, 75.7%; mostly involving chromosomes 5 and 7. *TP53* CNL was common and comparable across both groups: AML-MRC, 96/128 (75%); t-AML, 30/42 (71.4%). In both groups, most patients had 1 *TP53*mut: AML-MRC, 77.8%; t-AML, 66.7%. *TP53*mut was present as a dominant clone in all cases, and the median VAF of the dominant *TP53* clone was similar across the two groups: AML-MRC, 46%; t-AML, 43%. At least 75% of *TP53*mut were missense in both groups; ~23% being hotspot mutations, most commonly R248. The incidence of R248 was similar in both groups: AML-MRC 19/47 (40.4%); t-AML: 9/21 (42.8%). The second most common hotspot mutation in AML-MRC was Y220 (12/47; 25.5%) and in t-AML was R273 (4/21; 19%). Notably there was not statistically significant difference between the two groups across all TP53 and clinicopathologic parameters evaluated (Table 1 and Figure 1).

Variable	AML-MRC n = 167	t-AML n = 66
Age at diagnosis, median years (range)	71 (20-90)	70 (28-89)
Male (%)	93 (55.7%)	28 (42.4%)
Hemoglobin (g/dL), median (range)	8.7 (5.5-13)	8.8 (6.2-8.8)
White blood count (x10^9/L), median (range)	3.7 (0.5-113.6)	3.3 (0.5-143.6)
Platelet count (x10^9/L), median (range)	39 (2-242)	33.5 (0-207)
LDH, median (range)	636 (117-6623)	687 (180-9170)
Complex karyotype (%)	158 (94.6)	59 (89.3%)
Myelodysplasia-related cytogenetic abnormalities (%)	139 (87.7)	50 (75.7)
−5/del(5q) (%)	127 (77.4)[£]	47 (71.2)
−7/del(7q) (%)	78 (47.6)[£]	27 (41)
Overall survival, median months (range)	5.3 (0.1-53.5)	5.4 (0.1-32.7)
Number of *TP53* mutation(s) per case 1 mutation (%) 2 mutations (%) 3 mutations (%)	130 (77.8) 33 (19.8) 4 (2.4)	44 (66.7) 22 (33.3) 0

Type of *TP53* mutations	158 (76)	68 (77.3)
missense (%)	9 (4.3)	3 (3.4)
splice site (%)	14 (6.7)	9 (10.2)
nonsense (%)	23 (11)	5 (5.7)
frameshift (%)	4 (2)	3 (3.4)
deletion (%)		
TP53 hotspot mutations	47 (22.6)	21 (23.8)
R273H/C/S (%)	10 (21.3)	4 (19)
R175H/G (%)	3 (6.4)	3 (14.3)
R248Q/W (%)	19 (40.4)	9 (42.8)
Y220C/H/N/S (%)	12 (25.5)	2 (9.5)
M237I/K (%)	1 (2.1)	2 (9.5)
R282W/G (%)	2 (4.8)	1 (4.7)
TP53 VAF in dominant clone, median (range)	46 (1.5-95.4)	43 (1-95.2)
TP53 CNL	96 (75)[€]	30 (71.5)[¥]
1 mutation and CNL (%)	82 (64)	23 (54.8)
2 mutation and CNL (%)	13 (10.2)	7 (16.7)
3 mutation and CNL (%)	1 (0.8)	0
1 mutation (hotspot)	35	10
and CNL	24 (82.7)[§]	5 (62.5)[$]
1 mutation (non-hotspot)	95	34
and CNL	58 (79.5)[¶]	18 (78.2)[¶¶]
Base substitutions in 1 TP53 mutation		
Transitions		
C:G > T:A	54 (41.5)	21 (47.7)
T:A > C:G	27 (20.8)	13 (29.5)
Transversions		
C:G > A:T	8 (6.2)	3 (6.8)
C:G > G:C	10 (7.7)	2 (4.5)
T:A>A:T	10 (7.7)	1 (2.3)
T:A > G:C	3 (2.3)	2 (4.5)
Insertion/deletion/complex	18 (13.8)	2 (4.5)

[£]not available for 3 case; [¥]available for 42 cases; [€]available for 128 case; [$]not available for 2 case; [§]not available for 5 case; [¶]not available for 22 case; [¶¶]not available for 11 case; VAF: variant of allele frequency; CNL: copy number loss; all *p*-value ≥0.05.

Table 1. Clinical, cytogenetic and molecular features of AML-MRC and t-AML.

Figure 1 - 951

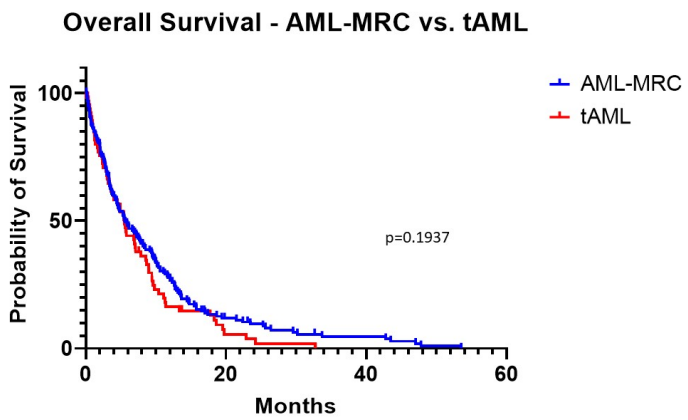

Conclusions: The similarities between *TP53* mutational signature in AML-MRC and t-AML suggest that *TP53* mutations in either group evolve through shared pathogenic mechanisms and evolutionary factors. Clinicopathologic overlap suggests that *TP53* mutation could be useful as a unifying factor for future classification.

952 Molecular Characterization of Chronic Lymphocytic Leukemia with Progression to Classic Hodgkin Lymphoma

Gerald Tiu[1], Guangwu Xu[1], Dita Gratzinger[2], Sebastian Fernandez-Pol[2]
[1]*Stanford Health Care, Stanford, CA,* [2]*Stanford University Medical Center, Stanford, CA*

Disclosures: Gerald Tiu: None; Guangwu Xu: None; Dita Gratzinger: None; Sebastian Fernandez-Pol: None

Background: In 5-10% of patients, chronic lymphocytic leukemia (CLL) may transform into a more aggressive lymphoma, most commonly of the diffuse large B-cell lymphoma (DLBCL) subtype. Rarely, CLL may also transform into classic Hodgkin lymphoma (CHL). Although the genetics of CLL transformation into DLBCL have been described, the molecular features of CLL transformation into CHL are not well-understood. Here, we describe the molecular characterization of CLL transformation into CHL (CLL/CHL) and related entities through targeted next generation sequencing (NGS).

Design: We retrospectively searched our institution's NGS database for patients with CLL/CHL who have undergone lymph node biopsies that show evidence of active disease. Targeted next generation sequencing was performed via our institution's clinical sequencing platform. Morphology, immunophenotype, and clinical data were also reviewed.

Results: We identified four patients with a history of CLL/CHL and one patient with progression to a B-cell lymphoproliferative disorder with Hodgkin-like features. Patient ages ranged from 48-78 years old (mean 69) with four males and one female. Three out of the five patient samples were positive for EBV by *in situ* hybridization.

Three of the five patient samples harbored pathogenic variants in either *IDH1* (n = 1) or *TET2* (n = 2), which are genes involved in the regulation of DNA 5-hydroxymethylcytosine (5hmC) levels. For the patient with the *IDH1* variant, mutation-specific immunohistochemistry (IHC) for *IDH1* R132H protein showed increased staining in tumor-associated histiocytes/dendritic cells rather than lymphocytes. Pathogenic variants were also identified in *SRSF2*, *KLF2*, and *MYD88*.

	Patient 1	Patient 2	Patient 3	Patient 4	Patient 5
Sex	Male	Male	Female	Male	Male
Age at diagnosis of CLL	71	72	64	63	41
Age at transformation and collection of specimen	71	78	78	70	48
Specimen type	Neck lymph node	Neck lymph node	Supraclavicular lymph node	Retroperitoneal lymph node	Cervical lymph node
Transformation type/Diagnosis	EBV-positive B-cell lymphoproliferative disorder with Hodgkin-like features	Classic Hodgkin lymphoma with atypical features	Classic Hodgkin lymphoma	Classic Hodgkin lymphoma	Classic Hodgkin lymphoma
Sequenced specimen with evidence of CHL/Transformation	Yes	Yes	Yes	Yes	Yes
Sequenced specimen with evidence of CLL	Yes	No	No	No	Yes
Reported pathogenic variants and variant allele frequency (VAF) of genes involved in 5-hydroxymethylcytosine pathways	IDH1 (R132H, 4% VAF)	TET2 (L615fs, 21% VAF); TET2 (Q831X, 13% VAF)	TET2 (Q884X, 27% VAF); TET2 (K244X, VAF 5%)	None	None
Other reported pathogenic variants and variant allele frequency (VAF)	SRSF2 (P95L, 4% VAF)	KLF2 (G280fs 12% VAF)	None	None	MYD88 (L265P, 43% VAF)
Reported variants of uncertain significance	None	DDX3X (N45D, 15%); JAK1 (G1097A, 12%); PRDM1 (K188E, 39%);	ALK (L1339V, 53% VAF); DNMT3A (R556_C557delinsSPG, 15% VAF); TET2 (Y1345D, 5% VAF)	PAX5 (P207L, 48% VAF); GATA3 (G246A, 36% VAF); SETD2 (K297R, 36% VAF)	None
Immunohistochemistry of Hodgkin and Reed/Sternberg (HRS) and HRS-like cells	CD30+, CD15-, CD20+, PAX5 variable, EBV+	CD30+, CD15-, CD20-, PAX5 rare/dim, EBV-	CD30+, CD15+ (subset, Golgi pattern), CD20-, PAX5 dim, EBV+	CD30+, CD15+, CD20-, PAX5 dim, EBV-	CD30+, CD15-, CD20-, PAX5 dim, EBV+
Other comments	IDH1 R132H+ tumor-associated histiocytes/dendritic cells by immunohistochemistry	N/A	N/A	N/A	N/A

Conclusions: To our knowledge, these are the first cases to characterize the genetics of CLL transformation to CHL with next generation sequencing. The most common mutations were in genes involved in oxidation of 5-methylcytosine (5mC) to 5hmC, which has previously been shown to play important roles in oxidogenesis and gene regulation. Furthermore, IHC for mutated IDH1 protein in the patient with a pathogenic *IDH1* variant showed expression in tumor-associated myeloid cells rather than in the malignant lymphocytes themselves, suggesting possible cell non-autonomous mechanisms by which genetic perturbation of 5hmC

pathway genes are associated with malignancy. Together, these findings provide a genetic foundation for further mechanistic and clinical characterization of CLL/CHL.

953 BAFF-R Expression in B Lymphoblastic Leukemia

Parastou Tizro[1], Ibrahim Aldoss[2], Aimin Li[3], Raju Pillai[4], Wanda Chan[5], Elizabeth Quirk[2], Wing Chan[4], Joo Song[4]
[1]City of Hope Cancer Center, Duarte, CA, [2]City of Hope, Duarte, CA, [3]City of Hope Medical Center, Duarte, CA, [4]City of Hope National Medical Center, Duarte, CA, [5]COH

Disclosures: Parastou Tizro: None; Ibrahim Aldoss: None; Aimin Li: None; Raju Pillai: None; Wanda Chan: None; Elizabeth Quirk: None; Wing Chan: None; Joo Song: None

Background: B cell activating factor (BAFF), as a member of tumor necrosis factor (TNF) family and its receptor (BAFF-R) are crucial for survival and maturation of B cells. Despite the lack of BAFF-R on pre-B cells and hematogones, recent studies show aberrant expression of BAFF-R in B lymphoblastic leukemia (B-ALL). Although CAR T cells against CD19 have shown an excellent response in CD19 positive B-cell malignancies, they have a limited efficacy in relapsed/refractory B-cell tumors partly due to CD19 antigen loss. We have recently developed a CAR T-cell targeting BAFF-R which shows promising therapeutic effects in B-ALL cases lacking CD19, and maybe an important alternative target for therapy.

Design: To determine the expression level of BAFF-R in tumor cells and normal hematopoietic elements in the bone marrow and peripheral blood, we used a commercially available BAFF-R antibody (clone 11C1, BD), starting with manufacturer's recommended volume of 5 µL which was added to 100 µL of patient sample and was incorporated in a standard panel for diagnosis of B-ALL (CD45, CD19, CD22, CD20, CD34, CD38). Determination of BAFF-R negative and BAFF-R positive was made by using T-cells and mature B cells as the reference internal negative and positive control, respectively. We analyzed 24 cases of B-ALL, 3 cases of chronic lymphocytic lymphoma (CLL), 1 primary myelofibrosis, 1 angioimmunoblastic T-cell lymphoma, 1 acute myeloid leukemia, and 5 negative cases by flow cytometry. We determined median fluorescent intensity (MFI) of the abnormal population divided by the MFI of the background normal T-cells to create an MFI ratio.

Results: The median MFI ratio in B-ALL was 2.51 (0.89-15.71). MFI ratio below 2.2 was considered negative, 2.3-7.9, dim positive, and >8 moderately positive. We found dim to moderate BAFF-R expression in 54% (13/24) of B-ALL cases. Patients who have failed prior blinatumomab show a higher percentage of cases with BAFF-R positivity compared to newly diagnosed patients (11/17, 65% vs 2/7, 29%). All cases of CLL and background mature B-cells showed moderate expression of BAFF-R.

Figure 1 - 953

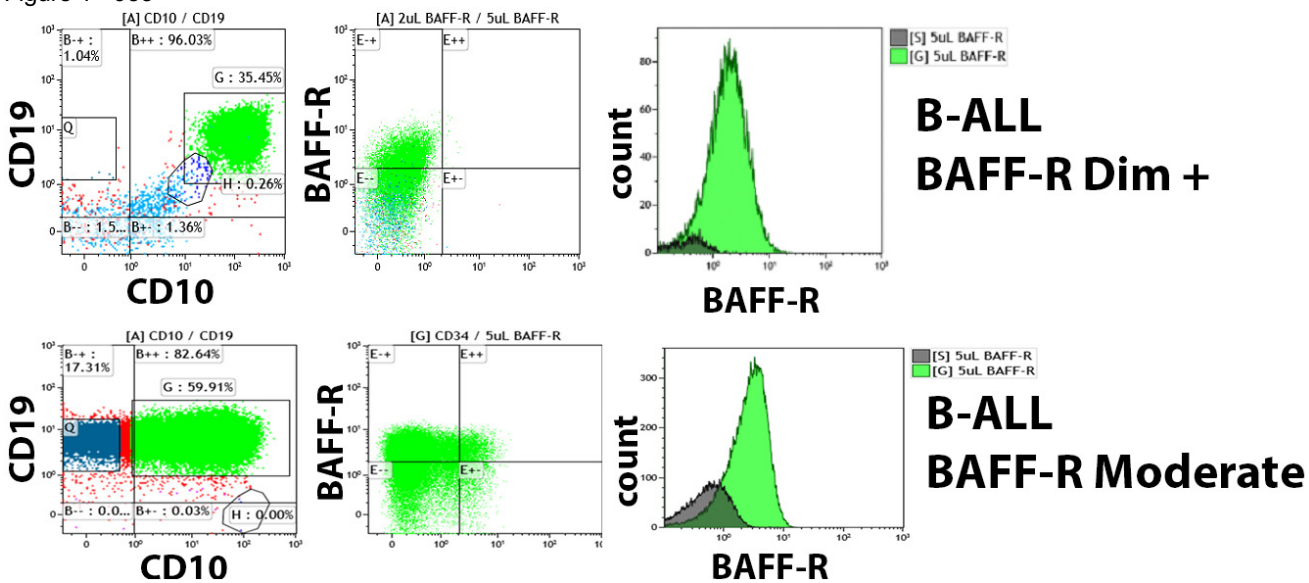

Conclusions: Our study showed that BAFF-R expression can be seen in B-ALL, particularly in relapsed/refractory cases. Expression of BAFF-R is important to detect as it can be therapeutic target for CAR T-cells or other immunotherapies and would benefit patients who have relapsed/refractory disease that have failed anti-CD19 therapy.

954 Characterization of the Tumor Microenvironment in Pediatric T-Cell Leukemia/Lymphoma

David Twa[1], Lorraine Liu[2], Douglas Morrison[2], Kate Chipperfield[2], Nicholas Au[2], Suzanne Vercauteren[2], Audi Setiadi[2]
[1]University of Calgary, Calgary, Canada, [2]BC Children's and Women's Hospital, Vancouver, Canada

Disclosures: David Twa: None; Lorraine Liu: None; Douglas Morrison: None; Kate Chipperfield: None; Nicholas Au: None; Suzanne Vercauteren: None; Audi Setiadi: None

Background: The tumor microenvironment (TME) of pediatric leukemia/lymphoma remains incompletely characterized and underutilized for potential risk stratification. While molecular and cytogenic profiling of tumor cells, in addition to minimal residual disease (MRD) testing following induction chemotherapy, have revolutionized disease outcomes, such improvements have preferentially favored B-cell entities.

Design: Using five and 10 channel flow cytometry, here, we interrogated the proportions of B-cells, and granulocytes, in addition to normal CD4+ and CD8+ T-cell populations in the diagnostic and post-induction (day-29) bone marrow samples of T-cell leukemia/lymphomas and mixed-phenotype (T-cell) acute leukemias diagnosed at BC Children's Hospital from January 2010 through November 2020 (n=44). The exposure variable for proportion of CD8 T-cells among the sum of single positive CD4 and CD8 populations was computed using the fraction of all events collected and was normalized to the averaged control bone marrow scores (n=2). Finally, the absolute value was taken to capture an index of T-cell diversity. TME constituents were compared (Wilcoxon) between bone marrow biopsy time points and correlated with MRD using Spearman's rho. T-cell diversity was interrogated using log-rank tests with overall and progression-free survival outcomes; patients with less than six months follow-up were excluded from this analysis.

Results: We found that following induction chemotherapy, there were appreciable increases in the number of CD4+ (P=2.40E-5) and CD8+ (P=5.22E-5) T-cells in the bone marrow and that the index of T-cell diversity was reduced (P=0.023). Correlating the T-cell diversity index with MRD, there was and inverse relationship (rho=-0.479; P=0.011), which remained significant following Bonferroni correction for multiple tests. Finally, we observed an association with T-cell diversity and overall survival (HR:5.2 95%CI:1.1-31.9; P=0.020). Binary tests of the T-cell index with clinical variables showed only a trend for significance for MRD (P=0.060). Accordingly, within the adjusted Cox model, we controlled for MRD, and the model remained significant (P=0.011).

Conclusions: This work reiterates the value of the TME in non-B-cell leukemia/lymphoma pathogenesis and demonstrates the potential clinical utility in identifying higher risk patient populations alongside preexisting risk factors.

955 Mechanisms of Programmed Death Ligand Structural Genomic Rearrangements

David Twa[1], Michael Skinnider[2], David Scott[3], Christian Steidl[4]
[1]University of Calgary, Calgary, Canada, [2]The University of British Columbia, Vancouver, Canada, [3]BC Cancer Agency, University of British Columbia, Vancouver, Canada, [4]BC Cancer Agency, Vancouver, Canada

Disclosures: David Twa: None; Michael Skinnider: None; David Scott: None; Christian Steidl: *Consultant*, Bayer, Seattle Genetics, Roche, AbbVie, AstraZeneca; *Grant or Research Support*, Bristol-Myers Squibb, Epizyme, Trillium Therapeutics

Background: The mechanisms that underlie common structural genomic rearrangements (SGR) in B-cell lymphomas have been studied extensively. V(D)J recombination, somatic hypermutation, and class-switch recombination are cellular processes that are critical to establishing the diversity and antigenic precision of B-cells. Rearrangements occurring at the programmed death ligand (PDL) locus (chromosome 9p24.1), for which immunoglobulin loci partners are rare and which occur in a malignant cell of origin that does not reproducibly express RAG/AID machinery at high levels, do not fit this model.

Design: To identify mechanisms involved in generating PDL SGRs, we analyzed the genomic sequences upstream and downstream of PDL breakpoints and cognate partner loci of 48 PDL rearrangements in B-cell lymphomas previously derived by our group, in addition to 31 PDL rearrangements derived from the literature. As a control, we used 176 BCL6 rearrangements that were observed from capture sequencing. DNA was interrogated for degenerate RAG/AID motifs, in addition to non-B DNA destabilizing forms, mobile elements, non-coding RNA, and novel motifs. Empirical enrichment for motifs was determined through bootstrapping 1,000 random genomic windows equal in size and number to the validated rearrangements.

Results: Among all PDL and partner breakpoints, we found that there was enrichment (119/132 90%; P=0.024) for inverted repeats, a type of destabilizing non-B DNA motif. Unlike for the control BCL6 rearrangements assessed, where we found significant AID CpG motif enrichment (P<0.001), there was no evident association of PDL SGRs with either RAG or AID mediated

mechanisms. We also observed that PDL SGR partners shared common ontologies, specifically there was an enrichment for an interferon gamma signature (R-HSA-877300; P=1.58E-6). Furthermore, PDL partner genes were highly expressed in non-Hodgkin lymphomas compared to other entities (P<0.050). Finally, we observed that 46/67 (69%) and 62/67 (98%) of rearrangements had no overlapping microhomology or flanking microhomology, respectively, favoring a pathogenesis model involving NHEJ repair.

Conclusions: These findings suggest that PDL SGRs are derived from DNA destabilizing motifs and while SGR partners are promiscuous compared to other B-cell rearrangements, these partners are highly expressed in B-cells and might be principally driven by an interferon gamma milieu.

956 Epstein Barr Virus Latency Patterns in Post-Transplant Lymphoproliferative Disorders and EBV+ Mucocutaneous Ulcer: Diagnostic and Prognostic Implications

Ashley Volaric[1], Atif Saleem[2], Lauren Lawrence[2], Sheren Younes[3], Diane Libert[3], Shuchun Zhao[1], Yasodha Natkunam[1]
[1]Stanford Medicine/Stanford University, Stanford, CA, [2]Stanford University, Stanford, CA, [3]Stanford Pathology, Stanford, CA

Disclosures: Ashley Volaric: None; Atif Saleem: None; Lauren Lawrence: None; Sheren Younes: None; Diane Libert: None; Shuchun Zhao: None; Yasodha Natkunam: None

Background: Epstein Barr Virus (EBV) is responsible for an array of lymphoproliferative disorders ranging from subclinical infection to immunodeficiency-related neoplasms. EBV establishes a latent infection in the host B cells as defined by discrete expression of latent membrane protein 1 (LMP-1) and EBV nuclear antigen 2 (EBNA-2). EBV latency is classified into three patterns, of which latency 3 is the most unrestrictive with full expression of LMP-1 and EBNA-2. Latency patterns are described in B lymphoblastoid transformation as distinct protein signatures. However, EBV latency patterns are not well understood in post-transplant lymphoproliferative disorders (PTLDs) and EBV+ mucocutaneous ulcers (MCU). Herein, we characterize the latency patterns of these disorders with LMP-1 and EBNA-2 immunohistochemistry in comparison to other B cell neoplasms.

Design: A total of 79 cases of EBV-positive PTLD, EBV+ MCU, classic Hodgkin lymphoma (CHL) and diffuse large B cell lymphoma (DLBCL) were evaluated for EBV-encoded small RNAs (EBER) by in situ hybridization and for LMP-1(Ventana Ultra, Dako M0897) and EBNA-2 (Leica Bond, Abcam ab90543) by immunohistochemistry.

Results: A full spectrum of EBV latency patterns is observed across PTLD, EBV+ MCU, CHL and DLBCL. DLBCL in the post-transplant setting show the greatest proportion of cases with EBV latency 3 pattern (Figures 1 and 2). In contrast, EBV+ DLBCL in immunocompetent patients show latency patterns 1-2. EBV+ MCU exhibit predominately latency 2 pattern, similar to the majority of CHL. Expression levels of EBER, LMP-1 and EBNA-2 vary (Table 1). In the post-transplant setting, DLBCL demonstrate the highest expression of EBNA-2 (>50%). Whereas, Burkitt lymphoma and plasmacytic hyperplasia are negative for EBNA-2 (<1%), which is indicative of a restrictive EBV latency pattern.

Table 1. LMP-1 and EBNA-2 Expression Patterns in B cell Lymphoproliferative Disorders.

Lesion Type	LMP-1		EBNA-2	
	Negative (<1%)	Positive (≥1%)	Negative (<1%)	Positive (≥1%)
PTLD, Florid Follicular Hyperplasia, EBV+	5/7 (71%)	2/7 (29%)	6/7 (86%)	1/7 (14%)
PTLD, Polymorphic, EBV+	2/7 (29%)	5/7 (71%)	5/7 (71%)	2/7 (29%)
PTLD, DLBCL, EBV+	3/26 (12%)	23/26 (88%)	4/26 (15%)	22/26 (85%)
PTLD, CHL, EBV+	2/3 (67%)	1/3 (33%)	3/3 (100%)	0
PTLD, Plasmacytic Hyperplasia, EBV+	3/3 (100%)	0	3/3 (100%)	0
PTLD, Burkitt Lymphoma, EBV+	1/1 (100%)	0	1/1 (100%)	0
EBV+ Mucocutaneous Ulcer	1/7 (14%)	6/7 (86%)	7/7 (100%)	0
EBV+ Classic Hodgkin Lymphoma	1/21 (5%)	20/21 (95%)	21/21 (100%)	0
EBV+ DLBCL	3/4 (75%)	1/4 (25%)	4/4 (100%)	0

Figure 1 - 956

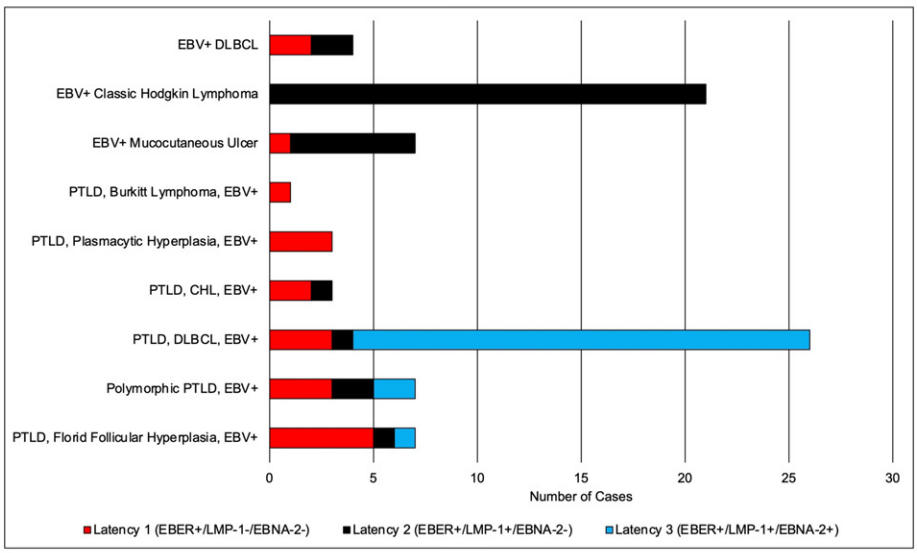

Figure 1. EBV Latency Patterns of B cell Lymphoproliferative Disorders. EBV latency patterns provide a unique signature to a variety of B cell lymphoproliferative disorders in both the post-transplant and non-transplant setting.

DLBCL= Diffuse large B cell lymphoma; PTLD= Post-transplant lymphoproliferative disorder; CHL= Classic Hodgkin lymphoma

Figure 2 – 956

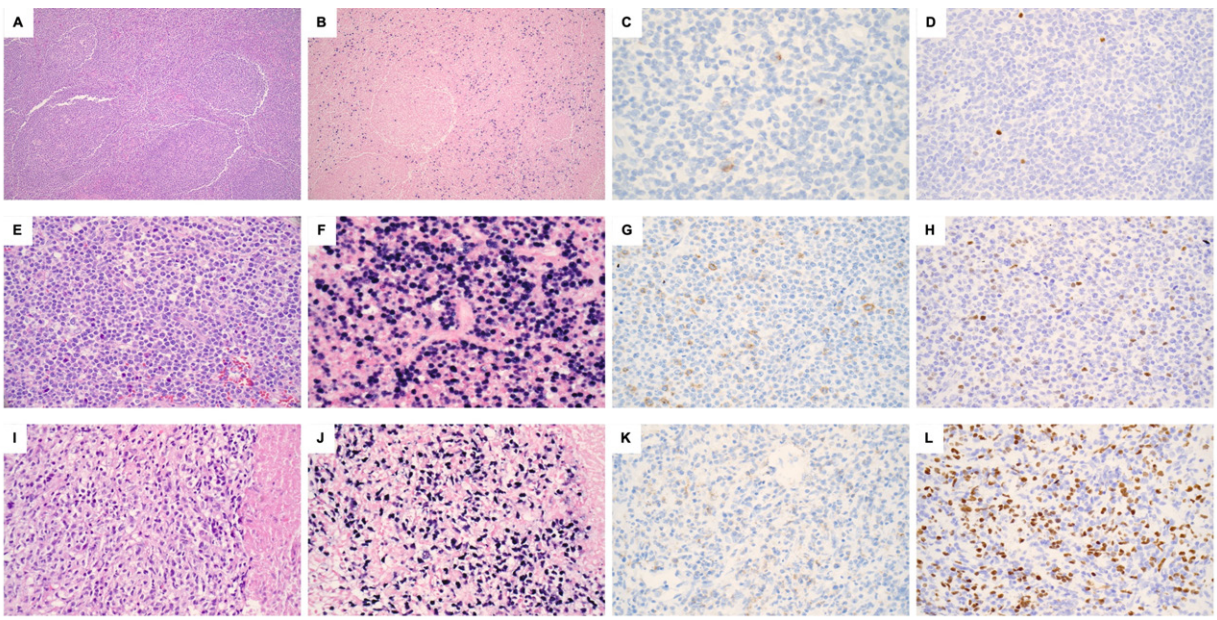

Figure 2. EBV Latency 3 Pattern in PTLD Cases. EBV Latency 3 pattern is illustrated in three representative cases of PTLD: florid follicular hyperplasia (A-D), polymorphic (E-H) and DLBCL (I-L). EBV latency is characterized by the expression pattern of EBV RNA in situ hybridization (EBER), (B, F, J), LMP-1 (C, G, K) and EBNA-2 (D, H, L). All three cases showed Latency 3 pattern, as defined by EBER positivity with co-expression of LMP-1 (membranous, cytoplasmic) and EBNA-2 (nuclear).

Conclusions: Immunohistochemistry for LMP-1 and EBNA-2 characterizes distinctive EBV latency profiles in a variety of B cell lymphoproliferative disorders. Our data show that the differences in expression of LMP-1 and EBNA-2 can be exploited for both diagnostic and therapeutic decision making. For example, the boundary between EBV+ CHL and polymorphic PTLD can be challenging. The latency profile as assessed by LMP-1 and EBNA-2 can aid in discerning the most appropriate diagnosis and guide subsequent clinical management. Additional biomarkers as well as correlation with EBV genome transcriptional profiles will more wholly define the pathogenic role of EBV in these disorders.

957 CD10-/CD15+/CD34- Immunophenotype Does Not Predict KMT2A Rearrangement in Adults with B-Lymphoblastic Leukemia/Lymphoma (B-LBL)

Xiaoqiong Wang[1], Hong Fang[1], Rashmi Kanagal-Shamanna[1], Guilin Tang[1], Wei Wang[1], Jie Xu[1], Elias Jabbour[1], Nitin Jain[1], Jeff Jorgensen[1], L. Jeffrey Medeiros[1], Sa Wang[1], Sergej Konoplev[1]
[1]The University of Texas MD Anderson Cancer Center, Houston, TX

Disclosures: Xiaoqiong Wang: None; Hong Fang: None; Rashmi Kanagal-Shamanna: None; Guilin Tang: None; Wei Wang: None; Jie Xu: None; Elias Jabbour: None; Nitin Jain: None; Jeff Jorgensen: None; L. Jeffrey Medeiros: None; Sa Wang: None; Sergej Konoplev: None

Background: B-LBL with *KMT2A* (*MLL*) rearrangement has an adverse outcome and has been reported to be associated with a unique CD10-/CD15+/CD34- immunophenotype. We reviewed the immunophenotype of adult patients to assess whether this immunophenotype can reliably predict the presence of *KMT2A* rearrangement.

Design: We retrospectively analyzed adult B-LBL patients with *KMT2A* rearrangement. Pediatric patients, patients who received prior therapy, and patients fulfilling the diagnostic criteria for mixed phenotype acute leukemia were excluded. Karyotyping and Fluorescence in-situ hybridization studies for *KMT2A* rearrangement were performed in all cases. Flow cytometry immunophenotype studies were performed using bone marrow aspirate specimens and a panel of antibodies from BD Biosciences on FACSCanto II instruments. In a subset of patients, PCR studies were performed to assess for *KMT2A-AFF1*.

Results: The cohort included 12 men and 14 women with a median age of 47 years (range, 19-83). All patients received chemotherapy; 16 (62%) patients achieved complete remission (CR) and 10 patients relapsed. Eleven (42%) patients died and 15 patients were alive at last follow-up (median 23 months; range, 1-115). Conventional karyotype showed loci involvement consistent with 4 partners: *AFF1* (n=13), *MLLT1* (n=4), *BTBD18* (n=1), and *CENPK* (n=1). *KMT2A-AFF1* was detected in 3 additional patients with normal karyotype patients using PCR studies. The remaining 4 patients had KMT2A rearrangement by FISH but its partners were unknown.

Somatic mutations were detected in 9 of 21 (43%) patients tested and predominantly involved the RAS pathway; no correlation between somatic mutations and *KMT2A* partner was identified.

The CD10-/CD15+/CD34- immunophenotype was identified in only 7 (27%) patients including 5 out of 16 patients with *KMT2A-AFF1*. CD10 was positive in one patient with unknown partner. CD15 was negative in 15 patients (*AFF1,* n=7; *MLLT1*, n=2; *BTBD18*, n=1; *CENPK*, n=1; unknown partner, n=4). CD34 was positive in 14 patients (*AFF1,* n=8; *MLLT1*, n=2; *BTBD18*, n=1; unknown partner, n=3).

Conclusions: The immunophenotype of *KMT2A* rearranged B-ALL is more diverse than previously understood. CD10-/CD15+/CD34- immunophenotype previously considered to be typical for this entity and particularly for *KMT2A-AFF1* rearrangement is observed in less than one third of adult patients with *KMT2A* rearrangement.

958 Clinical and Pathological Characteristics of Leukemic Phase of Double/Triple-Hit Lymphoma

Xiaoqiong Wang[1], Shimin Hu[1], L. Jeffrey Medeiros[1]
[1]The University of Texas MD Anderson Cancer Center, Houston, TX

Disclosures: Xiaoqiong Wang: None; Shimin Hu: None; L. Jeffrey Medeiros: None

Background: Double/triple-hit lymphoma (D/THL) is a heterogeneous group of aggressive large B-cell lymphomas defined by the presence of *MYC* and *BCL2* and/or *BCL6* rearrangements. This group comprises 1% of all non-Hodgkin lymphomas and these patients usually have a dismal clinical course. Occasionally patients with D/THL present with circulating lymphoma cells, mimicking acute leukemia. We aimed to investigate the clinicopathologic features and outcomes of the patients with a leukemic phase of D/THL.

Design: We retrospectively reviewed cases of D/THL with ≥10% circulating lymphoma cells in the peripheral blood, diagnosed at our institution from 1/1/2003 to 12/31/2020. *MYC, BCL2,* and *BCL6* rearrangements were confirmed by FISH analysis.

Results: We identified 49 patients with leukemic phase of D/THL. There were 32 men and 17 women with a median age of 56 years (range, 24-76). Thirty-seven (76%) patients had DHL harboring *MYC* and *BCL2* rearrangements, 3 (6%) patients had DHL with *MYC* and *BCL6* rearrangements, and 9 (18%) patients had THL harboring *MYC, BCL2,* and *BCL6* rearrangements. Thirty-nine (80%) patients presented at initial diagnosis with a leukemic phase of D/THL, with or without other nodal/extranodal involvement. Ten (20%) patients (9 DHL with *MYC* and *BCL2* rearrangements, 1 THL with *MYC, BCL2,* and *BCL6* rearrangements) developed leukemic phase following the diagnosis of follicular lymphoma (FL) (n=6), diffuse large-B cell lymphoma (DLBCL) (n=2), or DHL (n=2) with a median interval of 9.1 months. 36/40 (90%) patients had a complex karyotype, and 4/40 (10%) had a normal karyotype. *MYC* translocation was confirmed by FISH in all 49 cases. According to karyotype and FISH results, *MYC* was translocated with a variety of loci, including *IGK*/2p11 (n=3), *IGL*/22q11 (n=5), *IGH*/14q32 (n=14, 8 had other additional *MYC* rearrangements), and non-*IG* loci (n=6). All patients received chemotherapy, including 15 who received stem cell transplant. At last follow-up, 35 patients had relapsed or persistent disease, and 11 achieved complete remission including 3 who underwent stem cell transplant. With a median follow-up of 9.1 months, 35 of 49 (71%) patients died, with a median survival of 11.5 months from time of initial diagnosis.

Conclusions: Patients with D/THL can uncommonly develop a leukemic phase of the disease, mimicking acute leukemia. The leukemic phase of D/THL can arise de novo or transform/progress from FL, DLBCL or D/THL. It is associated with a complex karyotype and a poor prognosis.

959 EBV Positive Nodal T-Cell Lymphoma with Follicular Helper T-cell Phenotype

Zhe Wang[1], Zhaoxuan Zhang[2]
[1]Fourth Military Medical University, China, [2]The First Affiliated Hospital of University of Science and Technology of China, Hefei, China

Disclosures: Zhe Wang: None; Zhaoxuan Zhang: None

Background: Peripheral T-cell lymphoma with helper T-cell phenotype (PTCL-TFH) is a rare subtype. The most common pathological types of PTCL-TFH are angioimmunoblastic T-cell lymphoma (AITL) and follicular T-cell lymphoma (FTCL). RHOA Gly17Val is a characteristic mutation for PTCL-TFH and its examination is very valuable for the early detection of AITLs and PTCL-TFHs. Epstein-Barr virus (EBV) infection is often detected in PTCL-TFH, almost exclusively in B lymphocytes. However, we identified EBV-infected tumorous T-cells in our PTCL-TFH cases.

Design: Two cases with both CD4 and EBER expressed PTCLs from 2012 to 2019 were selected. The clinical data of each patient included sex, age, autoimmune disease, rash, B symptoms were collected. EBER-ISH, Immunohistochemistry(IHC), routine TCR rearrangement tests and whole exome sequencing were performed.

Results: Case 1: 59-year-old immunocompetent man with fever, multiple generalized lymphadenopathies and nasopharyngeal mass, histology showed classical pattern of FTCL based on the morphological and immunohistochemical results. EBER-CD3 double staining suggested that EBER ISH positivity mainly localized to CD3-positive tumor cells(Figure 1). Case 2: 58-year-old male with enlarged lymph nodes in the neck, supraclavicular region, axilla, mediastinum, and retroperitoneum, The morphology and IHC results demonstrated to be classical AITL pattern 3 (Figure 2). Both cases are positive for EBER and at least 2 TFH markers in the tumorous T cells, including Bcl-6, PD-1, CXCL-13 and ICOS. TET2 loss of function mutation, KMT2C p.K339N, and RHOA p.G17V were detected in both cases which have been reported in PTCL-NOS as well. Besides, both cases harbored BCR p.D1106N and PABPC1 p.F335Lfs*19 mutations(Table 1).

Table 1. Genetic aberrations of two studied samples and their mutation status in four major PTCL subtypes

Types / Gene	Mutations		Alleles (Frequency)	Involved Pathway
	Case1	Case2	PTCL-NOS	
TET2	p.L748*	p.M1333Rfs*28	Loss of function (38-49%)	Epigenetic regulators
KMT2C	p.K339N	p.K339N	SNV(8-46%)	Epigenetic regulators
RHOA	p.G17V	p.G17V	G17V(7-30%)	Rho GTPases Pathway
BCR	p.D1106N	p.D1106N	-	Rho GTPases Pathway
PABPC1	p.F335Lfs*19	p.F335Lfs*19	-	RNA binding
ARID1B	p.G327A	-	-	Chromatin remodeler
CHD2	-	p.Y1246Ifs*13	-	Chromatin remodeler
NUTM2B	p.Q665E	-	-	Nuclear/cytoplasmic shuttling
AFF1	c.2467-2A>G	-	-	Transcriptional activator
BRAF	p.R384G	-	-	MAPK signaling pathway
CBFA2T3	p.G303R	-	-	Tumor suppressor

CD209	p.L120Q	-		-		Pathogen recognition
MTOR	p.G793D	-		-		Cellular responses
RGPD3	p.E9Sfs*79	-		-		GTPase activator activity
SALL4	-	p.E889K		-		Transcription factor binding
TRIP11	p.K1607E	-		-		Transcription coactivator activity

Figure 1 - 959

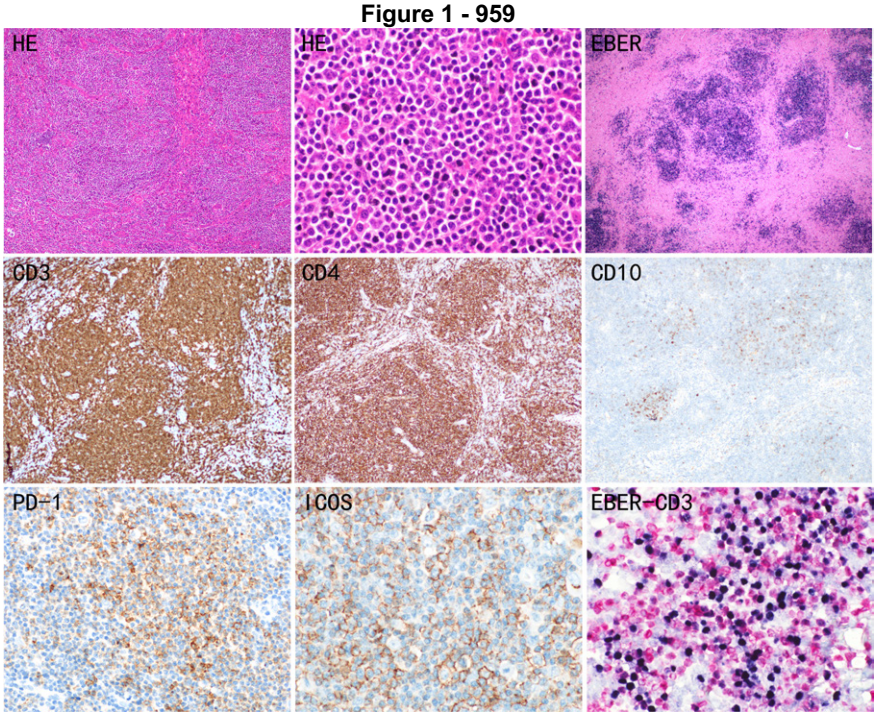

Figure 2 – 959

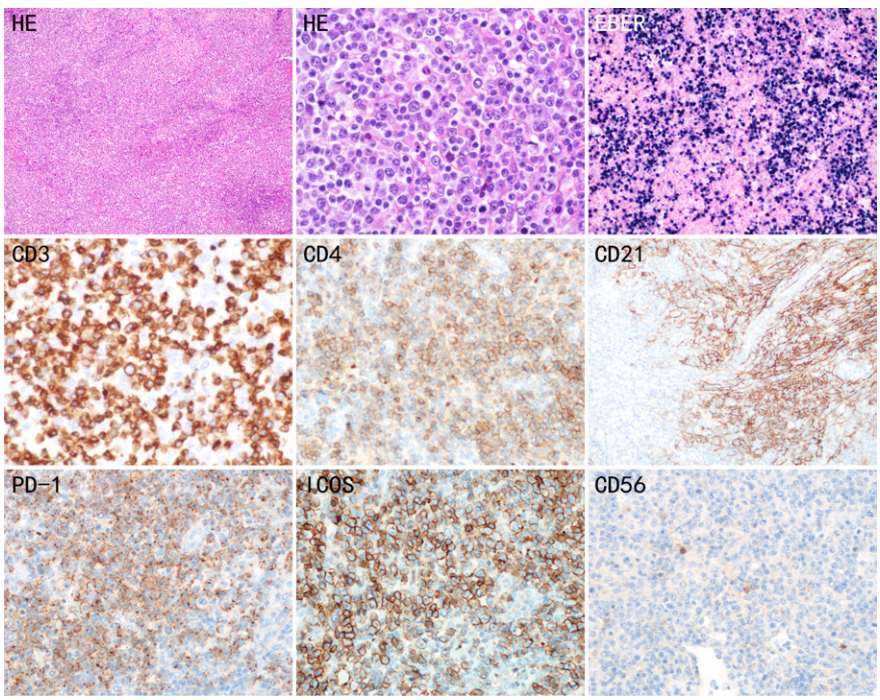

Conclusions: In general, we have found a kind of novel peripheral T-cell lymphoma with EBV infection in T cells, in view of the special gene mutation profile and immunophenotype, these cases represent a EBV positive peripheral T-cell lymphoma with TFH phenotype.

960 The Specific Expression of L-type Amino Acid Transporter 1 (LAT1) in Peripheral T-cell Lymphomas and Cutaneous T-cell Lymphomas Suggests a Predominant Upregulation in the Aggressive Counterparts, and a Novel Potential Therapeutic Target

Shaun Webb[1], Ryan Wilcox[2], Carlos Murga-Zamalloa[1]
[1]University of Illinois at Chicago, Chicago, IL, [2]Michigan Medicine, University of Michigan, Ann Arbor, MI

Disclosures: Shaun Webb: None; Ryan Wilcox: None; Carlos Murga-Zamalloa: None

Background: Peripheral T-cell lymphomas constitute one of the most aggressive types of hematolymphoid neoplasms and are characterized by frequent relapses and dismal outcomes. Currently, there are no standardized therapies available at relapse, and finding targeted therapies for these types of neoplasms would be a great step forward. Increased expression of the L-amino acid transporter 1 (LAT1) has been previously detected in different carcinomas, including esophageal, prostate, and lung adenocarcinoma. Importantly, upregulation of LAT1 has also been described in precursor T-cell acute lymphoblastic leukemia (T-ALL). The aberrant upregulation of LAT1 is associated with increased growth of tumor cells by specific activation of the mTORC1 pathway, which ultimately is associated with increased activity of the c-MYC oncoprotein. Due to its major role enabling tumor proliferation, novel compounds that selectively inhibit LAT1 have been designed with promising results at the pre-clinical stage.

Design: To investigate the oncogenic role of LAT1 in aggressive peripheral T-cell lymphomas, the expression of LAT1 was evaluated in a large cohort of peripheral T-cell lymphomas and cutaneous T-cell lymphomas (CTCLs). To further explore the therapeutic potential of LAT1, loss-of-function approaches with specific inhibition of LAT1 with a small compound drug was performed in cultured cell lines and in-vivo murine models of T-cell lymphomas.

Results: The findings were consistent with upregulation of LAT1 in 80% of PTCL-NOS (n = 30), 95% of AITL (n = 10), and 20% of ENKTCL (n = 5). In addition, LAT1 expression was not detected in mycosis fungoides (MF, n = 102), nor in CD30+ cutaneous T-cell lymphoproliferative neoplasms (n = 80). Importantly, expression of LAT1 was detected in 90% of Sézary Syndrome cases (SS, n = 10). Loss-of-function approaches in cultured T-cell lymphoma cell lines (MyLa, H9 and MAC1) with a selective LAT1 inhibitory compound demonstrated a marked decrease in proliferation and increase in apoptosis. Consistent with this, murine tumor xenografts of T-cell lymphoma lines featured decreased growth downstream of LAT1 in inhibition, in comparison with vehicle control.

Conclusions: LAT1 is predominantly upregulated in aggressive T-cell lymphomas. Furthermore, selective inhibition of LAT1 is associated with decreased tumor growth, which further supports that LAT1 is a potential therapeutic target in aggressive T-cell lymphomas.

961 High-Parameter Multiplex Ion Beam Imaging (MIBI) Reveals that Diffuse Large B Cell Lymphoma (DLBCL) is Spatially Defined by Three Distinct Immunological Microenvironments

Kyle Wright[1], Jason Weirather[2], Sizun Jiang[3], Katrina Kao[2], Margaret Shipp[2], Scott Rodig[4]
[1]Oklahoma University Health Sciences Center, Boston, MA, [2]Dana-Farber Cancer Institute, Boston, MA, [3]Beth Israel Deaconess Medical Center, Harvard Medical School, Boston, MA, [4]Brigham and Women's Hospital, Boston, MA

Disclosures: Kyle Wright: *Speaker*, Ionpath, Inc.; Jason Weirather: None; Sizun Jiang: None; Katrina Kao: None; Margaret Shipp: *Grant or Research Support*, Bristol-Myers Squibb, Merck, Bayer, Abbvie, AstraZeneca; *Advisory Board Member*, AstraZeneca, Immunitas Therapeutics; Scott Rodig: *Grant or Research Support*, Bristol Myers Squibb, Merck, Affimed, KITE/Gilead; *Advisory Board Member*, Immunitas

Background: DLBCL is the most common aggressive non-Hodgkin lymphoma and is biologically heterogeneous. Recent comprehensive genetic analyses revealed the molecular substructure of DLBCL. However, the DLBCL tumor-immune microenvironment (TIME) is less well defined, despite the increasing use of targeted immunotherapies.

Design: We employed a 26-plex antibody panel targeting cell lineage, functional, and architectural biomarkers which we applied to a cohort of 52 fixed *de novo* DLBCL samples. Stained tissue sections were imaged by MIBIscope (Ionpath), and then filtered and de-noised (MATLAB), cells segmented (Halo), and phenotyped (FlowSOM) using commercial software. Custom analytical tools were developed and employed to define cellular "neighborhoods" and their spatial arrangements in tissue. We supplemented these data with additional biomarkers captured by multiplex immunofluorescence and analyzed with Inform software (Akoya).

Results: We find DLBCLs are composed of shared and unique local cellular neighborhoods in defined spatial orientations (Fig 1A-C). The “immune-excluded” TIME (28/52 cases) is primarily composed of tumor-rich/immune cell-poor neighborhoods with adjacent regions rich in myeloid cells, and perivascular niches including T cells and myeloid cells. The “immune-active” TIME (14/52) is distinguished by neighborhoods rich in non-exhausted $CD4^+$ and $CD8^+$ T cells, $CD11c^+$ dendritic cells, and $CD68^+$ (M1) macrophages associated with tumor cells. The “immunosuppressive” TIME (10/52) is distinguished by neighborhoods composed of CD8 T cells and $CD163^+$ (M2) macrophages, robust LAG3, PD-1, IDO-1, FOXP3, and PD-L1, and reduced HLA-DR expression among tumor cells. Cases with the immuno-suppressive TIME were enriched in activated B-cell (ABC) type tumors and DLBCLs from genetic clusters 1 & 5.

Figure 1 - 961

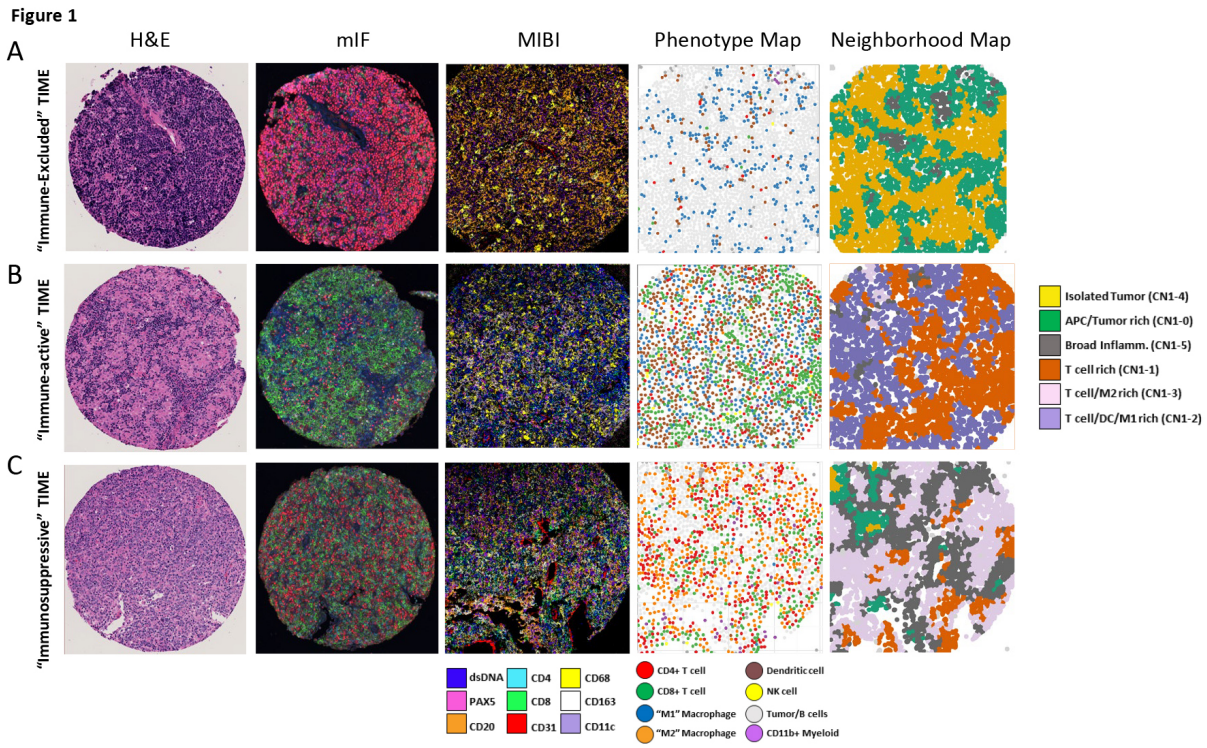

Conclusions: We find that DLBCL is organized into 3 distinct TIMEs characterized by common and unique cell neighborhoods with spatially-defined orientations. Our data suggest the immunological activity in DLBCL can be divided into those that are excluded, active, or suppressive. Recognition of these TIMEs helps refine our understanding of DLBCL biology and suggests a framework for optimizing strategies for immune therapy.

962 Expanding the Immunohistochemical Spectrum of Neoplastic and Reactive Plasmacytoid Dendritic Cells

Sarah Wu[1], Sam Sadigh[2], Geraldine Pinkus[1]
[1]Brigham and Women's Hospital, Boston, MA, [2]Brigham and Women's Hospital, Harvard Medical School, Boston, MA

Disclosures: Sarah Wu: None; Sam Sadigh: None; Geraldine Pinkus: None

Background: Dual expression of TCF-4 and CD123 was reported to be highly sensitive for diagnosis of Blastic Plasmacytoid Dendritic Cell Neoplasm (BPDCN). TCF-4/CD123 co-expression is also observed in non-neoplastic plasmacytoid dendritic cells

(pDCs). Advances in targeted therapies for BPDCN have presented a diagnostic dilemma of differentiating residual BPDCN from reactive pDCs, particularly in cases where concurrent flow cytometry is unavailable. We investigated IHC markers that may be differentially expressed between BPDCN and reactive pDCs such as CD56, SOX4 (identified through gene set enrichment profiling), and IRF8 (a key transcription factor in pDC development).

Design: BPDCN including post treatment samples, other hematologic malignancies, reactive lymph nodes, Kikuchi lymphadenitis, and normal skin, spleen, and bone marrow were included. Slides were stained using a double staining protocol for the following marker combinations (TCF-4/CD123, TCF-4/CD56, SOX4/CD123, IRF8/CD123), with a brown chromogen for TCF-4, SOX4, and IRF8 and a red chromogen for CD123 and CD56.

Results: BPDCN and post-treatment BPDCN with residual disease stained for TCF-4/CD123 and TCF-4/CD56 (Figure 1). In post-treatment samples of BPDCN that were negative by concurrent flow cytometry, 0/12 of TCF-4/CD56 samples showed double staining. However, 2/12 (17%) of these samples had positive scattered staining for TCF-4/CD123, likely representing reactive pDCs. Other hematologic malignancies did not exhibit co-staining for either TCF-4/CD123 or TCF-4/CD56. Non-neoplastic tissues known to contain pDCs exhibited staining with TCF-4/CD123 but no staining for TCF-4/CD56 (Kikuchi lymphadenitis, reactive lymphoid hyperplasia, spleen). In an initial cohort, all samples of BPDCN had double staining for SOX4/CD123 (Figure 2). None of the samples with reactive pDCs demonstrated staining for SOX4/CD123. IRF8/CD123 was positive in all samples of BPDCN as well as samples with reactive pDCs.

	n (%)	
Diagnosis	SOX4/CD123 +	IRF8/CD123+
BPDCN	9/9 (100%)	5/5 (100%)
Other Heme Malignancy		
ALCL	0/1 (0%)	
AML	0/1 (0%)	
B-ALL	0/1 (0%)	
CMML	0/1 (0%)	
CTCL	0/3 (0%)	
DLBCL	0/1 (0%)	
Myeloid Sarcoma	1/2 (50%)	
Non-neoplastic		
Skin	0/1 (0%)	
Kikuchi-Fujimoto Disease	0/1 (0%)	1/1 (100%)
Reactive Follicular Hyperplasia	0/6 (0%)	5/5 (100%)
Spleen	0/3 (0%)	3/3 (100%)
Bone Marrow	0/4 (0%)	0/2 (0%)

Figure 1 - 962

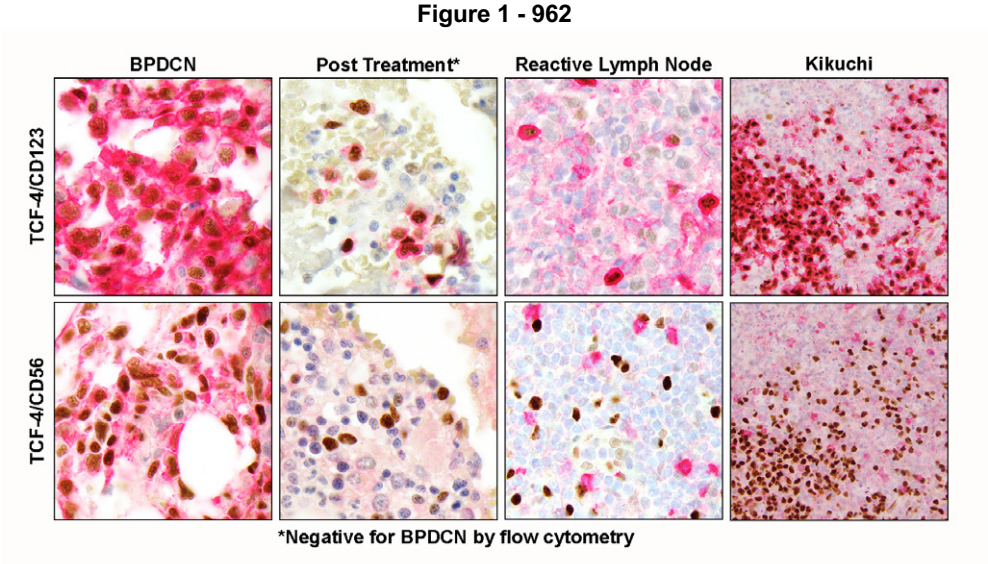

Figure 2 – 962

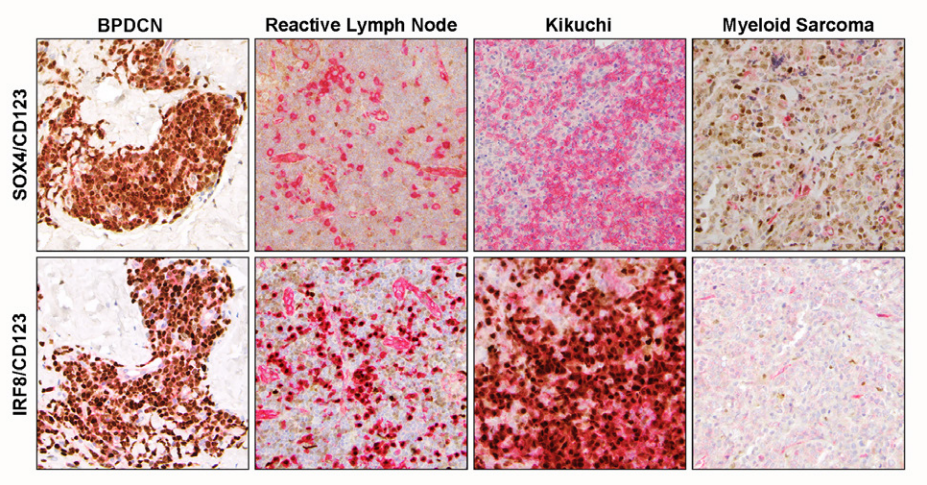

Conclusions: TCF-4/CD56 co-expression is as sensitive as TCF4/CD123 for diagnosis of BPDCN and more specific for distinguishing BPDCN from pDCs. SOX4 distinguishes BPDCN from reactive pDCs but is positive in other neoplastic entities. SOX4/CD123 can distinguish BPDCN from both pDCs and other neoplasms. Although IRF8 has been reported as a specific monoblast marker in AML, we found IRF8 is expressed in both BPDCN and reactive pDCs. Our study further highlights markers that expand the diagnostic armamentarium for plasmacytoid dendritic cell entities.

963 The Csn5/Jab1 Oncogene is Overexpressed and Suppresses Type 1 Interferon (IFN)-Associated Anti-Tumor Responses in Classical Hodgkin Lymphoma

Ioanna Xagoraris[1], Konstantina Stathopoulou[1], Georgia Kokaraki[1], Francois Claret[2], L. Jeffrey Medeiros[2], Drakos Elias[3], George Z. Rassidakis[4]

[1]Karolinska Institutet, Stockholm, Sweden, [2]The University of Texas MD Anderson Cancer Center, Houston, TX, [3]University of Crete, Heraklion, Greece, [4]Karolinska University Hospital, Stockholm, Sweden

Disclosures: Ioanna Xagoraris: None; Konstantina Stathopoulou: None; Georgia Kokaraki: None; Francois Claret: None; L. Jeffrey Medeiros: None; Drakos Elias: None; George Z. Rassidakis: None

Background: The Jab1 (cJun activation domain binding protein1), initially discovered as a cJun coactivator, represents the fifth component of an evolutionary highly conserved 8 subunit protein complex, named COP9 signalosome (CSN5). Accumulating evidence suggests that the Csn5/Jab1 gene operates as an oncogene in cancer through multiple mechanisms including cell cycle control via CDK inhibitors. Targeting Csn5/Jab1 activity in cancer is now possible since a novel inhibitor has been developed for clinical use. The potential role of Csn5/Jab1 in modulation of anti-tumor responses in cancer, and in particular in lymphomas, is largely unknown to date.

Design: The study group included 80 patients with classical Hodgkin Lymphoma (cHL) with available pre-treatment tissue samples and clinical data. Expression of Csn5/Jab1 was assessed by immunohistochemistry, a previously validated monoclonal antibody and standard methods. The *in vitro* system included 3 cHL cell lines (MDA-V, HDLM2, L428). Expression of various proteins at baseline and experimental conditions were analysed by Western blot and gene expression of type 1 interferons including interferon beta (IFN-β), CXCL10 and interferon gamma (IFN-γ), as well as, a control gene (GAPDH) at the RNA level with qRT-PCR. The cHL cell lines were treated with the specific CSN5i-3 inhibitor at different concentrations. Silencing of Csn5/Jab1 gene was performed using transient transfection with specific siRNA using the Amaxa Nucleofector System (Lonza).

Results: Csn5/Jab1 was positive in the neoplastic cells of cHL in 72 of 80 (90%) patients included in the study, with a predominantly nuclear and weaker cytoplasmic pattern. Treatment of HL cell lines with increasing concentrations of CSN5i-3 resulted in significant decrease in the cell growth associated with upregulation of the CDK inhibitors p21, p27 and p57. Similarly, Csn5/Jab1 gene silencing resulted in decreased cell growth associated with increased expression of similar cell cycle

inhibiting proteins. Inhibition of Csn5/Jab1 activity resulted in significantly increased gene expression of IFN-β, IFN-γ and CXCL10 at a variable degree among the cHL cell lines. Similarly, knocking down Csn5/Jab1 gene led to upregulation of type 1 interferons, particularly CXCL10.

Conclusions: The Csn5/Jab1 oncogene is overexpressed in the neoplastic cells of the majority of patients with cHL, promotes cell growth through cell cycle control and downregulates type 1 interferon (IFN)- associated anti-tumor responses in cHL.

964 Global Assessment of IRF8 as a Novel Cancer Biomarker

Mina Xu[1], Daniel McQuaid[2], Gauri Panse[1], Wei-Lien (Billy) Wang[3], Sam Katz[2]
[1]Yale University, New Haven, CT, [2]Yale School of Medicine, New Haven, CT, [3]The University of Texas MD Anderson Cancer Center, Houston, TX

Disclosures: Mina Xu: *Consultant*, Seattle Genetics, Pure Marrow, Blueprint Medicines; Daniel McQuaid: None; Gauri Panse: None; Wei-Lien (Billy) Wang: None; Sam Katz: None

Background: Interferon regulatory factor-8 (IRF8) is a member of the IRF family that is specific to the hematopoietic cell and is involved in regulating the development of human monocytic and dendritic-lineage cells, as well as B cells. Since its utility as a sensitive and specific monoblast marker in the context of acute monocytic leukemias (AMoLs) has been recently demonstrated, we hypothesized that it may also be useful as a novel immunohistochemical marker in myeloid sarcomas and blastic plasmacytoid dendritic cell neoplasms (BPDCN) with respect to their differential diagnoses.

Design: In this retrospective study, we analyzed the IHC expression pattern of 385 patient samples across 30 types of cancers, including soft tissue tumors that can mimic myeloid sarcoma and BPDCN. We also analyzed IRF8 staining in 35 cases of myeloid sarcoma and 13 cases of BPDCN, concomitantly staining for markers often included in the diagnostic panel for these malignancies. Additionally, we referenced IRF8 protein abundance in these various cancer types to their mRNA expression data available through TCGA.

Results: All 13 of 13 BPDCNs (100%) showed strong uniform expression of IRF8, which was occasionally more definitive than CD123. Twenty-four of 35 cases of myeloid sarcomas (68.5%) showed positivity for IRF8 with an inverse correlation to CD34 and MPO expression. IRF8 was negative in all desmoplastic small round cell tumors, Ewing sarcomas, synovial sarcomas, and undifferentiated pleomorphic sarcomas, as well as all epithelial malignancies tested except for 2 triple-negative breast cancers that showed subset weak staining.

Table 1: IRF8 expression in soft-tissue tumors. IRF8 expression in different types of sarcoma included in sarcoma-specific tissue microarrays (TMAs).

Sarcoma Type	Negative	Positive	Total
Desmoplastic small round cell tumor	30 (100%)	0	30
Ewing sarcoma	24 (100%)	0	24
Synovial sarcoma	45 (100%)	0	45
Undifferentiated pleomorphic sarcoma	12 (100%)	0	12

Figure 1 - 964

Figure 1: IRF8 staining in myeloid sarcoma. A) Heat map of myeloid sarcoma cases based on percent positivity of tumor cells for IRF8, CD34, or MPO by immunohistochemistry. B) Representative case of myeloid sarcoma at 2X, 20X magnification. This tumor shows strong IRF8 expression in the monoblastic population of tumor cells and MPO staining in the granulocytic population (case 8). IRF8 expression is dimly observed in the mantle zone B cells adjacent to neoplastic cells.

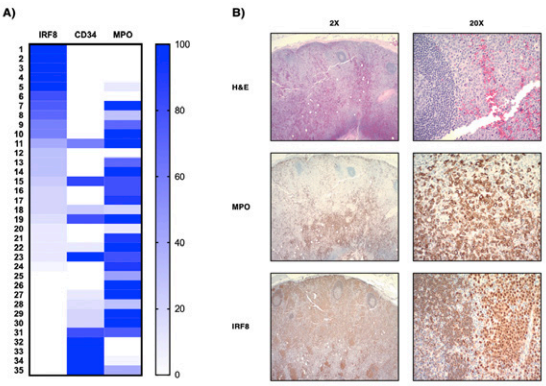

Figure 2 - 964

Figure 2: IRF8 staining in BPDCN. Expression patterns of BPDCN in three representative patients. Case 1 shows a mid-chest skin biopsy. Case 2 shows a bone marrow biopsy. Case 3 shows a left chest skin biopsy. All images taken at 200x magnification.

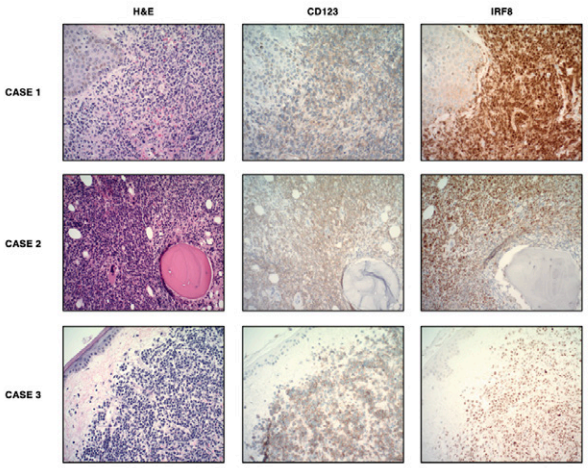

Conclusions: Taken together, these findings demonstrate that IRF8 is a novel marker helpful in identifying extranodal hematopoietic tumors that can otherwise be difficult to diagnose given the broad differential diagnoses and frequent loss of more common lineage-defining markers. Further validation of our observations will be critical in order to integrate IRF8 staining into pathologists' workflow for diagnosis of myeloid sarcoma and BPDCN.

965 Targeting the Innate Immune Landscape and Pro-Fibrotic Genetic Signatures for the Effective Treatment of Myelofibrosis

Guangwu Xu[1], Cristabelle De Souza[2], Yu Liu[3], Gerlinde Wernig[3]
[1]Stanford Health Care, Stanford, CA, [2]Stanford University, Stanford, CA, [3]Stanford University School of Medicine, Stanford, CA

Disclosures: Guangwu Xu: None; Cristabelle De Souza: None; Yu Liu: None; Gerlinde Wernig: None

Background: Myelofibrosis (MF) is characterized by bone marrow fibrosis and abnormal cytokine expression. There is an urgent need for anti-fibrotic therapeutics that can resolve pathogenic fibrosis that drives this disease phenotype. Our group has previously shown that activation of the AP-1 transcription factor JUN in fibroblasts promote a pro-fibrotic genetic signature via modulating several immune markers that ultimately function to aid in disease progression. One such molecular marker regulated by JUN is the '*don't eat me signal* CD47'. We have previously demonstrated that blocking CD47 using a monoclonal antibody has effectively reversed pathogenic fibrosis in animal models of liver and lung fibrosis (IPF). Here we sought to identify the expression levels of CD47 in patients with MF, to evaluate the potential of using CD47 as an effective molecular target for the treatment of MF.

Design: Using single-cell gene expression analyses, we have identified JUN and CD47 to be highly expressed in patients with MF. Further we demonstrate that the fibroblast clusters and innate immune cell clusters are enriched in MF patients thus warranting the need to target fibroblasts and activate the innate immune system simultaneously for enhanced therapeutic efficacy. We validated our results using immunohistochemical staining with anti-CD47 antibody. Staining was performed on FFPE tissue microarray (TMA) obtained from MF patients (n= 37). The reactivity of CD47, was scored for staining intensity and percentage of fibroblasts. Whole slides from four additional MF patients were also evaluated for CD47 expression.

Results: In TMA, CD47 were expressed in fibroblasts in nearly all the specimens (36 out of 37). CD47 expression in >50% fibroblasts were seen 5 specimens (14%; moderate to strong), CD47 expression in 10-50% fibroblasts were seen in 14 specimens (38%; weak to moderate), and CD47 expression <10% fibroblasts were seen in 17 specimens (46%; mostly weak). In the four whole slide specimens, moderate to strong CD47 expression was present in >50% of the fibroblasts in all of them.

Conclusions: Using single cell transcriptomic analyses and histopathological validation we demonstrate for the first time that CD47 is widely expressed in MF patients. This expression is correlated with a fibrotic phenotype and poor patient outcome. Based on the above findings, we believe CD47 is a promising target for the treatment of MF in patients.

966 Clinical and Prognostic Significance of LILRB4, a Potential Therapeutic Target for AML

Lijun Xue[1], John (Yahya) Daneshbod[2]
[1]LAC+USC Medical Center/Keck Medicine of USC, Los Angeles, CA, [2]Loma Linda University Medical Center, Loma Linda, CA

Disclosures: Lijun Xue: None; John (Yahya) Daneshbod: None

Background: Recent studies found that leukocyte immunoglobulin-like receptor subfamily B member 4 (LILRB4) fulfills unique escape mechanisms in acute myeloid leukemia (AML), particularly in acute myelomonocytic leukemia (AMML). LILRB4 signals monocytic leukemia cells but not normal monocytic cells to convey T cell suppression and tumor infiltration. Thus, LILRB4 may be a target for immunotherapy on AML/AMML. Here, the clinical relevance and prognostic significance of LILRB4 were analyzed to evaluate the potential of Anti-LILRB4 in immunotherapy for AML.

Design: The human AML mRNA gene expression datasets with survival information, including TCGA (n=173), GSE16432(n= 188), and GSE12417(n= 163), were obtained from TCGA and GEO databases. The hazard ratio (HR) was estimated by using Cox proportional model. The multivariate and stratification analyses were conducted to reduce biases and confounders. We also used Meta and Pooled analysis to combine HRs yielded from different datasets.

Results: LILRB4 gene expresses with different levels in different subtype of AML. It highly expresses in FAB M4 and M5 AML subtypes, ranking on the top of the list for all AML FAB subtypes. Among AML with recurrent genetic abnormalities, AML with t (9:11) genotype has about 10 times expression levels of average of all other subtypes (GSE 16432 datasets). Additionally, expression of LILRB4 significantly increase in AML patients as with the increase of age in both TCGA and GSE16432 datasets. With univariate Kaplan-Meier analysis, expression of LILRB4 significantly associates with poor overall survival of AML in the TCGA dataset (Log Rank p=0.023). A Meta-analysis also demonstrates that LILRB4 conveys poor outcomes when we combine all these datasets. The HR of LILRB4 is 1.06 per unit (95% CL 1.01-1.10, p<0.01). Further stratification analysis also demonstrates that LILRB4 specifically prognoses poor overall survival in male AML patients, rather than female, in both TCGA (Log-rank p=0.013. Adjusted HR=2.39, 95% CI 1.10-5.73) and GSE16432(Log-rank p=0.018, Adjusted HR=1.63; 95% CI 0.90-3.01) datasets.

Meta-analysis for LILRB4 expression and outcomes of AML

Data bases	HR	95%UCL	95%HCL	P-value
GSE12417A (n=163)	0.98	0.67	1.42	0.91
GSE16432B (n=188)	1.04	0.96	1.12	0.38
TCGA (n=173)	1.07	1.01	1.13	0.01
Meta analysis	1.06	1.01	1.10	0.01

HR is based on continue value of LILRB4 expression.

Figure 1 - 966

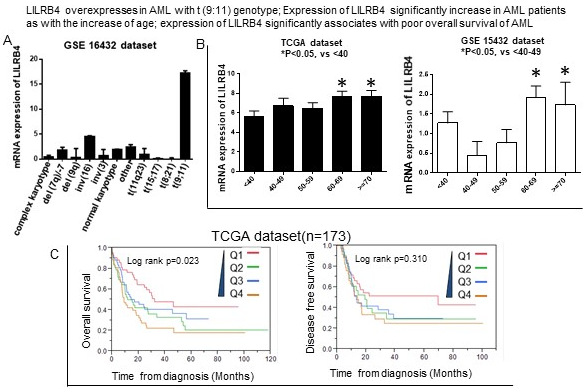

Figure 2 - 966

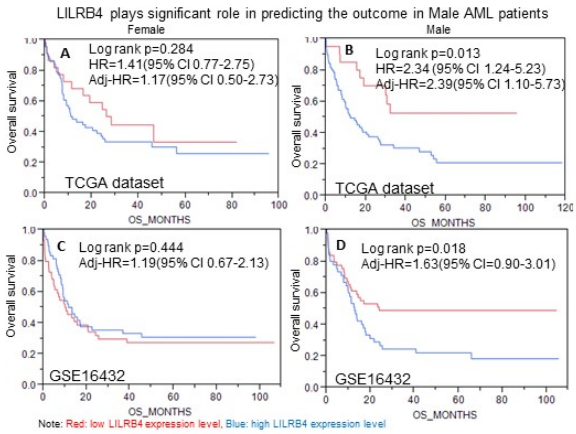

Conclusions: LILRB4 might be a therapeutic target and predictive biomarker for immunotherapy on AML, especially for males and in AML and those with t (9:11) genotype. It could also serve as a prognostic biomarker to predict the outcome of AML.

967 Identification of Hemophagocytes with Myeloid Cells in Bone Marrow Aspirates is Associated with Hemophagocytic Lymphohistiocytosis (HLH) Diagnosis and Worse Overall Prognosis

Mingfei Yan[1], Ramya Gadde[1], Rose Beck[2]
[1]Case Western Reserve University/University Hospitals Cleveland Medical Center, Cleveland, OH, [2]Seagen, Cleveland, OH

Disclosures: Mingfei Yan: None; Ramya Gadde: None; Rose Beck: None

Background: Presence of hemophagocytes (HPC) in bone marrow (BM) biopsies supports a diagnosis of hemophagocytic lymphohistiocytosis (HLH); however the presence of HPCs is non-specific and can be seen sporadically or be secondary to various non-HLH conditions. This study aims to investigate pathologic features in BM aspirates which may help to predict the diagnosis of HLH, thus facilitating prompt treatment for this aggressive condition.

Design: We identified 57 BM biopsies from 48 patients with HPC noted in BM reports over a 20-year period at our institution, and blindly re-reviewed BM aspirates to characterize pathological features. Number of HPC with either myeloid cells (Figure 1A) or non-myeloid nucleated cells (Figure 1B) were quantified by examining 2 entire aspirate smears from each biopsy. The number of phagocytosed cells in each HPC were also quantified. HPC with non-nucleated red blood cells were not included. The presence of binucleated HPC (Figure 1C) and megakaryocyte emperipolesis (Figure 1D) were also documented. Chart review was performed to categorize each patient as having a diagnosis of HLH or not based on HLH-2004 criteria, and to evaluate overall survival retrospectively.

Results: HLH patients had more phagocytosed nucleated cells per HPC than non-HLH cases (Table 1). Presence of HPC with myeloid cells (mHPC) was significantly associated with HLH diagnosis (p=0.008). In addition, the mHPC percentage of all HPC was significantly higher in HLH (17.7%) than non-HLH cases (7.4%) (p=0.007). Identification of either megakaryocyte emperipolesis or binucleated HPC was not correlated with HLH diagnosis. Analysis of lab values showed that patients with higher mHPC percentage tended to have lower hemoglobin level (p=0.026) (Figure 2A), and the highest number of phagocytosed cells per HPC in each case was positively correlated with triglyceride level (p=0.043) (Figure 2B). Finally, higher mHPC percentage in HLH patients was associated with poorer overall survival (p=0.037) (Figure 2C).

Table 1

	HLH cases	non-HLH cases	p-value
No. of HPC examined per case, median (range)	27 (1 - 192)	18 (1 - 157)	0.19
No. of phagocytosed cells per HPC			
Highest no. per case, median (range)	8.5 (2 - 51)	4 (1 - 20)	**0.01**
Median no. per case, median (range)	2 (1 - 5)	1.5 (1 - 3)	**0.01**
Myeloid HPC			
Present, no. (percentage)	22 (68.8%)	8 (32%)	**0.008**
Absent, no. (percentage)	10 (31.2%)	17 (68%)	
Percentage of myeloid HPC of all HPC, median (range)	17.7 (1.1 - 32.6)	7.4 (4.1 - 11.1)	**0.007**
Binucleated HPC			
Present, no. (percentage)	19 (59.4%)	10 (40%)	0.19
Absent, no. (percentage)	13 (40.6%)	15 (60%)	
Megakaryocyte emperipolesis			
Present, no. (percentage)	14 (43.8%)	6 (24%)	0.43
Absent, no. (percentage)	18 (56.2%)	19 (76%)	

Figure 1 - 967

Figure 1

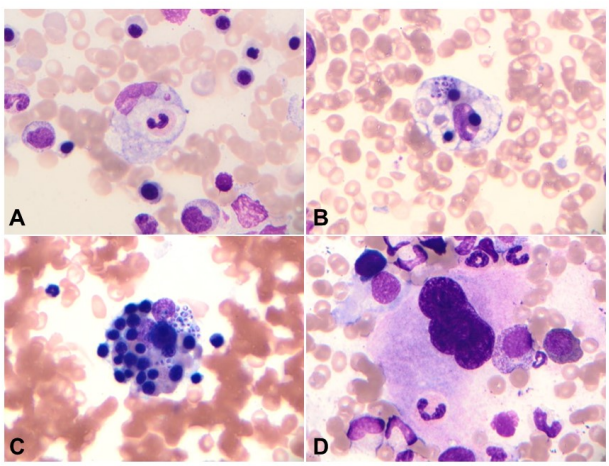

Figure 2 – 967

Figure 2

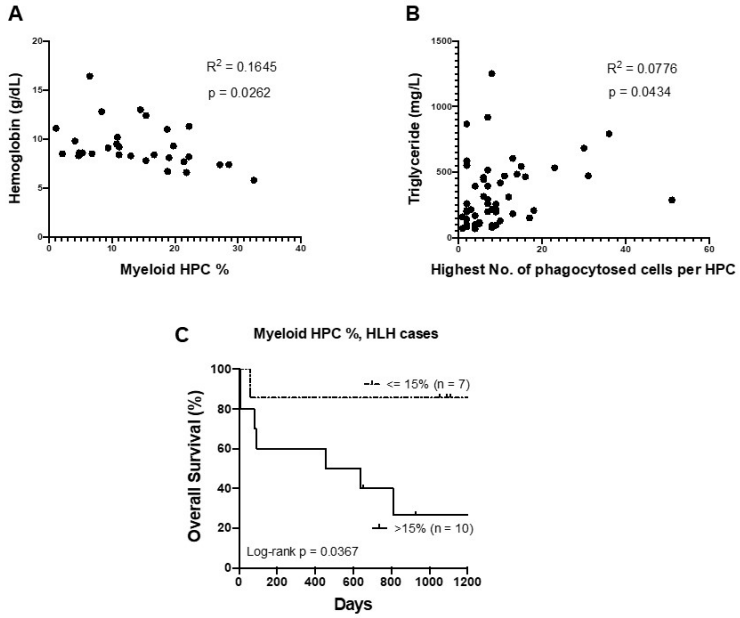

Conclusions: Distinct BM pathological features exist between HLH and non-HLH cases. By reporting the presence and prevalence of mHPC, pathologists may provide additional value when evaluating the risk of HLH and overall prognosis.

968 Detection of Aberrant CD58 Expression in a Wide Spectrum of Hodgkin and Non-Hodgkin Lymphomas: Implications for CAR T Cell Resistance

Sheren Younes[1], Diane Libert[1], Shuchun Zhao[2], Andrew Johnsrud[2], Sushma Bharadwaj[2], Robbie Majzner[2], Matthew Frank[3], David Miklos[4], Yasodha Natkunam[2]

[1]Stanford Pathology, Stanford, CA, [2]Stanford Medicine/Stanford University, Stanford, CA, [3]Stanford Hospital and Clinics, Stanford, CA, [4]Stanford University, Stanford, CA

Disclosures: Sheren Younes: None; Diane Libert: None; Shuchun Zhao: None; Andrew Johnsrud: None; Sushma Bharadwaj: None; Robbie Majzner: *Stock Ownership*, Syncopation Life Sciences; Matthew Frank: *Grant or Research Support*, Allogene Therapeutics, Adaptive Biotechnologies, Kite/Gilead; David Miklos: *Grant or Research Support*, Kite - Gilead; Yasodha Natkunam: None

Background: CD58 or lymphocyte function-associated antigen-3, is a ligand for CD2 receptors on T and NK cells and is required for their activation and target cell killing. We previously showed that CD58 aberrations (mutations and loss of expression of CD58 protein) are linked to lack of durable responses to CD19 CAR T-cells in diffuse large B-cell lymphoma (DLBCL). CD58 status is an important measure for patient selection and to engineer new generation CARs that overcome this mechanism of resistance. We therefore developed an immunohistochemical assay to evaluate CD58 status in lymphoma subtypes.

Design: Tissue microarrays (TMAs) of 702 lymphoma samples were used with Institutional Review Board approval. Immunohistochemistry was performed using an anti-CD58 antibody (rabbit monoclonal, 1:100, Sino Biological Inc., Beijing, China) on a Leica BOND-III platform (Leica Biosystems, Buffalo Grove, IL). Staining was optimized using CD58 wildtype (Nalm6) and mutant (CD58 KO) cell lines which also formed the benchmark for scoring. The percent positive cells were scored 0-100%, and the intensity, on a scale of 0-negative, 1-weak, 2-moderate, and 3-strong. An H-score of 0-300 was generated by multiplying the percentage and intensity. For Hodgkin lymphomas, tumor and microenvironment cells were evaluated separately.

Results: Aberrant loss of CD58 protein expression was found in a wide spectrum of lymphomas (Table 1). Among B-cell lymphomas, diminished CD58 expression was detected in DLBCL (13.7%), B lymphoblastic (25%), follicular (47.62%), marginal zone (76.81%), small lymphocytic (81.3%), and mantle cell (82.76%) lymphomas, and complete loss in lymphoplasmacytic, Burkitt, and plasmablastic lymphomas (Figure 1). Among T-cell lymphomas, diminished expression was detected in anaplastic large cell

(73.2%), angioimmunoblastic T-cell (81.8%) and T lymphoblastic (80%) lymphomas (Figure 2). CD58 loss was also seen in classic Hodgkin lymphoma, with a higher frequency in LP cells and the immune microenvironment of nodular lymphocyte predominant Hodgkin lymphoma (Table 2).

Table 1: Aberrant CD58 Expression in B and T cell Non-Hodgkin Lymphomas

Diagnosis	Number of cases	Positive (%)	Aberrant Expression		
			Weak (%)	Negative (%)	Total (%)
B-cell lymphoma subtypes					
Diffuse large B-cell lymphoma	102	88 (86.3%)	8 (7.8%)	6 (5.8%)	14 (13.7%)
B lymphoblastic lymphoma/leukemia	8	6 (75%)	0 (0%)	2 (25%)	2 (25%)
Follicular lymphoma	84	44 (52.38%)	29 (34.5%)	11 (13.1%)	40 (47.6%)
Primary mediastinal large B cell lymphoma	4	2 (50%)	1 (25%)	1 (25%)	2 (50%)
Marginal zone lymphoma (all types)	69	16 (23.19%)	19 (27.54%)	34 (49.2%)	53 (76.8%)
Small lymphocytic lymphoma	48	9(18.75%)	11(22.9%)	28(58.3%)	39(81.3%)
Mantle cell lymphoma	29	5 (17.24%)	9 (31.3%)	15 (51.7%)	24 (82.7%)
Lymphoplasmacytic lymphoma	5	0 (0%)	0 (0%)	5 (100%)	5 (100%)
Burkitt lymphoma	4	0 (0%)	0 (0%)	4 (100%)	4 (100%)
Plasmablastic lymphoma	2	0 (0%)	2 (100%)	0 (0%)	2 (100%)
T and NK cell lymphoma subtypes					
Anaplastic large cell lymphoma (all types)	112	30 (26.8%)	17 (15.2%)	65 (58%)	82 (73.2%)
T lymphoblastic lymphoma/leukemia	10	2 (20%)	2 (20%)	6 (60%)	8 (80%)
Angioimmunoblastic T cell lymphoma	11	2 (18.2%)	7 (63.6%)	2 (18.2%)	9 (81.8%)
Peripheral T cell lymphoma, NOS	11	1 (9.1%)	3 (27.3%)	7 (63.6%)	10 (90.9%)
Extranodal NK/T cell lymphoma	96	4 (4.2%)	12 (12.5%)	80 (83.3%)	92 (95.8%)
Hepatosplenic T cell lymphoma	4	0 (0%)	1 (25%)	3 (75%)	4 (100%)
Total	**599**	**209 (34.8%)**	**121 (20.2%)**	**269 (44.9%)**	**390 (65.1%)**

Table 2: Aberrant CD58 Expression in Hodgkin Lymphoma

Diagnosis	Number of cases	Positive (%)		Negative (%)
		Lymphoma	TME	
Classic Hodgkin lymphoma	84	44 (52.4%)	30 (35.7%)	9 (10.7%)
Nodular lymphocyte predominant Hodgkin lymphoma	19	8 (27.6%)	1 (5.2%)	9 (47.7%)

Figure 1 - 968

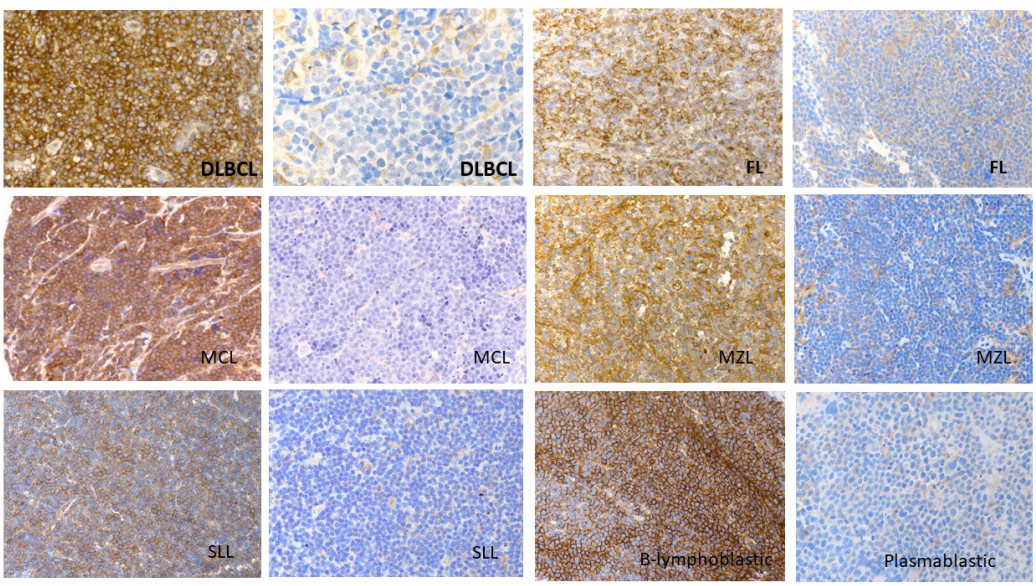

Figure 2 – 968

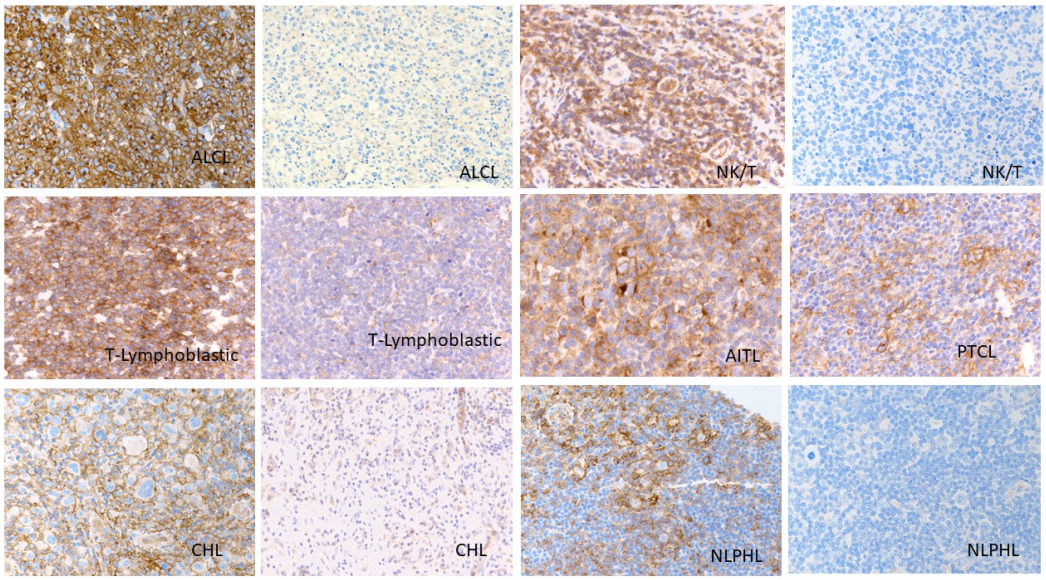

Conclusions: We show that CD58 is lost in a significant proportion of all subtypes of lymphomas. As eligibility for CAR T therapy is being extended to a broader spectrum of lymphomas, mechanisms of resistance, such as CD58 loss, may limit therapeutic success. CD58 status is therefore an important biomarker in lymphoma patients who may benefit from next generation CARs with increased efficacy and other novel approaches that mitigate immune escape.

969 Basophilia Predicts Poorer Outcomes in BCR-ABL1-Negative Myeloproliferative Neoplasms

Lisa Yuen[1], Tasos Gogakos[2], Leonardo Boiocchi[3], Gabriela Hobbs[2], Robert Hasserjian[1]
[1]Massachusetts General Hospital, Harvard Medical School, Boston, MA, [2]Massachusetts General Hospital, Boston, MA, [3]Memorial Sloan Kettering Cancer Center, New York City, NY

Disclosures: Lisa Yuen: None; Tasos Gogakos: None; Leonardo Boiocchi: None; Gabriela Hobbs: *Consultant*, AbbVie; *Advisory Board Member*, Novartis, Blueprint Medicines, Incyte; Robert Hasserjian: None

Background: Basophilia has been established as a poor prognostic indicator in chronic myeloid leukemia (CML), and high basophil level defines accelerated phase disease. For *BCR-ABL1*-negative myeloproliferative neoplasms (MPNs) the significance of basophilia is largely unknown. Prior studies found that patients with primary myelofibrosis (PMF) with high basophil counts have shortened survival. However, the significance of basophilia in other *BCR-ABL1*-negative MPNs, including associations with driver mutations and prognosis, has not been previously reported.

Design: We performed a retrospective analysis of 195 patients with MPN diagnosed on bone marrow biopsy (80 non-fibrotic essential thrombocythemia [ET], 13 non-fibrotic polycythemia vera [PV], 15 pre-fibrotic PMF, 71 MPN in fibrotic phase [MF] and 16 MPN unclassifiable [MPN-U]). Basophilia was defined as having a CBC within 6 months of the biopsy showing both relative (>3%) and absolute (>0.3 K/uL) increase in blood basophils, or >3% basophils in the bone marrow aspirate. Clinical, genetic, and morphologic features were recorded. Statistical significance was calculated using Fisher's exact test, chi-square test, t-test, or log rank test.

Results: Overall, 43 patients (22%) had basophilia. Patients with non-fibrotic ET/PV had a lower incidence of basophilia (6%) compared to patients with pre-fibrotic PMF, MF, or MPN-U (36%, p=0.0005). Basophilia was associated with more frequent abnormal cytogenetics (p=0.0002), higher WBC (17.27 vs 9.9 K/uL, p=0.0006), lower hemoglobin (11.3 vs 12.7 g/L, p=0.009) and platelet count (364 vs 600 K/uL, p=0.0001), and higher reticulin grade (1.79 vs 1.11, p=0.0007). Basophilia cases also had a greater number of mutations (2.9 vs 1.7, p<0.0001), and more frequent *JAK2* (p=0.0004), *SF3B1* (p=0.008), and *SRSF2* (p=0.016), but less frequent *CALR* mutations (p=0.002) (Fig 1). Patients with basophilia had significantly shorter overall (OS) and leukemia-free survival (LFS); OS and LFS were shorter in basophilia cases even when non-fibrotic ET/PV patients were excluded from analysis (Fig 2).

Figure 1 - 969

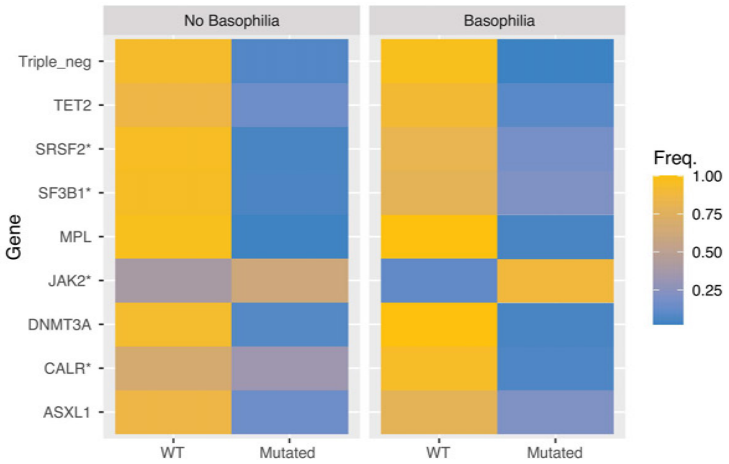

Figure 2 – 969

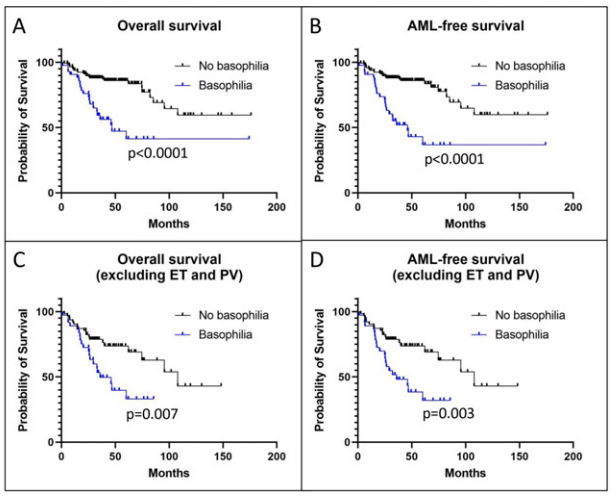

Conclusions: Basophilia in *BCR-ABL1*-negative MPNs is associated with more aggressive disease, characterized by more frequent abnormal cytogenetics, higher mutation burden, higher bone marrow reticulin grade, and poorer outcomes. Basophilia could represent a novel prognostic marker in MPN patients, who have heterogeneous clinical behavior.

970 Digital Image Analysis Utilizing an Artificial Neural Network in the Quantification of Bone Marrow Fibrosis on Reticulin-stained Trephine Core Biopsies

Christopher Zarbock[1], Bartosz Grzywacz[1]
[1]*University of Minnesota, Minneapolis, MN*

Disclosures: Christopher Zarbock: None; Bartosz Grzywacz: *Consultant*, MLM diagnostics; *Consultant*, Fate Therapeutics Inc; *Grant or Research Support*, Gamida Cell

Background: Bone marrow fibrosis is a well established pathogenic factor in myeloproliferative and other hematologic neoplasm and inflammatory conditions. We sought to develop a digital image analysis algorithm which would allow quantification of bone marrow fibrosis on reticulin-stained trephine core biopsies.

Design: We reviewed the pathology record and identified 43 cases which had reticulin staining performed during routine workup of myeloid neoplasms. This included 23 cases without a significant increase in reticulin fibrosis (MF-0 to MF-1) and 21 cases with increased reticulin fibrosis (MF-2 to MF-3). We utilized QuPath (an open-source software created by Bankhead, P. et al.) for digital image analysis with manual tissue segmentation.

Initially, an algorithm based on a pixel classifier using the thresholding approach was developed. This yielded quantitative evaluation, however we noted that in many instances nuclei were misinterpreted as reticulin fibers. In order to improve the algorithm's ability to exclude cells (round shapes) and emphasize reticulin fibers (longitudinal shapes) we trained a new pixel classifier via an artificial neural network with the Hessian max eigenvalue feature.

Results: The results demonstrated a significantly higher proportion of reticulin in cases with moderate to severe fibrosis (Figure 1 - Median 16.15 vs. 21.7, Mann - Whitney test p = 0.0001), supporting the notion that the digital image analysis can discriminate cases with severe reticulin fibrosis. Of note, there was a significant correlation with the degree of bone marrow cellularity and the proportion of reticulin fibrosis in minimal fibrosis group (R^2 = 0.47) but not in the group with severe fibrosis (R^2 = 0.05), pointing to a potential confounding effect of high cellularity. In the future stages of the project we will develop a mechanism for correction for tissue cellularity and will improve the algorithm to account for reticulin fiber thickness and intersection.

MF Grades Between 0 and 1						MF Grades Between 2 and 3				
Case		MF Grade	Proportion of Reticulin (%)	Cellularity (%)		Case		MF Grade	Proportion of Reticulin (%)	Cellularity (%)
20	1288	0	9.890512553	20		20	1125	3	26.37673523	15
20	1323	1	18.27200703	80		20	1362	2 to 3	21.93383269	5
20	1373	0	16.46099748	30		20	1406	2 to 3	19.40292592	85
20	1532	0	14.64994534	40		20	1517	2 to 3	26.06105057	85
20	1962	0 to 1	20.5848	90		20	2057	3	20.1396	85
20	2145	1	16.1538	65		20	2297	2 to 3	15.76562169	20
20	2561	1	14.37710469	60		20	2406	2 to 3	19.20321557	45
20	3045	0 to 1	13.17647506	20		20	2407	3	22.5637	30
20	3081	0 to 1	23.59078942	90		20	2689	2 to 3	19.99929295	15
20	3101	0	11.93198008	40		20	2793	3	23.96429535	10
20	3129	1	17.01425134	80		20	2848	2 to 3	18.00881493	20
20	3321	1	16.65021975	60		20	3592	3	30.02612687	80
20	3325	0	21.80205725	75		20	3619	3	24.41352469	60
20	3435	0 to 1	20.78344045	90		20	4040	3	20.42438007	90
20	3618	0	12.50103596	40						
20	3703	0	11.83712765	15		21	47	2 to 3	24.61497424	5
20	3729	0 to 1	18.45025274	40		21	77	3	21.52303807	90
20	4201	0	14.98600374	90		21	204	3	20.74534516	15
20	4321	0 to 1	9.607377645	30		21	332	2 to 3	25.33714237	50
20	4379	0 to 1	9.715992657	50		21	515	3	24.80015863	80
						21	827	3	27.60077428	70
21	360	0	16.98306309	80		21	957	3	21.2350008	35
21	706	0	15.74125699	70						
21	801	0 to 1	23.61332046	60						

Figure 1 - 970

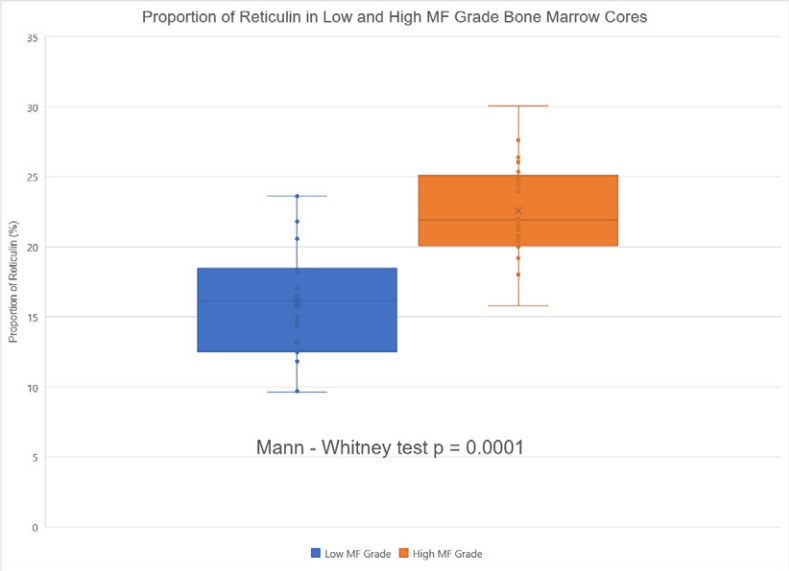

Figure 2 – 970

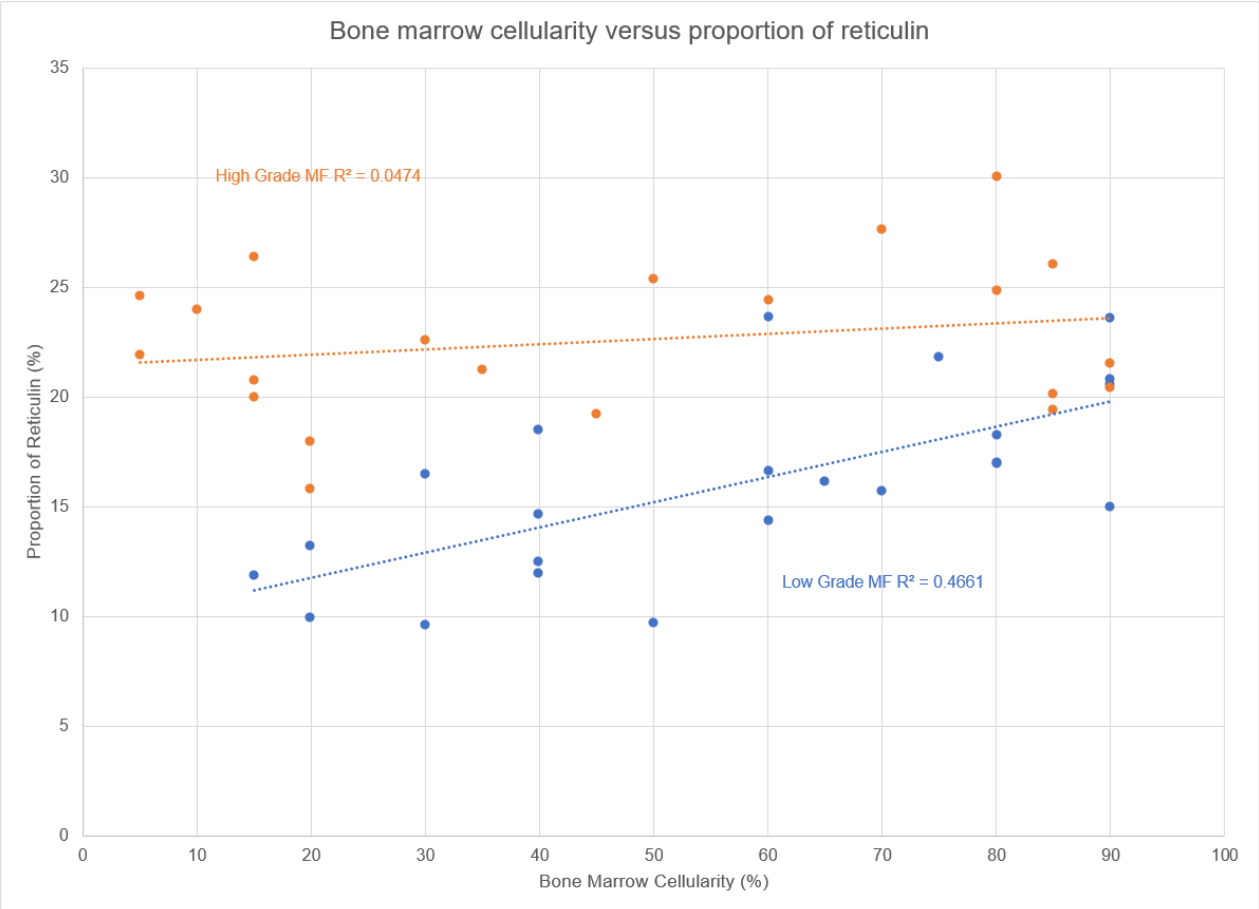

Conclusions: These results show applicability and acceptable performance of a digital image analysis algorithm using pixel classification trained via an artificial neural network emphasizing linear shapes for the quantification of bone marrow fibrosis. As the current algorithm sometimes appears to be influenced by bone marrow cellularity, we plan to analyze cases with no history of myeloid neoplasm to verify the effect of sample cellularity. Digital image analysis offers an objective method for quantitative evaluation of bone marrow fibrosis.

971 Expression of CD47 Protein in Hematolymphoid Neoplasms: Implications for CD47-Mediated Cancer Immunotherapy

Jingjing Zhang[1], Philip Bulterys[1], Sebastian Fernandez-Pol[2], Sheren Younes[3], Shuchun Zhao[1], Adnan Mansoor[4], Yasodha Natkunam[1]

[1]Stanford Medicine/Stanford University, Stanford, CA, [2]Stanford University Medical Center, Stanford, CA, [3]Stanford Pathology, Stanford, CA, [4]University of Calgary, Calgary, Canada

Disclosures: Jingjing Zhang: None; Philip Bulterys: None; Sebastian Fernandez-Pol: None; Sheren Younes: None; Shuchun Zhao: None; Adnan Mansoor: None; Yasodha Natkunam: None

Background: CD47, a surface glycoprotein, is overexpressed in some tumors and may predict poor clinical outcomes. Recent studies show blockade of CD47-SIRPα interactions to be a promising target in checkpoint inhibition for cancer immunotherapy. However, to date, the expression of CD47 is not well characterized. We explore CD47 reactivity in various hematolymphoid neoplasms to offer potential therapeutic candidates for anti-CD47 therapy.

Design: A total of 856 formalin-fixed, paraffin-embedded hematolymphoid neoplasms including 21 tumor types were studied. A portion of cases were scored from tissue microarrays. A rabbit anti-CD47 monoclonal antibody (Abcam, SP279) was used on a Leica Bond automated staining system. An H-score (percent positive tumor cells multiplied by intensity) was calculated for each tumor type and averaged (Figure 1).

Results: CD47 expression varied widely among tumor types and within individual samples in both intensity and percentage. The highest CD47 expressions in both percentage of positive lymphoma cells and intensity was seen in small B-cell lymphomas, particularly CLL/SLL (H score 224.9), mantle cell (245.2), marginal zone (252.1), and follicular lymphomas (209.8). T and B lymphoblastic, diffuse large B cell, peripheral T cell, gamma-delta T cell, angioimmunoblastic T-cell lymphomas and myelodysplastic syndrome showed moderate CD47 expression (mean H score range: 98.5-149.6). Acute and chronic myeloid leukemia as well as classic Hodgkin, anaplastic large cell, Natural Killer/T cell, and Burkitt lymphomas showed low expression (mean H scores below 50).

Figure 1 - 971

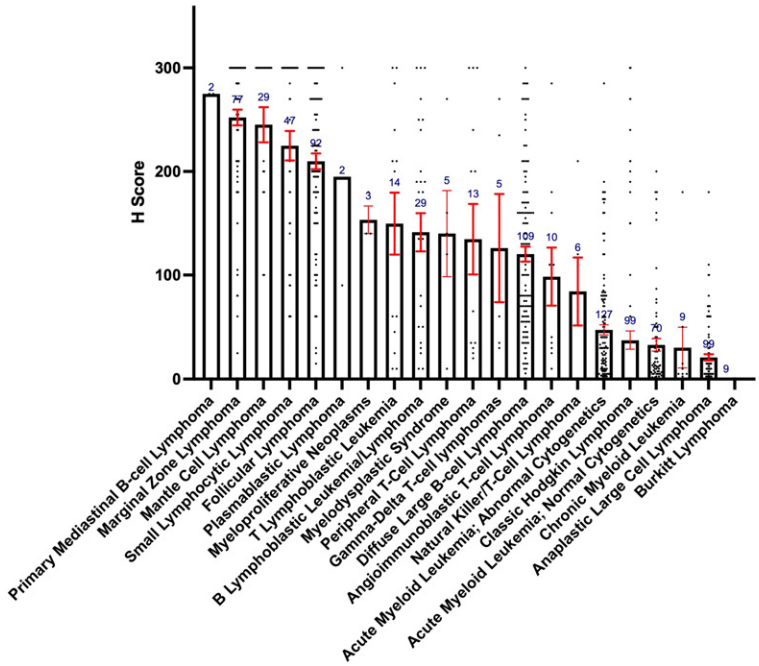

Conclusions: This is the largest study to date that describes the expression of CD47 across hematolymphoid neoplasms. Interestingly, the highest CD47 expression is seen in low-grade B cell lymphomas. The prognostic significance of these findings require further correlation with clinicopathologic and molecular data to elucidate whether CD47 expression is reflective of potential to respond to anti-CD47 therapy and to inform future clinical trial design.

972 Mutated CSF3R is a Shared Genetic Feature of CNL and MDS/MPN Overlap Syndromes

Lily Zhang[1], Eric Duncavage[2], Yi-Shan Lee[1]
[1]Washington University School of Medicine, St. Louis, MO, [2]Washington University in St. Louis, St. Louis, MO

Disclosures: Lily Zhang: None; Eric Duncavage: None; Yi-Shan Lee: None

Background: Chronic neutrophilic leukemia (CNL) is a rare myeloproliferative neoplasm, of which the differential diagnoses include atypical chronic myeloid leukemia (aCML), chronic myelomonocytic leukemia (CMML), and myelodysplastic/myeloproliferative neoplasm, unclassifiable (MDS/MPN-U). *CSF3R* mutations have been previously shown to be sensitive and specific for CNL. We describe the clinical, morphologic, and genetic findings of all *CSF3R*-mutated cases detected by our targeted NGS assay, Myeloseq.

Design: Bone marrow and peripheral blood samples from patients with a suspected or prior history of myeloid disorder were sequenced using Myeloseq, which targets 40 commonly mutated genes. We conducted a retrospective search of over 2,000 MyeloSeq cases for *CSF3R* mutated cases from 8/2018 to 8/2021. Clinical data were obtained from electronic medical records. Morphologic findings on the concurrent sample were collected from the initial report.

Results: Thirty-one unique cases with mutated *CSF3R* were identified. Of these, a concurrent diagnosis of MPN, MDS, or MDS/MPN overlap was made in 14 cases; AML in 8; therapy-related myeloid neoplasm in 1; and other in 8, in which the *CSF3R* variant was thought to represent a germline polymorphism. Of the non-germline cases (n=23), the most common *CSF3R* variant was p.T816I (14/23). All cases showed co-mutations in other genes, with an average of 4.2 co-mutations per case (range 1-9). Of the *CSF3R*-mutated cases associated with a diagnosis of MPN, MDS, or MDS/MPN overlap (n=14), the average patient age was 73 and the cohort showed a male predominance. The average WBC was 49 K/cumm, ANC 36 K/cumm, and absolute monocyte count 4.5 K/cumm. Morphologic analysis showed that 13 of 14 cases had a hypercellular marrow; one case had a suboptimal biopsy. Seven of the 13 cases presented for a first-time diagnosis. Using strict 2017 WHO criteria to retrospectively classify these 7 cases, zero would qualify for a diagnosis of CNL; 4 for MDS/MPN-U; 2 for CMML; and 1 for aCML.

Conclusions: *CSF3R* mutations have been described as a specific marker for CNL. However, no patients in our cohort of *CSF3R*-mutated cases meet strict 2017 WHO criteria for a diagnosis of CNL, as cases often had concurrent monocytosis or dysplasia. As clinical trials for kinase inhibitors have shown benefit in CNL patients with mutated *CSF3R*, a broader definition of CNL should be considered.

973 Significance of Co-mutations in BCR-ABL1 Negative Myeloproliferative Neoplasms

Yi Zhou, University of Miami, Miami, FL

Disclosures: Yi Zhou: None

Background: Mutation in JAK2 (V617F), CALR and MPL are the hallmark of BCR-ABL1 negative myeloproliferative neoplasms. These neoplasms have commonalities in megakaryocytic proliferation but diverse in morphology and progression to myelofibrosis and secondary acute myeloid leukemia. Genetic abnormalities revealed by NGS has shed light on the heterogeneity in this group of diseases. Myelofibrosis with co-mutations in SRSF2, U2AF1, EZH1, CBL, KRAS, NRAS, IDH1/IDH2, or TP53 have significantly higher risk of transformation and are associated with shorter overall survival than the diseases without these co-mutations. The finding raises a notion that BCR-ABL1 negative myeloproliferative neoplasms can be better stratified based on the underpinning genetic abnormalities. In this study, we correlated genetic abnormalities detected by NGS with the diagnosis based on the WHO classification criteria.

Design: In this retrospective study, we identified consecutive myeloid neoplasms that harbored JAK2V617F, MPLW515L or mutated CALR and tested using a 44-gene NGS panel. The co-mutation profile was divided into five groups: group1: absence of co-mutation; group2: mutation in DNMT3A, ASXL1 or TET2; group3: single mutation in SF3B1, SRSF2, U2AF1, ZRSR2, EZH2, IDH1/2, CBL, KRAS, NRAS, PTPN11 or NF1 with or without group2 mutation; group4: more than one group3 mutations; group5: mutations in TP53, PHF6 or RUNX1. The mutation profiles were correlated diagnosis based on WHO criteria.

Results: Total 62 unique patients were identified. All the cases carried JAK2V617F, MPLW515L or mutated CALR in more than 30% of nucleated cells. The co-mutations were divided into 5 groups. Patients' age distribution, and diagnosis based on WHO criteria for each genetic group are listed in Table 1. We found that single co-mutation in SF3B1, SRSF2, U2AF1, ZRSR2, EZH2, IDH1/2, CBL, KRAS, NRAS, PTPN11 or NF1 MPN was associated with increase in myelofibrosis and features of dysplasia, whereas more than one co-mutation in this group was more likely presented as MDS/MPN. Acquiring mutation in TP53, PHF6 and RUNX1 were associated with increased risk of secondary AML in patients with long history of myeloproliferative neoplasm.

	Group1	Group2	Group3	Group4	Group5
N	17	11	12	8	13
age	61 (37-76)	70 (61-87)	66 (45-84)	70 (65-81)	71 (56-87)
ET	1	1	0		
PV	6	2	1		
PMF-C	4	1	0		
MF (MF2-3)	6	7	7	1	2
MDS/MPN			4	7	3
AML					8

Conclusions: Co-mutation in genes involving spliceosome and signaling pathway can result in the features of MDS/MPN, whereas mutation in TP53, PHF6 or RUNX1 are associated high-risk of secondary acute myeloid leukemia. Monitoring co-mutation in MPN may improve assessment of disease progression.

974 Angioimmunoblastic T-cell Lymphoma: The Significance of HAVCR2/TIM3 in CD8+ Tumour Infiltrating Lymphocytes

Qiqi Zhu[1], Xueqin Deng[1], Weiping Liu[1], Wen-yan Zhang[1], Sha Zhao[1]
[1]*West China Hospital, Sichuan University, Chengdu, China*

Disclosures: Qiqi Zhu: None; Xueqin Deng: None; Weiping Liu: None; Wen-yan Zhang: None; Sha Zhao: None

Background: Angioimmunoblastic T-cell Lymphoma (AITL) originates from T follicular helper (TFH) cells and has a substantial inflammatory tumor microenvironment (TME). Our previous study focusing on tumour-infiltrating lymphocytes (TILs) related risk

factor in AITL suggested that CD8+TILs was a significant risk factor of OS. And we had also found the obviously increasement of CD8+TIM3+ in AITL compared with reactive lymph node hyperplasia in the former research. With TIM3-related drugs gradually application in clinical practice, the significance of HAVCR2/TIM3 in CD8+ TILs is needed to be investigated in AITL.

Design: The expression of TIM3 on CD8+TILs was evaluated in fresh lymph node tissue samples from 20 de novel AITL cases by flow cytometry (FCM). The expression of HAVCR2 (which encode TIM3) in Formalin-fixed paraffin-embedded (FFPE) samples was detected from 48 de novel AITL cases through qPCR. The cut-off for the CD8+TIM3+ in FCM and HAVCR2 in qPCR were defined as the point where the sensitivity plus specificity was maximized in the receiver operating characteristic (ROC) curves for predicting the overall survival (OS) respectively, and COX regression was used to evaluate the impact of HAVCR2/TIM3 on the prognosis of patients. Subsequently, RNA-sequencing was performed on FFPE samples from 20 de novel AITL cases to explore the potential HAVCR2-related genes in CD8+TILs.

Results: Twenty AITL cases were divided into high CD8+TIM3+ (>=3.55%) (n=7) group and low CD8+TIM3+ (<3.55%) group (n=13) (p<0.001, Fig 1a) in FCM and high CD8+TIM3+ was a significant risk factor of OS (p=0.008, Fig 1b). Similarly, 48 AITL cases were divided into high HAVCR2 (>=1.2) group (n=40) and low HAVCR2 (<1.2) group (n=8) (p<0.001, Fig 1c) based on the result of qPCR and the inferior impact of HAVCR2 on prognosis in AITL was confirmed (p=0.011, Fig 1d). RNA-seq analysis results demonstrated that HAVCR2 was not only strongly associated with cytotoxic T lymphocyte related signature including CD8A (r=0.6, p=0.004), CD8B (r=0.71, p<0.001), GZMA (r=0.71, p<0.001), GZMB (r=0.8, p<0.001), PRF1 (r=0.78, p<0.001) and IFNG (r=0.57, p=0.009), but also positively correlated with other inhibitor receptors such as LAG3 (r=0.7, p<0.001), CD244 (r=0.55, p=0.012) and PTGER4 (r=0.57, p=0.008), and negatively correlated with the transcription-related factor TCF7 (r= -0.66, p=0.001) and VHL (r=-0.48, p=0.032) (Fig 2).

Figure 1 - 974

Fig 1

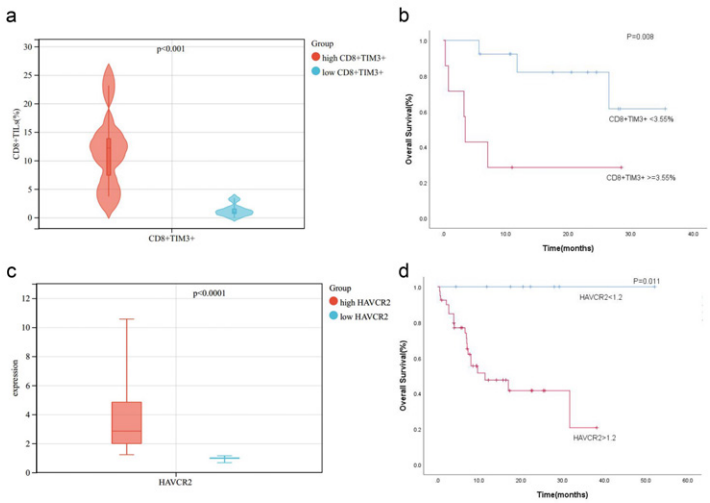

Figure 1. The results of TIM3/HAVCR2 in AITL.
a. Comparison of FCM results in high CD8+TIM3+ group (n=7) and low CD8+TIM3+ group (n=13).
b. Overall survival rate for CD8+TIM3+ in AITL by FCM.
c. Comparison of qPCR results in high HAVCR2 group (n=40) and low HAVCR2 group (n=8).
d. Overall survival rate for HAVCR2 in AITL by qPCR.

Figure 2 – 974

Fig 2

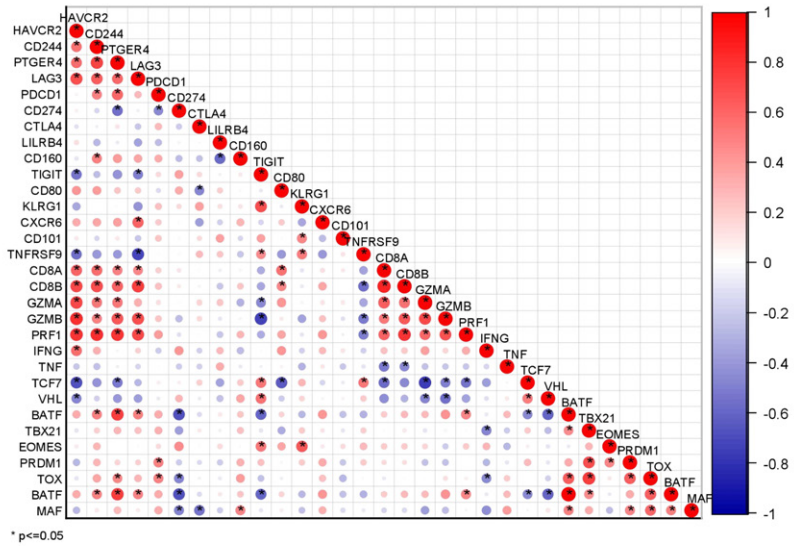

Figure 2. The correlation between HAVCR2 and cytotoxic T lymphocyte related signature, other inhibitor receptors and transcription-related factor.

Conclusions: Our research demonstrates that HAVCR2/TIM3 was closely related to CD8+TILs both in protein and gene level, and exhibited an inferior OS in AITL. The function of HAVCR2/TIM3 could be regulated by some transcriptional genes, and the synergistic action of HAVCR2/TIM3 and other inhibitory receptors might lead to CD8+TILs exhaustion in AITL and result in poor prognosis, which indicate HAVCR2/TIM3 could be a novel target in AITL therapy and deserve further research.

975 Applying LymphGen Classification to a Clinically Validated 400-gene Targeted Next-Generation Sequencing (NGS) Panel in Diffuse Large B-cell Lymphoma (DLBCL)

Menglei Zhu[1], Esther Drill[1], Erel Joffe[1], Maria Arcila[1], Ahmet Dogan[1]
[1]*Memorial Sloan Kettering Cancer Center, New York, NY*

Disclosures: Menglei Zhu: None; Esther Drill: None; Erel Joffe: None; Maria Arcila: None; Ahmet Dogan: None

Background: DLBCL is a pathologically, phenotypically, and genetically heterogeneous disease. Several recent studies utilized high-resolution genomic analysis to describe molecular subtypes based on genetic alterations and revealed broader biological heterogeneity than the ABC/GCB paradigm. A probabilistic classification algorithm, LymphGen, was developed by NCI group (Wright, et.al) to subclassify DLBCL into six groups based on mutation profiles with superior prognostic correlation. However, genetic classification has not been reported on a clinical available molecular testing platform.

Design: In this study, we applied the LymphGen algorithm to our clinically validated 400-gene targeted NGS panel (referred as 400-gene panel below). We extracted mutations and copy number alteration (CNA) of 417 clinical DLBCL samples submitted for NGS evaluation in our institution during 2017-2021. In addition, BCL2, BCL6, and MYC translocation were obtained from the clinical cytogenetic report. To evaluate the LymphGen performance on the 400-gene panel, we obtained published genetic data (mutations, cytogenetics, and CNA) from the NCI DLBCL cohort. The data was filtered to the alterations that can only be detected by the 400-gene panel and applied to LymphGen. The classification outcome was compared to the NCI panel.

Results: Comparable to NCI cohorts, 54.8% of 417 cases from our DLBCL cohort were assigned to one of the six or combined categories (MCD:10.1%, EZB:21.7%, BN2:9.9%, N1:2.8%, ST2:6.8%, A53:1.8%, combined:1.8%) (Figure 1A). Within these cases, about two-thirds of cases were called with high confidence (Core group, >90% probability), and one-third was called with lower confidence (Extended group) (Figure 1B). The correlation of genetic subtypes and cell of origin based on Hans' algorithm is similar to the published study (Figure 1C). Forty significant genes with high prevalence in each subtype were identified (Figure 1D).

Different Immunophenotypical features were observed in each genetic subtype (Figure 1E). Compared to the NCI panel, the accuracy and specificity by 400-gene panel were 92% and 98 overall, with the highest performance in EZB and N1 subtypes. Promisingly, the accuracy and specificity were 96% and 99% in the Core group (Figure 2).

Figure 1 - 975

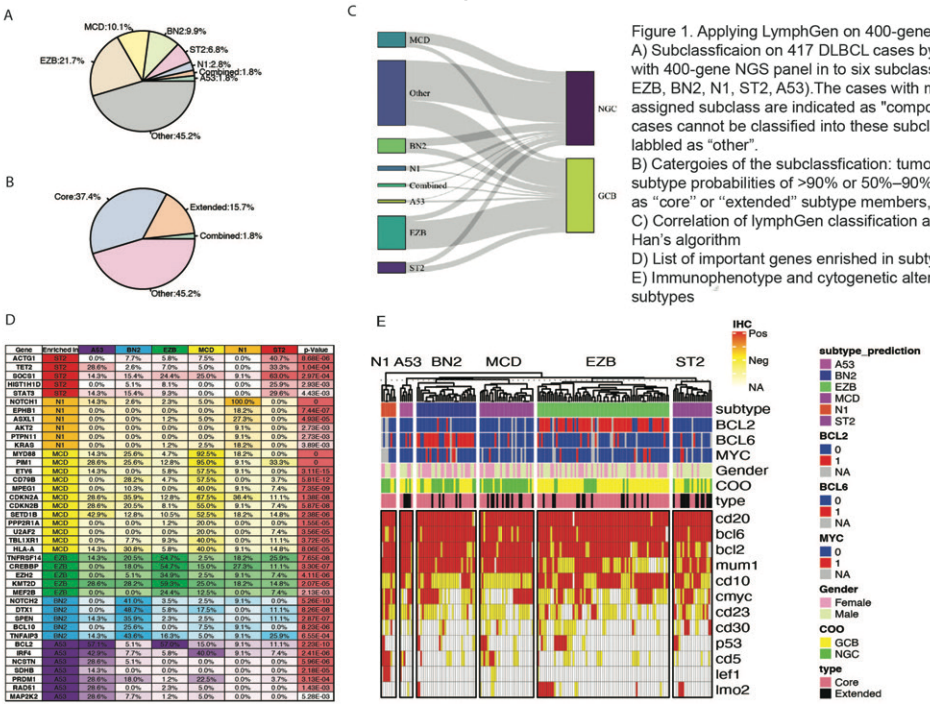

Figure 1. Applying LymphGen on 400-gene NGS panel
A) Subclassficaion on 417 DLBCL cases by lymphGen with 400-gene NGS panel in to six subclasses (MCD, EZB, BN2, N1, ST2, A53).The cases with more than one assigned subclass are indicated as "composite." The cases cannot be classified into these subclasses are labbled as "other".
B) Catergoies of the subclassfication: tumors with subtype probabilities of >90% or 50%–90% were defined as "core" or "extended" subtype members, respectively.
C) Correlation of lymphGen classification and COO by Han's algorithm
D) List of important genes enrished in subtypes
E) Immunophenotype and cytogenetic alterations in subtypes

Figure 2 – 975

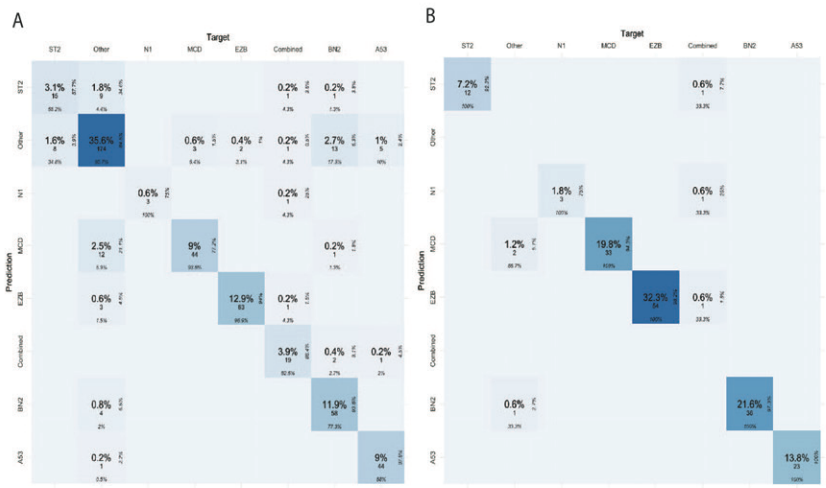

Figure 2. NCI cohort data filtered by 400-gene panal
A)Confusion matrix of 400-gene panel vs NCI panel (all cases)
B) Confusion matrix of 400-gene panel vs NCI panel (core group)
C) Analysis of 400-gene panel vs NCI panel(all cases)
D) Analysis of 400-gene panel vs NCI panel (core cases)

C

	Accuracy	F1	Sensitivity	Specificity	Pos Pred Value	Neg Pred Value
ALL	0.92	0.84	0.86	0.98	0.83	0.98
A53	0.94	0.88	1.00	0.98	0.99	0.93
BN2	0.88	0.77	0.99	0.94	0.96	0.85
Combined	0.91	0.83	0.99	0.86	0.99	0.84
EZB	0.98	0.97	0.99	0.94	1.00	0.95
MCD	0.95	0.94	0.97	0.77	0.99	0.85
N1	1.00	1.00	1.00	0.75	1.00	0.86
Other	0.87	0.86	0.89	0.84	0.90	0.85
ST2	0.81	0.65	0.98	0.58	0.98	0.61

D

	Accuracy	F1	Sensitivity	Specificity	Pos Pred Value	Neg Pred Value
ALL	0.96	NaN	0.75	0.99	NaN	1.00
A53	1.00	1.00	1.00	1.00	1.00	1.00
BN2	1.00	1.00	0.99	0.97	1.00	0.99
EZB	1.00	1.00	0.99	0.98	1.00	0.99
MCD	0.99	1.00	0.99	0.94	1.00	0.97
N1	1.00	1.00	0.99	0.75	1.00	0.86
ST2	1.00	1.00	0.99	0.92	1.00	0.96

Conclusions: We validated genetic classification for DLBCL by LymphGen on the clinical 400-gene NGS panel. This approach could open an avenue of incorporating genetic classification of DLBCL into the clinical trials design and therapeutic decision.

976 Automatic Triaging of Hematopathology Tissue Specimens by Neural Network on Whole Slide Image (WSI)

Menglei Zhu[1], Michael Hazoglou[1], Anyi Li[1], Ahmet Dogan[1]
[1]Memorial Sloan Kettering Cancer Center, New York, NY

Disclosures: Menglei Zhu: None; Michael Hazoglou: None; Anyi Li: None; Ahmet Dogan: None

Background: Recently, digital pathology's rapid growth provides a platform for machine learning applications in clinical pathology. A few studies showed the decent performance of machine learning algorithms on lymphoid tissue classification in limited tumor types. Definitive hematopathology diagnosis is primarily based on a combination of morphology and immunohistochemistry studies. Selection of appropriate immunohistochemistry (IHC) workup is an essential but time-consuming process during hematopathology diagnosis. This study developed a machine-learning model to classify clinically common lymphoma and facilitate automatic IHC ordering in hematopathology.

Design: 4247 H&E-stained WSI from our institution's slides archive were collected for clinical specimens submitted to Hematopathology Service between 2017-2021, including 1129 follicular lymphoma (FL), 212 chronic lymphocytic leukemia/small lymphocytic lymphoma (CLL), 613 mantle cell lymphoma (MCL), 1002 diffuse large B-cell lymphoma (DLBCL), 232 Classic Hodgkin lymphoma (CHL), 888 marginal zone lymphoma (MZL), 76 angioimmunoblastic lymphoma (AITL), and 95 Burkitt's lymphoma (BL). The WSIs were split into training (50%), validation (25%), and test (25%) datasets following by pre-processing. A variant of ResNet with ten layers was applied to the training set. Multiple versions of this ResNet were trained using Adam with decoupled weight decay regularization, and a cross-entropy loss accepts only the models that improve the validation loss (Figure 1A).

Results: The neural network model classified the WSI into one of the 8 diagnoses with 81% accuracy overall. The confusion matrix and performance on each tumor type are shown in Figure1 B-D. An AI-assisted workflow was developed based on the predicted tumor type. The images with a low prediction confidence score (19.7%) or scant tissue (3%) by automatic tissue detection were directed to pathologist manual review. Based on the classification, the rest of the images were assigned to one of the 5 IHC panels (DLBCL/FL/BL; MCL/CLL; AITL, CHL, or MZL). Overall, the IHC panel of 84% cases was correctly determined by this system (Figure 2).

Figure 1 - 976

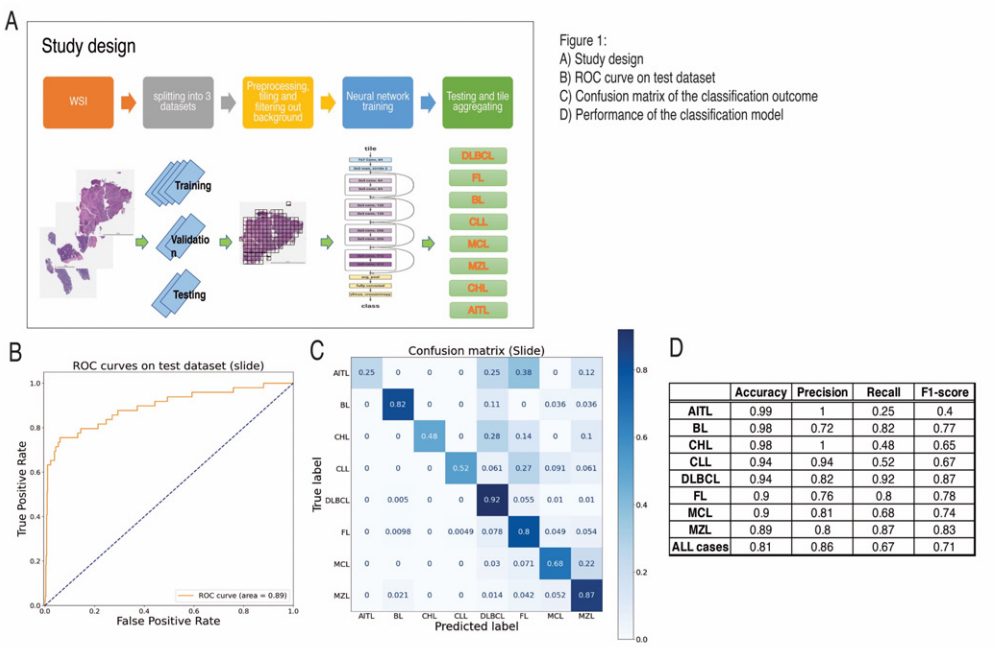

D

	Accuracy	Precision	Recall	F1-score
AITL	0.99	1	0.25	0.4
BL	0.98	0.72	0.82	0.77
CHL	0.98	1	0.48	0.65
CLL	0.94	0.94	0.52	0.67
DLBCL	0.94	0.82	0.92	0.87
FL	0.9	0.76	0.8	0.78
MCL	0.9	0.81	0.68	0.74
MZL	0.89	0.8	0.87	0.83
ALL cases	0.81	0.86	0.67	0.71

Figure 2 – 976

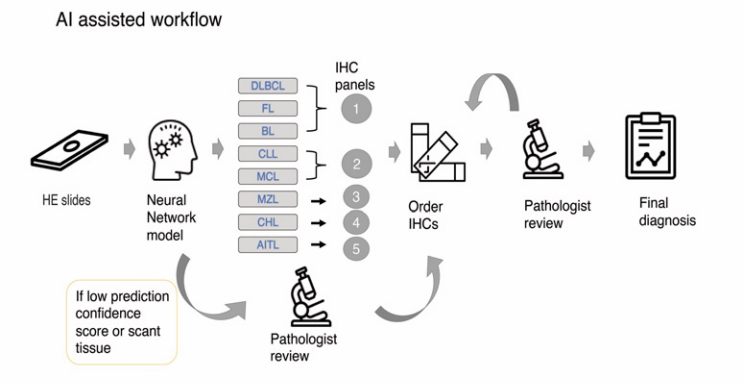

Conclusions: We developed an AI-based triaging system for automatic IHC ordering. Incorporating this system into clinical workflow could potentially markedly reduce turnaround time and cost. In addition, to our knowledge, this study is the first large-scale/multiple categories cohort on utilizing deep learning to classify lymphoma.